Identification and Control of Chaotic Maps: A Frobenius-Perron Operator Approach

Xiaokai Nie

A thesis submitted to the University of Sheffield for the degree of

Doctor of Philosophy

Department of Automatic Control and Systems Engineering

The University of Sheffield

Sheffield, United Kingdom

January 2015

Abstract

Deterministic dynamical systems are usually examined in terms of individual point trajectories. However, there are some deterministic dynamical systems exhibiting complex and chaotic behaviour. In many practical situations it is impossible to measure the individual point trajectories generated by an unknown chaotic dynamical system, but the evolution of probability density functions generated by such a system can be observed. As an alternative to studying point trajectories, such systems can be characterised in terms of sequences of probability density functions. This thesis aims to develop new approaches for inferring models of one-dimensional dynamical systems from observations of probability density functions and to derive new methodologies for designing control laws to manipulate the shape of invariant density function in a desired way.

A novel matrix-based approach is proposed in the thesis to solve the generalised inverse Frobenius-Perron problem, that is, to recover an unknown chaotic map, based on temporal sequences of probability density function estimated from data generated by the underlying system. The aim is to identify a map that exhibits the same transient as well as the asymptotic dynamics as the underlying system that generated the data. The approach involves firstly identifying the Markov partition, then estimating the associated Frobenius-Perron matrix, and finally constructing the underlying piecewise linear semi-Markov map. The approach is subsequently extended to more general one-dimensional nonlinear systems. Compared with the previous solutions to the inverse Frobenius-Perron problem, this approach is able to uniquely construct the transformation over the identified partition.

The method is applied to heterogeneous human embryonic stem cell populations for inferring its dynamical model that describes the dynamical evolution based on sequences of experimentally observed flow cytometric distributions of cell surface marker SSEA3. The model that delineates the transitions of SSEA3 expression over one-day interval, can predict the long term evolution of SSEA3 sorted cell fractions, particularly, how different cell fractions regenerate the invariant parent distribution,

and can be used to investigate the equilibrium points which are believed to correspond to functionally relevant substates, as well as their transitions.

A new inverse problem is further studied for one-dimensional chaotic dynamical systems subjected to additive bounded random perturbations. The problem is to infer the unperturbed chaotic map based on observed temporal sequences of probability density functions estimated from perturbed data, and the density function of the perturbations. This is the so-called inverse Foias problem. The evolution of probability density functions of the states is formulated in terms of the Foias operator. An approximate matrix representation of Foias operator corresponding to the perturbed dynamical system, which establishes the relationship with Frobenius-Perron matrix associated with the unknown chaotic map, is derived.

Inspired from the proposed approach for solving the generalised inverse Frobenius-Perron problem, a novel two-step matrix-based method is developed to identify the Frobenius-Perron matrix which gives rise to the reconstruction of the unperturbed chaotic map.

The asymptotic stability of the probability density functions of the one-dimensional dynamical systems subjected to additive random perturbations is proven for the first time. The new result establishes the existence as well as the uniqueness of invariant densities associated to such transformations.

Finally, this thesis addresses the problem of controlling the invariant density function. Specifically, given a one-dimensional chaotic map, the purpose of controller design is to determine the optimal input density function so as to make the resulting invariant density function as close as possible to a desired distribution. The control algorithm is based on the relationship between the input density function and the invariant density function derived earlier on.

Acknowledgements

I would like to express my sincere gratitude to my supervisor Prof. Daniel Coca for his excellent supervision, constant encouragement, support and helpful insights on my PhD project research.

I also would like to gratefully acknowledge the financial support from the Department of Automatic Control and Systems Engineering of the University of Sheffield, and China Scholarship Council.

Besides, I wish to thank Dr. Veronica Biga, Dr. Yuzhu Guo, and Dr. Andrew Hills for the inspiring discussion with them and their great help, and thank James Mason from the Centre for Stem Cell Biology at the University of Sheffield, for providing experimental data and relevant useful materials. Moreover, my appreciations would go to my colleagues and all of my friends, Dr. Yang Li, Jia Zhao, Dr. Zhuoyi Song, Dr. Dazhi Jiang, etc, and the support staff of the Department for their kind help and the fantastic experience with them in Sheffield.

Finally, yet importantly, I am extremely grateful to my beloved parents, my sister and my brother, and girlfriend Jingjing Luo for their love, encouragement and support.

Contents

List of Acronyms

IFPP	inverse Frobenius-Perron problem
GIFPP	generalised inverse Frobenius-Perron problem
PRE	percentage root-mean-square error
MAPE	mean absolute percentage error
RMSE	root mean square error
SSEA3	surface specific embryonic antigen
ESC	embryonic stem cell
hESC	human embryonic stem cell
FACS	fluorescence activated cell sorting

List of Important Symbols

I	The bounded interval
$\mathbb{R}$	The real line
S	Measurable transformation
$\mathbb{C}^r$	Space of all r-times continuously differentiable real functions
χ	Normalised Lebesgue measure
A	Arbitrary measurable set
χ_A	Characteristic function for the set A
f	Probability density function of bounded variation
P_S	The Frobenius-Perron operator with respect to S
$\mathfrak{R}$	Markov partition
N	Number of subintervals of partition $\mathfrak{R}$
L^1	Space of Lebesgue integrable functions
R_i	The i-th subinterval of a partition
M	Frobenius-Perron matrix
$\lambda(\cdot)$	Lebesgue measure
$Q_j^{(i)}$	Subinterval in interval R_i
$p(i)$	Number of subintervals in interval R_i
$\mathfrak{F}$	Space of the piecewise constant functions
f^*	Invariant density function
$q_k^{(i)}$	Interval points in $Q_j^{(i)}$
$E(\cdot)$	Mathematical expectation
$\mathfrak{B}$	Borel σ-algebra of subsets in I
μ	Normalized Lebesgue measure on I
$\hat{S}$	Identified transformation

$\hat{\alpha}_{i,j}$, $\hat{\beta}_{i,j}$	Parameters of identified transformation
δS	Absolute percentage error between the original and identified maps
$\mathfrak{D}$	Space of probability density functions
$\|\|\cdot\|\|_F$	Frobenius norm
ξ	Noise maximum magnitude
u_n	Input variable
Q	Foias operator
Prob{·}	Probability of {·} taking place
ω_n	Stochastic noise
$\boldsymbol{H}$	Matrix representation of Foias operator
U	Input samples
Ω	Noise samples
f_u	Probability density function of input
$g(\omega)$	Probability density function of noise

List of Figures

List of Tables

Chapter 1
Introduction

1.1 Research background and motivation

1.1.1 Modelling of chaotic dynamical systems from probability density functions

It is well known that even simple one-dimensional discrete time deterministic systems can exhibit complex and unpredictable random-like dynamical behaviour, the so-called chaos. In many practical situations, the underlying dynamical system is unknown, and the critical problem is to infer the mathematical description of the system from the observations. The mathematical model characterising the system dynamics can be used to predict the evolution of the dynamical behaviour, and analyse the system stability. Chaotic behaviour can be observed in many natural systems, and one-dimensional chaotic maps describes many real dynamical processes, encountered in engineering, biology, physics and economics (Ott 1993), which generate density of states. Examples include modelling particle formation in emulsion polymerization (Coen, Gilbert et al. 1998), papermaking systems (Wang, Baki et al. 2001) bursty packet traffic in communication (Mondragó C. 1999), networks (Rogers, Shorten et al. 2004), cellular uplink load in WCDMA systems (Wigren 2009). A major challenge is that of inferring the chaotic map which describes the evolution of the unknown chaotic system, solely based on experimental observations.

Starting with seminal research of Farmer and Sidorovich (1987), Casadgli (1989), and Abarbanel et al (1989), the problem of inferring dynamical models of chaotic

systems directly from time series data has been addressed by many authors using neural networks (Principe, Rathie et al. 1992), polynomial (Aguirre & Billings 1995a), or wavelet models (Billings & Coca 1999).

In many practical applications, it is more convenient to observe experimentally the evolution of the probability density functions instead of individual point trajectories, generated by such systems. There are even many cases in which individual point trajectories are not allowed to be recorded but sequences of probability density functions are available (Lozowski, Lysetskiy et al. 2004, Altschuler & Wu 2010). As a consequence, the traditional perspective of studying the chaotic systems needs to be shifted. Such systems can be studied in terms of probability density functions they generate, rather than point trajectories.

The problem of inferring the chaotic map given probability density functions observed from the unknown systems, known as inverse Frobenius-Perron Problem (IFPP), has been investigated by a number of researchers in the case when the only information available is the invariant density function associated with the unknown map over the past few years. Typical relevant research has been presented by Friedman & Boyarsky (1982), Ershov & Malinetskii (1988), Góra & Boyarsky (1993), Baranovsky & Daems (1995), Diakonos & Schmelcher (1996), Pingel, Schmelcher & Diakonos (1999), Diakonos, Pingel & Schmelcher (1999), et al. In particular, a matrix approach (Ulam 1960, Góra & Boyarsky 1993, Rogers, Shorten et al. 2004, Rogers, Shorten et al. 2008a) to the inverse problem has been developed to reconstruct Markov transformation with prescribed invariant density function.

It needs to be noted that all the existing methods are used to construct a map on the given condition that the invariant density is known. This leads to the limitation of these approaches that the solution to the inverse problem is not unique. Typically, there exist many transformations, exhibiting a wide variety of dynamical behavious, but which the same invariant density. Therefore, the reconstructed map does not necessarily exhibit the same dynamics as the underlying systems even though it preserves the required invariant density. Additional constraints and model validity tests have to be used to ensure that the reconstructed map captures the dynamical properties of the underlying system (Lyapunov exponents, fixed points etc.) and

predicts its evolution. This is of paramount importance in a many practical applications ranging from modelling and control of particulate processes (Coen, Gilbert et al. 1998, Crowley, Meadows et al. 2000), characterising the formation and evolution of the persistent spatial structures in chaotic fluid mixing (Pikovsky & Popovych 2003), characterising the chaotic behaviour of electrical circuits (Wyk & Ding 2002), chaotic signal processing (Götz, Abel et al. 1997, Isabelle & Wornell 1997), analysing and interpreting cellular heterogeneity (Altschuler & Wu 2010, MacArthur & Lemischka 2013) and identification of molecular conformations (Schütte, Huisinga et al. 2001).

Another noteworthy limitation of the existing matrix-based reconstruction algorithms is the assumption that a Markov partition is known. In general, no *a priori* information about the unknown map is available, so the partition identification problem has to be solved as part of the reconstruction method. In a whole, as for a specific unknown dynamical system, the uniqueness of identified transformation cannot be guaranteed with current available approaches, which implies that they cannot be used to predict the long-term evolution of dynamical behaviour and to analyse the complete stability of the dynamical systems.

In view of the shortages stated above, this research will focus on utilising the temporal sequences of probability density functions to address the inverse Frobenius-Perron problem and further generalise the solution to nonlinear systems.

Furthermore, practical systems are usually subjected to stochastic perturbations. It follows that, given the same initial density function, the perturbed and the noise-free systems will generate different sequence of probability density functions compared with those of the noise-free system. To date the research in this area focused on the study of invariant measures of discrete-time systems with constantly or randomly applied stochastic perturbations (Lasota & Mackey 1994, Boyarsky & Góra 1997, Kuske & Papanicolaou 1998, Bollt, Góra et al. 2008, Islam & Góra 2011).

So, whilst the problem of modelling chaotic dynamical systems from noisy time series data has been widely studied (Billings, Jamaluddin et al. 1992, Brown,

Rulkov et al. 1994, Aguirre & Billings 1995a, Billings & Coca 1999, Coca & Billings 2001, Voss, Timmer et al. 2004, Zhiwei & Min 2007), the inverse Frobenius-Perron problem has only been studied for purely deterministic dynamical systems. For this reason, one of the objectives of this thesis is to address the more realistic inverse Foias problem for one-dimensional chaotic maps subjected to stochastic perturbations.

1.1.2 Modelling the heterogeneity of human embryonic stem cell populations

Stem cell research has become the frontier field of modern clinical medicine committed to treating neurodegenerative diseases and conditions such as diabetes, Parkinson's, Alzheimer's diseases and cancer. In many tissues, stem cells act as a class of repair system for a live body, having unlimited potential of dividing to replenish other cells.

Embryonic stem cells (ESCs) are an unspecialised type of cells which are capable of differentiating to any type of cells with specialised functions such as neurons, retinal pigment cells, hepatic cells etc. At the same time, when grown *in vitro,* ESCs have the capability to divide indefinitely whilst maintaining pluripotency (self-renewal).

Human embryonic stem cells are pluripotent stem cells derived from the inner cell mass of blastocysts that are embryos of 4 to 5 days old consisting of 50 to 150 cells. They can develop into the derivatives of the three primary germ layers: ectoderm, endoderm and mesoderm that involve a great number of over 200 cell types existing in adult body.

It has been found that human embryonic stem cell (hESC) cultures are not homogeneous but are, instead composed of cells occupying inter-convertible substates (Chambers, Silva et al. 2007, Chang, Hemberg et al. 2008, Hayashi, Lopes et al. 2008a). These substates represent cells with distinct functions, which behave differently in response to same stimuli (Olariu, Coca et al. 2009). Cells in these substates may be biased in their probability of adopting particular fates upon

differentiation, while interactions between cells in different sub-states may profoundly influence cell fate decisions during self-renewal and differentiation. Human embryonic stem cell lines have been used as the best tool to study the cell differentiation associated with the embryonic development (Andrews 1998). Changes in the expression of cell surface antigens SSEA3 can be used to characterise the heterogeneity of stem cell cultures.

In this work, the NTERA2 cell line, a pluripotent human embryonal carcinoma cell line which exhibits biochemical and developmental properties similar to the cells of the early embryo, was used as a model for studying the heterogeneity of human embryonic stem cells.

Specifically, the research was focused on applying the new methods for inferring the dynamical model based on observed sequences of density functions (i.e. solving the Inverse Frobenius-Perron Problem) to the problem of characterising the dynamic evolution of heterogeneous cell populations using sequences of flow cytometric distributions of cell surface markers.

1.1.3 Controlling the invariant densities of dynamical systems

Over the past few decades there has been a large number of research on control of chaotic dynamical systems (Shinbrot, Grebogi et al. 1992, Lai & Grebogi 1993, Góra & Boyarsky 1996, Góra & Boyarsky 1998, Bollt 2000a). In the early stage, the major strategy developed was aimed to stabilise periodic orbits by applying a local feedback control on the motion of a chaotic attractor to direct the individual trajectory to a desired periodic orbit. This was achieved by making small perturbations to the motion. Sensitive dependence to initial conditions of the chaotic systems requires the control to be applied to each individual trajectory to achieve overall regulation on the chaotic behaviour. Another disadvantage is that these methods will change the chaotic nature of the underlying system.

The later proposed methodologies of controlling chaotic systems were focused on more global strategies (Góra & Boyarsky 1996, Góra & Boyarsky 1998, Bollt

2000b, Bollt 2000a, Góra & Boyarsky 2001, Rogers, Shorten et al. 2008a). Specifically, instead of controlling individual trajectories of attractors, the idea is to take advantage of the probabilistic description of the chaotic dynamics to control the invariant probability density function which represents the desired long term statistical behaviour.

It can be clearly seen that, compared with the schemes of controlling individual orbits, controlling probability density function can avoid continuous local optimisation for each orbit but can cover all the individual orbits (Boyarsky & Góra 1997). All the existing approaches of controlling probability density function of chaotic systems work by modifying the original transformation to achieve the desired invariant density function. The main limitation of these methods is that in practice the transformation which describes the evolution of the system cannot be modified arbitrarily to achieve the desired invariant density.

Moreover, the existing methods for controlling invariant density function have not considered the effect of stochastic perturbations. Since all practical systems are subjected to stochastic perturbations it is important to devise control schemes that take into account the effect of such perturbations on the long term evolution of the system.

Some other research in (Wang, Baki et al. 2001, Wang & Zhang 2001, Wang 2002, Forbes, Forbes et al. 2003b, Wang 2003, Forbes, Forbes et al. 2004) presented ideas of controlling shape of probability density functions of stochastic nonlinear processes through selecting optimal deterministic control input.

This thesis introduces alternative strategies of controlling the invariant density function of a chaotic dynamical system subjected to an additive input and stochastic noise.

1.2 Research objectives and strategies

The main aims of this thesis are to develop new methodologies for inferring chaotic maps based on sequences of probability density functions, to develop new strategies for controlling the invariant density functions of stochastically perturbed chaotic

maps and to apply the developed methods to characterise heterogeneous human embryonic stem cell population.

The aims and objectives of this work can be summarised as following:

- *Modelling one-dimensional chaotic systems from sequences of probability density functions*

The aim is to develop new methods for solving the inverse Frobenius-Perron problem, that is, to infer an unknown chaotic map based on sequences of density functions estimated from data such that the resulting map exhibits the same transient as well as asymptotic dynamics as the underlying system that generated the data. The proposed methodology involves the identification of the Markov partition, estimation of the Frobenius-Perron matrix and the reconstruction of the underlying map that generated the data.

- *Modelling the dynamical evolution of heterogeneous human embryonic stem cell populations*

The aim is to apply the new methods for solving the inverse Frobenius-Perron problem to infer models that describe the evolution of subpopulations of NTERA2 cells, stained for the SSEA3 cell surface marker, over a number of days. The inferred dynamical model can then be used to predict the evolution of stem cell populations and to determine the equilibrium points which correspond to potential cellular substates that could be subsequently tested.

- *Modelling of chaotic dynamical systems subjected to stochastic perturbations from sequences of probability density functions*

The aim is to develop new methods for inferring the chaotic maps based on sequences of probability density functions generated by the underlying system perturbed by additive stochastic perturbation. Two cases of bounded perturbed systems are to be studied: a chaotic system subjected to an additive bounded input; a chaotic system subjected to an additive random noise, given the probability density function of input or noise. The evolution of probability densities will be

formulated. A matrix based approach is proposed to recover an approximate Frobenius-Perron matrix associated with the chaotic map.

- *Control of invariant density functions for stochastic dynamical systems*

The aim is to derive new strategies for controlling the invariant density function of a chaotic map subjected to an additive bounded input and noise. The objective is to determine the input density function so as to make the invariant density function of the system as close as possible to a targeted distribution function. The control algorithm is derived based on the asymptotic stability of the system by exploiting the relationship between the invariant density function and the input density function.

1.3 Overview of the thesis

This thesis consists of eight chapters. Chapter 2 introduces the fundamental concepts of the Frobenius-Perron operator and Foias operator, and reviews on the modelling and control problems. Chapter 3 to 7 are dedicated to development of the new techniques of modelling and control, as well as the related application in stem cell biology. Finally in Chapter 8, results in previous chapters are briefly summarised and discussion on further studies is presented. A more detailed summary of Chapters 2-8 is as follows.

Chapter 2 compares chaotic systems with stochastic systems, and introduces the Frobenius-Perron operator associated with a one-dimensional piecewise monotonic and expanding transformation, which describes the evolution of probability densities under the operation of the transformation. This chapter provides a comprehensive literature review concerning the inverse Frobenius-Perron problem and introduces the Foias operator with respect to stochastic dynamical systems. The literature review on the inverse Foias problem and on controlling the probability density functions is also presented.

Chapter 3 introduces two special classes of piecewise monotonic transformation, namely Markov and semi-Markov transformations, the explicit derivation of the associated Frobenius-Perron operator and the invariant density functions for these

transformations. The generalised inverse Frobenius-Perron problem is presented in this chapter and a new methodology for solving it for piecewise-linear semi-Markov transformations is proposed. The effectiveness of the proposed approach is demonstrated by numerical simulation examples of a noise-free system as well as in the presence of additive Gaussian white noise of different magnitudes.

In Chapter 4, the developed approach to reconstructing piecewise linear semi-Markov transformations from sequences of densities is extended to more general nonlinear maps. Numerical examples of noise-free as well as noise perturbed system are provided to demonstrate the performance of the proposed algorithms.

Chapter 5 focuses on applying the developed modelling techniques to characterising the dynamic evolution of heterogeneous cell populations based on a sequence of flow cytometric distributions of cell surface markers. The reconstructed model is used to identify potential cellular substates and to characterize their stability properties.

Chapter 6 introduces new approaches to modelling for one-dimensional dynamical systems subjected to additive random inputs or noise given their probability density functions. The Foias operator associated with the perturbed systems, which describes explicitly the evolution of the density functions, is derived explicitly.

Chapter 7 introduces a new strategy for controlling the invariant densities of stochastic dynamical systems. The existence of invariant density functions is analysed first then, using the newly developed modelling methods, a model of the chaotic dynamical system subjected to an additive input and random noise is derived based on from sequences of probability density functions. The model, which relates the invariant density function to the input density function, is used as a basis for deriving the controller design algorithm.

Chapter 8 summarises the main contributions of this thesis provides an overview of potential further work to be carried out.

1.4 Publications arising from the thesis

Some publications arising from the thesis are as follows

- X. Nie, D. Coca, A new approach to solving the inverse Frobenius-Perron problem, The 12th European Control Conference, Zurich, Switzerland, 17-19 July 2013, 2916-2920.
- X. Nie, D. Coca, Reconstruction of one-dimensional chaotic maps based on sequences of probability density functions, Nonlinear Dynamics, 2015, 80(3): 1373-1390. DIO: 10.1007/s11071-015-1949-9.
- X. Nie, D. Coca, Modelling of one-dimensional chaotic systems subjected to additive stochastic noise from sequences of probability density functions, *to be submitted*.
- X. Nie, D. Coca, Modelling of one-dimensional stochastic chaotic systems from sequences of probability density functions, *to be submitted*.
- X. Nie, D. Coca, Control of invariant density functions of stochastic chaotic systems, *to be submitted*.

Chapter 2

Literature Review

2.1 Introduction

The chapter provides a review of the relevant research literature on the identification and control law design approaches presented in this thesis.

This chapter is organised as follows: Section 2.2 gives the definition of chaotic systems and the difference with stochastic systems. Section 2.3 introduces the Frobenius-Perron operator which plays an important role throughout the work, and gives the literature review of studies on inverse Frobenius-Perron problem. In Section 2.4 a new operator defined as Foias operator is introduced for the dynamical systems with stochastic perturbations, and the inverse Foias Problem is reviewed. The literature review of research on control of probability density function is provided in Section 2.5. The summary is presented in Section 2.6.

2.2 Chaotic systems

In contrast with stochastic systems in which future states are not determined from the previous ones, chaotic systems are deterministic. Chaotic systems are dynamcial systems that are highly sensitive to initial conditions. It means even small initial conditions can results in very diverging states, which makes long term predictions generally impossible. This phenomena is also called deterministic chaos. Although such displayed dynamical behaviour looks random, the future states of chaotic systems are fully determined by mathematical formulas and the initial conditions without stochastic perturbation involved, but not predictable due to the nature of

high sensitivity to initial conditions. Chaotic systems exist in many practical fields including biology (Gleick 2008), meterology (Lorenz 1995), chemistry (Srivastava, Srivastava et al. 2013), economics (Medio & Gallo 1995), mechanical devices (Holmes & Moon 1983), celestial mechanics (Laskar 1989, Laskar 1994), etc. Particularly, there are many systems that can be described by one-dimensional chaotic maps, for example, congestion control of communication networks (Rogers, Shorten et al. 2008a), olfactory systems (Lozowski, Lysetskiy et al. 2004), electrical circuits (van Wyk & Ding 2002), packet traffic (Mondragó C. 1999), etc.

2.3 Inverse Frobenius-Perron problem

2.3.1 The Frobenius-Perron operator

Let $I=[a,b]\subset\mathbb{R}$ be a bounded interval of the real line. Let $S:I\to I$ be a one-dimensional non-singular, piecewise monotonic transformation. It is assumed that the interval is partitioned as $a=a_0<a_1<\ldots<a_N=b$, and that $S\big|_{(a_{i-1},\,a_i)}\in\mathbb{C}^r$ for $i=1,2,\ldots,N$, $r\geq 1$, where $\mathbb{C}^r$ denotes the space of all *r*-times continuously differentiable real functions. If $|S'(x)|>1$ wherever the derivative exists, *S* is called expanding. An example of this class of transformations is illustrated in Figure 2.1.

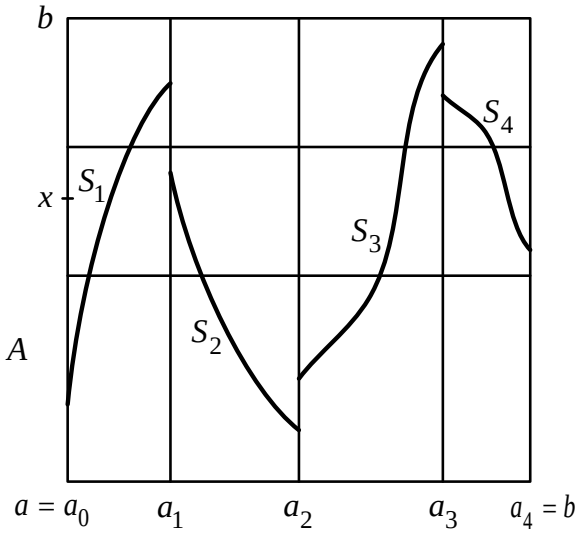

Figure 2.1 An example of one-dimensional piecewise monotonic transformation.

Let $X_n = \{x_n^1, x_n^2, \ldots, x_n^\theta\}$ be a set of θ states at time *n*. Through iterating the transformation with X_n , a set of θ new states can be yielded as $X_{n+1} = \{x_{n+1}^1, x_{n+1}^2, \ldots, x_{n+1}^\theta\}$, where $x_{n+1}^i = S(x_n^i)$ for $1 \le i \le \theta$. Let $f_n \in L^1$ denotes the probability density function of X_n, then the probability of the points falling into an arbitrary measurable set $A \subset I$ is given by

$$\int_A f_n(x)\, dx \cong \frac{1}{\theta}\sum_{i=1}^{\theta} \chi_A(x_n^i), \tag{2.1}$$

where *x* is normalised Lebesgue measure (Boyarsky & Góra 1997) on *I*, $\chi_A(x)$ is the characteristic function for the set *A*, defined by

$$\chi_A(x) = \begin{cases} 1, & \text{if } x \in A; \\ 0, & \text{if } x \notin A. \end{cases}, \tag{2.2}$$

Likewise, the probability density function of set X_{n+1} is denoted by f_{n+1}. It can be given that

$$\int_A f_{n+1}(d)\, dx \cong \frac{1}{\theta}\sum_{i=1}^{\theta} \chi_A(x_{n+1}^i). \tag{2.3}$$

Since *S* is non-singular, $x_{n+1}^i \in A$ if and only if $x_n^i \in S^{-1}(A)$. Then the following relationship is held

$$\chi_A(x_{n+1}^i) = \chi_{S^{-1}(x)}(x_n^i). \tag{2.4}$$

From (2.3) and (2.4), it can be obtained that

$$\int_A f_{n+1}(x)\, dx \cong \frac{1}{\theta}\sum_{i=1}^{\theta} \chi_{S^{-1}(A)}(x_n^i). \tag{2.5}$$

By contrasting (2.1) and (2.5), it can be seen that

$$\int_A f_{n+1}(x)\, dx = \int_{S^{-1}(A)} f_n(x)\, dx. \tag{2.6}$$

(2.6) reveals an integral equation relationship between f_{n+1} and f_n . If let $A = [a, x]$, it can be wrote as

$$\int_a^x f_{n+1}(x)\,dx = \int_{S^{-1}([a,\,x])} f_n(x)\,dx\,. \tag{2.7}$$

By differentiating both sides of (2.7) with respect to *x*, the following expression is obtained

$$f_{n+1}(x) = \frac{d}{dx}\int_{S^{-1}([a,\,x])} f_n(x)dx\,, \tag{2.8}$$

To show the transforming of the density functions, an operator is defined by $P_S f_n = f_{n+1}$, then (2.8) can be written in the following general form

$$P_S f = \frac{d}{dx}\int_{S^{-1}([a,\,x])} f(x)\,dx\,. \tag{2.9}$$

The Frobenius-Perron operator is defined as follows (Lasota & Mackey 1994).

Definition 2.1 If $S : I \to I$ is a non-singular transformation, the unique operator $P_S : L^1 \to L^1$ defined by (2.9) is referred to as the Frobenius-Perron operator associated with *S*.

Let $B_i = S((a_{i-1}, a_i))$ denotes the image of each interval (a_{i-1}, a_i) under transformation *S*. Let the inverse function for B_i be denoted by $\tau_i = S^{-1}\big|_{B_i}$.

Because *S* is piecewise on the intervals, $S^{-1}(A)$ is allowed to have multiple branches, and is made up of a union of disjointed intervals, written as

$$S^{-1}(A) = \bigcup_{i=1}^{k} \tau_i(A \cap B_i)\,. \tag{2.10}$$

By substituting (2.10) into (2.9) we obtain that

$$\begin{aligned} P_S f(x) &= \frac{d}{dx}\int_{S^{-1}(A)} f(x)\,dx = \frac{d}{dx}\int_{\bigcup_{i=1}^{k}\tau_i(A\cap B_i)} f(x)\,dx \\ &= \sum_{i=1}^{k} \frac{d}{dx}\int_{\tau_i(A\cap B_i)} f(x)\,dx. \end{aligned} \tag{2.11}$$

Thus from (2.10), (2.11) can to be written as

$$P_S f(x) = \sum_{i=1}^{k} \frac{d}{dx} \int_{S^{-1}(A \cap B_i)} f(x)\, dx, \tag{2.12}$$

After differentiating, since $A = [a, x]$, and $B_i = S((a_{i-1}, a_i))$, (2.12) becomes

$$P_S f(x) = \sum_{i=1}^{k} \frac{f(S_i^{-1}(x))}{\left|S'(S_i^{-1}(x))\right|} \chi_{S((a_{i-1}, a_i))}(x), \tag{2.13}$$

where $S_i = S\big|_{(a_{i-1}, a_i)}$. This equation describes the Frobenius-Perron operator P_S associated with the class of piecewise monotonic transformations.

2.3.2 Solution to the inverse Frobenius-Perron problem

The problem of inferring a point transformation given probability density functions observed from the dynamical system is referred to as the inverse Frobenius-Perron problem (IFPP). It is aimed to make use of the probability density functions observed from a dynamical system, rather than trajectories of individual points to recover the model of the system.

The inverse problem for one-dimensional maps has been studied under the assumption that only the invariant density of the unknown dynamical system is known. Friedman and Boyarsky (1982) proposed a graph-theoretic approach to construct a piecewise linear transformations given an invariant density function belonging to a very restrictive class of piecewise constant density functions whose relative minima points are 0. Ershov and Malinetskii (1988) developed a numerical algorithm for constructing a one-dimensional unimodal transformation which has a given unique invariant density. Diakonos and Schmelcher (1996) considered the inverse problem for a class of symmetric maps that have invariant symmetric beta density functions given by

$$f^*(x) = \frac{2^{2\gamma-1} B_0(\frac{1}{2}, 1-\gamma)}{x^{\gamma}(1-x)^{\gamma}}, \tag{2.14}$$

where γ is an arbitrary real number smaller than unity, and B_0 is the beta function. For the given symmetry constraints they show that this problem has a unique solution. A generalization of this approach, which deals with a broader class of one-dimensional continuous unimodal maps for which each branch of the map covers the complete interval and assumes that the invariant density belongs to a special class of two-parametric asymmetric beta density functions

$$f^*(x) = \frac{x^\alpha (1-x)^\beta}{B(\alpha+1, \beta+1)}, \quad \alpha, \beta > -1, \tag{2.15}$$

where *B* is the beta function, was proposed in (Pingel, Schmelcher et al. 1999). Huang presented approaches to constructing smooth chaotic transformation with closed form (Huang 2006, Huang 2009b) and multi-branches complete chaotic map (Huang 2009a), given invariant densities. (Boyarsky & Góra 2008) studied the problem of modelling for a dynamical system, of which the trajectories of probability density function are reversible. Potthast and Roland (Potthast 2012) investigated solving the Frobenius-Perron equation to derive the evolution law of nonlinear dynamical automata of Turing machines. Baranovsky and Daems (1995) investigated the problem of synthesizing one-dimensional piecewise linear Markov maps with a prescribed autocorrelation function, The desired invariant density was then obtained by performing a suitable coordinate transformation. They also considered the problem of reconstructing one-dimensional chaotic maps which have a given invariant density and their trajectories are characterised by a given autocorrelation function. An alternative stochastic optimization approach was proposed by (Diakonos, Pingel et al. 1999) to address the inverse problem for the class of smooth complete unimodal maps with given combined statistical involving the invariant density and autocorrelation function. Koga (1991) introduced an analytical approach to solving the IFPP for two specific types of one-dimensional symmetric maps by deriving the formula between the difference system and the invariant density of which an analytic form was given.

Ulam (1960) hypothesised that the infinite-dimensional Frobenius-Perron operator can be approximated by a finite-dimensional Markov transformation defined over a uniform partition of the interval of interest. The conjecture was proven by Li (1976)

who also provided a rigorous numerical algorithm for constructing the finite-dimensional operator when the one-dimensional transformation *S* is known. Góra and Boyarsky (1997) introduced a matrix method for constructing a 3-band transformation such that an arbitrary given piecewise constant density is invariant under the transformation. Provided a stochastic matrix $\boldsymbol{M}$ representing the Frobenius-Perron operator is known, let $\mathfrak{R}$ be a uniform partition with *N* intervals, and the subinterval $Q_k^{(i)} = (q_k^{(i)}, q_{k-1}^{(i)})$, $i = 1, \ldots, N$, $k = 1, \ldots, p(i)$, then

$$q_k^{(i)} = a + \frac{1}{N}\left(\sum_{j=j_1}^{j_k} m_{i,j} + i - 1\right)(b-a), \tag{2.16}$$

where j_k denotes the column index of positive entry in the *i*-th row, thus, piecewise linear transformation on each subinterval can be expressed as

$$S(x)\big|_{Q_k^{(i)}} = \frac{1}{m_{i,j_k}}(x - q_k^{(i)}) + \frac{(j_k - 1)(b-a)}{N}, \tag{2.17}$$

which demonstrates the relationship between the transformation and the Frobenius-Perron matrix defined from the invariant density.

Furthermore, a technique of constructing a piecewise linear Markov map that preserves a given invariant density and has the metric entropy close to observed one was presented in (Boyarsky & Góra 2002). A direct method for constructing discrete chaotic maps with arbitrary piecewise constant invariant densities and arbitrary mixing properties, using positive matrix theory, was introduced in (Rogers, Shorten et al. 2004), which was based on the theory of positive matrices. By choosing the parameters in the Perron eigenvector of the induced Ulam transition matrix, the dominate eigenvector representing the invariant density can be fully determined. The approach has been further exploited to synthesise dynamical systems with desired characteristics i.e. Lyapunov exponent and mixing properties that share the same invariant density, and to analyse and design the communication networks based on TCP-like congestion control mechanisms (Rogers, Shorten et al. 2008a). An extension of this work to randomly switched chaotic maps is studied in (Rogers, Shorten et al. 2008b). It is also shown how the method can be extended to higher dimensions and how the approach can be used to encode images. In (Bollt

2000a) the inverse problem was treated for globally stabilising the target invariant density of a perturbed dynamical system. The open-loop IFPP was solved by finding a perturbation matrix based on the matrix approach given a stochastic matrix and invariant density. The inverse problem was reduced into a constrained optimisation problem that was solved in L^2. In view of usefulness of the obtained solution, an L^∞ algorithm based on linear programming was presented in (Bollt 2000b) to solve the optimisation.

In addition, the problem has been investigated in numerous practical applications. An optimisation approach to finding the elements of the Frobenius-Perron matrix, offering a way to characterize the patterns of activity in the olfactory bulb, based on the invariant density functions of interspike intervals, was also proposed in (Lozowski, Lysetskiy et al. 2004). Setti, Mazzini et al. (2002) investigated the Markov approach to constructing piecewise-affine Markov maps with application to two signal processing issues: generation of low-EMI timing signals and performance optimisation for DS-CDMA systems. The algorithms were generalised to the case of piecewise-affine Markov maps with infinite number of Markov intervals in (Rovatti, Mazzini et al. 2002). Mondragó C. (1999) considered the problem of modelling for packet traffic in computer networks by introducing the random wall map and taking advantage of the fact that the invariant density of this map could be easily approximated analytically.

2.4 Inverse Foias problem

2.4.1 Foias operator

In this section, a more general dynamical system that involves random perturbations is considered and the derivation of the formula linking the probability density functions with the potential transformation is reviewed.

The general form of the dynamical system with stochastic perturbations is represented as follows

$$x_{n+1} = H(x_n, \omega_n), \quad \text{for } n = 0, 1, 2, \ldots, \tag{2.18}$$

where H is the transformation of the perturbed dynamical system, x_n is the state variable defined on Borel measurable $I \subset \mathbb{R}$, ω_n is the independent random variable, $\omega_n \in I_\omega \subset \mathbb{R}$. For every fixed ω, the function $H(x_n, \omega_n)$ is continuous in x, and for every fixed x it is measurable in ω. The probability density function of ω_n is denoted by g. the random numbers x_0, $\omega_0, \omega_1, \omega_2, \ldots$ are independent with each other.

Assume a bounded measurable function $G : I \to I$. The mathematical expectation of $G(x_{n+1})$ is given by

$$E(G(x_{n+1})) = \int_I G(x_{n+1}) f(x_{n+1})\, dx, \tag{2.19}$$

Let $f_n(x)$ denote the probability density function of x_n, thus $f_{n+1}(x) = f(x_{n+1})$. (2.19) can be expressed as

$$E(G(x_{n+1})) = \int_I G(x) f_{n+1}(x)\, dx. \tag{2.20}$$

By submitting (2.18) into the right side of (2.19), the expectation can be written as

$$\begin{aligned} E(G(x_{n+1})) &= E(G(H(x_n, \omega_n)) \\ &= \int_I \int_{I_\omega} G(H(x, \omega)) f_n(x) g(\omega)\, dx d\omega. \end{aligned} \tag{2.21}$$

Let $y = H(x, \omega)$, then $\omega = H^{-1}(y \mid x)$. (2.21) can be written as

$$\begin{aligned} E(G(x_{n+1})) &= \int_I \int_I G(y) f_n(x) g(H^{-1}(y \mid x))\, dx d(H^{-1}(y \mid x)) \\ &= \int_I \int_I \frac{1}{H'(H^{-1}(y \mid x))} G(y) f_n(x) g(H^{-1}(y \mid x))\, dx dy. \end{aligned} \tag{2.22}$$

Equating (2.19) and (2.22), we can obtain the following formula

$$f_{n+1}(x) = \int_I \frac{1}{H'(H^{-1}(x \mid y))} f_n(y) g(H^{-1}(x \mid y))\, dy\,. \tag{2.23}$$

It follows that the Foias operator associated with the stochastic dynamical system is defined as follows

Definition 2.2 if $H : I \times I_\omega \to I$ is a non-singular function, then the operator $Q_H : I \to I$ defined by

$$Q f_n(x) = \int_I \frac{1}{H'(H^{-1}(x \mid y))} f_n(y) g(H^{-1}(x \mid y))\, dy\,, \tag{2.24}$$

is called the Foias operator (Lasota & Mackey 1994) corresponding to the dynamical system described in (2.18).

It can be seen from (2.24) that the Foias operator is a Markov operator (Boyarsky & Góra 1997). Given an initial density function f_0, the evolution of probability densities can be denoted by $f_{n+1} = Q_H^n f_0$. The invariant density of the stochastic dynamical system is defined as follows

Definition 2.3 For a Foias operator Q_H with respect to the dynamical system (2.18), if $Q_H f^* = f^*$, the density f^* is called invariant or stationary density preserved by the dynamical system.

The theorem below about the existence of a invariant density for a regular dynamical system was proved in (Lasota & Mackey 1994).

Theorem 2.1 *Let Q_H be the Foias operator corresponding to a regular dynamical system (2.18). Assume that there is a $f_0 \in L^1$ having the following property. For every $\varepsilon > 0$ there is a bounded set $B \in \mathfrak{B}(I)$ such that*

$$f_n(B) = Q_H^n f_0(B) \geq 1 - \varepsilon, \quad \text{for } n = 0, 1, 2, \ldots, \tag{2.25}$$

then Q_H has an invariant density.

2.4.2 Solution to the inverse Foias problem

Practical dynamical systems are usually subjected to random perturbations. Assuming that the probability density function of the perturbation is known, the problem of reconstructing the deterministic transformation based on a sequence of probability density functions generated by the stochastic dynamical system (2.18) is called inverse Foias problem.

In the literature, there are only few solutions to the inverse Foias problem. Most research studies focus on the invariant measure of the stochastically perturbed dynamical systems. Kuske and Papanicolaou (1998) considered a chaotic dynamical system with small noise and developed a method to approximate the invariant density. Ostruszka & Życzkowski (2001) addressed the problem of approximating the spectrum and eigenvectors of the Frobenius-Perron operator associated with a discrete dynamical system with an additive, small amplitude stochastic perturbation. Islam and Góra (2011) also considered a dynamical system that is stochastically perturbed by an additive noise and employed Fourier approximation to obtain an approximation to the Frobenius-Perron operator. In (Bollt, Góra et al. 2008) an algorithm was introduced approximate the stochastic transition matrix of a finite size N to represent the Frobenius-Perron operator for a dynamical system with small additive noise.it was concluded that when the size $N \to \infty$ the sequence of the invariant densities of the perturbed systems converges to the invariant density of the deterministic system.

2.5 Controlling the invariant density function

It is well-known that many practical deterministic systems are subjected to stochastic disturbances. Stochastic control has been widely studied for many years. The mean and variance of the systems' outputs have been usually regarded as the control objectives (Åström 1970, Goodwin & Sin 1984, Åström & Wittenmark 1989, Papoulis 1991, Lu & Skelton 1998, Iourtchenko 2000, Wojtkiewicz & Bergman 2001). This is generally applied to the systems that are subjected to Gaussian perturbations. But for the systems that are subjected to non-Gaussian

perturbations, it becomes quite limited to continue targeting the two quantities as these do not characterise in full the probability density function associated with the systems' outputs. The general objective of this class of control problems is to find the optimal input so as to attain a desired target output probability density function, or to make the shape of the output probability density function as close as possible to a given distribution.

Over the past decades, a few control algorithms were developed to control the output probability density function of a dynamical system. Kárný (1996) proposed a randomised controller aimed to find the optimal probability density function generated by the controller by means of minimising the distance between closed-loop probability density function and the desired distribution function. The distance is measured by Kullback-Leibler divergence. The closed-loop probability density function is calculated by directly multiplying the probability density function of the stochastic system and that of the controller. The solution was generalised and extended for stochastic state-space models by solving the fully probabilistic control design in (Kárný & Guy 2006).

For general nonlinear stochastic systems, there is no easy way of analytic methods to formulate the mathematical relationships between the output probability density functions and the control inputs due to the nonlinearity of both the systems and densities. Wang (1999b, 1999c, 2000, 2001, 2002) introduced a B-spline function based model in which the output probability density functions can be expanded as a linear combination of the basis functions, thus by relating the control input to the weights, the system dynamics is converted into a formula linking the weights of output probability density function to the control input. As a result, based on this model, the controller is designed to select a deterministic input to make the output density function as close as possible to a targeted one. The algorithm was applied to the papermaking systems for controlling the density distribution of paper web (Wang, Baki et al. 2001), pseudo-ARMAX stochastic systems for bounded control of the output distribution in (Wang & Zhang 2001), general nonlinear dynamical systems subjected to non-Gaussian to control the conditional output probability density function (Wang 2003), and singular stochastic dynamical systems for shaping the output density function (Yue, Leprand et al. 2005). Based on the linear

B-spline model, pseudo PID controllers were developed for general non-Gaussian stochastic systems in (Guo & Wang 2003, Guo & Wang 2005b), moreover, there are some other new techniques proposed to extend the control strategy to Lyapunov based control algorithm (Wang, Kabore et al. 2001), control of output probability density function of NARMAX stochastic systems with non-Gaussian noise (Guo, Wang et al. 2008), a generalised PI control (Guo & Wang 2005a), constrained PI tracking control using two-step neural networks (Yang, Lei et al. 2009), predictive probability density function control for molecular weight distributions in industrial polymerisation processes (Yue, Zhang et al. 2004), multi-step predictive control (Wang, Zhang et al. 2005a), and iterative learning control (Wang, Zhang et al. 2005b, Hong & Afshar 2006, Wang, Afshar et al. 2008).

Crespo and Sun (2002, 2003) proposed a discontinuous nonlinear feedback law to achieve a target stationary probability density function of a one-dimensional stochastic continuous-time systems that is described by an Itô differential equation. But this noise involved in the equation is restricted to Gaussian noise. Pigeon, Perrier et al. (2011) considered a switching linear controller for shaping the output probability density function. Besides, a feedback control law using Gram-Charlier function to approximate the stationary probability density was developed for a first-order and discrete-time nonlinear system with Gaussian noise in (Forbes, Guay et al. 2002, Forbes, Forbes et al. 2003a, Forbes, Forbes et al. 2003b, Forbes, Forbes et al. 2004, Forbes, Guay et al. 2004b, Forbes, Forbes et al. 2006). Moreover, in (Zhu & Zhu 2011), targeting a given stationary probability density function, a feedback control of multi-degree-of-freedom nonlinear stochastic systems was investigated, based on a technique of obtaining five classes of exact stationary solutions of dissipated multi-degree-of-freedom system. Another approach proposed by the same authors (2012) uses Fokker-Planck-Kolmogorov equation to target a given stationary probability density function of nonlinear systems subjected to Poisson white noise.

Some researchers focused on the control of invariant density of chaotic dynamical systems without noise. For a given one-dimensional point transformation S which admits an absolutely continuous invariant density, Góra and Boyarsky (1996)

proposed a method of slightly modifying S to achieve a desired invariant density. The modified transformation is approximated by a piecewise linear and expanding transformation even though the original map is nonlinear or nonexpanding on the defined partition. Another analytic method was introduced in (Góra & Boyarsky 1998) to attain a desired invariant density which is allowed to have 0 on some targeted partition. Bollt (2000a, 2000b) considered the control problem that, given a point transformation S which preserves an invariant density function f^*, the aim is to construct a nearby transformation $S + \Delta S$ whose invariant density is or close to be a desired one $f^* + \Delta f$. The optimisation algorithm for finding ΔS was improved in (Góra & Boyarsky 2001). In (Rogers, Shorten et al. 2008a), a synthesis approach based on the matrix method was developed for controlling the invariant densities of chaotic maps.

2.6 Summary

This chapter introduced the Frobenius-Perron operator, the main tool that is used to study the evolution of probability density functions under the action of a chaotic transformation, and the inverse Frobenius-Perron problem, moreover, provided an overview of the existing solutions, a major limitation of which is the fact that they cannot guarantee uniqueness of the estimated map. As a result the reconstructed map in general cannot predict the underlying dynamical behaviour. The extended inverse Foias problem which takes into account the effect of stochastic perturbations was discussed.

Finally, the chapter introduced the problem of controlling the probability density function and provided an overview of the relevant literature.

Chapter 3

Reconstruction of Piecewise Linear semi-Markov Maps from Sequences of Probability Density Functions

3.1 Introduction

One-dimensional deterministic maps can display chaotic behaviour. Chaotic maps, capable of generating density of states, can be used to model a multitude of chaotic processes encountered in engineering, biology, physics and economics (Ott 1993). Example applications include modelling particle formation in emulsion polymerization (Coen, Gilbert et al. 1998), papermaking systems (Wang, Baki et al. 2001), synchronized communication networks (Rogers, Shorten et al. 2004), cellular uplink load in WCDMA systems (Wigren 2009), etc.

Instead of studying the evolution of individual point trajectories, it is often more convenient to observe experimentally the evolution of the probability density functions generated by such systems. A major challenge is that of inferring the chaotic map which describes the evolution of the unknown chaotic system, solely based on experimental observations. While solutions exist for the case when observations of individual point trajectories are available, currently no method is available to uniquely recover the chaotic map given only sequences of density functions derived from experimental observations. As reviewed in the previous chapter, this problem known as the Inverse Frobenius-Perron Problem (IFPP), has been investigated by a number of researchers in the case when the only information

available is the invariant density function associated with the unknown map. Although all existing methods can be used to construct a map with a given invariant density, the uniqueness of the solution can be guaranteed only under very restrictive conditions. In other words, whilst the identified transformation may have the same invariant density, it will not exhibit the same dynamics as the underlying system of interest. In general, the reconstructed maps will not resemble the actual transformation that generated the data and therefore these maps cannot predict the dynamical properties of the underlying system (Lyapunov exponents, fixed points etc.) or predict its evolution, which is of paramount importance in many practical applications. Moreover, the matrix-based algorithms proposed so far assume that the Markov partition is known *a priori* but in practice this is rarely the case.

This chapter proposes for the first time a systematic method for determining an unknown piecewise linear semi-Markov map given sequences of density functions estimated from data. In other words, the inverse problem studied in this work is that of determining the map that exhibits the same transient as well as asymptotic dynamics as the underlying system that generated the data. To avoid confusion, this is called the generalised inverse Frobenius-Perron problem (GIFPP).

This chapter is organized as follows: Section 3.2 introduces some relevant preliminary fundamental theoretical concepts and results including the evolution of probability densities for point transformations and the existence of absolutely continuous invariant measure described in Section 3.2.1, a special class of piecewise monotonic transformation called Markov transformation and its some important properties in terms of invariant density introduced in Section 3.2.2, and a much more general class of piecewise linear transformations, semi-Markov transformation introduced in Section 3.2.3, where the matrix form of associated Frobenius-Perron equation, properties with respect to the invariant density are also presented. Formulation of the GIFPP was given in section 3.3. The new methodology for solving the GIFPP for piecewise-linear semi-Markov transformations is presented in Section 3.4. Numerical simulation examples of a noise-free system and the same system perturbed by an additive white Gaussian noise of different magnitudes are given in Section 3.5. Conclusions are presented in Section 3.6.

3.2 Preliminaries

3.2.1 Evolution of probability densities

The Frobenius-Perron operator associated with a transformation *S* maps an initial probability density function to its transformed probability density function by the action of *S*. Instead of studying the orbits of individual points of the dynamical systems, it allows us to take advantage of flow of densities to uncover the dynamical behaviour. The Frobenius-Perron operator P_S becomes a useful tool to study the evolution of probability densities.

Let the initial density be denoted by f_0, then the evolution of the probability density functions can be represented by $\{f, P_S f, P_S^2 f, \ldots, P_S^n f\}$. P_S is a bounded linear operator on L^1 (Boyarsky & Góra 1997), thus it is a convenient way to study the asymptotic probabilistic behaviour of the dynamical systems with P_S, and a mathematical relationship between the dynamics and the transformation *S* of underlying system can be revealed from the Frobenius-Perron equation.

The existence of absolutely continuous invariant measure for some examples of transformations was found by (Ulam & von Neumann 1947), and a defined class of transformations was firstly proven by (Rényi 1957). The results were generalised by (Lasota & Yorke 1973) who proved, by means of the theory of bounded variation, that the Frobenius-Perron operator associated with the class of piecewise expanding transformations was contractive. It was further extended to be a general theorem for bounded intervals (Jabłoński, Góra et al. 1996). The following theorem proves the existence of an absolutely continuous invariant measure for a piecewise expanding transformation (Boyarsky & Góra 1997):

Theorem 3.1 *The transformation $S: I \to I$ admits an absolutely continuous invariant measure whose density is of bounded variation, if S satisfies the following conditions:*

i) *S is piecewise expanding, i.e., there exists a partition* $\Re = \{R_i = (a_{i-1}, a_i)\}_{i=1,N}$ *of I such that* $S|_{R_i} \in \mathbb{C}^1$, *and* $S_i'(x) \geq \alpha > 1$ *for* $x \in (\alpha_{i-1}, \alpha_i), i = 1, \ldots, N$;

ii) $\frac{1}{S'(x)}$ *is of bounded variation, where* $S'(x)$ *is the appropriate one-sided derivative at the endpoints of* $\Re$.

The Frobenius-Perron operator for the non-singular transformation *S* is a Markov operator (Boyarsky & Góra 1997), which is defined as follows

Definition 3.1 A linear operator $P_S : L^1 \to L^1$ satisfying

(a) $P_S f_n \geq 0$ for $f_n \geq 0$, $f_n \in L^1$;

(b) $\|P_S\|_{L^1} < 1$, and $\|P_S f_n\|_{L^1} = \|f_n\|_{L^1}$, for $f_n \geq 0$, $f_n \in L^1$,

is called a Markov operator.

The strong constrictiveness of a Markov operator is defined as follows

Definition 3.2 A Markov operator $P_S : L^1 \to L^1$ is called strongly constrictive if there exists a compact set $\mathcal{F} \subset L^1$ such that for any $f \in D = \{f \in L^1 : f \geq 0, \|f\|_{L^1} = 1\}$, $\lim_{n\to\infty} \operatorname{dist}(P^n f, \mathcal{F}) = 0$, where $\operatorname{dist}(P^n f, \mathcal{F}) = \inf_{f\in\mathcal{F}} \|f - P^n f\|_{L^1}$.

The density of the invariant measure for the transformation can also be discussed from the perspective of spectral decomposition of the Frobenius-Perron operator associated with the transformation. If P_S is strongly constrictive, according to the spectral decomposition theorem (Boyarsky & Góra 1997), there exists a sequence of densities $f_1, \ldots, f_r$ and a sequence of bounded linear functionals $g_1, \ldots, g_r$ such that

$$\lim_{n\to\infty} \left\| P_s^n \left(f - \sum_{i=1}^{r} g_i(f) f_i \right) \right\|_{L^1} = 0 \text{, for any } f \in L^1. \tag{3.1}$$

where P_S^n is the *n*-th iteration of *P*, the densities $f_1,\ldots, f_r$ have mutually disjoint supports ($f_i f_j = 0$ for $i \neq j$), and $P_S f_i = f_{\alpha(i)}$, where $i = 1,\ldots,r$, and $\{\alpha(1),\ldots,\alpha(r)\}$ is a permutation of the integers $\{1,\ldots,r\}$.

Every constrictive Markov operator admits a stationary density (Lasota & Mackey 1994). Let f^* denote the invariant density of the transformation *S*. From (3.1) it follows that, $P_S^n f$ converges to an invariant density f^*which satisfies $f^* = P_S f^*$. The invariant measure on *A* is denoted by $\mu(A) = \int_A f^*(x)\,dx$, then $\mu(A) = \int_A P_S f^*(x)\,dx = \int_{S^{-1}(A)} f^*(x)\,dx$, therefore, $\mu(S^{-1}(A)) = \mu(A)$. f^* is called the fixed point of the associated Frobenius-Perron operator P_S.

3.2.2 Markov transformation

The focus of this research is on a special class of piecewise monotonic transformation that is defined as follows

Definition 3.3 Let $\Re = [R_1, R_2, \ldots, R_N]$ be a partition of *I* into *N* intervals, and $\text{int}(R_i) \bigcap \text{int}(R_j) = \varnothing$ if $i \neq j$. A transformation $S : I \to I$ is said to be Markov with respect to the partition $\Re$ (or $\Re$-Markov) if *S* is monotonic on every interval R_i and $S(R_i)$ is a connected union of intervals of $\Re$ for $i = 1, 2,\ldots, N$. The partition $\Re$ is called a Markov partition with respect to *S*.

If S_i on R_i is linear, *S* is referred to as a piecewise linear Markov transformation. The Frobenius-Perron operator associated with this class of transformations can be represented by a matrix that is of the form $\boldsymbol{M} = (m_{i,j})_{1\le i,j\le N}$, where

$$m_{i,j} = \begin{cases} |S_i'|^{-1}, & \text{if } R_j \subset S(R_i); \\ 0, & \text{otherwise.} \end{cases} \tag{3.2}$$

Let $\mathfrak{F}$ be the class of the functions that are piecewise constant on the partition $\mathfrak{R}$. For a step function $f(x) \in \mathfrak{F}$,

$$f(x) = \sum_{i=1}^{N} h_i \chi_{R_i}(x), \tag{3.3}$$

where $\chi_{R_i}(x)$ is the indicator function defined as

$$\chi_{R_i}(x) = \begin{cases} 1, & \text{if } x \in R_i; \\ 0, & \text{if } x \notin R_i. \end{cases} \tag{3.4}$$

and h_i are the expansion coefficients. $f(x)$ can also be represented in the form of a row vector $\boldsymbol{h}^f = [h_1^f, h_2^f, \ldots, h_N^f]$. The relationship between the probability density functions and the matrix represented Frobenius-Perron operator can be derived as follows (Boyarsky & Góra 1997)

$$\boldsymbol{h}^{P_S f} = \boldsymbol{h}^f \boldsymbol{M}, \tag{3.5}$$

where $\boldsymbol{h}^{P_S f} = [h_1^{P_S f}, h_2^{P_S f}, \ldots, h_N^{P_S f}]$ is the vector form of density $P_S f$.

The following theorem with regard to the eigenvalue of maximum modulus is given in (Friedman & Boyarsky 1981)

Theorem 3.2 *Let $S : I \to I$ be a piecewise linear Markov transformation, and **M** be the induced Frobenius-Perron matrix. Then **M** has 1 as the eigenvalue of maximum modulus. If **M** is also irreducible, then the algebraic and geometric multiplicity of the eigenvalue is also 1.*

This implies that there always exists a piecewise constant invariant density under *S*. The existence of invariant density for expanding transformation was further proven by (Boyarsky & Góra 1997), which is stated as follows

Theorem 3.3 *Let S be a piecewise linear Markov transformation, and the absolute value of the slope of S is greater than 1, then any S-invariant density function f^* is piecewise constant on the partition $\mathfrak{R}$.*

Thus, expanding piecewise linear Markov transformations have piecewise constant invariant densities. This theorem was further generalised for some case when the transformation cannot satisfy the expanding condition that $|S_i'|>1$. If the derivative after *k* iterations is greater than 1, $|(S^k)'|$ can be equivalently regarded as $|S'|$, then the following theorem (Boyarsky & Góra 1997) can be obtained

Theorem 3.4 *Let S be a piecewise linear Markov transformation, as long as there exist some* $k \geq 1$ *such that* $|(S^k)'(x)|>1$, *S admits an invariant density function which is piecewise constant on the partition* $\mathfrak{R}$.

For a partition $\mathfrak{R}$ comprised of *N* equal sized intervals $R_1, R_2, \ldots, R_N$, Lebesgue measure on each interval R_i is denoted by $\lambda(R_i)=1/N$. The definition of the stochastic matrix with respect to $\mathfrak{R}$ representing the Frobenius-Perron operator can be simplified as

$$m_{i,j}=\frac{\lambda(R_i \cap S^{-1}(R_j))}{\lambda(R_i)}, \tag{3.6}$$

which define the fraction of interval R_i which is mapped into interval R_j by *S*. This matrix was applied to the so-called Ulam method by (Ulam 1960) for approximating the Frobenius-Perron operator. Entry $m_{i,j}$ denotes the transition probability of moving from interval R_i to interval R_j. The stochastic matrix can be approximated using a set of finite individual orbits $\{x_k\}$ in the following alternative way to (3.6)

$$m_{i,j} \cong \frac{\sum_k (\chi_{R_i}(x_k)\cdot \chi_{R_j}(S(x_k)))}{\sum_k \chi_{R_i}(x_k)}, \tag{3.7}$$

The resulting matrix ***M*** satisfies the following equality

$$\sum_{j=1}^{N} m_{i,j} = 1, \text{ for } i = 1, 2, \ldots, N. \tag{3.8}$$

This means that the total sum of the transition probability of given states mapped from an interval to any other interval of $\mathfrak{R}$ is 1.

3.2.3 Semi-Markov transformation

A richer class of piecewise linear transformations than piecewise linear Markov transformation is introduced in this section. For a given partition $\mathfrak{R} = [R_1, R_2, \ldots, R_N]$, $\text{int}(R_i) \bigcap \text{int}(R_j) = \varnothing$ if $i \neq j$, this class of transformations is called $\mathfrak{R}$-semi-Markov transformation that is defined as follows

Definition 3.4 A transformation $S : I \to I$ is said to be semi-Markov with respect to the partition $\mathfrak{R}$ (or $\mathfrak{R}$-semi-Markov) if there exist disjoint subintervals $Q_j^{(i)}$ so that $R_i = \bigcup_{j=1}^{k(i)} Q_j^{(i)}$ for $i = 1, \ldots, N$, $S|_{Q_j^{(i)}}$ is monotonic and $S(Q_j^{(i)}) \in \mathfrak{R}$ where $S|_{Q_j^{(i)}}$ denotes the restriction of S to $Q_j^{(i)}$, and $S(Q_j^{(i)})$ denotes the image of $Q_j^{(i)}$ mapped by S.

The restriction $S|_{Q_k^{(i)}}$ is a homeomorphism from R_i to a union of intervals of $\mathfrak{R}$

$$I_i = \bigcup_{k=1}^{p(i)} R_{r(i,k)} = \bigcup_{k=1}^{p(i)} S(Q_k^{(i)}), \tag{3.9}$$

where $R_{r(i,k)} = S(Q_k^{(i)}) \in \mathfrak{R}$, $Q_k^{(i)} = [q_{k-1}^{(i)}, q_k^{(i)}]$, $i = 1, \ldots, N$, $k = 1, \ldots, p(i)$ and $p(i)$ denotes the number of disjoint subintervals $Q_k^{(i)}$ corresponding to R_i.

Piecewise linear semi-Markov transformations preserve the same important property with piecewise linear Markov transformation that the invariant density is piecewise constant on each interval of the defining partition (Boyarsky & Góra 1997).

Theorem 3.5 *if a transformation $S: I \to I$ is piecewise linear semi-Markov with respect to a partition $\mathfrak{R}$, and slope of $S|_{Q_j^{(i)}}$ is greater than 1, $j = 1, \ldots, k(i)$, $i = 1, \ldots, N$, then any S-invariant density is constant on the intervals of $\mathfrak{R}$.*

The Frobenius-Perron matrix associated with a piecewise linear semi-Markov transformation *S*, $\boldsymbol{M} = (m_{i,j})_{1 \le i,j \le N}$ is defined by as follows (Boyarsky & Góra 1997)

$$m_{i,j} = \begin{cases} \left| \left(S|_{Q_k^{(i)}} \right)' \right|^{-1}, & \text{if } S(Q_k^{(i)}) = R_j \in \mathfrak{R}; \\ 0, & \text{otherwise.} \end{cases} \tag{3.10}$$

Then the Frobenius-Perron equation can be converted into the following matrix form linking the probability density function *f* and Frobenius-Perron matrix

$$\boldsymbol{h}^{P_S f} = \boldsymbol{h}^{f} \boldsymbol{M}, \tag{3.11}$$

where $\boldsymbol{h}^{f} = [h_1^{f}, h_2^{f}, \ldots, h_N^{f}]$ and $\boldsymbol{h}^{P_S f} = [h_1^{P_S f}, h_2^{P_S f}, \ldots, h_N^{P_S f}]$ are the vector form of density functions $f \in \mathfrak{F}$ and $P_S f \in \mathfrak{F}$ respectively.

Given an arbitrary density function *f* that is constant on the intervals of $\mathfrak{R}$, there always exists a $\mathfrak{R}$-semi-Markov transformation of which *f* is the invariant density. (Boyarsky & Góra 1997) utilised a special class of transformation called 3-band transformation to illustrate the construction of a piecewise linear transformation from any density and prove the existence of such a transformation. The generalised mathematic relationship between a given invariant density and the supposed 3-band transformation is further derived based on the results in (Boyarsky & Góra 1997) as follows

Let *S* be a 3-band transformation on the partition $\mathfrak{R} = \{R_1, \ldots, R_N\}$ with Frobenius-Perron matrix $\boldsymbol{M} = (m_{i,j})_{1 \le i,j \le N}$, and $f \in \mathfrak{F}$ be an arbitrary density invariant density function of *S*. The following equations can be obtained from (3.11)

$$h_1^f \cdot m_{1,1} + h_2^f \cdot m_{2,1} = h_1^f \,, \tag{3.12}$$

for i=1; and

$$h_{i-1}^f \cdot m_{i-1,i} + h_i^f \cdot m_{i,i} + h_{i+1}^f \cdot m_{i+1,i} = h_i^f \,, \tag{3.13}$$

for $2 \le i \le N-1$; and

$$h_{N-1}^f \cdot m_{N-1,N} + h_N^f \cdot m_{N,N} = h_N^f \,, \tag{3.14}$$

for i=N.

At the same time, the following equalities should hold

$$\lambda(R_1) \cdot m_{1,1} + \lambda(R_2) \cdot m_{1,2} = \lambda(R_1) \,, \tag{3.15}$$

for i=1; and

$$\lambda(R_{i-1}) \cdot m_{i,i-1} + \lambda(R_i) \cdot m_{i,i} + \lambda(R_{i+1}) \cdot m_{i,i+1} = \lambda(R_i) \,, \tag{3.16}$$

for $2 \le i \le N-1$; and

$$\lambda(R_{N-1}) \cdot m_{N,N-1} + \lambda(R_N) \cdot m_{N,N} = \lambda(R_N) \,, \tag{3.17}$$

for i =N.

Assuming that $h_i^f > 0$, $\lambda(R_i) > 0$, it can be obtained from (3.13) and (3.16) that

$$\frac{h_{i-1}^f}{h_i^f} \cdot m_{i-1,i} + m_{i,i} + \frac{h_{i+1}^f}{h_i^f} \cdot m_{i+1,i} = 1 \,, \tag{3.18}$$

and

$$\frac{\lambda(R_{i-1})}{\lambda(R_i)} \cdot m_{i,i-1} + m_{i,i} + \frac{\lambda(R_{i+1})}{\lambda(R_i)} \cdot m_{i,i+1} = 1 \,. \tag{3.19}$$

It was proven by (Boyarsky & Góra 1997) that

$$m_{i,i-1} \cdot h_i^f = m_{i-1,i} \cdot h_{i-1}^f \,. \tag{3.20}$$

Then it follows from (3.18) and (3.19) that

$$\frac{h_{i+1}^f}{h_i^f} \cdot m_{i+1,i} = \frac{\lambda(R_{i+1})}{\lambda(R_i)} \cdot m_{i,i+1}. \tag{3.21}$$

For $1 \le i \le N-1$, the entry $m_{i+1,i}$ in the ith row is given by

$$m_{i+1,i} = \frac{\lambda(R_{i+1}) \cdot h_i^f}{\lambda(R_i) \cdot h_{i+1}^f} \cdot m_{i,i+1}. \tag{3.22}$$

For $2 \le i \le N-1$ The entry $m_{i,i+1}$ in the ith row is obtained from (3.16) as follows

$$m_{i,i+1} = \frac{\lambda(R_i) - \lambda(R_{i-1}) \cdot m_{i,i-1} - \lambda(R_i) \cdot m_{i,i}}{\lambda(R_{i+1})}. \tag{3.23}$$

For i =1,

$$m_{1,2} = \frac{\lambda(R_1) \cdot (1 - m_{1,1})}{\lambda(R_2)}, \tag{3.24}$$

Consequently, it can be found out that, for a 3-band transformation with respect to a partition $\mathfrak{R}$, if the elements on any band of the associated Frobenius-Perron matrix are known, the Frobenius-Perron matrix $\boldsymbol{M}$ can be uniquely determined.

3.3 Problem Formulation

Let $\mathfrak{B}$ be a Borel σ-algebra of subsets in I, and μ denote the normalized Lebesgue measure on I. Let $S : I \to I$ be a measurable, non-singular transformation, that is, $\mu(S^{-1}(A)) \in \mathfrak{B}$ for any $A \in \mathfrak{B}$ and $\mu(S^{-1}(A)) = 0$ for all $A \in \mathfrak{B}$ with $\mu(A) = 0$. If x_n is a random variable on I having the probability density function $f_n \in \mathfrak{D}(I, \mathfrak{B}, \mu)$, $\mathfrak{D} = \{ f \in L^1(I, \mathfrak{B}, \mu) : f \ge 0, \| f \|_1 = 1 \}$, such that

$$\text{Prob}\{x_n \in A\} = \int_A f_n \, d\mu, \tag{3.25}$$

then x_{n+1} given by

$$x_{n+1} = S(x_n), \tag{3.26}$$

is distributed according to the probability density function $f_{n+1} = P_S f_n$ where $P_S : L^1(I) \to L^1(I)$ is the Frobenius-Perron operator associated with the transformation *S* defined in Section 3.2.1.

The inverse Frobenius-Perron problem is usually formulated as the problem of determining the point transformation *S* such that the dynamical system $x_{n+1} = S(x_n)$ has a given invariant probability density function f^*. In general, the problem does not have a unique solution.

The generalised inverse problem addressed in this chapter, is that of inferring the point transformation which generated a sequence of density functions and has a given invariant density function. Specifically, let $\{x_{0,i}^j\}_{i,j=1}^{\theta,K}$ and $\{x_{1,i}^j\}_{i,j=1}^{\theta,K}$ be two sets of initial and final states observed in *K* separate experiments, where $x_{1,i}^j = S(x_{0,i}^j)$, $i = 1,\ldots,\theta$, $j = 1,\ldots,K$, and $S : I \to I$ is an unknown, nonsingular point transformation. It is assumed that for practical reasons we cannot associate to an initial state $x_{0,i}^j$ the corresponding image $x_{1,i}^j$ but we can estimate the probability density functions f_0^j and f_1^j associated with the initial and final states, $\{x_{0,i}^j\}_{i=1}^{\theta}$ and $\{x_{1,i}^j\}_{i=1}^{\theta}$ respectively. Moreover, let f^* be the invariant density of the system. The inverse problem is to determine $S : I \to I$ such that $f_1^j = P_S f_0^j$ for $j = 1,\ldots,K$ and $f^* = P_S f^*$.

3.4 A solution to the GIFPP for piecewise linear semi-Markov transformations

This section presents a method for solving the GIFPP for a class of piecewise monotonic and expanding semi-Markov transformations defined on the partition $\mathfrak{R}$ called $\mathfrak{R}$-semi-Markov.

$$\mathfrak{R} = \{R_1, R_2, \ldots, R_N\} = \{[c_0, c_1], (c_1, c_2], \ldots, (c_{N-1}, c_N]\}, \qquad (3.27)$$

is a partition of $I=[a,b]$, $c_0=a$, $c_N=b$.

Let S be an unknown piecewise-linear $\Re$-semi-Markov transformation and $\{f_{t,i}\}_{t,i=1}^{T,K}$ be a sequence of probability density functions generated by the unknown map S, given a set of initial density functions $\{f_{0,i}\}_{i=1,K}$. Assuming that the invariant density function f^* of the Frobenius-Perron operator associated to the unknown transformation S can be estimated based on observed data, the proposed identification approach can be summarised as follows:

Step 1: Given the samples, construct a uniform partition C and an initial piecewise constant density estimate f_C^* of the true invariant density f^* which maximises a penalised log-likelihood function.

Step 2: Select a sub-partition $C_d(\bar{l}_j)$ of C.

Step 3: Estimate the matrix representation of the Frobenius-Perron operator over the partition $C_d(\bar{l}_j)$ based on the observed sequences of densities generated by S.

Step 4: Construct the piecewise linear map $\hat{S}^{(\bar{l}_j)}$ corresponding to the matrix representation.

Step 5: Compute the piecewise constant invariant density $f^*_{C_d(\bar{l}_j)}$ associated with the identified transformation $\hat{S}^{(\bar{l}_j)}$ and evaluate performance criterion.

Step 6: Repeat steps 2) to 5) to identify the partition and map which minimise the performance criterion.

3.4.1 Identification of the Markov partition

Let $f^* \in \mathfrak{F}$ be the invariant density associated with a $\Re$-semi-Markov transformation S. Let $\{x_i^*\}_{i=1}^{\theta}$ be a finite number of independent observations of f^*. The aim is to determine an orthogonal basis set $\{\chi_{R_i}(x)\}_{i=1}^{N}$ such that

$$f^*(x) \approx \sum_{i=1}^{N} h_i \chi_{R_i}(x),, \tag{3.28}$$

where $\chi_{R_i}(x)$ is the indicator function and h_i are the expansion coefficients given by

$$h_i = \frac{1}{\theta \cdot \lambda(R_i)} \sum_{j=1}^{\theta} \chi_{R_i}(x_j^*), \tag{3.29}$$

$\lambda(R_i)$ denotes the length of the interval R_i.

We start by constructing a uniform partition Δ with intervals N' that maximises the following penalised log-likelihood function (Rozenholc, Mildenberger et al. 2010)

$$L_\theta(N') - p(N') = \left[\sum_{i=1}^{N'} D_i \log(N' D_i/\theta)\right] - \left[N' - 1 + (\log N')^{2.5}\right], \tag{3.30}$$

where $1 \le N' \le \theta/\log\theta$, $D_i = \sum_{j=1}^{\theta} \chi_{\Delta_i}(x_j^*)$ and

$$\Delta_i = \begin{cases} [a, (b-a)/N'], & i = 1; \\ ((i-1)(b-a)/N', i(b-a)/N'], & i = 2, \ldots, N'. \end{cases}$$

The coefficients h_i' for the regular histogram are given by

$$h_i' = \frac{N'}{\theta(b-a)} \sum_{j=1}^{\theta} \chi_{\Delta_i}(x_j^*), \tag{3.31}$$

Let $C = \{c_1, \ldots, c_{N'-1}\}$ be the strictly increasing sequence of cut points corresponding to the resulting uniform partition $\Delta = \{\Delta_i\}_{i=1}^{N'}$. Let $L = \{l_j\}_{j=1}^{N'-1}$, $l_j = N' \cdot \left|(h_{j+1}' - h_j')\right| / (b-a)$ and $\bar{L} = \{\bar{l}_j\}_{j=1}^{N''}$, $0 \le N'' \le N' - 1$, be the longest strictly increasing subsequence of L.

The final Markov partition $\mathfrak{R}$ is determined by solving

$$\min_{\bar{l}_j \in \bar{L}} \left\{ J(\Re) = \int_I (f_C^*(x) - f_{C_d(\bar{l}_j)}^*(x))^2 dx \right\}, \tag{3.32}$$

where $C_d(\bar{l}_j) = \{c_{d_1(\bar{l}_j)}, ..., c_{d_\rho(\bar{l}_j)}\}$ is a longest subsequence of C which, for the selected threshold $\bar{l}_j \in \bar{L}$, satisfies $d_1(\bar{l}_j) = 1$ if $l_1 > \bar{l}_j$ and in general $d_{i+1}(\bar{l}_j) = d_i(\bar{l}_j) + 1$ if $l_{d_i+1} > \bar{l}_j$ for $i = 1, \ldots, \rho - 1$. In equation (3.32), $f_{C_d(\bar{l}_j)}^*$ denotes the piecewise constant invariant density associated with the transformation $\hat{S}^{(\bar{l}_j)}$ identified over the partition

$$\Re^{(\bar{l}_j)} = \{\underbrace{[a, c_{d_1(\bar{l}_j)}]}_{R_1^{(\bar{l}_j)}}, \underbrace{(c_{d_1(\bar{l}_j)}, c_{d_2(\bar{l}_j)}]}_{R_2^{(\bar{l}_j)}}, ..., \underbrace{(c_{d_\rho(\bar{l}_j)}, b]}_{R_\rho^{(\bar{l}_j)}}\}. \tag{3.33}$$

3.4.2 Identification of the Frobenius-Perron matrix

Let $\Re = \{R_1, R_2, \ldots, R_N\} = \{[a, c_1], (c_1, c_2], \ldots, (c_{N-1}, b]\}$ be a candidate Markov partition and $\{f_{t,i}\}_{t,i=1}^{T,K}$ be the piecewise constant densities on $\Re$, which are estimated from the samples.

Let $f_0(x)$ be an initial density function that is piecewise constant on the partition $\Re$

$$f_0(x) = \sum_{i=1}^{N} w_{0,i} \chi_{R_i}(x), \tag{3.34}$$

where the coefficients satisfy $\sum_{i=1}^{N} w_{0,i} \lambda(R_i) = 1$.

Let $X_0 = \{x_{0,j}\}_{j=1}^{\theta}$ be the set of initial conditions obtained by sampling $f_0(x)$ and

$$X_t = \{x_{t,j}\}_{j=1}^{\theta}, \tag{3.35}$$

be the set of states obtained by applying t times the transformation S such that $x_{t,j} = S^t(x_{0,j})$ for some $x_{0,j} \in X_0$, $j = 1, \ldots, \theta$.

The density function associated with the states X_t is given by

$$f_t(x) = \sum_{i=1}^{N} w_{t,i} \chi_{R_i}(x), \tag{3.36}$$

where the coefficients $w_{t,j} = \frac{1}{\lambda(R_j)\cdot\theta} \sum_{j=1}^{\theta} \chi_{R_j}(x_{t,j})$. Let $\boldsymbol{w}^{f_t} = [w_{t,1},...,w_{t,N}]$ be the vector defining $f_t(x)$, $t = 0,\ldots,T$ where typically $T \geq N$. In practice, the observed $f_t(x)$, $t = 0,\ldots,T$, are approximations of the true density functions, which are inferred from experimental observations.

It follows that

$$\boldsymbol{W}_1 = \boldsymbol{W}_0 \boldsymbol{M}, \tag{3.37}$$

where

$$\boldsymbol{W}_0 = \begin{bmatrix} \boldsymbol{w}^{f_0} \\ \boldsymbol{w}^{f_1} \\ \vdots \\ \boldsymbol{w}^{f_{T-1}} \end{bmatrix} = \begin{bmatrix} w_{0,1} & w_{0,2} & \cdots & w_{0,N} \\ w_{1,1} & w_{1,2} & \cdots & w_{1,N} \\ \vdots & \vdots & \ddots & \vdots \\ w_{T-1,1} & w_{T-1,2} & \cdots & w_{T-1,N} \end{bmatrix}, \tag{3.38}$$

and

$$\boldsymbol{W}_1 = \begin{bmatrix} \boldsymbol{w}^{f_1} \\ \boldsymbol{w}^{f_2} \\ \vdots \\ \boldsymbol{w}^{f_T} \end{bmatrix} = \begin{bmatrix} w_{1,1} & w_{1,2} & \cdots & w_{1,N} \\ w_{2,1} & w_{2,2} & \cdots & w_{2,N} \\ \vdots & \vdots & \ddots & \vdots \\ w_{T,1} & w_{T,2} & \cdots & w_{T,N} \end{bmatrix}. \tag{3.39}$$

The matrix $\boldsymbol{M}$ is obtained as a solution to a constrained least-squares optimisation problem

$$\min_{\{m_{i,j}\}_{i,j=1}^{N} \geq 0} \| \boldsymbol{W}_1 - \boldsymbol{W}_0 \boldsymbol{M} \|_F, \tag{3.40}$$

subject to

$$\sum_{j=1}^{N} m_{i,j}\lambda(R_j) = \lambda(R_i), \quad \text{for } i = 1,\ldots,N, \tag{3.41}$$

where $\|\cdot\|_F$ denotes the Frobenius norm.

The matrix $\Phi = \boldsymbol{W}_0^T \boldsymbol{W}_0$ has to be non-singular for the estimate to be unique.

Proposition 3.1 *Given a sequence of density functions $f_0,\ldots, f_T$ generated by a transformation S(x), the matrix $\Phi = \boldsymbol{W}_0^T \boldsymbol{W}_0$ is non-singular if $f_{N-2}(x) \neq f^*(x)$.*

Proof. If $f_{N-2}(x) = f^*(x)$ then $f_t(x) = f^*(x)$ for $t = N-1,\ldots,T$, that is, the matrix $\boldsymbol{W}_0$ has at most *N*-2 rows that are distinct from $f^*(x)$.

Using Cauchy-Binet formula, the determinant of Φ can be written as

$$\det(\boldsymbol{W}_0^T \boldsymbol{W}_0) = \sum_{S \in \binom{[T]}{N}} \det(\boldsymbol{W}_{0,S,[T]}^T)\det(\boldsymbol{W}_{0,S,[T]}), \tag{3.42}$$

where [*T*] denotes the set $\{1,...,T\}$, $\binom{[T]}{N}$ denotes the set of subsets of size *N* of [*T*] and $\boldsymbol{W}_{0,S,[T]}$ is a $N \times N$ matrix whose rows are the rows of $\boldsymbol{W}_0$ at indices given in *S*. Since $\boldsymbol{W}_0$ has at most *N*–2 rows that are distinct from $f^*(x)$, it follows that $\boldsymbol{W}_{0,S,[T]}$ has at least two rows that are identical, hence $\det(\boldsymbol{W}_{0,S,[T]}) = 0$ for any $S \in \binom{[T]}{N}$. Consequently, $\det(\boldsymbol{W}_0^T \boldsymbol{W}_0) = 0$, which concludes the proof.

Proposition 3.2 *A $\Re$-semi-Markov, piecewise linear and expanding transformation S can be uniquely identified given N linearly independent, piecewise constant densities $f_0^i \in \mathfrak{F}$ and their images $f_1^i \in \mathfrak{F}$ under the transformation.*

Proof. Let

$$f_0^i(x) = \sum_{j=1}^{N} w_{i,j}^0 \chi_{R_j}(x), \qquad i = 1, \ldots, N, \tag{3.43}$$

Since $\{f_0^i\}_{i=1}^N$ are linearly independent, $\{\boldsymbol{w}_i^0\}_{i=1}^N$, $\boldsymbol{w}_i^0 = [w_{i,1}^0, \ldots, w_{i,N}^0]$ are also linearly independent. Moreover, given that S is a $\Re$-semi-Markov, piecewise linear and expanding, we have

$$f_1^i(x) = \sum_{j=1}^{N} w_{i,j}^1 \chi_{R_j}(x), \qquad i = 1, \ldots, N, \tag{3.44}$$

where $\boldsymbol{w}_i^1 = [w_{i,1}^1, \ldots, w_{i,N}^1] = \boldsymbol{w}_i^0 \boldsymbol{M}$, $i = 1, ..., N$. Alternatively, this can be written as

$$\boldsymbol{W}_1' = \boldsymbol{W}_0' \boldsymbol{M} \,, \tag{3.45}$$

where

$$\boldsymbol{W}_0' = \begin{bmatrix} \boldsymbol{w}_1^0 \\ \boldsymbol{w}_2^0 \\ \vdots \\ \boldsymbol{w}_2^0 \end{bmatrix} = \begin{bmatrix} w_{1,1}^0 & w_{1,2}^0 & \cdots & w_{1,N}^0 \\ w_{21}^0 & w_{22}^0 & \cdots & w_{2,N}^0 \\ \vdots & \vdots & \ddots & \vdots \\ w_{N,1}^0 & \cdots & \cdots & w_{N,N}^0 \end{bmatrix}, \tag{3.46}$$

and

$$\boldsymbol{W}_1' = \begin{bmatrix} \boldsymbol{w}_1^1 \\ \boldsymbol{w}_2^1 \\ \vdots \\ \boldsymbol{w}_2^1 \end{bmatrix} = \begin{bmatrix} w_{1,1}^1 & w_{1,2}^1 & \cdots & w_{1,N}^1 \\ w_{21}^1 & w_{22}^1 & \cdots & w_{2,N}^1 \\ \vdots & \vdots & \ddots & \vdots \\ w_{N,1}^1 & \cdots & \cdots & w_{N,N}^1 \end{bmatrix}. \tag{3.47}$$

Since $\boldsymbol{W}_0'$ is non-singular, the Frobenius-Perron matrix $\boldsymbol{M}$ is given by

$$\boldsymbol{M} = \boldsymbol{W}_0'^{-1} \boldsymbol{W}_1' \,. \tag{3.48}$$

The derivative of $S\big|_{Q_k^{(i)}}$ is $1/m_{i,j}$, the length of $Q_k^{(i)}$ is given by

$$\lambda(Q_k^{(i)}) = q_k^{(i)} - q_{k-1}^{(i)} = m_{i,j} \lambda(R_j) \,, \tag{3.49}$$

which allows computing iteratively $q_k^{(i)}$ for each interval R_i starting with $q_0^{(i)} = c_{i-1}$. By assuming each branch $S|_{R_i}$ is monotonically increasing, the piecewise linear semi-Markov mapping is given by

$$S|_{Q_k^{(i)}}(x) = \frac{1}{m_{i,j}}(x - q_{k-1}^{(i)}) + c_{j-1}, \tag{3.50}$$

for $k = 1,\ldots, p(i)$, j is the index of image R_j of $Q_k^{(i)}$, i.e. $S(Q_k^{(i)}) = R_j$, $i = 1,\ldots, N$, $j = 1,\ldots, N$, where $m_{i,j} \neq 0$.

The map is constructed as depicted in Figure 3.1.

In practice, we can choose the piecewise constant probability density functions $f_0^{\,j}(x) = \frac{1}{\lambda(R_j)}\chi_{R_j}(x)$. These are sampled in order to generate *N* sets of initial conditions

$$X_0^i = \{x_{0,j}^i\}_{j=1}^{\theta}, \quad i = 1,...,N, \tag{3.51}$$

that will be used in the experiments. For each set of initial conditions X_1^i we measure a corresponding set of final states

$$X_1^i = \{x_{1,j}^i\}_{j=1}^{\theta}, \quad i = 1,...,N, \tag{3.52}$$

where $x_{1,j}^i = S(x_{0,k}^i)$ for some $x_{0,k}^i \in X_0^i$. The density function f_1^i associated with the set X_1^i of final states is given by

$$f_1^i(x) = \sum_{j=1}^{N} v_{ij}\chi_{R_j}(x), \qquad i = 1, \ldots, N, \tag{3.53}$$

where $v_{i,j} = \frac{1}{\lambda(R_j)\cdot\theta}\sum_{k=1}^{\theta}\chi_{R_j}(x_{1,k}^i)$.

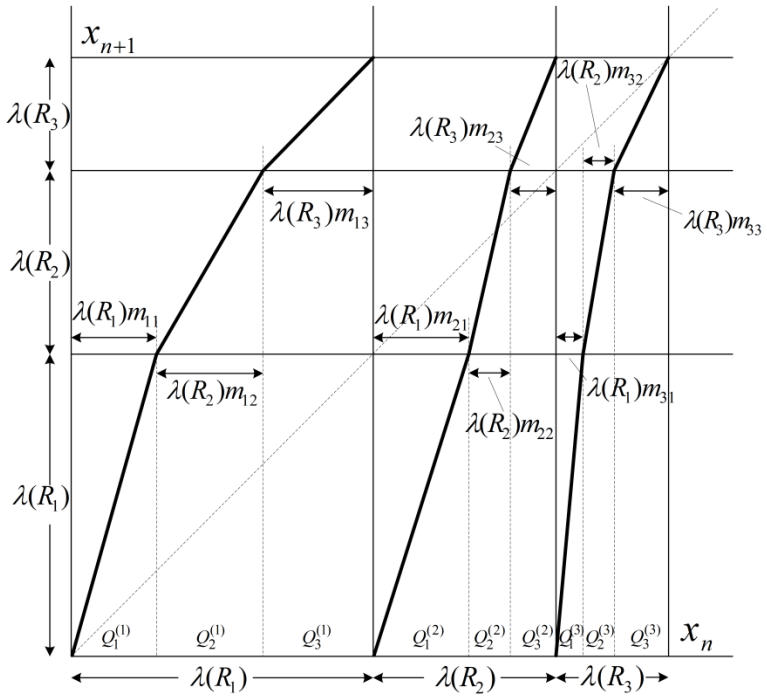

Figure 3.1 Construction of 1-D piecewise-linear semi-Markov transformation based on the Frobenius-Perron matrix.

Remark. We only need to generate initial conditions for the densities that correspond to the finest uniform partition $N = N'$. Coarser partitions are obtained by merging adjacent intervals, for example R_j and R_{j+1}, leading to the new partition $\{\overline{R}_1,...,\overline{R}_{N-1}\}$. It follows that the initial and final states corresponding to the merged interval $\overline{R}_j = R_j \cup R_j$ are given by $\overline{X}_0^j = X_0^j \cup X_0^{j+1}$ and $\overline{X}_1^j = X_1^j \cup X_1^{j+1}$ respectively. The initial and final densities corresponding to the merged interval are given by $\overline{f}_0^j(x) = \frac{1}{\lambda(\overline{R}_J)} \chi_{\overline{R}_j}(x)$ and $\overline{f}_1^j(x) = \frac{1}{2\lambda(\overline{R}_i)\cdot\theta} \sum_{i=1}^{N-1}\sum_{k=1}^{\theta} \chi_{\overline{R}_i}(x_{1,k}^j)\chi_{\overline{R}_i}(x)$ respectively.

In general, initial density functions are not piecewise constant over the partition $\Re$. Let $f \in L^1 \supset \mathfrak{F}(\Re_Q)$, $P^{N_Q} : L^1 \to \mathfrak{F}(\Re_Q)$ be the orthogonal projector operator and $Z^{N_Q} = I - P^{N_Q}$ such that $f = P^{N_Q} f + Z^{N_Q} f = f_p + f_z$ where

$\Re_Q = \{Q_1^{(1)},...,Q_1^{p(1)}, \ ...,Q_N^{p(N)}\} = \{Q_1,...,Q_{N_Q}\}$, $R_i = \bigcup_{k=1}^{p(i)} Q_k^{(i)}$, $i = 1, \ldots, N$,

$\mathfrak{F}(\Re_Q) = span\{\chi_{Q_k^{(i)}}\}$ and $N_Q = \sum_{i=1}^{N} p(i)$.

Theorem 3.6 *A $\Re$-semi-Markov, piecewise linear and expanding transformation, where $R_i = \bigcup_{k=1}^{p(i)} Q_k^{(i)}$, i=1, .., N,* can *be uniquely identified given a set of initial densities* $\{f_0^i\}_{i=1}^{N_Q}$, $N_Q = \sum_{i=1}^{N} p(i)$, *and their images* $\{f_1^i\}_{i=1}^{N_Q}$ *under the transformation, if* $\{P^{N_Q} f_0^i\}_{i=1}^{N_Q}$ *are linearly independent.*

Proof. The Frobenius-Perron operator associated with *S* is given by

$$P_S f_0^i(x) = \sum_{z_i = f^{-1}(x)} \frac{f_0^i(z_i)}{|f_0^{i\prime}(z_i)|}. \tag{3.54}$$

It follows that

$$\begin{aligned} f_1^i(x) &= P_S f_0^i(x) = P_S p_0^i(x) + P_S q_0^i(x) \\ &= \sum_{z_i = f^{-1}(x)} \frac{p_0^i(z_i)}{|f_0^{i\prime}(z_i)|} + \sum_{z_i = f^{-1}(x)} \frac{q_0^i(z_i)}{|f_0^{i\prime}(z_i)|}, \end{aligned} \tag{3.55}$$

where $|f_0^{i\prime}(S|_{Q_k^{(i)}}^{-1}(x))| \in \{\beta_1,....,\beta_{N_Q}\}$.

$$\begin{aligned} & P^{N_Q} f_1^i(x) \\ &= P^{N_Q} P_S p_0^i(x) + P^{N_Q} P_S q_0^i(x) \\ &= P^{N_Q} \sum_{i,j: x \in S|_{Q_k^{(i)}}(Q_k^{(i)})} \frac{p_0^i(S|_{Q_k^{(i)}}^{-1}(x))}{|f_0^{i\prime}(S|_{Q_k^{(i)}}^{-1}(x))|} + P^{N_Q} \sum_{i,j: x \in S|_{Q_k^{(i)}}(Q_k^{(i)})} \frac{q_0^i(S|_{Q_k^{(i)}}^{-1}(x))}{|f_0^{i\prime}(S|_{Q_k^{(i)}}^{-1}(x))|}. \end{aligned} \tag{3.56}$$

Then,

$$P^{N_Q} \sum_{i,j:x\in S|_{Q_k^{(i)}}(Q_k^{(i)})} \frac{q_0^i(S|_{Q_k^{(i)}}^{-1}(x))}{|f_0^{i\prime}(S|_{Q_k^{(i)}}^{-1}(x))|}$$

$$= \sum_{i,j:x\in S|_{Q_k^{(i)}}(Q_k^{(i)})} \frac{\chi_{Q_k^{(i)}}(x)}{\beta_{i,k}} \int_{Q_k^{(i)}} q_0^i(S|_{Q_k^{(i)}}^{-1}(x))dx = 0. \tag{3.57}$$

Hence,

$$P^{N_Q} P_S f_0^i(x) = P_S p_0^i(x) = \sum_j^{N_Q} w_{i,j}^1 \chi_{Q_k^{(j)}}(x)$$

$$= \sum_{j,k:x\in S|_{Q_k^{(i)}}(Q_k^{(i)})} \frac{\chi_{Q_k^{(j)}}(x)}{\beta_{j,k}} w_{i,k}^{0,j}. \tag{3.58}$$

$i = 1,\ldots, N_Q$.

Alternatively, (3.45) can be written as

$$\boldsymbol{W}_1'' = \boldsymbol{W}_0'' \boldsymbol{M}_{N_Q}, \tag{3.59}$$

where

$$\boldsymbol{W}_0'' = \begin{bmatrix} w_{1,1}''^0 & w_{1,2}''^0 & \cdots & w_{0,N_Q}''^0 \\ w_{2,1}''^0 & w_{2,2}''^0 & \cdots & w_{2,N_Q}''^0 \\ \vdots & \vdots & \ddots & \vdots \\ w_{N_Q,1}''^0 & w_{N_Q,2}''^0 & \cdots & w_{N_Q,N_Q}''^0 \end{bmatrix}, \tag{3.60}$$

and

$$\boldsymbol{W}_1'' = \begin{bmatrix} w_{1,1}''^1 & w_{1,2}''^1 & \cdots & w_{0,N_Q}''^1 \\ w_{2,1}''^1 & w_{2,2}''^1 & \cdots & w_{2,N_Q}''^1 \\ \vdots & \vdots & \ddots & \vdots \\ w_{N_Q,1}''^1 & w_{N_Q,2}''^1 & \cdots & w_{N_Q,N_Q}''^1 \end{bmatrix}, \tag{3.61}$$

$\boldsymbol{M}_{N_Q} = \boldsymbol{W}_0''^{-1}\boldsymbol{W}_1'' = \{m_{i,j}\}_{i,j=1}^{N_Q}$ is the Frobenius-Perron matrix that corresponds to a unique piecewise linear and expanding transformation *S* given by

$$S|_{Q_k^{(i)}}(x) = \frac{1}{m_{s(i)+1,s(j)+1}}(x - q_{k-1}^{(i)}) + c_{j-1}, \tag{3.62}$$

for $k = 1,\ldots, p(i)$, j is the index of image R_j of $Q_k^{(i)}$, i.e. $S(Q_k^{(i)}) = R_j$, $i = 1,\ldots,N$, $j = 1,\ldots,N$, $s(1)=0$ and $s(i) = s(i-1) + p(i-1)$ for $i > 1$.

To summarise, the full procedure of the approach is described as follows

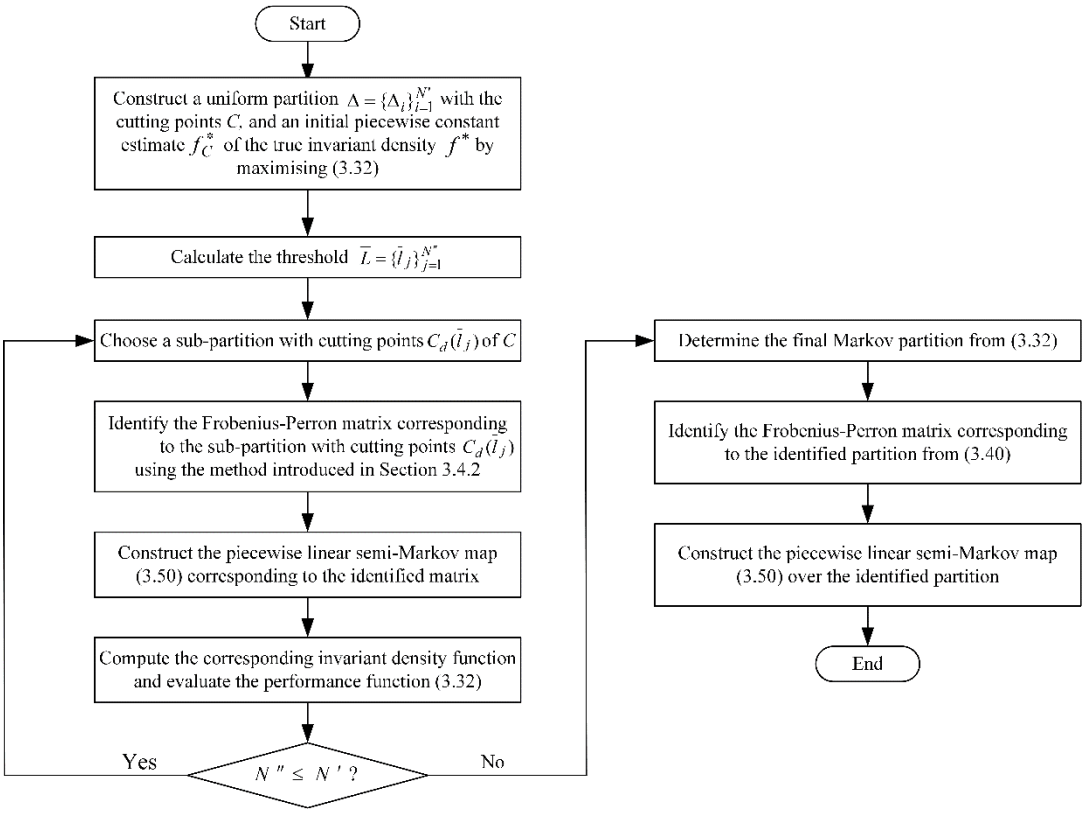

Figure 3.2 Flow chart of the proposed identification approach.

3.5 Numerical example

The applicability of the proposed algorithm is demonstrated using numerical simulation. Consider the following piecewise linear and expanding transformation $S : [0,1] \to [0,1]$

$$S|_{R_i}(x) = \alpha_{i,j}x + \beta_{i,j}, \tag{3.63}$$

for $i = 1,\ldots,4$, $j = 1,\ldots,4$, defined on the partition $\Re = \{R_i\}_{i=1}^{4} = \{[0, 0.3], (0.3, 0.4], (0.4, 0.8], (0.8, 1]\}$, where

$$(\alpha_{i,j})_{1\le i,j\le 4} = \begin{bmatrix} 2.50 & 1.67 & 13.33 & 2.22 \\ 15.00 & 3.33 & 20.00 & 6.67 \\ 7.50 & 1.25 & 3.33 & 1.25 \\ 7.50 & 2.50 & 5.00 & 5.00 \end{bmatrix},$$

$$(\beta_{i,j})_{1\le i,j\le 4} = \begin{bmatrix} 0 & 0.10 & -2.00 & 0.33 \\ -4.50 & -0.77 & -6.60 & -1.67 \\ -3.00 & -0.25 & -1.33 & 0 \\ -6.00 & -1.80 & -4.00 & -4.00 \end{bmatrix}.$$

The graph of *S* is shown in Figure 3.3.

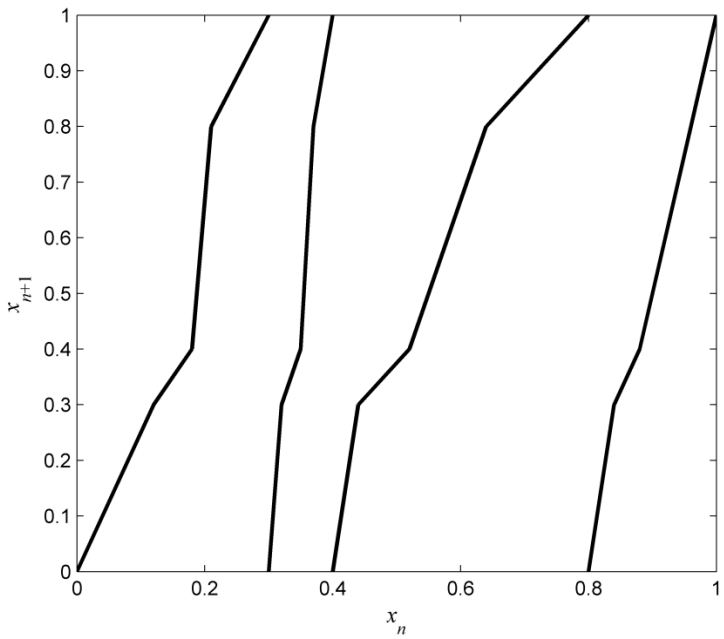

Figure 3.3 Original piecewise linear transformation *S*.

A set of initial states $X_0 = \{x_{0,j}\}_{j=1}^{\theta}$, $\theta = 5\times 10^3$, generated by sampling from a uniform probability density function $f_0(x) = \chi_{[0,1]}(x)$, were iterated using *S* to generate a corresponding set of final states $X_T = \{x_{T,j}\}_{j=1}^{\theta}$ where $T = 20{,}000$. The data set X_T was used to determine the uniform partition Δ with N' intervals, $1 \le N' \le \lfloor \theta / \log\theta \rfloor = 587$, which maximizes the penalised log-likelihood function in

equation (3.30). In this example $N' = 10$, i.e. $C = \{0.1, ..., 0.9\}$ and the estimated invariant density $f_C^*(x)$ with respect to the 10-interval partition is shown in Figure 3.4.

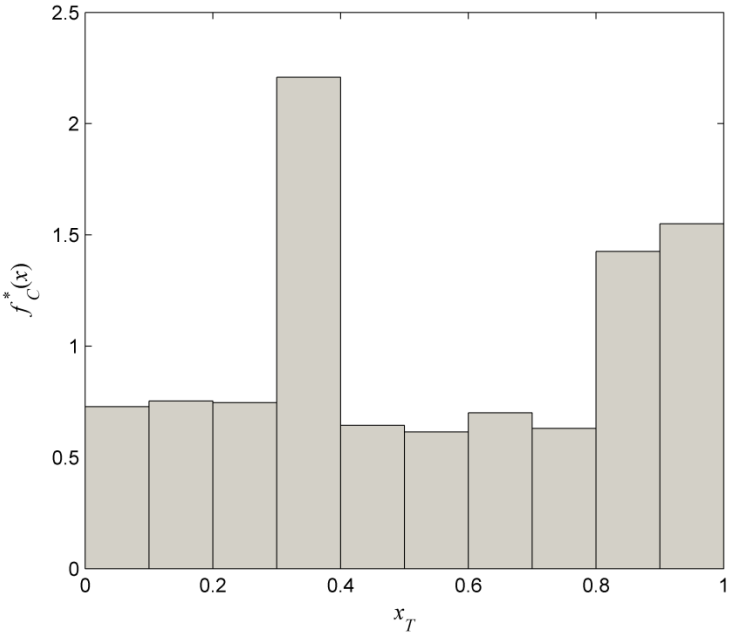

Figure 3.4 The invariant density estimated over the initial uniform partition with $N' = 10$ intervals.

The sequence $L = \{l_j\}_{j=1}^{9}, l_j = 10 \,|\, h'_{j+1} - h'_j \,|$ is shown in Figure 3.5.

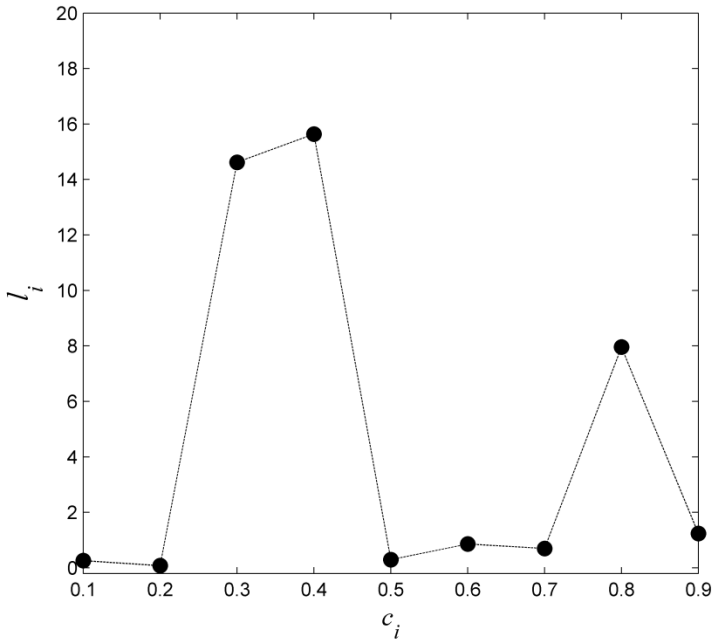

Figure 3.5 A piecewise linear example: The *L* sequence.

In this example, $\bar{L} = \{\bar{l}_j\}_{j=1}^{9} = \{0.08, 0.26, 0.30, 0.70, 0.86, 1.24, 7.96, 14.62, 15.64\}$.

In order to explicitly show the process of searching the final Markov partition, Figure 3.6 illustrates the formation of a Markov partition for $\bar{l}_7 = 7.96$. $\bar{l}_7 = l_8$. From Figure 3.5, it can be found that $l_j < \bar{l}_7$, $j = 1, 2, 5, 6, 7, 9$, therefore, the adjacent uniform intervals connected by the cut points $\{c_j, j = 1, 2, 5, 6, 7, 9\}$ at which $l_j < \bar{l}_7$, are merged, which results in the non-uniform partition shown in Figure 3.6. Specifically, intervals {[0, 0.1), [0.1, 0.2), [0.2, 0.3)} are merged into one interval [0, 0.3), and intervals {[0.4, 0.5), [0.5, 0.6), [0.6, 0.7) , [0.7, 0.8)} are merged into one interval [0.4, 0.8) , and intervals {[0.8, 0.9), [0.9, 1.0)} are merged into one interval [0.8, 1.0). Based on the new formed non-uniform candidate partition, sequences of probability density function are generated to identify the corresponding piecewise linear semi-Markov transformation, as described in Sectioin 4.2.2 and 4.2.3. Then the associated invariant density function $f^*_{C_d(\bar{l}_7)}$ is predicted and the loss function

$$\min_{\bar{l}_j \in \bar{L}} \left\{ J(\Re) = \int_I (f^*_C(x) - f^*_{C_d(\bar{l}_j)}(x))^2 dx \right\}, \tag{3.64}$$

corresponding to $\bar{l}_7$ is calculated.

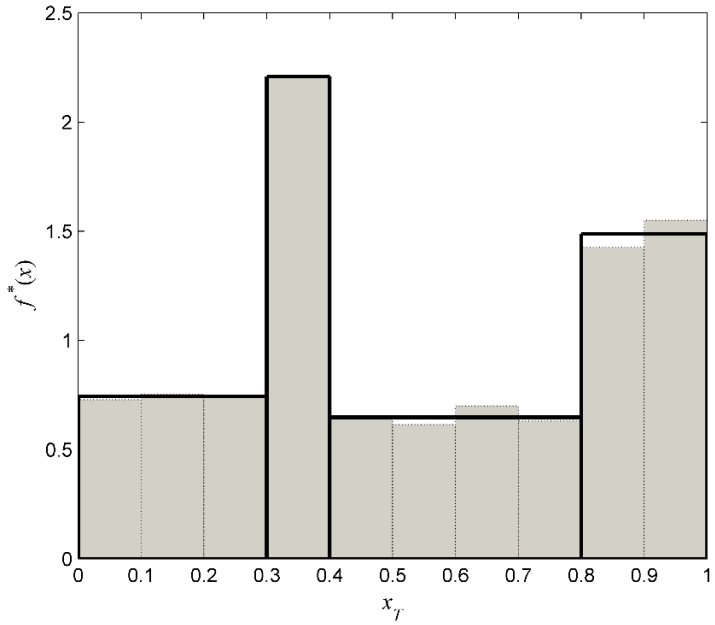

Figure 3.6 Chapter 3 numerical example: Formation of the final Markov partition corresponding to the obtained minimum loss function for $\bar{l}_7$. The bold line is the invariant density histogram estimated over the final Markov partition; the dotted line is the invariant density histogram estimated over the initial uniform partition.

Consequently, the minimum is obtained for $\bar{l}_7$, as shown in Figure 3.7.

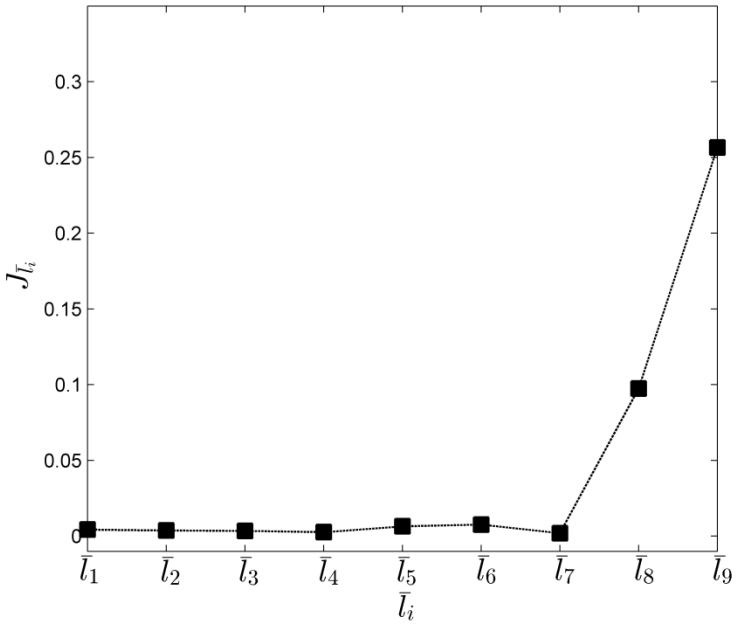

Figure 3.7 Chapter 3 numerical example: The value of the cost function given in equation (3.32) for each threshold.

This corresponds to the final Markov partition $\mathfrak{R} = \{R_1, R_2, R_3, R_4\}$ where $R_1 = [0, 0.3]$, $R_2 = (0.3, 0.4]$, $R_3 = (0.4, 0.8]$ and $R_4 = (0.8, 1]$. Figure 3.8 shows the

initial density functions used to generate the set of the initial conditions and the final density functions estimated from the corresponding final states for T=1.

For the identified partition, the estimated Frobenius-Perron matrix is

$$\boldsymbol{M} = \begin{bmatrix} 0.4044 & 0.5874 & 0.0753 & 0.4491 \\ 0.0673 & 0.3062 & 0.0482 & 0.1497 \\ 0.1363 & 0.7968 & 0.2988 & 0.7996 \\ 0.1345 & 0.4052 & 0.1995 & 0.1966 \end{bmatrix}, \tag{3.65}$$

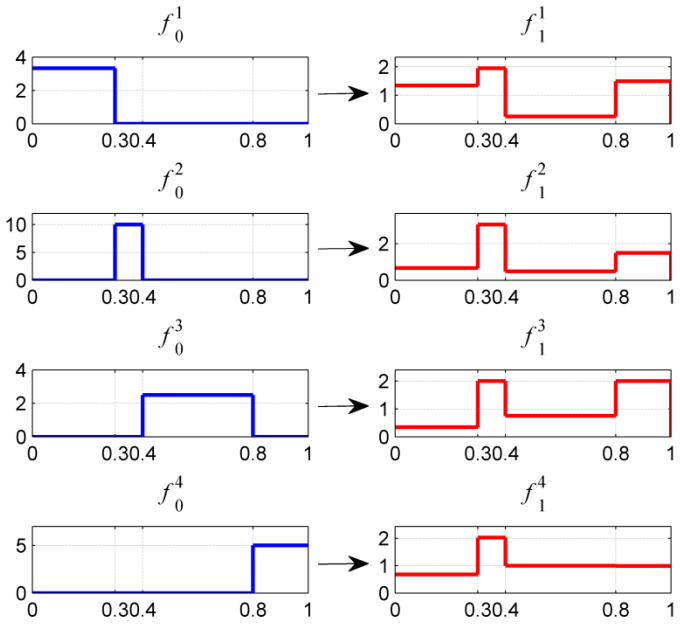

Figure 3.8 A piecewise linear example: The initial and final density functions $f_0^i(x)$ and $f_1^i(x)$ corresponding to the identified four-interval partition.

The corresponding identified mapping $\hat{S}$ is shown in Figure 3.9.

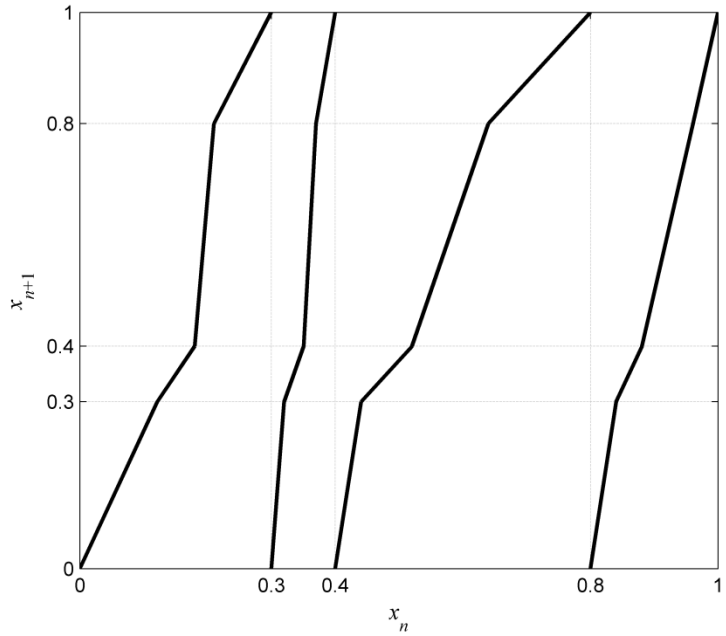

Figure 3.9 Chapter 3 numerical example: The identified transformation $\hat{S}$ of the underlying system.

The estimated coefficients of the identified piecewise linear semi-Markov transformation $\hat{S}\big|_{R_i}(x) = \hat{\alpha}_{i,j}x + \hat{\beta}_{i,j}$ are

$$(\hat{\alpha}_{i,j})_{1\le i,j\le 4} = \begin{bmatrix} 2.47 & 1.70 & 13.28 & 2.23 \\ 14.87 & 3.27 & 20.77 & 6.68 \\ 7.33 & 1.26 & 3.34 & 1.25 \\ 7.43 & 2.47 & 5.01 & 5.09 \end{bmatrix},$$

$$(\hat{\beta}_{i,j})_{1\le i,j\le 4} = \begin{bmatrix} 0 & 0.09 & -1.99 & 0.33 \\ -4.46 & -0.75 & -6.89 & -1.67 \\ -2.94 & -0.25 & -1.34 & 0 \\ -5.95 & -1.77 & -4.02 & -4.09 \end{bmatrix}.$$

To show the identification performance of the algorithms, the absolute percentage error is evaluated by

$$\delta S(x) = 100 \times \frac{\left|S(x) - \hat{S}(x)\right|}{S(x)}, \tag{3.66}$$

for $x \in X = \{0.01, 0.02, ..., 0.99\}$. As shown in Figure 3.10 the relative error between the identified and original map is less than 2.5%.

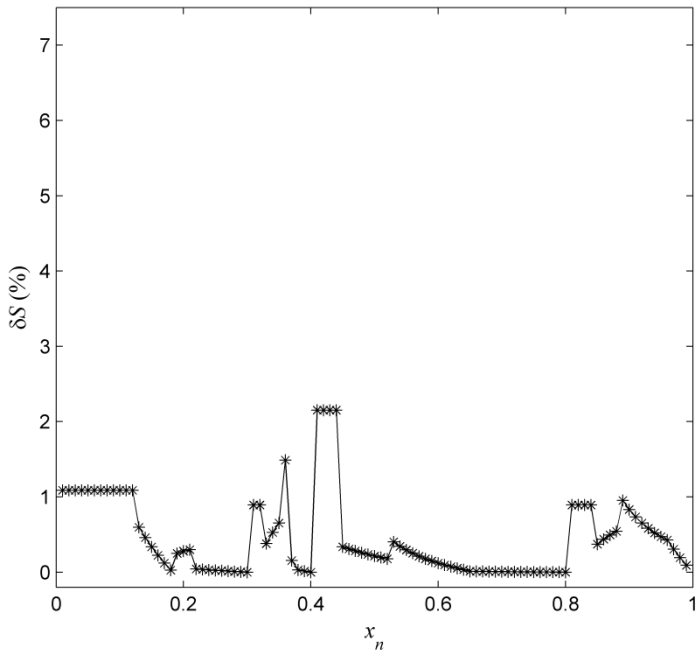

Figure 3.10 Chapter 3 numerical example: Relative error between the original map S and the identified map $\hat{S}$ evaluated for 99 uniformly spaced points.

Furthermore, Figure 3.11 shows the true invariant density f^* associated with S superimposed on the invariant density $\hat{f}^*$ associated with the identified map $\hat{S}$. The *percentage root-mean-square error* (PRE) is calculated by

$$\mathrm{PRE} = \frac{\sqrt{\int_I (\hat{f}^*(x) - f^*(x))^2 dx}}{\sqrt{\int_I (f^*(x))^2 dx}} \times 100\% . \tag{3.67}$$

It follows that $\mathrm{PRE} = 1.48\%$.

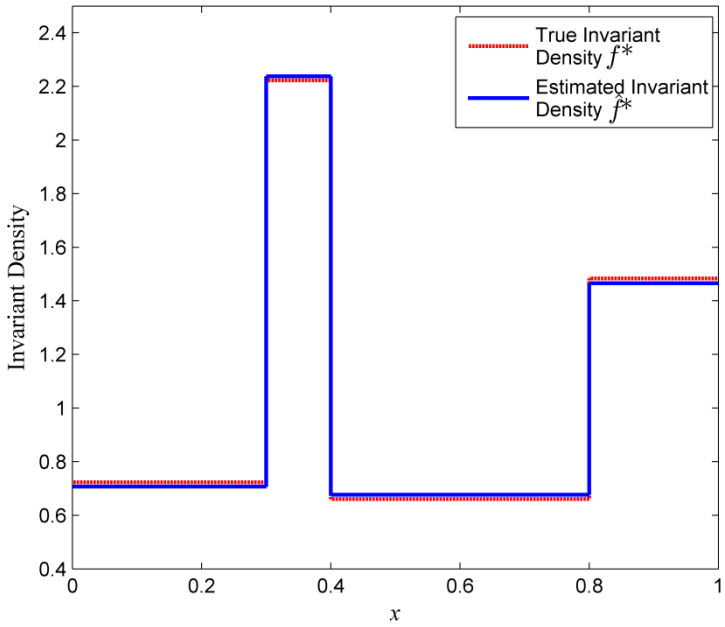

Figure 3.11 Chapter 3 numerical example: The true invariant density (red dashed line) and the estimated invariant density (blue solid line) of the identified map.

In practical situations, measurements are corrupted by noise. Given the process

$$x_{n+1} = S(x_n) + \omega_n, \tag{3.68}$$

where $S : R \to R$ is a measurable transformation and $\{\omega_n\}$ is a sequence of independent random variables with density *g*, it can be shown (Lasota & Mackey 1994) that the evolution of densities for this transformation is described by the Markov operator $\overline{P} : L^1 \to L^1$ defined by

$$\overline{P}f(x) = \int_R f(y)g(x - S(y))dy, \tag{3.69}$$

Furthermore, if $\overline{P}$ is constrictive then $\overline{P}$ has a unique invariant density f^* and the sequence $\{\overline{P}^n f\}$ is asymptotically stable for every $f \in D$ (Lasota & Mackey 1994).

To study how noise affects the performance of the developed algorithm the following process is considered

$$x_{n+1} = S(x_n) + \alpha\omega_n \pmod 1, \tag{3.70}$$

where $S:[0,1]\to[0,1]$ is a measurable transformation that has a unique invariant density f^*, $\{\omega_n\}$ is i.i.d. N (0,1) (the results apply for general density functions) and α is a known noise level. This leads to an integral operator P_α which has a unique invariant density f_α^* (Lasota & Mackey 1994). It can be shown that $\lim_{\alpha\to 0}\|P_\alpha f - Pf\| = 0$ for all $f \in D$ and that, for $0<\alpha<\alpha_0$, if $\lim_{\alpha\to 0} f_\alpha^*$ exists then the limit is f^*.

To evaluate the performance of the proposed algorithm in the presence of noise, the map for different values of α is reconstructed and the *mean absolute percentage error* (MAPE) between *S* and $\hat{S}$ is computed by

$$\delta S(x) = \frac{100}{\theta_{\delta S}} \sum_{i=1}^{\theta_{\delta S}} \left| \frac{S(x_i) - \hat{S}(x_i)}{S(x_i)} \right|, \tag{3.71}$$

where $\{x_i\}_{i=1}^{\theta_{\delta S}} = \{0.01,...,0.99\}$, $\theta_{\delta S} = 99$.

Table 3.1 Reconstruction errors for different noise levels – Example: a piecewise linear system example in Chapter 3.

$\alpha = \sigma_\alpha^2 / \sigma_x^2$	0 (noise-free)	0.0335%	0.1588%	0.8819%	2.2234%	3.9414%
MAPE (%)	0.43	1.08	1.34	8.52	33.35	37.74

The results demonstrate that the algorithm is robust to noise i.e. the approximation error remains relatively small even for significant levels of noise which in practice would make it extremely difficult to reconstruct the map based on time series data (Aguirre & Billings 1995b, Aguirre & Billings 1995a).

3.6 Conclusions

There are some practical situations in which the individual point trajectories of a chaotic system cannot be measured directly, and the only information available is in the form of probability density functions. As a result, the problem of inferring the

mathematical model can be studied with sequences of probability density functions, instead of massive individual point orbits by means of traditional strategies of model identification.

Previous research generally focused on the problem of deriving a potential transformation only based on the invariant density, which is the so-called classical inverse Frobenius-Perron problem. The shortcoming of the approach is that it cannot guarantee uniqueness of the solution. There are many transformations that share the same invariant density but exhibit distinct dynamical behaviour. The new methodology introduced in this chapter addresses this issue by using a temporal sequence of density functions generated by the underlying system, which allows the unique chaotic map can be recovered. The system identification approach involves determining the Markov partition by minimising the established cost function firstly, then recovering the Frobenius-Perron matrix, finally constructing the piecewise linear semi-Markov transformation on the Markov partition. The effectiveness of the algorithms was demonstrated using numerical simulations for a noise-free system. Furthermore, small noise perturbed case was also studied to show the applicability of the method to practical systems.

Chapter 4
A Solution to the Generalised Inverse Frobenius-Perron Problem for Continuous One-Dimensional Chaotic Maps

4.1 Introduction

The previous chapter introduced a matrix-based approach to the generalised inverse Frobenius-Perron problem (GIFPP) for a special class of one-dimensional bounded piecewise monotonic transformations known as piecewise linear semi-Markov transforms. These transformations can be regarded as a special type of nonlinear transformations constituted by finite linear branches on disjointed intervals. Nonetheless, in general most practical systems are nonlinear on each interval of domain, and even fractions of transformations are not homeomorphism, therefore, they are not Markov transformations. It is interesting to explore the strategy of reconstructing the nonlinear map with observed sequences of probability density functions yielded by the system.

Since Frobenius-Perron matrix is non-negative, and positive entry is defined by $|(S|_{Q_k^{(i)}})'|^{-1}$, for a known piecewise linear semi-Markov transformation *S*, there exists a unique corresponding Frobenius-Perron matrix ***M***, but not vice versa. i.e. *S* is not the only transformation that possesses the Frobenius-Perron matrix ***M***.

Therefore, given a Frobenius-Perron matrix, the monotonicity of the transformation $S|_{R_i}$ is not determined as the slope could be positive or negative. The developed approach to GIFPP for piecewise linear semi-Markov transformations is devised under the assumption that each branch $S|_{R_i}$ is monotonically increasing. But for continuous nonlinear transformations, it is imperative to determine the monotonicity of $S|_{R_i}$ i.e. monotonically increasing or decreasing.

This chapter extends the approach to reconstructing piecewise linear semi-Markov transformations from sequences of densities to more general nonlinear maps. Ulam (1960) conjectured that for one-dimensional systems the infinite-dimensional Frobenius-Perron operator can be approximated arbitrarily well by a finite-dimensional Markov transformation defined over a uniform partition of the interval of interest. The conjecture was proven by Li (1976) who also provided a rigorous numerical algorithm for constructing the finite-dimensional operator when the one-dimensional transformation *S* is known. The purpose in this chapter is to generalise the developed solution to GIFPP for continuous nonlinear systems, specifically, to construct from sequences of probability density functions a piecewise linear semi-Markov transformation $\hat{S}$ which approximates the original continuous nonlinear map *S*.

In the following section, the methodology of deriving the map for continuous nonlinear systems is presented. In particular, it involves the algorithms of a two-step optimisation calculation for obtaining the Frobenius-Perron matrix of the corresponding the approximate piecewise linear $\Re$-semi-Markov transformations to the nonlinear map, and determining the monotonicity of the nonlinear map on each interval of $\Re$. A numerical example is then given to illustrate the applicability of the algorithms.

4.2 Methodology

The main assumptions of the developed methodology are as follows

a) The transformation $S: I \to I$ is continuous, $I = [a, b]$;

b) The Frobenius-Perron operator $P_S : L^1 \to L^1$ associated with the transformation S has a unique stationary density f^* which can be estimated based on the observed data;

c) For $n \to \infty$, $P_S^n f \to f^*$ for every $f \in \mathfrak{D}$ i.e. the sequence $\{P_S^n\}$ is asymptotically stable.

Asymptotic stability of $\{P_S^n\}$ has been established for certain classes of piecewise $\mathbb{C}^2$ maps. For example, the following theorem was proven in (Lasota & Mackey 1994).

Theorem 4.1 *If* $S:[0,1] \to [0,1]$ *is a piecewise monotonic transformation satisfying the conditions*:

a) There is a partition $0 < c_1 < \ldots < c_{N-1} < 1$ *such that the restriction of S to an interval* $R_i = (c_{i-1}, c_i)$ *is a* $\mathbb{C}^2$ *function*;

b) $S(R_i) = (0,1)$;

c) $|S'(x)| > 1$ *for* $x \neq c_i$;

d) There is a finite constant ψ *such that*

$$-S''(x)/[S'(x)]^2 \leq \psi\ ,\ x \neq c_i,\ i = 1, \ldots, N-1, \tag{4.1}$$

then $\{P_S^n\}$ *is asymptotically stable*.

By using a change of variables, it is sometimes possible to extend the applicability of the above theorem to more general transformations, such as the logistic map (Lasota & Mackey 1994) , which does not satisfy the restrictive conditions on the derivatives of *S*.

The procedures of the generalised solution are briefly stated as follows

Step 1: Identify the optimal Markov partition $\mathfrak{R}$ prepared for deriving the Frobenius-Perron matrix corresponding to the piecewise linear semi-Markov map close to the original continuous nonlinear map;

Step 2: Identify the Frobenius-Perron matrix ***M*** from the sequences of probability densities generated by *S* in the first stage. Then refine the resulting matrix by implementing a second optimisation in which the zero entries are specified.

Step 3: determine the monotonicity (monotonically increasing or decreasing) of the constructed point transformation $\hat{S}\big|_{R_i}$ on each interval of $\mathfrak{R}$.

Step 4: Smooth the constructed piecewise linear map to make it more close to the potential continuous nonlinear map.

4.2.1 Identification of the optimal Markov partition

For a nonlinear transformation $S: I \to I$, $I = [a,b]$, the invariant density $f^* \in \mathfrak{D}$ is not piecewise constant. The Frobenius-Perron operator associated with *S* cannot be represented by a square matrix. By constructing a piecewise linear semi-Markov transformation $\hat{S}$ close the original continuous nonlinear map, the Frobenius-Perron equation can also be written in the following matrix form of equality.

$$P_{\hat{S}} f_n = f_n \boldsymbol{M}_{\hat{S}}, \tag{4.2}$$

where $P_{\hat{S}}$ is the Frobenius-Perron operator associated with $\hat{S}$, and $\boldsymbol{M}_{\hat{S}}$ is the Frobenius-Perron matrix induced by $\hat{S}$.

For the invariant density, it follows that

$$\hat{f}^* = \hat{f}^* \boldsymbol{M}_{\hat{S}}. \tag{4.3}$$

where $\hat{f}^* \in \mathfrak{F}$ denotes the piecewise constant density approximating f^*.

As a consequence, the approach used to determine the Markov partition for piecewise linear transformation in Section 3.3.1 of the previous chapter is also used here to determine the optimal Markov partition for the piecewise linear approximation of the unknown nonlinear map.

4.2.2 Identification of the Frobenius-Perron matrix

For the Markov partition

$$\Re = \{R_1, R_2, \ldots, R_N\} = \{[a, c_1], (c_1, c_2], \ldots, (c_{N-1}, b]\}, \tag{4.4}$$

the Frobenius-Perron matrix can be tentatively identified using the approaches described in Section 3.3.2, and is denoted by $\tilde{\boldsymbol{M}} = (\tilde{m}_{i,j})_{1 \le i, j \le N}$.

Since S is continuous on I, $\bigcup_{k=1}^{p(i)} R_{r(i,k)}$ is a connected union of intervals where $R_{r(i,k)} = S(Q_k^{(i)}) \in \Re$, $i = 1, \ldots, N$, $k = 1, \ldots, p(i)$. Here $r(i,k) \in \{1,..., N\}$ are the column indices of non-zero entries on the i-th row of the Frobenius-Perron matrix which satisfy

$$r(i, k+1) = r(i, k) + 1, \tag{4.5}$$

for $i = 1, ..., N$, $k = 1, \ldots, p(i) - 1$. This implies that the positive entries are contiguous, and that the else entries on the i-th row should be 0, which can be expressed as

$$m_{i,j} = 0, \tag{4.6}$$

for $i = 1, ..., N$, $j = 1, \ldots, N, j \neq r(i,k)$.

In order to ensure the identified Frobenius-Perron matrix meets the above conditions, the first step is to determine the indices $r(i,k)$ of the non-zero entries on each row. Let $r^m(i, k^m)$ be the index of the entry of which

$$\lambda(Q_{k^m}^{(i)}) = \max\{\lambda(Q_k^{(i)})\}_{k=1}^{p(i)} = \max\{\lambda(R_r) \cdot \tilde{m}_{i,r}\}. \tag{4.7}$$

It represents the longest subinterval within the interval R_i which can be interpreted as the predominant support of the transformation $\hat{S}\big|_{R_i}$.

Therefore,

$$m_{r^m(i,k^m)} \neq 0, \tag{4.8}$$

Thus, $r^m(i,k^m) \in \{r(i,k)\}_{k=1}^{p(i)}$, $r(i,1) \leq r^m(i,k^m) \leq r(i,p(i))$.

$\bigcup_{k'=k'_1}^{k'_{p(i)}} R_{r'(i,k')}$ is the connected union of intervals involving $R_{r^m(1,k^m)}$, where $R_{r'(i,k')} = \tilde{S}(Q_{k'}^{(i)}) \in \Re$. Consequently, the indices of non-zero entries on the *i*-th row of the desired Frobenius-Perron matrix $\boldsymbol{M} = (m_{i,j})_{1 \leq i,j \leq N}$ associated with the piecewise linear $\Re$ -semi-Markov transformation which is more closer to the nonlinear map can be determined by

$$\begin{aligned} r(i,1) &= r'(i,k'_1), \\ r(i,p(i)) &= r'(i,k'_{p(i)}). \end{aligned} \tag{4.9}$$

As a result, for the *i*-th row of matrix $\boldsymbol{M}$

$$\begin{cases} m_{i,j} > 0, & r'(i,k'_1) \leq j \leq r'(i,k'_{p(i)}); \\ m_{i,j} = 0, & \text{otherwise.} \end{cases} \tag{4.10}$$

The final Frobenius-Perron matrix $\boldsymbol{M}$ is obtained as a solution to the following constrained optimisation problem

$$\min_{\{m_{i,j}\}_{i,j=1}^{N} \geq 0} \| \boldsymbol{W}_1 - \boldsymbol{W}_0 \boldsymbol{M} \|_F, \tag{4.11}$$

where $\boldsymbol{W}_0$ and $\boldsymbol{W}_1$ are the densities matrices produced in Section 3.3.2,

subject to

$$\sum_{k=1}^{p(i)} m_{i,r(i,k)} \lambda(R_{r(i,k)}) = \lambda(R_i), \tag{4.12}$$

$m_{i,j} \geq 0$ if $j = r(i,k), k = 1,..., p(i)$, and $m_{i,j} = 0$ if $j \neq r(i,k), k = 1,..., p(i)$.

4.2.3 Reconstruction of the transformation from the Frobenius-Perron matrix

The method for constructing a piecewise linear approximation $\hat{S}(x)$ over the partition $\Re$ is augmented to take into account the fact that the underlying transformation is continuous and that on each interval of the partition, $S|_{R_i}$ is either monotonically increasing or decreasing. The entries of the positive Frobenius-Perron matrix are used to calculate the absolute value of the slope of $\hat{S}_{Q_k^{(i)}}$ as $|\hat{S}|_{Q_k^{(i)}}| = 1/m_{i,j}$. A simple algorithm was derived to decide if the slope of $\hat{S}|_{Q_k^{(i)}}$ on the interval R_i is positive or negative.

Let $I_i = [c_{r(i,1)-1}, c_{r(i,p(i))}]$ for $i = 1, \ldots, N$, be the image of the interval R_i under the transformation $\hat{S}$ which induce the identified Frobenius-Perron matrix $\boldsymbol{M}$. $c_{r(i,1)-1}$ is the starting point of $R_{r(i,1)}$ which is the image of the subinterval $Q_1^{(i)}$, and $c_0 = a$ if $r(i,1) = 1$. $c_{r(i,p(i))}$ is the end point of $R_{r(i,p(i))}$ which is the image of the subinterval $Q_{p(i)}^{(i)}$. As before, $\{r(i,k)\}_{k=1}^{p(i)}$ denote the column indices corresponding to the non-zero entries in the *i*-th row of $\boldsymbol{M}$.

Let $\bar{c}_i = \frac{1}{2}[c_{r(i,1)-1}, c_{r(i,p(i))}]$ be the midpoint of the image I_i. The sign $\sigma(i)$ of $\{\hat{S}'(x)|_{Q_k^{(i)}}\}_{k=1}^{p(i)}$ is given by

$$\sigma(i) = \begin{cases} -1, & \text{if } \bar{c}_i - \bar{c}_{i-1} < 0; \\ 1, & \text{if } \bar{c}_i - \bar{c}_{i-1} > 0;, \\ \sigma(i-1) & \text{if } \bar{c}_i = \bar{c}_{i-1}, \end{cases} \tag{4.13}$$

for $i = 2, \ldots, N$ and $\sigma(1) = \sigma(2)$.

Given that the derivative of $S|_{Q_k^{(i)}}$ is $1/m_{i,j}$, the end point $q_k^{(i)}$ of subinterval $Q_k^{(i)}$ within R_i is given by

$$q_k^{(i)} = \begin{cases} c_{i-1} + \sum_{j=1}^{k} m_{i,r(i,j)} \lambda(R_{r(i,j)}), & \text{if } \sigma(i) = +1; \\ c_{i-1} + \sum_{j=1}^{k} m_{i,r(i,p(i)-k+1)} \lambda(R_{r(i,p(i)-k+1)}), & \text{if } \sigma(i) = -1. \end{cases} \tag{4.14}$$

where $k = 1,..., p(i)-1$ and $q_{p(i)}^{(i)} = c_i$.

The piecewise linear semi-Markov transformation for each subinterval $Q_j^{(i)}$ is given by

$$\hat{S}_{Q_j^{(i)}}(x) = \begin{cases} \frac{1}{m_{i,j}}(x - a - q_{k-1}^{(i)}) + c_{j-1}, & \text{if } \sigma(i) = +1; \\ -\frac{1}{m_{i,j}}(x - a - q_{k-1}^{(i)}) + c_j, & \text{if } \sigma(i) = -1, \end{cases} \tag{4.15}$$

for $i = 1,\ldots, N,\ j = 1,\ldots, N,\ k = 1,..., p(i)-1,\ m_{i,j} \neq 0$.

The construction of the piecewise linear semi-Markov transformation $\hat{S}(x)$ to approximate the original continuous nonlinear map $S(x)$ is depicted in Figure 4.1.

4.2.4 Smoothing of the constructed piecewise linear semi-Markov map

Since the constructed map is piecewise on the identified Markov partition, in order to make it more close to the original map that is continuous on *I*, a smooth version of the estimated transformation can be obtained by fitting a polynomial smoothing spline.

A set of initial states $X_0 = \{x_{0,j}\}_{j=1}^{\theta}$ which are uniformly distributed on *I* were iterated one time using the constructed piecewise linear $\Re$ -semi-Markov transformation $\hat{S}(x)$ to yield a corresponding new states $X_0 = \{x_{1,j}\}_{j=1}^{\theta}$. The new states can be regarded as noise-like data to smooth the piecewise map. The smoothing spline can be obtained as the solution of the following optimisation problem

$$\min\left\{\frac{\gamma}{\theta}\sum_{j=1}^{\theta}(\bar{S}(x_{0,j})-x_{1,j})^2+(1-\gamma)\int_I\left(\frac{d^2\bar{S}}{dx^2}\right)^2 dx\right\}, \tag{4.16}$$

where γ is the smoothing parameter.

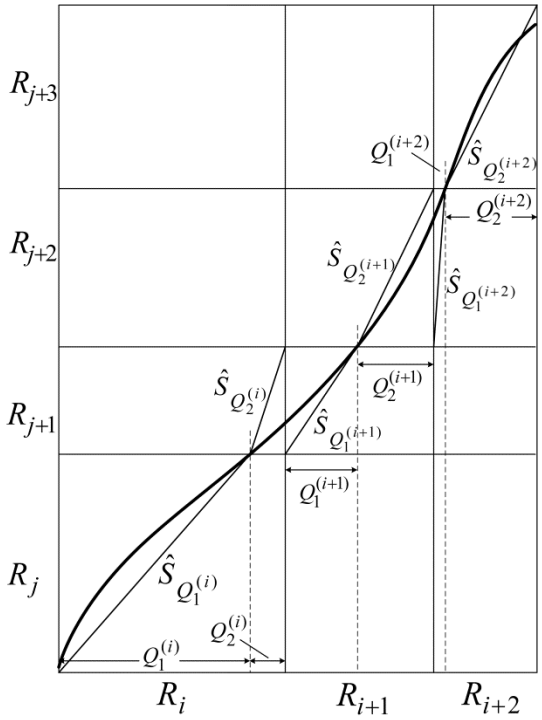

Figure 4.1 Construction of a piecewise linear semi-Markov transformation approximating the original continuous nonlinear map.

4.3 Numerical simulations

To demonstrate the use of the extended algorithm, the following quadratic (logistic) transformation without noise disturbance depicted in Figure 4.2 is considered.

$$S(x)=4x(1-x), \tag{4.17}$$

It can be shown that $\{P_S^n\}$ associated with this transformation is asymptotically stable.

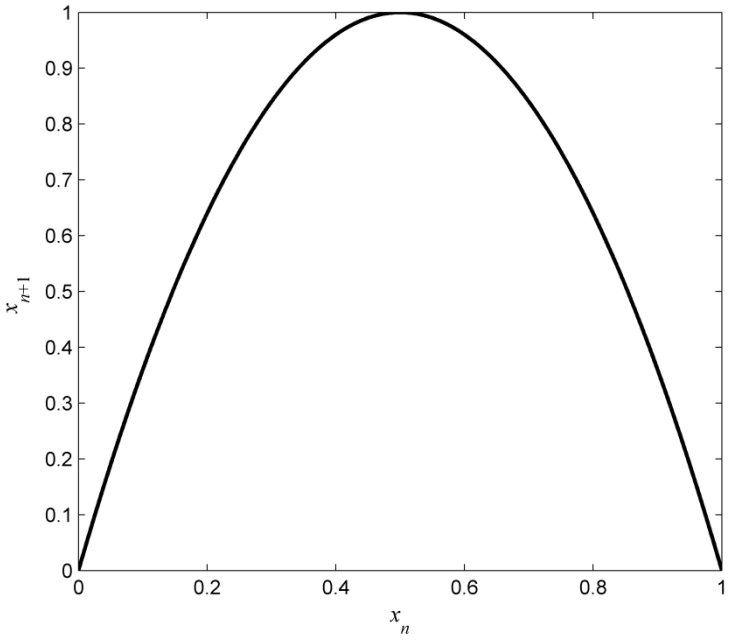

Figure 4.2 Original continuous nonlinear transformation *S*.

A set of initial states $X_0 = \{x_{0,j}\}_{j=1}^{\theta}$, $\theta = 5 \times 10^3$, generated by sampling from a uniform probability density function $f_0(x) = \chi_{[0,1]}(x)$, were iterated using S to generate a corresponding set of final states $X_T = \{x_{T,j}\}_{j=1}^{\theta}$ where $T = 30{,}000$. The data set X_T was used to search for an uniform partition Δ with N' intervals, $1 \le N' \le \lfloor \theta / \log \theta \rfloor = 587$, which maximises the penalised log-likelihood function

$$L_\theta(N') - p(N') = \left[\sum_{i=1}^{N'} D_i \log(N' D_i / \theta) \right] - \left[N' - 1 + (\log N')^{2.5} \right], \qquad (4.18)$$

defined in Section 3.4.1. It is obtained that $N' = 145$ for this case. The estimated invariant density $f_C^*(x)$ with respect to the 145-interval partition is shown in Figure 4.3.

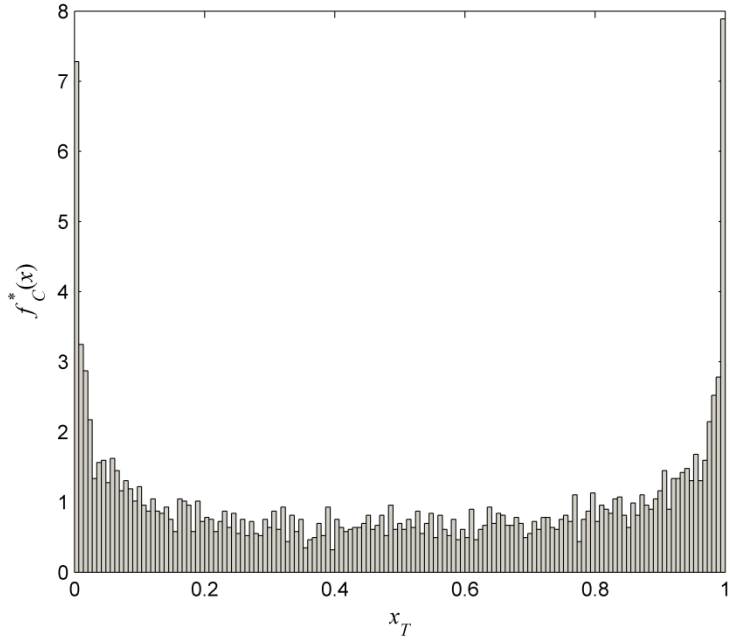

Figure 4.3 Chapter 4 numerical example: Initial regular histogram based on a 145-interval uniform partition.

In this example, the longest strictly monotone subsequence $\overline{L}$ of $L=\{l_j\}_{j=1}^{144}$, $l_j=145|h'_{j+1}-h'_j|$ has 52 elements and the minimisation of

$$\min_{l_j\in\overline{L}}\left\{J(\Re)=\int_I (f_C^*(x)-f_{C_d(\bar{l}_j)}^*(x))^2\,dx\right\}, \tag{4.19}$$

is achieved for $\bar{l}_{20}=0.1560$, as shown in Figure 4.4.

This corresponds to a final Markov partition with 72 intervals. The invariant density on the irregular partition $\Re$ with 72 intervals is shown in Figure 4.5.

To identify the Frobenius-Perron matrix, 100 densities (see Appendix) were randomly sampled to generate 100 sets of initial states $X_0^i=\{x_{0,j}^i\}_{j=1}^{\theta}$, i=1,...,100, $\theta=5\times10^3$. The initial states X_0^i and their images X_1^i under the transformation S were used to estimate the initial and final density functions on $\Re$. Examples of initial and final densities are shown in Figure 4.6.

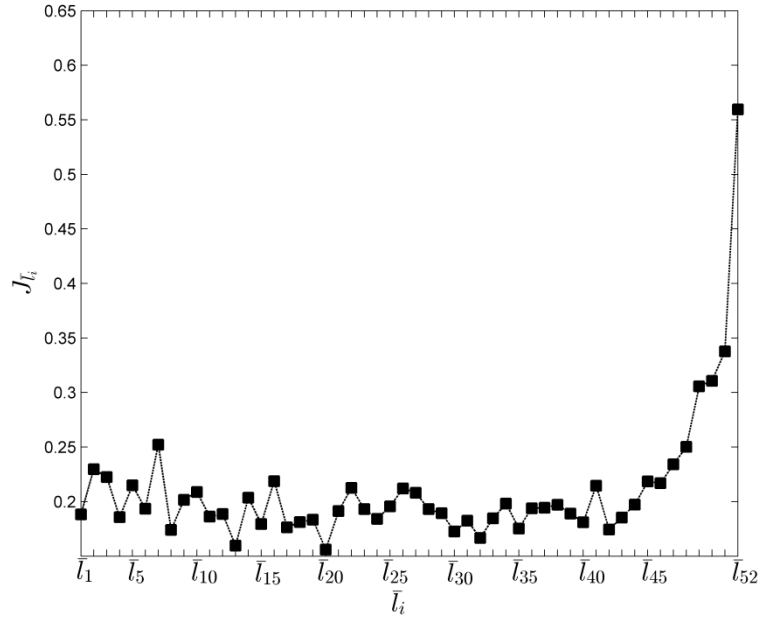

Figure 4.4 Chapter 4 numerical example: The cost function $J_{\bar{l}_j}$, j =1, …, 52.

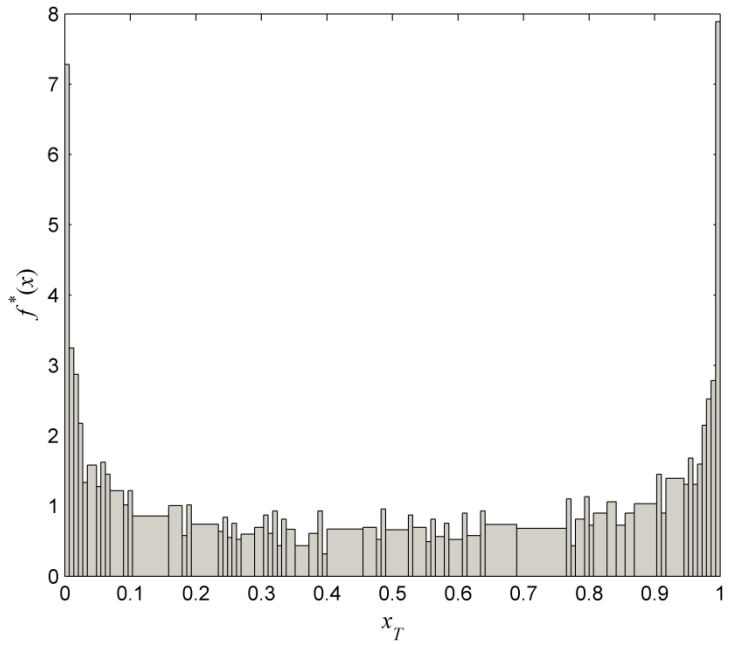

Figure 4.5 Chapter 4 numerical example: The invariant density estimated over the partition $\Re = \{R_i\}_{i=1}^{72}$.

The constructed piecewise linear semi-Markov transformation with respect to the partition $\Re$ is shown in Figure 4.7.

The smoothed map, obtained by fitting a cubic spline (smoothing parameter: 0.999), is shown in Figure 4.8.

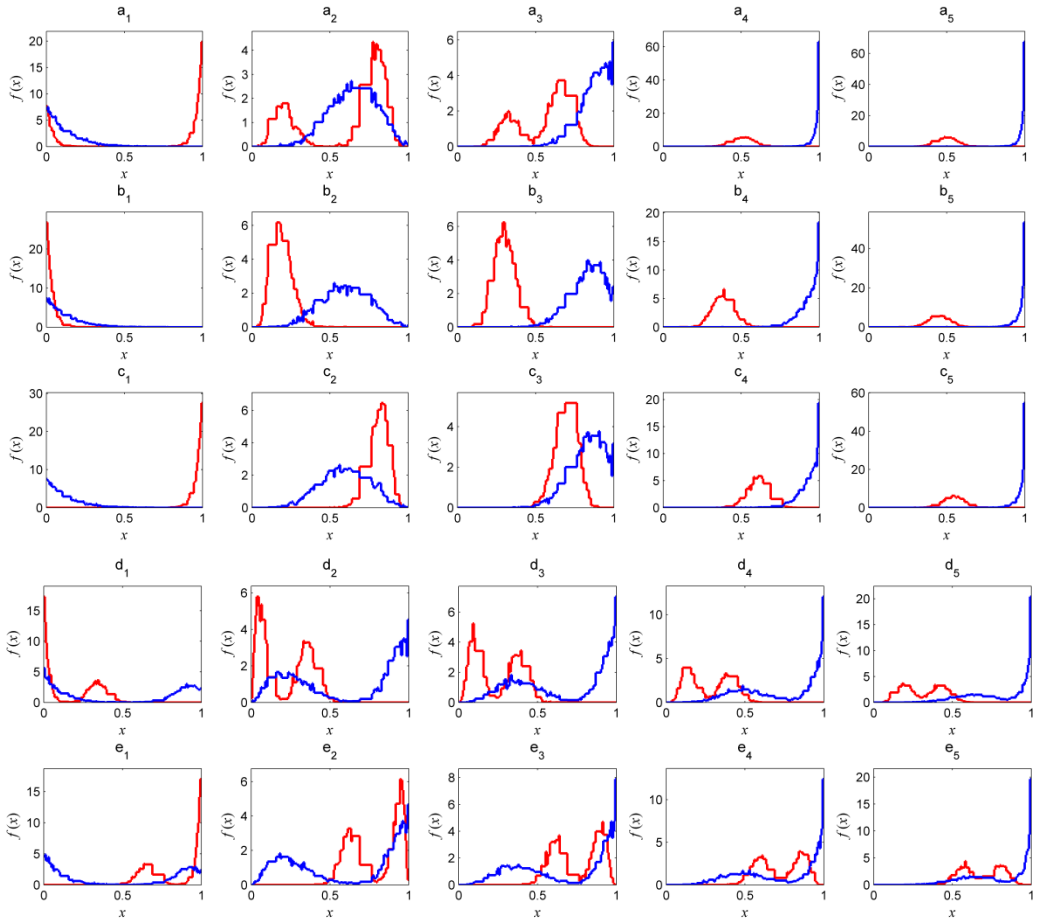

Figure 4.6 Chapter 4 numerical example: Examples of initial densities (red lines) and the corresponding densities after one iteration (blue lines):

a_1: $f^1_{0,1}$, $f^1_{1,1}$; a_2: $f^8_{0,1}$, $f^8_{1,1}$; a_3: $f^{15}_{0,1}$, $f^{15}_{1,1}$; a_4: $f^{27}_{0,1}$, $f^{27}_{1,1}$; a_5: $f^{30}_{0,1}$, $f^{30}_{1,1}$;

b_1: $f^1_{0,2}$, $f^1_{1,2}$; b_2: $f^7_{0,2}$, $f^7_{1,2}$; b_3: $f^{13}_{0,2}$, $f^{13}_{1,2}$; b_4: $f^{27}_{0,2}$, $f^{27}_{1,2}$; b_5: $f^{30}_{0,2}$, $f^{30}_{1,2}$;

c_1: $f^1_{0,3}$, $f^1_{1,3}$; c_2: $f^7_{0,3}$, $f^7_{1,3}$; c_3: $f^{13}_{0,3}$, $f^{13}_{1,3}$; c_4: $f^{27}_{0,3}$, $f^{27}_{1,3}$; c_5: $f^{30}_{0,3}$, $f^{30}_{1,3}$;

d_1: $f^1_{0,4}$, $f^1_{1,4}$; d_2: $f^3_{0,4}$, $f^3_{1,4}$; d_3: $f^5_{0,4}$, $f^5_{1,4}$; d_4: $f^7_{0,4}$, $f^7_{1,4}$; d_5: $f^{10}_{0,4}$, $f^{10}_{1,4}$;

e_1: $f^1_{0,5}$, $f^1_{1,5}$; e_2: $f^3_{0,5}$, $f^3_{1,5}$; e_3: $f^5_{0,5}$, $f^5_{1,5}$; e_4: $f^7_{0,5}$, $f^7_{1,5}$; e_5: $f^{10}_{0,5}$, $f^{10}_{1,5}$.

The relative approximation error between the identified smooth map and the original map calculated in (3.66) is shown in Figure 4.9. It can be seen that for 97 out of the 99 linearly spaced points $x \in X = \{0.01, 0.02, ..., 0.99\}$ $\delta S(x) < 5\%$.

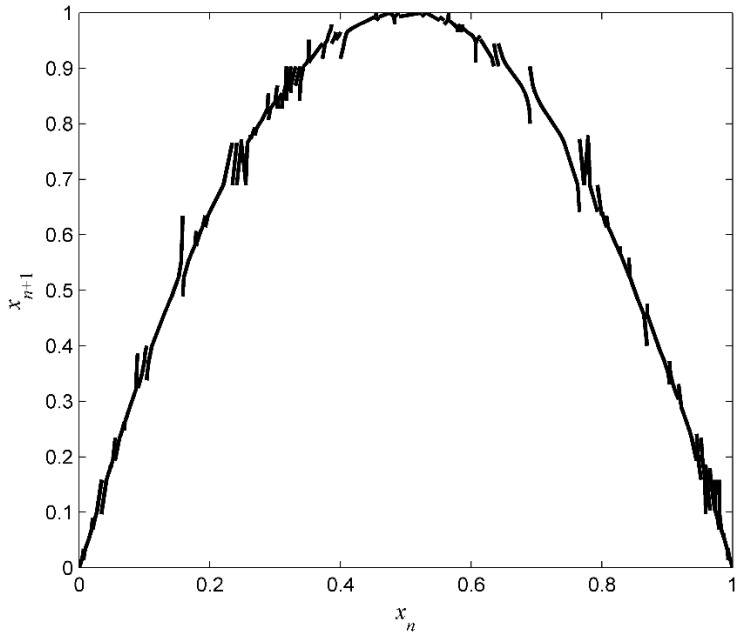

Figure 4.7 Chapter 4 numerical example: Reconstructed piecewise linear semi-Markov map over the irregular partition $\mathfrak{R}$.

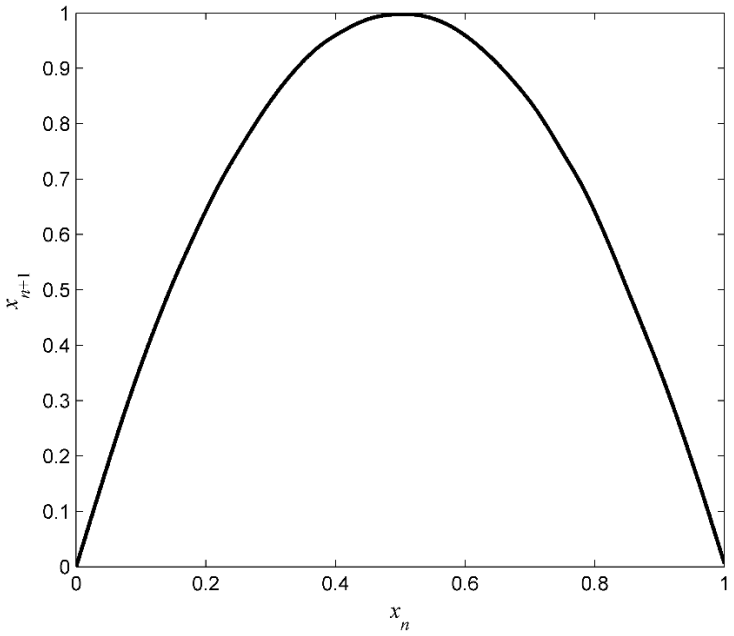

Figure 4.8 Chapter 4 numerical example: Identified smooth map.

The estimated invariant density on $\mathfrak{R}$, obtained by iterating the smoothed map 20,000 times with the initial states X_0, and is shown in Figure 4.10, compared with the true invariant density.

$$f^*(x) = \frac{1}{\pi\sqrt{x(1-x)}}. \tag{4.20}$$

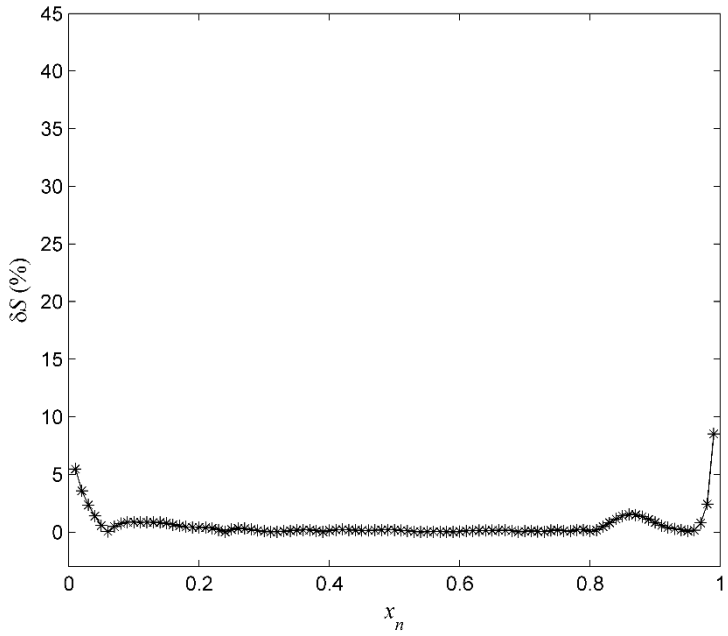

Figure 4.9 Chapter 4 numerical example: Relative error between the original map *S* and the identified map $\overline{S}$ evaluated for 99 uniformly spaced points.

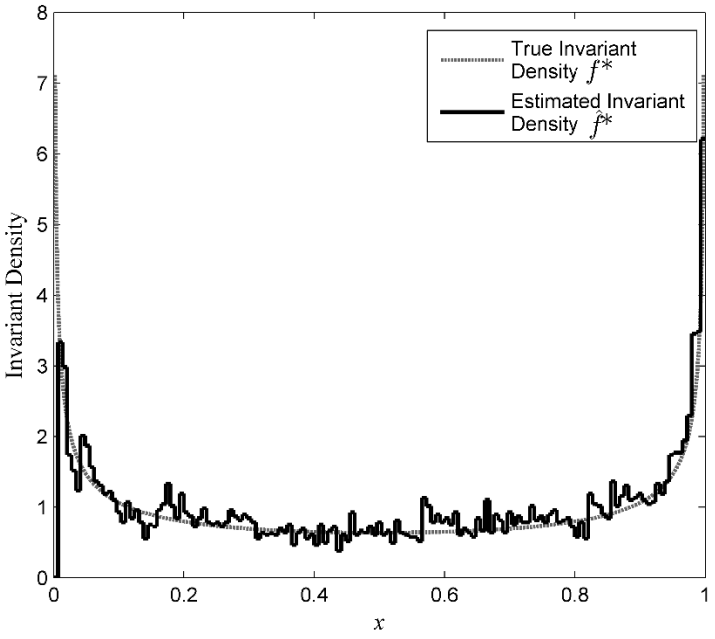

Figure 4.10 Chapter 4 numerical example: The true invariant density of the underlying system (dashed line) and the estimated invariant density of the identified map (solid line) on a uniform partition with 145-intervals.

To examine how noise affects the performance of the generalised solution for continuous one-dimensional chaotic maps, an additive random noise is applied to the logistic map as expressed as follows

$$x_{n+1} = 4x_n(1-x_n) + \alpha\omega_n \qquad (\text{mod } 1), \tag{4.21}$$

where $\{\omega_n\}$ is i.i.d. $N(0,1)$ (white Gaussian noise), and α is a known noise level. A set of Gaussian noise $\Omega = \{\omega_i\}_{i=1}^{\theta}, \theta = 5\times10^3$, the noise maximum magnitude (i.e. $\xi \geq \max(|\omega_n|)$) $\xi = 1/50$ and $\alpha = 0.0335\%$ is taken for example in the first instance.

The invariant density was obtained by iterating S for T times with the noise ω_i applied per iteration. Still using the penalised log-likelihood maximisation for searching the preliminary uniform partition, the resulting invariant density with respect to the uniform partition containing 67 intervals is shown in Figure 4.11.

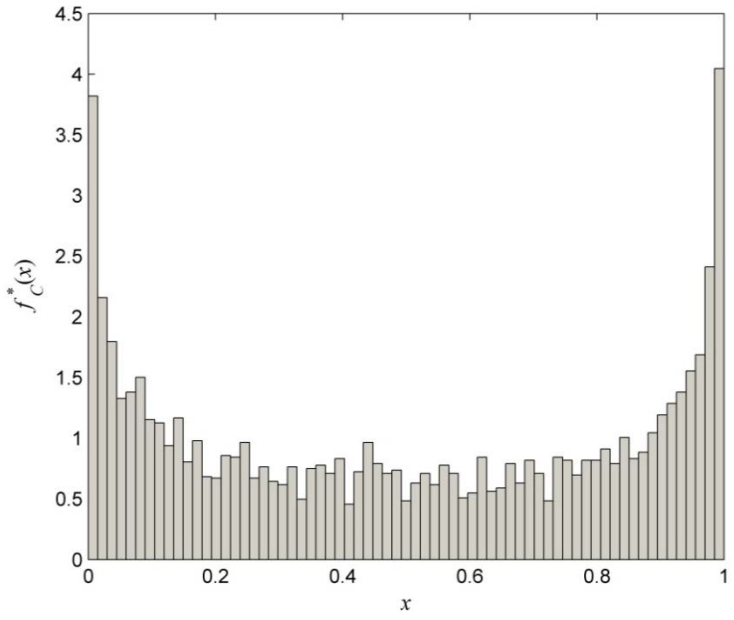

Figure 4.11 Chapter 4 numerical example: Initial regular histogram based on a 67-interval uniform partition.

Figure 4.12 shows the results of the loss function (4.19) corresponding to $\bar{l}_i$ for $i = 1, \ldots, 66$. It can be seen that the minimisation is found at $\bar{l}_{39} = 0.0304$ which

corresponds to a Markov partition involving 31 non-uniform intervals, as shown in Figure 4.12.

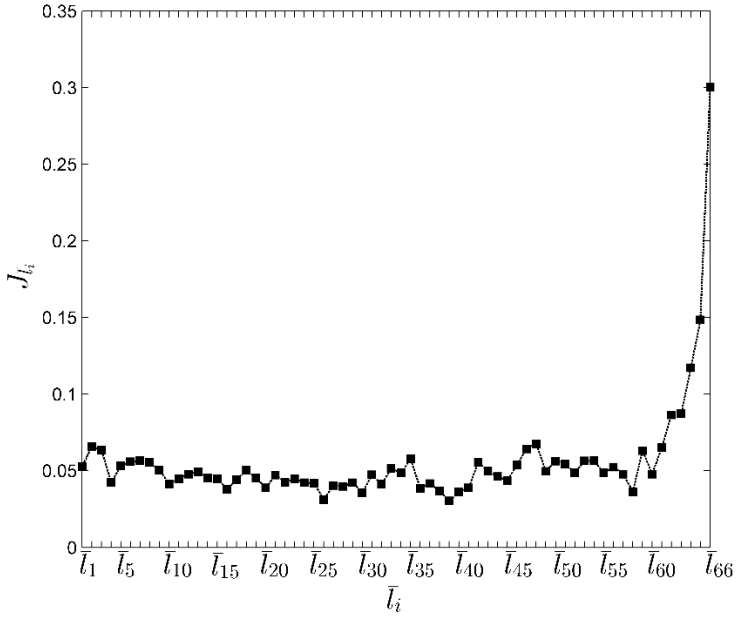

Figure 4.12 Chapter 4 numerical example: The cost function $J_{\bar{l}_j}$, j =1, …, 66.

Figure 4.13 shows the estimated invariant density on the obtained Markov partition $\mathfrak{R}$.

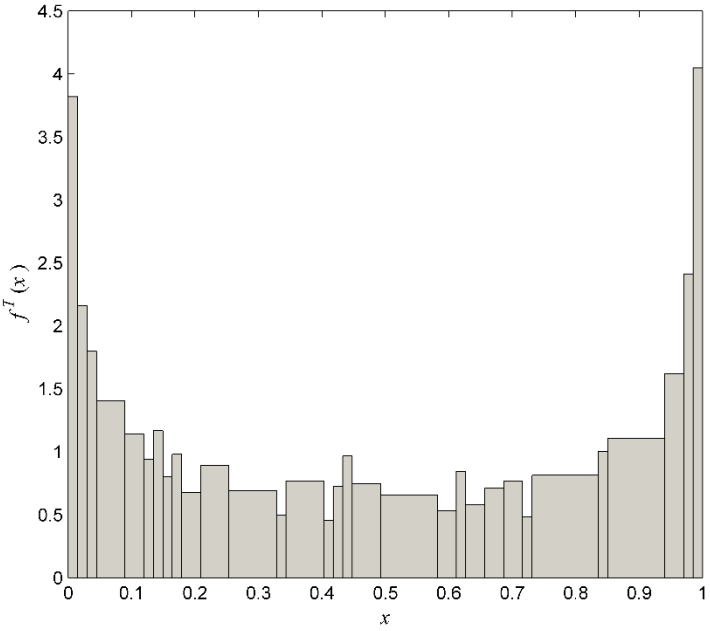

Figure 4.13 Chapter 4 numerical example: The invariant density estimated over the partition $\mathfrak{R} = \{R_i\}_{i=1}^{31}$.

The 100 sets of initial states X_0^i, i=1,...,100, generated in the noise-free case was used to yield the corresponding sets of images X_1^i under the noisy system (4.21). The constructed piecewise linear $\mathfrak{R}$-semi-Markov map is shown in Figure 4.14.

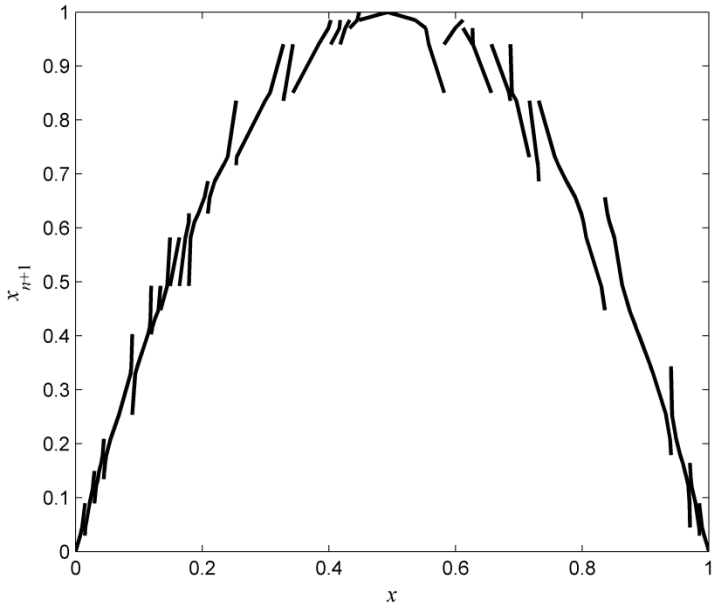

Figure 4.14 Chapter 4 numerical example: Reconstructed piecewise linear semi-Markov map over the irregular partition $\mathfrak{R}$.

The smoothed map obtained with the same smoothing parameter 0.999 is shown in Figure 4.15.

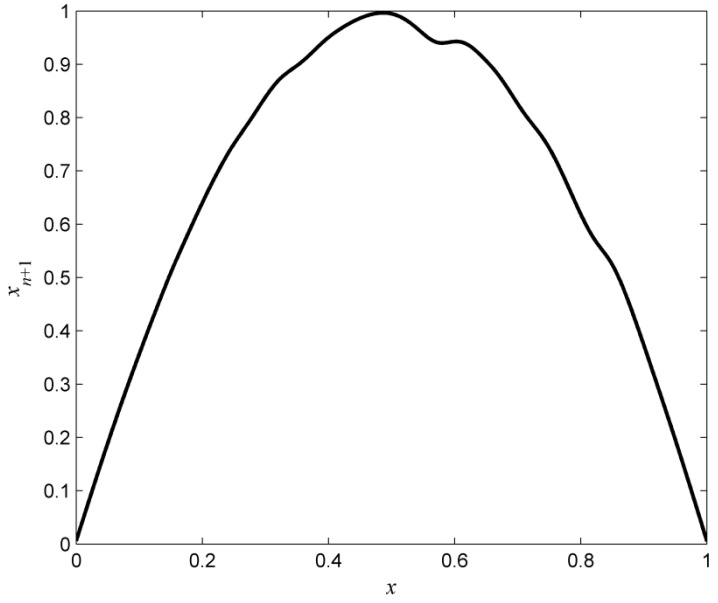

Figure 4.15 Chapter 4 numerical example: Identified smooth map $\overline{S}$.

Figure 4.16 shows the calculated relative error δS on the 99 uniformly spaced points. It can be seen that $\delta S < 5\%$ for 96 points out of them.

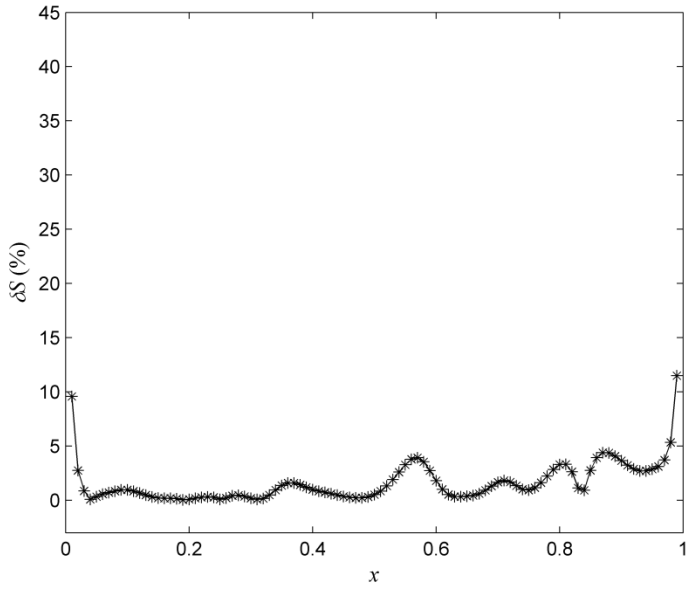

Figure 4.16 Chapter 4 numerical example: Relative error between the original map *S* and the identified smooth map $\overline{S}$ evaluated for 99 uniformly spaced points.

In order to evaluate the performance of the developed algorithms for larger noise levels, Figure 4.17 and Figure 4.18 give the reconstructed maps and relative error for noise level $\alpha = 0.0978\%, 0.5431\%$ ($\xi = 0.04, 0.10$) respectively.

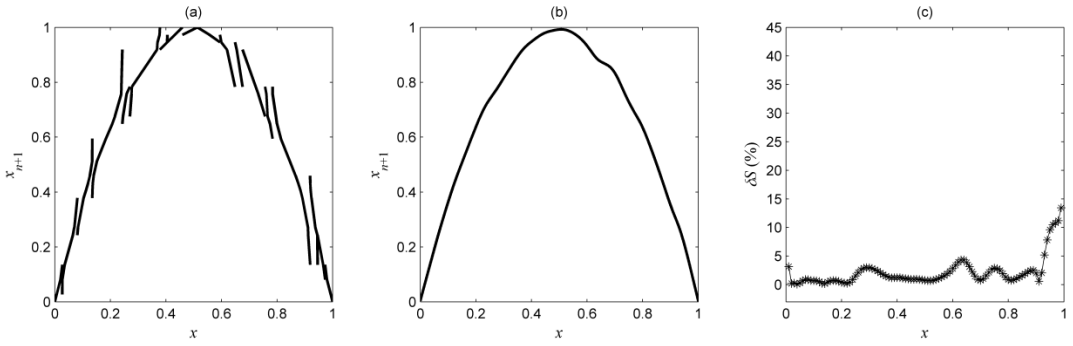

Figure 4.17 Chapter 4 numerical example: (a) Constructed piecewise linear semi-Markov map for $\alpha = 0.0978\%$ ($\xi = 0.04$); (b) The resulting smooth map from the piecewise linear semi-Markov map; (c) The relative error calculated on the 99 uniformly spaced points.

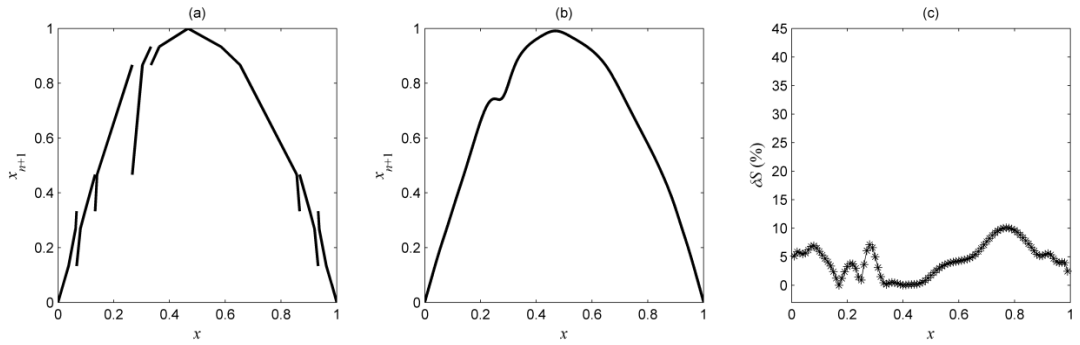

Figure 4.18 Chapter 4 numerical example: (a) Constructed piecewise linear semi-Markov map for $\alpha = 0.5431\%$ ($\xi = 0.10$); (b) The resulting smooth map from the piecewise linear semi-Markov map; (c) The relative error calculated on the 99 uniformly spaced points.

Table 4.1 summarises the MAPE between the reconstructed map $\overline{S}$ and the original map *S* for some various noise levels.

Table 4.1 Reconstruction errors for different noise levels – Example: a continuous nonlinear system example in Chapter 4.

α	0 (noise-free)	0.0206%	0.0978%	0.5431%	1.3692%	2.4272%
ξ	0	0.02	0.04	0.10	0.15	0.20
MAPE (%)	0.61	1.59	2.10	4.424	79.60	84.84

As it can be seen the approximation error remains relatively low (<5%) for levels $\alpha = 0.0206\%,\ 0.0978\%,$ and 0.5431% (noise samples with $\xi = 0.02, 0.04,$ and 0.10 correspondingly) of noise that normally cause severe problems to reconstruction algorithms that use time series data.

4.4 Conclusions

This chapter proposed an extension to the solution to the generalised inverse Frobenius-Perron problem for piecewise linear semi-Markov transformations to more general one-dimensional smooth chaotic maps. The proposed method infers directly from data a piecewise linear semi-Markov map approximation of the original map, which can be subsequently smoothed.

As before, proposed method involves identifying the optimal Markov partition, $\mathfrak{R}$ estimating the Frobenius-Perron matrix and reconstructing the map. Additional algorithms were introduced to identify the non-zero entries Frobenius-Perron matrix and to determine the monotonicity over each interval of the partition. The last step smoothing the piecewise linear map further helps reducing the approximation error.

Numerical simulations involving noise-free as well as noisy data were used to demonstrate the effectiveness of the developed method.

Chapter 5

Characterising the Dynamical Evolution of Heterogeneous Human Embryonic Stem Cell Populations

5.1 Introduction

Human pluripotent stem cells cultured *in vitro* exist as heterogeneous mixture (Stewart, Bossé et al. 2006, Chambers, Silva et al. 2007, Chang, Hemberg et al. 2008, Hayashi, Lopes et al. 2008a, Olariu, Coca et al. 2009, Tonge, Olariu et al. 2010, Tonge, Shigeta et al. 2011). It has been proposed that the heterogeneity with human pluripotent stem cells reflects the existence of a number of functionally relevant, unstable substates that are interconvertible, each of which could be characterised by higher propensity to differentiate into particular somatic cell. In practice, heterogeneity of hESCs has been studied by measuring using flow cytometry the level of particular stem cell surface marker such as that of the Surface Specific Embryonic Antigen (SSEA3) which is used to identify pluripotent hESCs. One of the characteristics of heterogeneous stem cell cultures is that subpopulations sorted according to their level of SSEA3 expression, can regenerate the original parent population in about five – seven days after plating. The process by which the parent population is regenerated produces similar sequence of density functions in separate experiments, suggesting that it could reflect deterministic chaos rather than a purely stochastic process. In this context, the equilibrium

distribution of SSEA3 expression in a population could be seen as the invariant density function associated with the chaotic map.

Here the aim was to apply the methods developed in previous chapters to infer a one-dimensional chaotic map to characterise the dynamical evolution of stem cell populations based on the experimentally observed probability distributions. The reconstructed model could be used to predict the long term evolution of different fractions, to determine equilibrium points and perform local and global stability analysis.

This chapter is organised as follows. The biological background involving NTERA-2 cell line, heterogeneity of the human embryonic stem cells, the cell surface marker SSEA3 used for isolating distinct subpopulations, the fluorescence activated cell sorting machine and the brief experimental process is firstly introduced in Section 5.1. The modelling algorithms are briefly described in Section 5.3. This is followed by the simulation results with experimental data shown in Section 5.4.

5.2 Biological background

This section will briefly introduce related knowledge of the background biological system and the experimental process conducted by the Centre for Stem Cell Biology at the University of Sheffield which is the data provider.

5.2.1 Heterogeneity of hESCs

Embryonic stem (ES) cell are used for analysis of multilineage differentiation within *in vivo* development. The formation of embryoid bodies can show the multilineage differentiation. The orbits of the cell differentiation can be affected by the body size. Thus, the differentiation can be changed by manipulating the size. hESC lines are morphologically and phenotypically heterogenecus. The starting populations of undifferentiated human ES cells are important, as they may affect the differentiation to or away from the desired phenotype. If they are heterogeneous, the differentiated derivatives may also be heterogeneous. Spontaneous differentiation of cells is a source of cell heterogeneity in ES cell cultures (Tonge,

Shigeta et al. 2011). hESCs in culture can be divided into different subsets that can interconvert. The cells are able to interconvert reversibly between different subsets that are functionally non-equivalent but having the capability of multilineage differentiation (Enver, Pera et al. 2009). For example, heterogeneity has been identified in mouse ES cultures for the expression of Nanog and Stella (Tonge, Shigeta et al. 2011). Mouse ES cell can switch reversibly between Nanog positive and negative states (Chambers, Silva et al. 2007). A dynamic equilibrium within the ES cultures is represented by the fluctuating levels of Stella expression (Hayashi, Lopes et al. 2008b). The different expression marks functionally distinct cells. It has been known that undifferentiated hESCs contain functionally distinct subsets. The regulatory genes associated with the pluripotent state are co-expressed with lineage specific transcription factors at early stage of stem cell differentiation (Laslett, Grimmond et al. 2007).

5.2.2 NTERA-2

The experimental data was generated using the NTERA-2 cell line which is a clonally derived, pluripotent human embryonal carcinoma cell line (Stevens 1966, Solter & Damjanov 1979, Andrews, Damjanov et al. 1984, Lee & Andrews 1986). It has many similar characteristics to hESCs, in particular, expresses the same markers of pluripotency as hESCs, including the SSEA3 marker (Pera, Cooper et al. 1989, Draper, Pigott et al. 2002a, Walsh & Andrews 2003). The NTERA-2 cell line has been extensively used as a model of human neurogenesis. It can differentiate into neuronal, glial, and oligodendrocytic lineages *in vitro* (Fenderson, Andrews et al. 1987, Rendt, Erulkar et al. 1989, Pleasure & Lee 1993, Miyazono, Lee et al. 1995, Bani-Yaghoub, Felker et al. 1999, Philips, Muir et al. 1999), in response to retinoic acid (Andrews 1984). The differentiated derivatives of the human embryonal carcinoma cell line contain cells with phenotypic properties of neurons. By manipulating the exposure to retinoic acid, the differentiation can be easily controlled. When NTERA-2 cells mature, the differentiation results in a relatively homogenous population of neurons with functionally appropriate properties. NTERA-2 cell line is a useful tool to explore the early development of human nervous system and identify the genes that are engaged in neurogenesis.

5.2.3 Cell surface antigen maker SSEA3

Undifferentiated hESCs are highly unstable and tend to spontaneously differentiate under standard culture conditions. The differentiation is characterised by marked changes in gene expression (Ackerman, Knowles et al. 1994). In other words, the differentiation can be monitored by observing the changes in the expression of cell surface antigens, because the expression of cell surface antigen can be readily evaluated on single cell in complex differentiating populations, and the isolated single antigen can be used to analyse the properties and explore the further differentiation of the individual antigen. Functionally distinct subsets of undifferentiated hESCs can be studied by surface antigen markers such as SSEA3 (Enver, Soneji et al. 2005).

SSEA3 is a cell surface antigen that is rapidly down-regulated as hESCs differentiate to more mature cell types (Shevinsky, Knowles et al. 1982, Draper, Pigott et al. 2002b). It can be used to observe the changes from undifferentiated state to differentiated state of the cells. The NTERA2 pluripotent cell line is comprised of stem cells which have different expression levels of SSEA3 surface antigen. It has been reported that SSEA3 expression positively correlates with the probability of a NTERA2 cell to clonal expansion (Andrews 1984). It has been found that substates $SSEA3^{positive}$ and $SSEA3^{negative}$ that are divided from undifferentiated hESCs in culture have different expression of SSEA3.

5.2.4 Fluorescence activated cell sorting

Fluorescence activated cell sorting (FACS) is a flow cytometry approach that allows fractionating a population of live cells that are phenotypically different from each other into sub-populations based on fluorescent labelling. FACS enables fast and quantitative recording fluorescent signals of individual cells as well as physically isolating cells of particular interest. Figure 5.1 shows the diagram explaining FACS. The process begins injecting some samples containing cells into a flask, and the sample is then funnelled to generate a single cell line. When the cells flow down, they are scanned by a laser beam that is used to count the cells as well as measure the size of the cells. Each single cell enters a single droplet which

is then given electronic charge. When the cells are in the area between the deflection plates, the cell will be attracted or repelled into corresponding plates. Then the sorted cell can be cultured.

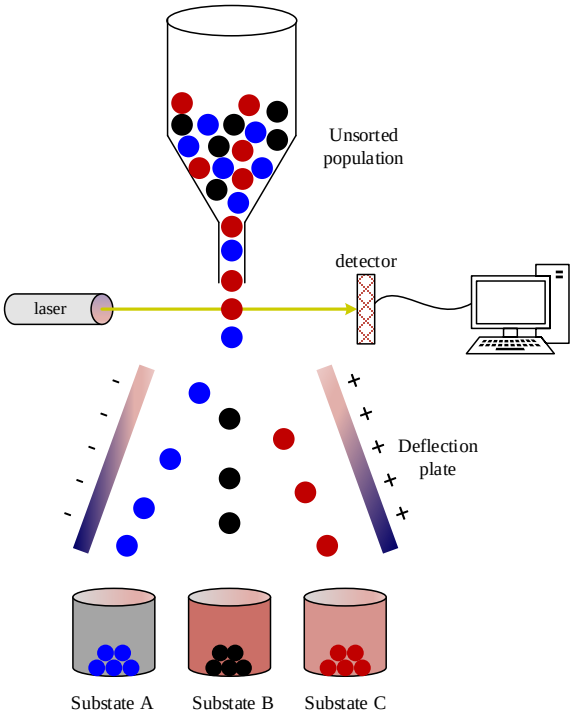

Figure 5.1 Diagram of FACS machine.

5.2.5 Experimental process

Figure 5.2 shows the process of cell culturing experiments. The initial unsorted cell populations are prepared for sorting by the FACS machine into some different subpopulations which are isolated by the cell surface marker SSEA3. On the initial day, the sorted cell subpopulations are treated as the initial state for the following differentiation. On each sampling day, the flow cytometry distributions of markers are measured. This will generate the sequences of probability density functions of the SSEA3 $\{f_1^i, f_2^i, f_3^i, \ldots\}$, which will be used for modelling for the heterogeneous cell populations.

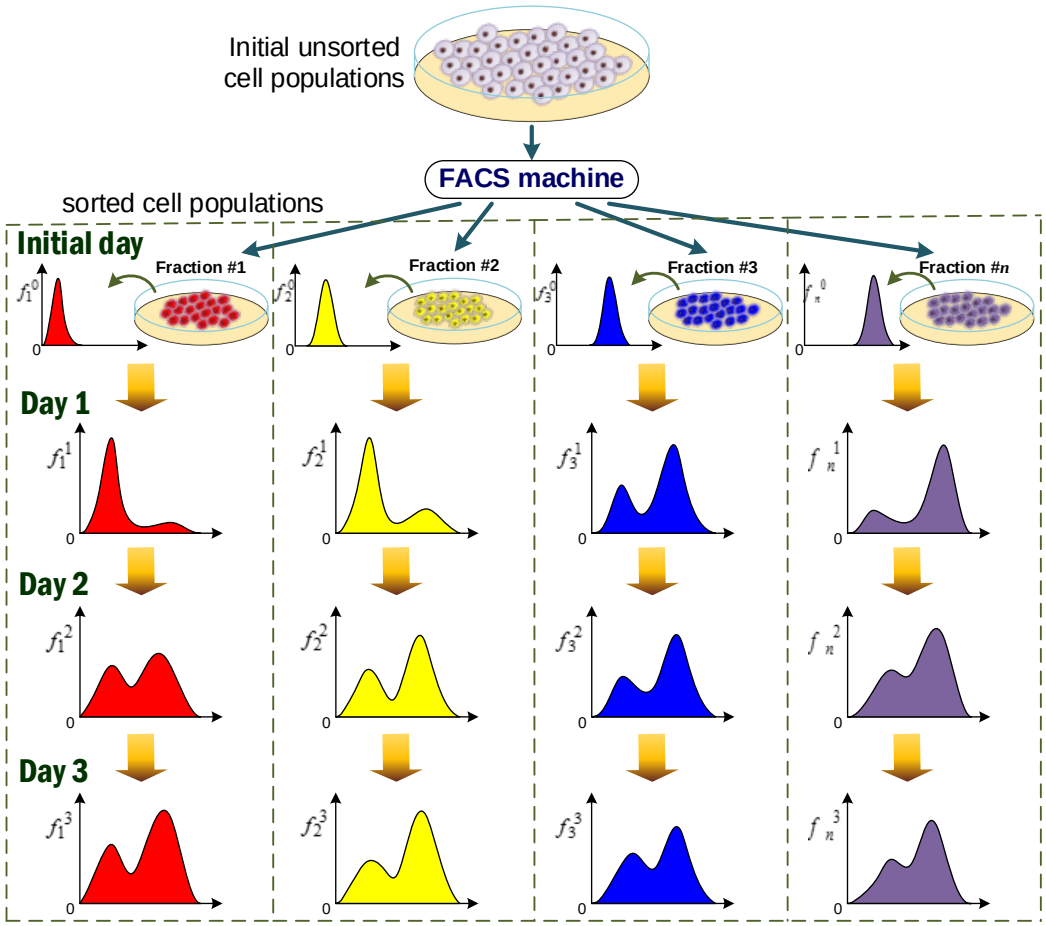

Figure 5.2 Diagram of the experimental process example. For each measured distribution, the horizontal axis represents the SSEA3-FITC (Fluorescein isothiocyanate) fluorescent intensity; the vertical axis represents the probability density.

5.3 Modelling algorithms

The aim is to reconstruct a piecewise linear semi-Markov transformation for the stem cell population, which characterises the dynamical evolution of the heterogeneous cell populations based on temporal sequences of probability density function generated from the cell culturing experiments. For each substate, starting from a distinct initial population, a sequence of probability density functions can be observed as listed in Table 5.1.

Table 5.1 Observed sequences of probability density functions for each fraction.

Fraction	Density observations
#1	$f_1^0, f_1^1, f_1^2, \ldots, f_1^T$

#2	$f_2^0, f_2^1, f_2^2, \ldots, f_2^T$
#3	$f_3^0, f_3^1, f_3^2, \ldots, f_3^T$
⋮	⋮
$\# F_N$	$f_{F_N}^0, f_{F_N}^1, f_{F_N}^2, \ldots, f_{F_N}^T$

It is assumed that a stationary distribution can be reached after T days of evolution from an initial unsorted population, whereby the invariant density f^* associated to the unknown semi-Markov transformation is measured.

The procedures of reconstructing the piecewise linear semi-Markov estimate are stated as follows:

Step 1: An initial uniform partition Δ with N' equal intervals can be determined from the invariant density observed from an unsorted cell population $F_{unsorted}$ on the sampling day T, by solving the maximisation of the following penalised log-likelihood function

$$\max_{N' \in [1, \theta/\log\theta]} \left\{ \left[\sum_{i=1}^{N'} D_i \log(N' D_i / \theta) \right] - \left[N' - 1 + (\log N')^{2.5} \right] \right\}, \tag{5.1}$$

where θ is the number of $F_{unsorted}$ samples $\{x_j^*\}_{j=1}^{\theta}$ at sampling day T, $D_i = \sum_{j=1}^{\theta} \chi_{\Delta_i}(x_j^*)$.

Step 2: Select a non-uniform partition of which the cut points are included by that of the uniform partition Δ, over which the probability density functions of the observed experimental data are estimated.

Step 3: Identify the Frobenius-Perron matrix estimate over the non-uniform partition based on the constructed density functions, using the proposed approach in Section 3.3.2.

Step 4: Construct the piecewise linear map $\hat{S}$ corresponding to the Frobenius-Perron matrix representation.

Step 5: Compute the invariant density $f^*_{C_d(\bar{l}_j)}$ associated with the identified transformation $\hat{S}$, and evaluate the performance criterion

$$\min_{\bar{l}_j \in \bar{L}} \left\{ J(\Re) = \int_I (f^*_C(x) - f^*_{C_d(\bar{l}_j)}(x))^2 dx \right\}. \tag{5.2}$$

Step 6: Repeat step 2 to 5 to identify the partition and piecewise linear semi-Markov map which minimise the performance criterion, as introduced in Section 3.4.

5.4 Simulation results

In the experiment, cells were separated by FACS into four subpopulations: $SSEA3^{-VE}$, $SSEA3^{low}$, $SSEA3^{MH}$, $SSEA3^{H++}$. -ve, low, MH and H++ correspond to different sorted fractions based upon SSEA3 expression, where -ve (negative - no expression of SSEA3); low (lowly expressing SSEA3); MH (mid-high expression) and H++ (very high expression). The initial densities of the subpopulations of experimental data Batch #1 are designed as shown in Figure 5.3. The probability density functions are measured on logarithmic scale of SSEA3 FITC fluorescent intensity for $1\text{-}10^4$. In order to compare the differentiation of each subpopulation, and to show the evolving shapes of the probability distribution, the probability density functions were normalised based on the maximum density values, e.g.

$$f'(x) = \frac{f(x)}{\max\{f\}}. \tag{5.3}$$

where x denotes the logarithmic SSEA3 FITC fluorescent intensity.

Apart from the four fractions used for separately observing the differentiation, three more populations were also cultured, which were UU (unstained for SSEA3 and unsorted); SU (stained for SSEA3 and unsorted) and US (unstained for SSEA3, but run through the FACS machine). The observed distributions are shown in Figure 5.4.

To sum up, the available probability density functions of Batch #1 experimentally observed are given in Table 5.2.

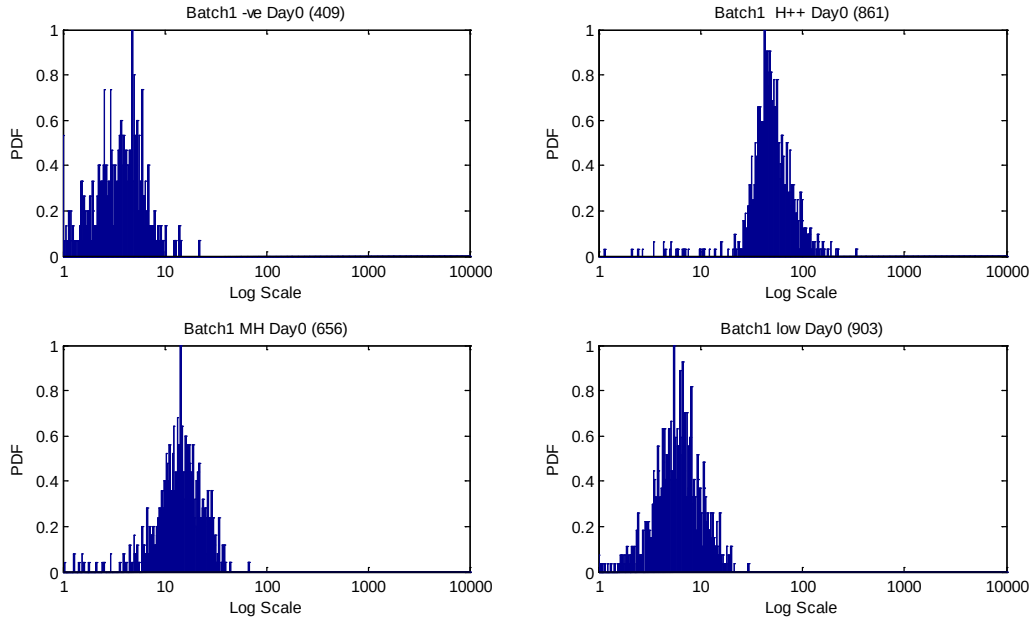

Figure 5.3 Initial probability distribution of the four subpopulations

Table 5.2 List of probability density functions observed from experiment.

	Sorted fractions				Unsorted		
Date	-ve	low	MH	H++	UU	SU	US
0	f_0^1	f_0^2	f_0^3	f_0^4			
1	f_1^1	f_1^2	f_1^3	f_1^4	f_1^5	f_1^6	f_1^7
2	f_2^1	f_2^2	f_2^3	f_2^4	f_2^5	f_2^6	f_2^7
3	f_3^1	f_3^2	f_3^3	f_3^4	f_3^5	f_3^6	f_3^7
4	f_4^1	f_4^2	f_4^3	f_4^4	f_4^5	f_4^6	f_4^7
5	f_5^1	f_5^2	f_5^3	f_5^4	f_5^5	f_5^6	f_5^7

5.4.1 Identification of Markov partition

It is assumed that the density of US on Day 5 is the invariant density of the underlying dynamical system. It is given that

$$f^* = f_5^7, \tag{5.4}$$

The uniform partition Δ with N' equal sized intervals can be obtained by maximising the penalised log-likelihood function

$$L_\theta(N') - p(N') = \left[\sum_{i=1}^{N'} D_i \log(N' D_i/\theta)\right] - \left[N' - 1 + (\log N')^{2.5}\right], \tag{5.5}$$

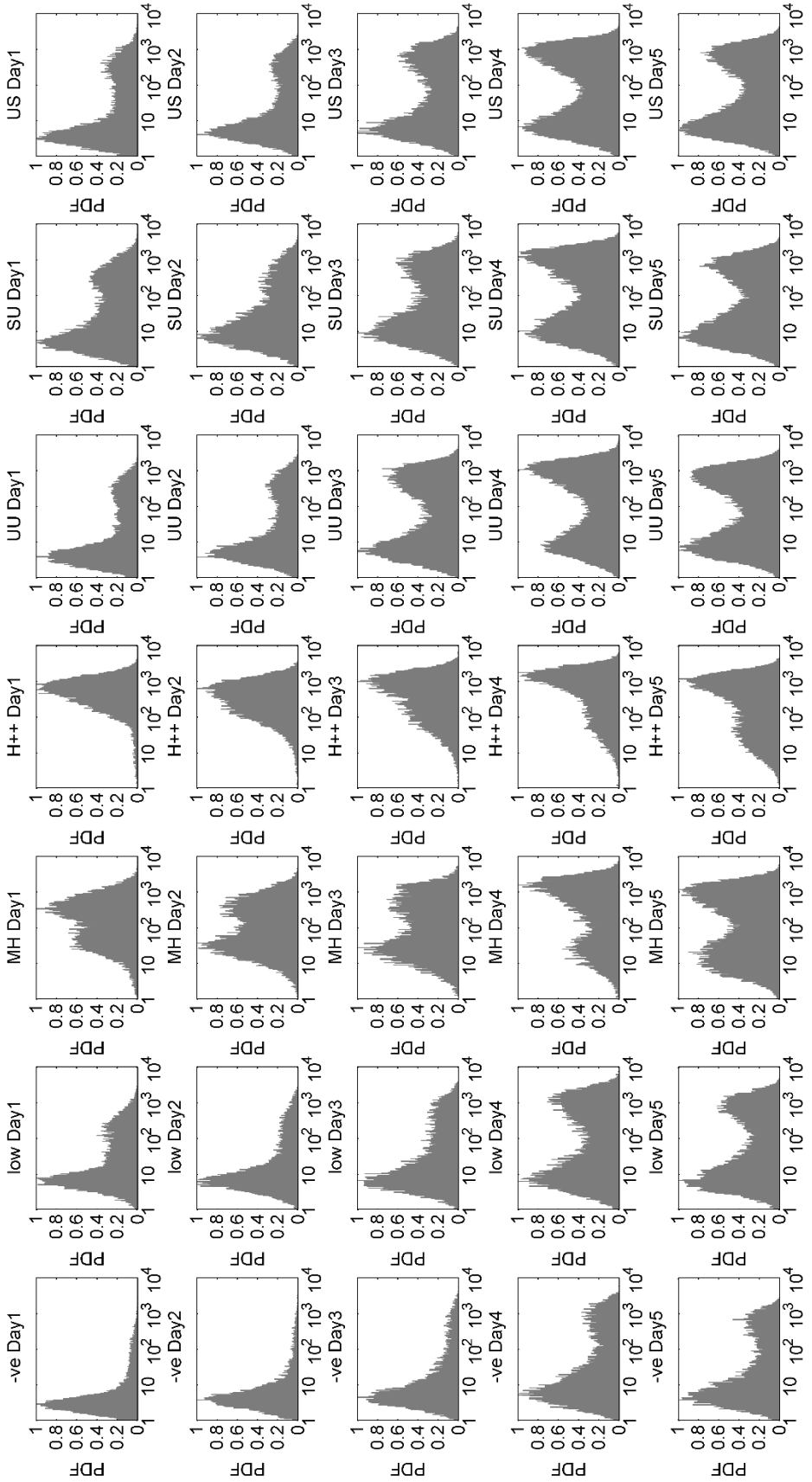

Figure 5.4 Observed probability distribution of each subpopulation from day 1 to day 5

where $\theta = 67983$ is the number of population of US on Day 5, $1 \le N' \le \theta / \log\theta = 6109$, $D_i = \sum_{j=1}^{\theta} \chi_{\Delta_i}(x_j^*)$, and

$$\Delta_i = \begin{cases} [0, 4/N'], & i = 1; \\ 4(i-1)/N', & i = 2, \ldots, N'. \end{cases}$$

It is obtained that the finest uniform partition contains $N' = 120$ intervals. The estimated invariant density function with respect to the regular partition is shown in Figure 5.5.

From Table 5.2, it can be seen that 32 sets of density mapping are available for map reconstruction, which involve 7 sequences of density functions.

The longest strictly monotone sequence is $L = \{l_j\}_{j=1}^{119}$, $l_j = 30\left|(h'_{j+1} - h'_j)\right|$. The final Markov partition $\Re$ is determined by minimising

$$\min_{\bar{l}_j \in \bar{L}} \left\{ J(\Re) = \int_I (f_C^*(x) - f_{C_d(\bar{l}_j)}^*(x))^2 dx \right\}, \tag{5.6}$$

$\bar{L} = \{\bar{l}_j\}_{j=1}^{N''}$, $0 \le N'' \le 31$.

It is found that $\{\bar{l}_j\}_{j=1}^{24}$ correspond to partitions with $N \le 32$.

$\bar{L} = \{\bar{l}_j\}_{j=1}^{24}$

={0.8076, 0.8077, 0.8473, 0.8605, 0.8737, 0.8870, 0.9267, 0.9664, 0.9665, 0.9929, 0.9930, 1.0326, 1.0458, 1.0988, 1.1650, 1.2577, 1.2709, 1.2710, 1.2974, 1.3239, 1.3901, 1.3902, 1.4562, 1.6681}.

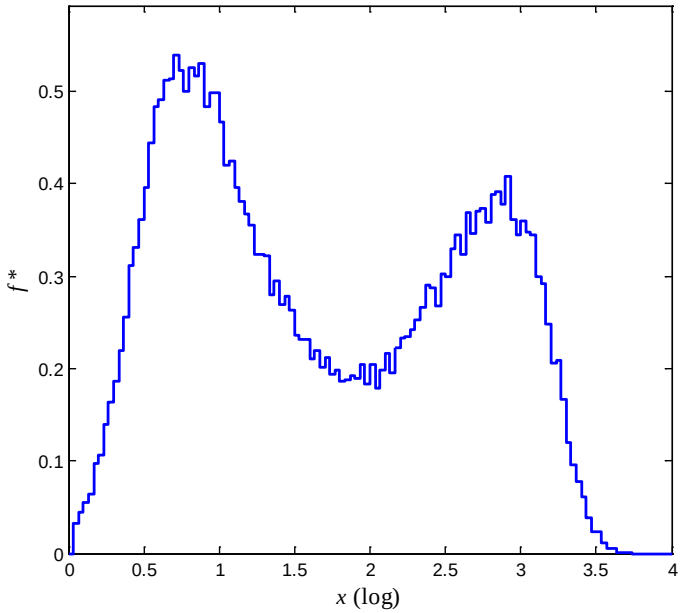

Figure 5.5 Invariant density function estimated on the initial uniform partition with $N' = 120$ intervals (x axis: logarithmic SSEA3 FITC fluorescent intensity)

Figure 5.6 shows the value of loss function (5.6). The minimum is obtained for $\bar{l}_{11}$, which leads to the final Markov partition $\mathfrak{R} = \{R_i\}_{i=1}^{18}$.

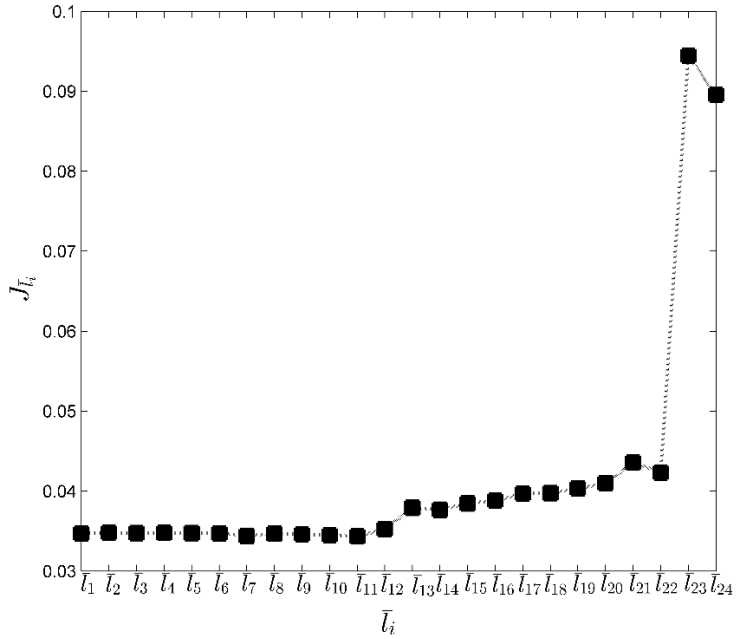

Figure 5.6 The value of the cost function corresponding to $\{\bar{l}_j\}_{j=1}^{24}$.

Figure 5.7 shows the invariant density function with respect to the identified Markov partition.

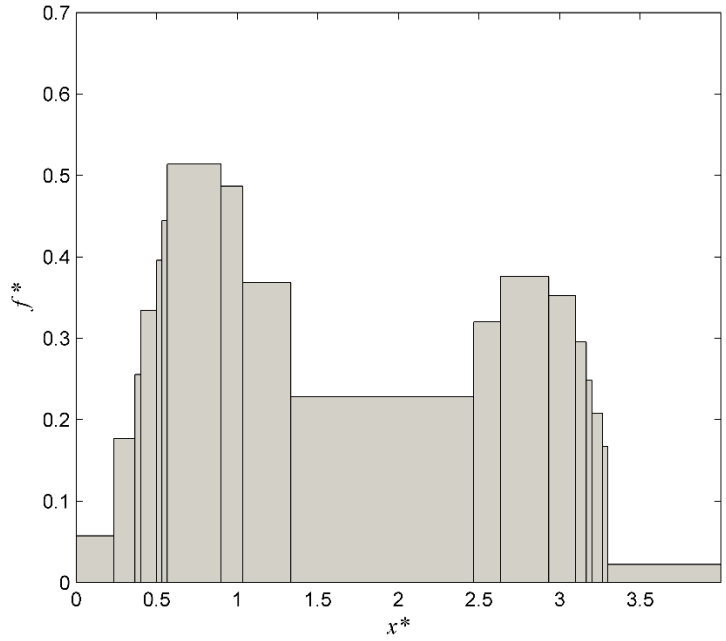

Figure 5.7 Invariant density function over the identified Markov partition $\Re = \{R_i\}_{i=1}^{18}$. (x axis: logarithmic SSEA3 FITC fluorescent intensity)

5.4.2 Identification of the chaotic map

Based on the identified Markov partition, the observed density functions are given by

$$f_t^i(x) = \sum_{j=1}^{18} w_{t,j}^i \chi_{R_j}(x), \tag{5.7}$$

where $R_j \in \Re$, $w_{t,j}^i = \frac{1}{\lambda(R_j)\theta_t^i} \sum_{k=1}^{\theta_t^i} \chi_{R_j}(x_{t,k}^i)$, θ_t^i denotes the number of cell population associated with fraction i on day t, for $i = 1,\ldots 4$, $t = 0,\ldots,5$, and for $i = 5,\ldots 7$, $t = 1,\ldots,5$.

The Frobenius-Perron matrix associated with the piecewise linear semi-Markov transformation is obtained as a solution to the following constrained optimisation problem.

$$\min_{\{m_{i,j}\}_{i,j=1}^{18} \geq 0} \| \boldsymbol{W}_1 - \boldsymbol{W}_0 \boldsymbol{M} \|_F, \tag{5.8}$$

where

$$\boldsymbol{W}_0 = \begin{bmatrix} \boldsymbol{w}^{f_0^1} \\ \vdots \\ \boldsymbol{w}^{f_4^1} \\ \vdots \\ \boldsymbol{w}^{f_0^4} \\ \vdots \\ \boldsymbol{w}^{f_4^4} \\ \boldsymbol{w}^{f_1^5} \\ \vdots \\ \boldsymbol{w}^{f_4^5} \\ \vdots \\ \boldsymbol{w}^{f_1^7} \\ \vdots \\ \boldsymbol{w}^{f_4^7} \end{bmatrix} = \begin{bmatrix} w_{0,1}^1 & w_{0,2}^1 & \cdots & w_{0,N}^1 \\ \cdots & \cdots & \cdots & \cdots \\ w_{4,1}^1 & w_{4,2}^1 & \cdots & w_{4,N}^1 \\ \vdots & \vdots & \vdots & \vdots \\ w_{0,1}^4 & w_{0,2}^4 & \cdots & w_{0,N}^4 \\ \cdots & \cdots & \cdots & \cdots \\ w_{4,1}^4 & w_{4,2}^4 & \cdots & w_{4,N}^4 \\ w_{1,1}^5 & w_{1,2}^5 & \cdots & w_{1,N}^5 \\ \cdots & \cdots & \cdots & \cdots \\ w_{4,1}^5 & w_{4,2}^5 & \cdots & w_{4,N}^5 \\ \vdots & \vdots & \vdots & \vdots \\ w_{1,1}^7 & w_{1,2}^7 & \cdots & w_{1,N}^7 \\ \cdots & \cdots & \cdots & \cdots \\ w_{4,1}^7 & w_{4,2}^7 & \cdots & w_{4,N}^7 \end{bmatrix}, \tag{5.9}$$

$$\boldsymbol{W}_1 = \begin{bmatrix} \boldsymbol{w}^{f_1^1} \\ \vdots \\ \boldsymbol{w}^{f_5^1} \\ \vdots \\ \boldsymbol{w}^{f_1^4} \\ \vdots \\ \boldsymbol{w}^{f_5^4} \\ \boldsymbol{w}^{f_2^5} \\ \vdots \\ \boldsymbol{w}^{f_5^5} \\ \vdots \\ \boldsymbol{w}^{f_2^7} \\ \vdots \\ \boldsymbol{w}^{f_5^7} \end{bmatrix} = \begin{bmatrix} w_{1,1}^1 & w_{1,2}^1 & \cdots & w_{1,N}^1 \\ \cdots & \cdots & \cdots & \cdots \\ w_{5,1}^1 & w_{5,2}^1 & \cdots & w_{5,N}^1 \\ \vdots & \vdots & \vdots & \vdots \\ w_{1,1}^4 & w_{1,2}^4 & \cdots & w_{1,N}^4 \\ \cdots & \cdots & \cdots & \cdots \\ w_{5,1}^4 & w_{5,2}^4 & \cdots & w_{5,N}^4 \\ w_{2,1}^5 & w_{2,2}^5 & \cdots & w_{2,N}^5 \\ \cdots & \cdots & \cdots & \cdots \\ w_{5,1}^5 & w_{5,2}^5 & \cdots & w_{5,N}^5 \\ \vdots & \vdots & \vdots & \vdots \\ w_{2,1}^7 & w_{2,2}^7 & \cdots & w_{2,N}^7 \\ \cdots & \cdots & \cdots & \cdots \\ w_{5,1}^7 & w_{5,2}^7 & \cdots & w_{5,N}^7 \end{bmatrix}, \tag{5.10}$$

subject to

$$\sum_{j=1}^{18} m_{i,j}\lambda(R_j) = \lambda(R_i), \quad \text{for } i = 1,\ldots,18. \tag{5.11}$$

The Frobenius-Perron matrix is obtained as follows

$$\boldsymbol{M} = \begin{bmatrix}
0 & 0.72 & 1.41 & 0.66 & 0.55 & 0.16 & 0 & 0 & 0 & 0 & 0 & 0 & 0 & 0 & 0 & 0 & 0 & 0 \\
0 & 0 & 0 & 0 & 0.43 & 0.48 & 0.31 & 0 & 0 & 0 & 0 & 0 & 0 & 0 & 0 & 0 & 0 & 0 \\
0.14 & 0 & 0 & 0 & 0 & 0 & 0 & 0 & 0 & 0 & 0 & 0 & 0 & 0 & 0 & 0 & 0 & 0 \\
0 & 0.22 & 0.20 & 0.47 & 0.22 & 0.29 & 0 & 0 & 0 & 0 & 0 & 0 & 0 & 0 & 0 & 0 & 0 & 0 \\
0 & 0 & 0 & 0 & 0 & 0 & 0.03 & 0.18 & 0 & 0 & 0 & 0 & 0 & 0 & 0 & 0 & 0 & 0 \\
0 & 0 & 0 & 0 & 0 & 0 & 0.10 & 0 & 0 & 0 & 0 & 0 & 0 & 0 & 0 & 0 & 0 & 0 \\
0.05 & 0.08 & 0.09 & 0.14 & 0.23 & 0.28 & 0.40 & 0.19 & 0.19 & 0.05 & 0 & 0 & 0 & 0 & 0 & 0 & 0 & 0 \\
0 & 0 & 0 & 0 & 0 & 0 & 0.11 & 0.33 & 0.17 & 0 & 0 & 0 & 0 & 0 & 0 & 0 & 0 & 0 \\
0 & 0 & 0 & 0 & 0 & 0 & 0 & 0 & 0.07 & 0.18 & 0.20 & 0.11 & 0.04 & 0.02 & 0.02 & 0.02 & 0.03 & 0 \\
0 & 0 & 0 & 0 & 0.02 & 0.01 & 0.09 & 0.11 & 0.18 & 0.32 & 0.63 & 0.88 & 0.83 & 0.67 & 0.62 & 0.47 & 0.34 & 0.08 \\
0 & 0 & 0 & 0 & 0 & 0.02 & 0.08 & 0.16 & 0.23 & 0.04 & 0 & 0 & 0 & 0 & 0 & 0 & 0 & 0 \\
0 & 0 & 0 & 0 & 0 & 0 & 0 & 0 & 0 & 0.21 & 0.29 & 0.03 & 0 & 0 & 0 & 0 & 0 & 0.01 \\
0 & 0 & 0 & 0 & 0 & 0 & 0 & 0 & 0 & 0 & 0.01 & 0.33 & 0.29 & 0.07 & 0 & 0.13 & 0.17 & 0 \\
0 & 0 & 0 & 0 & 0 & 0 & 0 & 0 & 0 & 0 & 0 & 0 & 0.15 & 0.39 & 0.48 & 0 & 0 & 0 \\
0 & 0 & 0 & 0 & 0 & 0 & 0 & 0 & 0 & 0 & 0 & 0 & 0 & 0.08 & 0 & 0.27 & 0.29 & 0 \\
0 & 0 & 0.03 & 0 & 0 & 0 & 0 & 0 & 0 & 0 & 0 & 0 & 0.09 & 0 & 0.03 & 0.14 & 0 & 0.06 \\
0 & 0 & 0.03 & 0.07 & 0.10 & 0.06 & 0 & 0 & 0 & 0 & 0 & 0 & 0 & 0 & 0 & 0 & 0 & 0.03 \\
0 & 0.14 & 0.09 & 0.18 & 0.31 & 0.41 & 0.68 & 0.76 & 0.71 & 0.08 & 0 & 0 & 0 & 0 & 0 & 0 & 0 & 0
\end{bmatrix}.$$

By assuming the map is continous nonlinear, the monotonocity of each segment is determined from Section 4.2.3. Figure 5.8 shows the constructed piecewise linear semi-Markov map. Figure 5.9 shows the smooth map obtained by fitting a cubic spline (smoothing parameter: 0.999). The model describes the transitions of SSEA3 cell-surface marker expression over one day intervals, and can be used to predict the long term evolution of SSEA3-sorted cell fractions.

Predictions of SSEA3 probability density functions from day 2 to 5 based on the density funcitons on day 1 of Batch #1 are demonstrated in Figure 5.10.

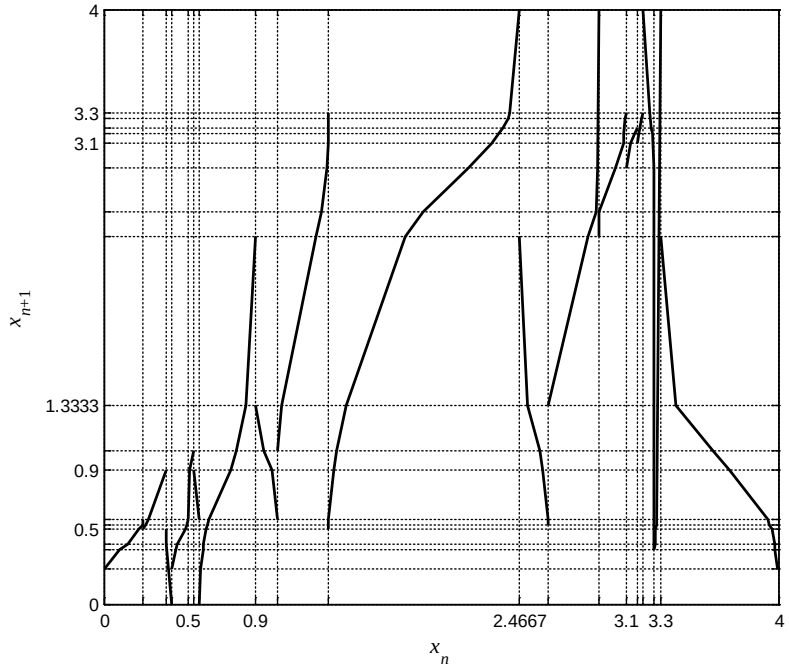

Figure 5.8 Constructed piecewise linear semi-Markov map characterising the dynamics of cell population.

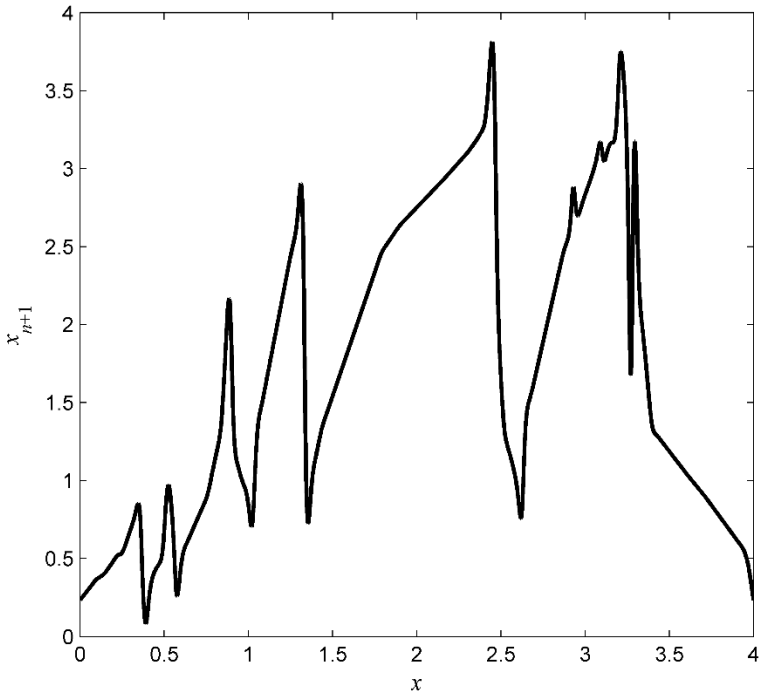

Figure 5.9 Identified smooth map from the reconstructed piecewise linear semi-Markov transformation.

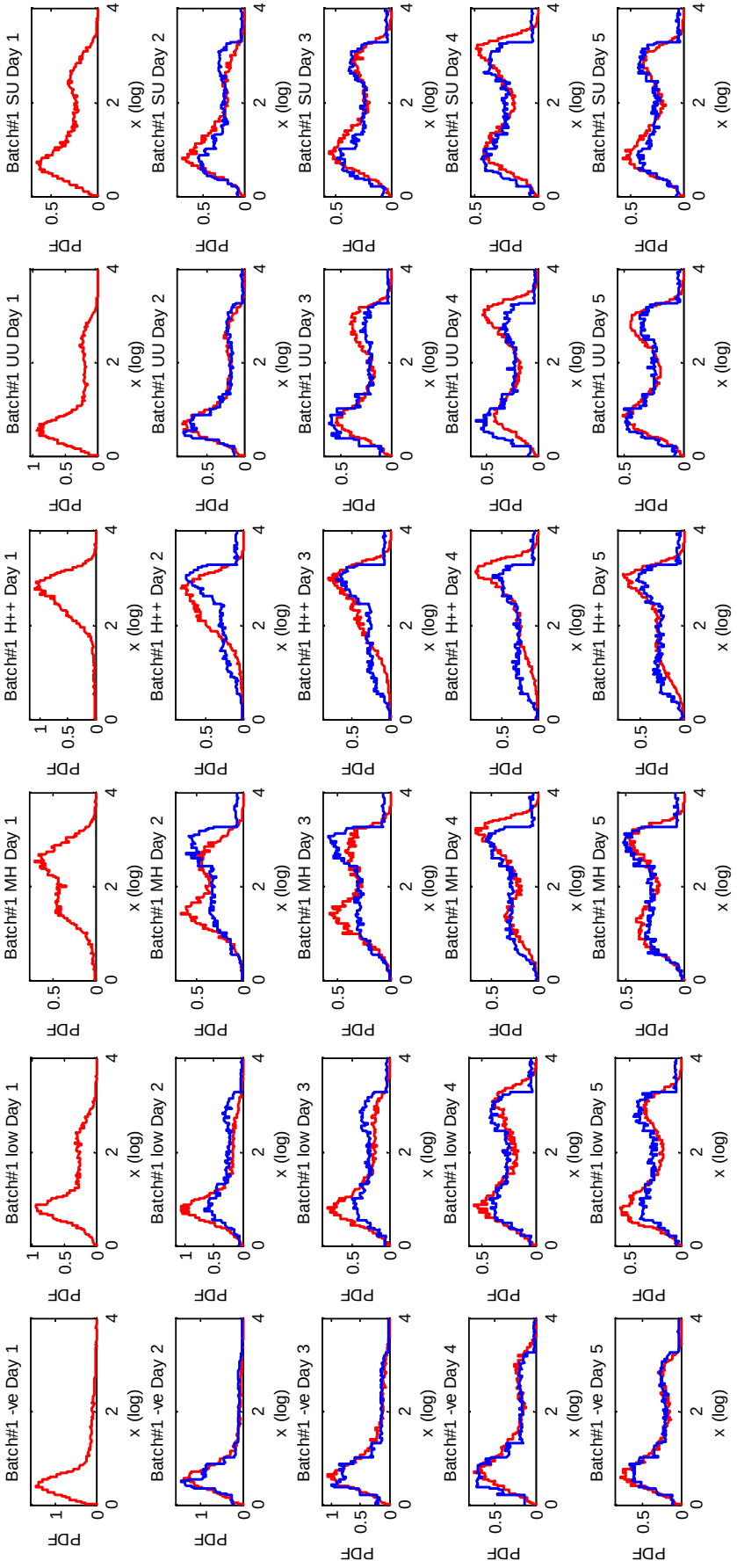

Figure 5.10 Predictions of probability density functions of SSEA3 for the four fractions (-ve, low, MH, H++) and three populations (UU, SU, US) based on distributions on day 1 in Batch #1 (red lines: true density functions; blue lines: predicted density functions).

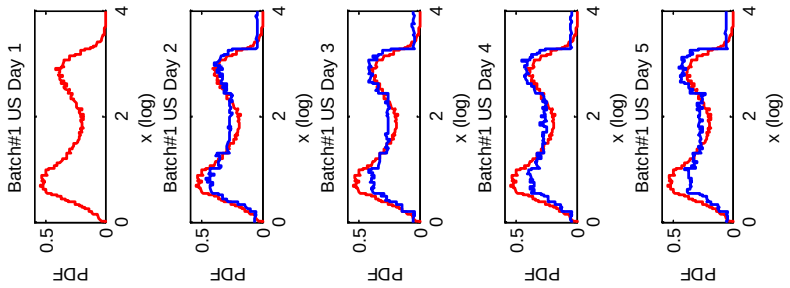

(7)

To quantitatively demonstrate the prediction performance using the training data Batch #1, the Bhattacharyya distances (Aherne, Thacker et al. 1998) between the predicted and true densities, calculated by

$$D_B = -\ln(\int_0^4 \sqrt{f(x)\hat{f}(x)}dx), \tag{5.12}$$

where $f(x)$ is the true density function, and $\hat{f}(x)$ is the predicted result, were given in Table 5.3. Bhattacharyya distance is a measure of divergence between two probability distributions. Lower D_B implies higher similarity of the compared density functions, particularly, $D_B = 0$ when $f(x) = \hat{f}(x)$.

Table 5.3 The Bhattacharyya distances between the true density functions of training data Batch #1 and the predicted results by the reconstructed model.

	Day 2	Day 3	Day 4	Day 5	Mean
-ve	0.0207	0.0157	0.0176	0.0138	0.0169
Low	0.0464	0.0339	0.0210	0.0237	0.0312
MH	0.0419	0.0264	0.0404	0.0180	0.0317
H++	0.0687	0.0563	0.0801	0.0302	0.0588
UU	0.0141	0.0185	0.0319	0.0145	0.0197
SU	0.0242	0.0168	0.0250	0.0166	0.0206
US	0.0141	0.0168	0.0183	0.0215	0.0176

Another group of experimental data Batch #2 was used to test the identified model. Figure 5.11 shows the prediction results for day 2 to 5 based on the distribution on day 1.

Table 5.4 gives the calculated Bhattacharyya distances between the estimated densities and true densities of Batch #2.

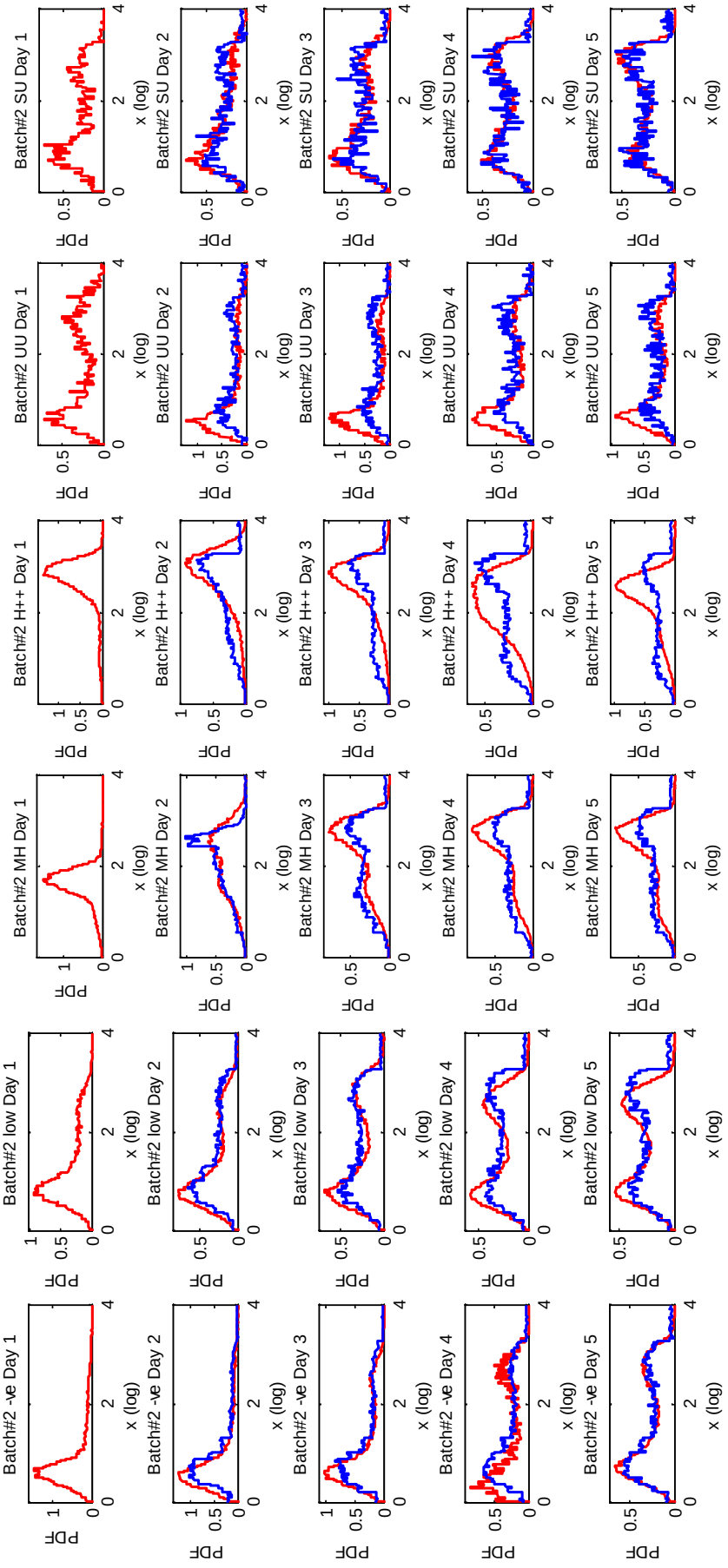

Figure 5.11 Predictions of probability density functions of SSEA3 for the four fractions (-ve, low, MH, H++) and three populations (UU, SU, US) based on distributions on day 1 in Batch #2 (red lines: true density functions; blue lines: predicted density functions).

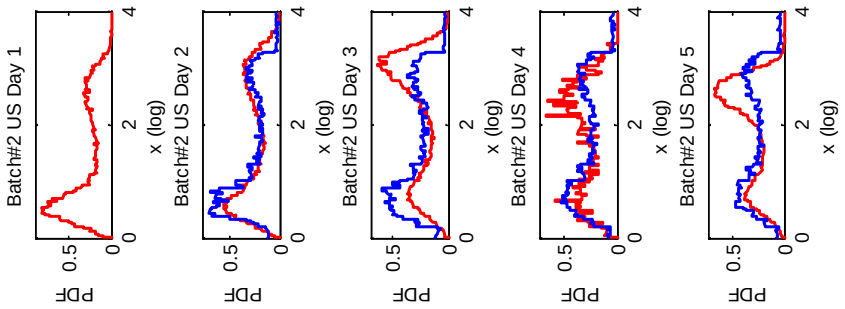

(7)

The identified model reveals how different cell fractions evolve towards and reconstitute the invariant parent density as well as the presence of unstable equilibrium points, some of which become stable attractors in response to changes in culture conditions.

Table 5.4 The Bhattacharyya distances between the true density functions of test data Batch #2 and the predicted results by the reconstructed model.

	Day 2	Day 3	Day 4	Day 5	Mean
-ve	0.0268	0.0208	0.0533	0.0132	0.0285
Low	0.0155	0.0161	0.0210	0.0271	0.0225
MH	0.0265	0.0257	0.0293	0.0378	0.0298
H++	0.0579	0.0673	0.0771	0.1126	0.0787
UU	0.0720	0.0917	0.0474	0.0600	0.0678
SU	0.0324	0.0271	0.0203	0.0240	0.0260
US	0.0206	0.0537	0.0360	0.0478	0.0395

Figure 5.12 depicts the bifurcation diagram of a one-parameter family associated with the identified chaotic map.

$$S_\alpha = \alpha S(x), \tag{5.13}$$

where the varying parameter $\alpha \in [0,1]$, $S(x)$ is the constructed dynamical map for the cell population. It is found that S_α has one equilibrium point when $0 < \alpha < 0.425$. As α increases from 0.425, the attractor becomes period chaotic.

For the first time, the identified model allows for deriving analytically several equilibrium points of the system that are believed to correspond to functionally relevant substates. Using cell mapping method (Hsu 1987) where I was divided

into 9×10^3 equal cell, the equilibrium points of the model and the domain of attraction were calculated.

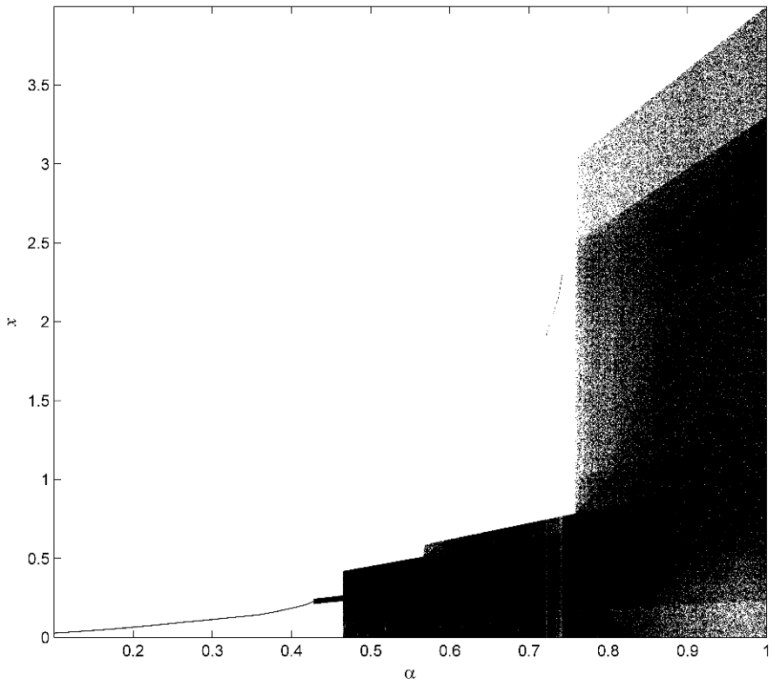

Figure 5.12 Bifurcation diagram of a one-parameter family associated with the reconstructed map.

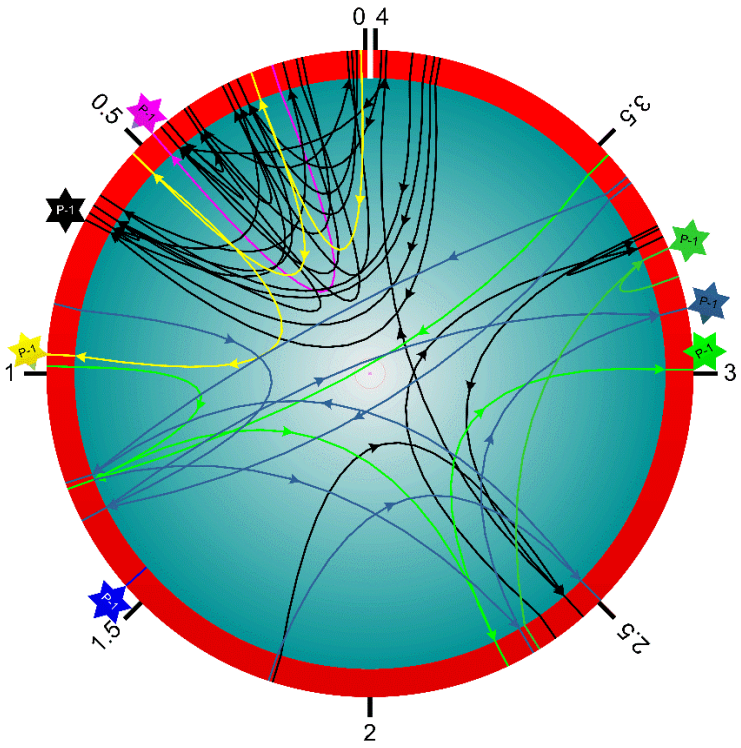

Figure 5.13 Predicted state transitions (changes in fluorescent intensity) that give rise to the observed evolution of the distribution SSEA3 expression following re-plating. Coloured stars indicate predicted equilibrium points.

Figure 5.13 shows the predicted equilibrium points and the individual state transitions. The coloured stars represent the predicted equilibrium points. The identified states transfer from the domain of attraction to the corresponding unique equilibrium point. This reveals the changes in the fluorescent intensity that leads to the observed dynamical evolution of each fracation.

5.5 Conclusions

In this chapter, using the proposed approaches to solving the generalised inverse Frobenius-Perron problem, the dynamical model of the hESC populations has been developed based on the sequences of flow cytometric distributions of cell surface markers. The model describes the one-day period transitions of cells expressed by SSEA3 cell surface marker, and can be used to predict how different cell fractions regenerate the equilibrium SSEA3 distribution after isolation and re-culturing. The equilibrium points of the underlying chaotic system were derived to help understanding the corresponding functionally relevant substates. The model reveals unstable equilibrium points become stable attractors by changing cell culture conditions. The identified equilibrium points are now being validated experimentally by using FACS to isolate narrow cell fractions for each of the predicted equilibrium points, plating, monitoring and re-analysing cells in culture over a number of days.

Chapter 6
Modelling of One-Dimensional Dynamical Systems Subjected to Additive Perturbations with Sequences of Probability Density Functions

6.1 Introduction

The preceding chapters study methodologies of reconstructing one-dimensional chaotic maps directly from sequences of probability density functions. In practice, physical systems are always subjected to additional perturbation (input or random noise). This chapter considers more rigorously the problem of inferring a one-dimensional chaotic transformation perturbed by an additive perturbation from temporal sequences of probability density functions that are measured from the perturbation-corrupted data. To distinguish from the previous IFPP, this problem is referred to as inverse Foias problem. Specifically, two cases of perturbations are analysed respectively:

a) A chaotic map $S : I \to I$ subjected to an additive input bounded in I. The input density function can be arbitrarily assigned on I.
b) A chaotic map $S : I \to I$ subjected to an additive random noise spanning $[-\varepsilon, \varepsilon]$, $\varepsilon \le b/2$. The probability density function of noise is assumed to be known.

It is aimed to reveal the effects of two separate forms of perturbations that are usually encountered in practice. Case a) concerns a dynamical system involving an input variable on *I*, of which the nature of dynamics can be manipulated by choosing the input density function. Case b) treats the more realist noisy system compared with the noise-free system considered in the previous chapters, but for which the probability density function of the stochastic noise cannot be adjusted in general. Although many approaches have been presented for solving the IFPP, really few solutions to the inverse Foias problem has been proposed by far.

This chapter is organised as follows: Section 6.2 introduces the method for identifying the model of a one-dimensional dynamical system subjected to an additive input. Section 6.3 presents algorithms of modelling for a one-dimensional dynamical systems subjected to an additive random noise. Numerical simulation examples for the two cases are given to demonstrate effectiveness of the developed algorithms.

6.2 Modelling of a one-dimensional dynamical systems subjected to an additive input

This section will study the problem of reconstructing a one-dimensional transformation with an additive input, for which the probability density function is assumed to be known, given sequences of probability density functions generated by the unknown system.

6.2.1 Formulation of the evolution of probability densities

In this section, the following one-dimensional, discrete-time and bounded chaotic dynamical system with an additive input is considered.

$$x_{n+1} = S(x_n) + u_n \pmod{b}, \quad n = 0, 1, 2, \ldots, \tag{6.1}$$

where $S : I \to I$, $I = [0, b]$, is a measurable nonlinear and non-singular transformation; x_n is a random variable bounded in *I*, having probability density

function $f_n \in \mathfrak{D}(I, \mathfrak{B}, \mu)$, $\{u_n\}$ is i.i.d. input variable bounded in I having the probability density function $f_u \in \mathfrak{D}$.

Since x_{n+1} is the sum of $S(x_n)$ and input u_n, the density function of x_{n+1}, f_{n+1} is related with f_n and f_u. In the first place the aim is to find out the relationship between f_{n+1} and f_n, f_u that reveals mathematically the propagation of densities functions from one sampling time n to the next time n+1.

The system bounded on I can be rewritten in the following alternative form

$$x_{n+1} = \begin{cases} S(x_n) + u_n, & 0 \le S(x_n) + u_n \le b; \\ S(x_n) + u_n - b, & b < S(x_n) + u_n \le 2b, \end{cases} \tag{6.2}$$

or in a more compact way

$$x_{n+1} = S(x_n) + u_n - b \cdot \chi_{(b,\,2b]}[S(x_n) + u_n], \tag{6.3}$$

By assuming that $\tau(x_n)$ is a measurable bounded function in terms of x_n, the mathematical expectation of $\tau(x_{n+1})$ can be expressed as

$$E\big(\tau(x_{n+1})\big) = \int_I \tau(x)\, f_{n+1}(x)\, dx, \tag{6.4}$$

$E\big(\tau(x_{n+1})\big)$ can also be given in an alternative way in terms of f_n and f_u.

$$\begin{aligned} E\big(\tau(x_{n+1})\big) &= E\{\tau[S(x_n) + u_n - b\chi_{(b,\,2b]}(S(x_n) + u_n)]\} \\ &= \int_I \int_I \left\{ \tau\big[S(x) + u\big] \cdot \frac{1}{2} f_n(x)\, f_u(u) + \tau\big[S(x) + y - b\big] \cdot \frac{1}{2} f_n(x)\, f_u(u) \right\} dxdu \\ &= \int_I \int_I \tau\Big[S(x) + u - b\chi_{(b,\,2b]}(S(x) + u)\Big] \cdot f_n(x)\, f_u(u)\, dxdu. \end{aligned} \tag{6.5}$$

Let $w' = S(x) + u - \chi_{(b,\,2b]}(S(x) + u)$, and $v' = x$. It can be further obtained from (6.4) that

$$E\big(\tau(x_{n+1})\big) = \int_I \int_I \tau(w')\, f_n(v')\, f_u(w' - S(v') + b\chi_I(S(v') - w'))\, dv'dw'. \tag{6.6}$$

From (6.4) and (6.6), by changing the variables, it can be seen that

$$f_{n+1}(x) = \int_I f_n(z)\, f_u(x - S(z) + b\chi_I(S(z) - x))\, dz\,, \tag{6.7}$$

This directly reflects the relationship connecting f_{n+1} with f_n and f_u, and formulates the transformation from the density of the states at sample time *n* into a new density at sample time $n+1$.

Assumptions are made as follows: 1) probability density functions $\{f_0^j\}_{j=1}^K$ and $\{f_1^j\}_{j=1}^K$ can be estimated from the initial and final states $\{x_{0,i}^j\}_{i,j=1}^{\theta,K}$ and $\{x_{1,i}^j\}_{i,j=1}^{\theta,K}$ which are observed in practical experiment but lose correspondence; 2) input density function f_u is known.

6.2.2 The Foias operator

Let $Q f_n = f_{n+1}$ in (6.7), where $Q : \mathfrak{D} \to \mathfrak{D}$ is referred to as the Foias operator corresponding to the perturbed dynamical system, which transforms one probability density function into another under the action of *S* and f_u. Thus, (6.7) can be written as

$$Q f_n(x) = \int_I f_n(z)\, f_u(x - S(z) + b\chi_I(S(z) - x))\, dz\,, \tag{6.8}$$

It is supposed that for a specified value of u_n, there exist N_1 intervals $\{I_i^{(N_1)}\}_{i=1}^{N_1}$ on which $S(x_n) + u_n \in I$, and N_2 intervals $\{I_i^{(N_2)}\}_{i=1}^{N_2}$ on which $S(x_n) + u_n \notin I$, the corresponding partition of I is given by $0 = a_0 < a_1 < \ldots < a_{N_1+N_2} = b$, then the right side of (6.8) can be decomposed as follows

$$\begin{aligned} Q f_n(x) = &\sum_{i=1}^{N_1} \int_I f_n(z)\, f_u(x - S(z))\chi_{I_i^{(N_1)}}(z)\, dz \\ &+ \sum_{j=1}^{N_2} \int_I f_n(z)\, f_u(x - S(z) + b)\chi_{I_j^{(N_2)}}(z)\, dz. \end{aligned} \tag{6.9}$$

By replacing $S(z)$ by y, then $z = S^{-1}(y)$. It follows that

$$\begin{aligned} Q f_n(x) = & \sum_{i=1}^{N_1} \int_I f_n(S^{-1}(y))\, f_u(x-y)\, \chi_{I_i^{(N_1)}}(S^{-1}(y))\, d(S^{-1}(y)) \\ & + \sum_{j=1}^{N_2} \int_I f_n(S^{-1}(y))\, f_u(x-y+b)\, \chi_{I_j^{(N_2)}}(S^{-1}(y))\, d(S^{-1}(y)). \end{aligned} \tag{6.10}$$

Then,

$$\begin{aligned} Q f_n(x) = & \sum_{i=1}^{N_1} \int_I f_u(x-y) \frac{f_n(S^{-1}(y))}{S'(S^{-1}(y))} \chi_{S(I_i^{(N_1)})}(y)\, dy \\ & + \sum_{j=1}^{N_2} \int_I f_u(x-y+b) \frac{f_n(S^{-1}(y))}{S'(S^{-1}(y))} \chi_{S(I_j^{(N_2)})}(y)\, dy. \end{aligned} \tag{6.11}$$

This can be further converted to

$$\begin{aligned} & Q f_n(x) \\ & = \int_I f_u(x-y) \sum_{i=1}^{N_1} \left[\frac{f_n(S_i^{-1}(y))}{S'(S_i^{-1}(y))} \chi_{S(I_i^{(p)})}(y) \right] dy \\ & + \int_I f_u(x-y+b) \sum_{j=1}^{N_2} \left[\frac{f_n(S_j^{-1}(y))}{S'(S_j^{-1}(y))} \chi_{S(I_j^{(N_2)})}(y) \right] dy \\ & = \int_I f_u(x-y+b\chi_I(y-x)) \left\{ \sum_{i=1}^{N_1} \left[\frac{f_n(S_i^{-1}(y))}{S'(S_i^{-1}(y))} \chi_{S(I_i^{(N_1)})}(y) \right] \right. \\ & \left. + \sum_{j=1}^{N_2} \left[\frac{f_n(S_j^{-1}(y))}{S'(S_j^{-1}(y))} \chi_{S(I_j^{(N_2)})}(y) \right] \right\} dy. \end{aligned} \tag{6.12}$$

It can be found that the right side can be related to the Frobenius-Perron operator corresponding to *S* because of the following equality

$$P_S f_n(y) = \sum_{i=1}^{N_1} \left[\frac{f_n(S_i^{-1}(y))}{S'(S_i^{-1}(y))} \chi_{S(I_i^{(N_1)})}(y) \right] + \sum_{j=1}^{N_2} \left[\frac{f_n(S_j^{-1}(y))}{S'(S_j^{-1}(y))} \chi_{S(I_j^{(N_2)})}(y) \right]. \tag{6.13}$$

Therefore, it can be further obtained that

$$Q f_n(x) = \int_I f_u(x-y+b\chi_I(y-x)) \cdot P_S f_n(y)\, dy\,. \tag{6.14}$$

This equation reveals that the Foias operator *Q* associated with the dynamical system with an additive input is able to be connected with the Frobenius-Perron operator corresponding to the noise-free map *S*.

It is assumed that S is a piecewise linear semi-Markov transformation on a N-interval partition of I, $\mathfrak{R} = \{R_1, R_2, \ldots, R_N\}$, for which $\text{int}(R_i) \bigcap \text{int}(R_j) = \varnothing$ if $i \neq j$. The restriction $S\big|_{R_i}$ is a homeomorphism from R_i to a union of intervals of $\mathfrak{R}$

$$\bigcup_{k=1}^{p(i)} R_{r(i,k)} = \bigcup_{k=1}^{p(i)} S(Q_k^{(i)}), \tag{6.15}$$

where $R_{r(i,k)} = S(Q_k^{(i)}) \in \mathfrak{R}$, $Q_k^{(i)} = [q_{k-1}^{(i)}, q_k^{(i)}]$, $i = 1, \ldots, N$, $k = 1, \ldots, p(i)$ and $p(i)$ denotes the number of disjoint subintervals $Q_k^{(i)}$ corresponding to R_i.

Let $f_n(x) = \sum_{i=1}^{N} w_i \chi_{I_i}(x)$ and $P_S f_n(x) = \sum_{i=1}^{N} \upsilon_i \chi_{I_i}(x)$. The Frobenius-Perron equation can be written as

$$P_S f_n(x) = \sum_{j=1}^{N} \left(\sum_{i=1}^{N} (w_i m_{i,j}) \right) \chi_{I_j}(x). \tag{6.16}$$

where $\boldsymbol{M} = (m_{i,j})_{1 \leq i,j \leq N}$. It can be simplified as follows

$$\upsilon_j = \sum_{i=1}^{N} w_i m_{i,j}, \tag{6.17}$$

for $j = 1, \ldots, N$.

By integrating both sides of (6.17) over the interval $R'_k \in \mathfrak{R}' \square \{R'_1, R'_2, \ldots, R'_P\}$ that is a regular partition of I into P equal sized intervals, it can be obtained that

$$\int_{R'_k} Q f_n(x)\, dx = \int_{R'_k} \int_I f_u(x - y + b\chi_I(y - x)) \cdot P_S f_n(y)\, dy dx. \tag{6.18}$$

Using rectangle method to approximate the integral, $Q f_n(x)$ is given by

$$Q f_n(x) = \sum_{k=1}^{P} v_k \chi_{I_k}(x), \tag{6.19}$$

As a result, the coefficients of $Q f_n$ can be given by

$$v_k = \frac{1}{\lambda(R_k')} \int_{R_k'} \int_I f_u(x - y + b\chi_I(y - x)) \cdot P_S f_n(y)\, dydx, \tag{6.20}$$

where $\lambda(R_k')$ denotes Lebesgue measure on R_k'. Then, it can be written as follows

$$\begin{aligned} v_k &= \frac{1}{\lambda(R_k')} \int_{R_k'} \sum_{j=1}^{N} \left[\int_{I_j} f_u(x - y + b\chi_I(y - x))\, dy \cdot \upsilon_j \right] dx \\ &= \frac{P}{b} \sum_{j=1}^{N} \left[\int_{R_k'} \int_{I_j} f_u(x - y + b\chi_I(y - x))\, dydx \cdot \upsilon_j \right]. \end{aligned} \tag{6.21}$$

It is defined a matrix $\boldsymbol{D} = (d_{k,j})_{1 \le k \le P;\, 1 \le j \le N}$ where

$$d_{k,j} = \frac{P}{b} \int_{R_k'} \int_{R_j} f_u(x - y + b\chi_I(y - x))\, dydx, \tag{6.22}$$

as a consequence, (6.8) can be converted into the following equation of matrix form

$$\begin{bmatrix} v_1 \\ v_2 \\ \vdots \\ v_k \\ \vdots \\ v_P \end{bmatrix} = \begin{bmatrix} d_{11} & d_{12} & \cdots & d_{1j} & \cdots & d_{1N} \\ d_{21} & d_{22} & \cdots & d_{2j} & \cdots & d_{2N} \\ \vdots & \vdots & \ddots & \vdots & \vdots & \vdots \\ d_{k1} & d_{k2} & \cdots & d_{kj} & \cdots & d_{kN} \\ \vdots & \vdots & \vdots & \vdots & \ddots & \vdots \\ d_{P1} & d_{P2} & \cdots & d_{Pj} & \cdots & d_{PN} \end{bmatrix} \cdot \begin{bmatrix} \upsilon_1 \\ \upsilon_2 \\ \vdots \\ \upsilon_j \\ \vdots \\ \upsilon_N \end{bmatrix}, \tag{6.23}$$

from which it can be found that an estimated matrix representation of the Foias operator can be obtained based on the Frobenius-Perron matrix associated with the transformation *S*.

By submitting (6.17) into (6.23), it can be obtained that

$$\boldsymbol{v}^{f_1} = \boldsymbol{w}^{f_0} \cdot \boldsymbol{M} \cdot \boldsymbol{D}^T, \tag{6.24}$$

where $\boldsymbol{w}^{f_0} = [w_1, \ldots, w_N]$, $\boldsymbol{v}^{f_1} = [v_1, \ldots, v_P]$.

The Foias operator can be represented by an estimated matrix $\boldsymbol{H}$ as follows

$$\boldsymbol{H} = \boldsymbol{M} \cdot \boldsymbol{D}^T, \tag{6.25}$$

6.2.3 Identification of the Frobenius-Perron matrix

Provided the evolving probability density function at each sampling time *T* can be measured, two scenarios of identifying the Frobenius-Perron matrix are provided here.

1. F-P matrix identification based on a set of initial probability density functions $f_0^1,..., f_0^N$ and their images $f_1^1,..., f_1^N$ under the transformation

Given a partition $\mathfrak{R}$ with *N* intervals, the Frobenius-Perron matrix associated with *S* can be identified given at least *N* distinct initial density functions $\{f_0^i\}_{i=1}^N$ and their images $\{f_1^i\}_{i=1}^N$. Using the same way of constructing the initial conditions described in Chapter 3, piecewise constant densities f_0^i are constructed in the following way

$$f_0^i(x) = \sum_{j=1}^{N} w_{i,j}\chi_{I_j}(x); \quad i = 1, 2, \ldots, N, \tag{6.26}$$

where $w_{i,j} = 1/\lambda(I_i) = b/N$ for $j = i$; and $w_{i,j} = 0$ for $j \neq i$. *N* sets of initial conditions are generated by sampling each initial density function f_0^i

$$X_0^i = \{x_{0,j}^i\}_{j=1}^{\theta}, \quad i = 1, ..., N, \tag{6.27}$$

and θ random input values are generated by sampling the input density function

$$U = \{u_i\}_{i=1}^{\theta}, \tag{6.28}$$

which will be used in the experiments. The corresponding set of final states observed at *T*=1 are measured as follows

$$X_1^i = \{x_{1,j}^i\}_{j=1}^{\theta}, \quad i = 1,...,N, \tag{6.29}$$

where $x_{1,j}^i = S(x_{0,k}^i) + u_k \mod b$, for some $x_{0,k}^i \in X_0^i$, $u_k \in U$. The density function f_1^i associated with the set X_1^i of final states is estimated on the *P*-interval uniform partition given by

$$f_1^i(x) = \sum_{j=1}^{P} v_{ij} \chi_{I_j}(x), \qquad i = 1, \ldots, N, \tag{6.30}$$

where the coefficients $v_{i,j} = \frac{P}{b\theta} \sum_{k=1}^{\theta} \chi_{I_j}(x_{1,k}^i)$.

In order to recover the Frobenius-Perron matrix, it can be seen from (6.23) and (6.24) that the first step is to determine $P_S f_0^i(x)$ which correspond to $f_0^i(x)$, for $1 \le i \le N$. Let $\boldsymbol{v}^{P_S f_0^i} = [w_{i,1}, \ldots, w_{i,N}]$, $\boldsymbol{v}^{f_1^i} = [v_{i,1}, \ldots, v_{i,P}]$. It follows that

$$\boldsymbol{V} = \boldsymbol{Y} \cdot \boldsymbol{D}^T, \tag{6.31}$$

where

$$\boldsymbol{V} = \begin{bmatrix} \boldsymbol{v}^{f_1^1} \\ \boldsymbol{v}^{f_1^2} \\ \vdots \\ \boldsymbol{v}^{f_1^N} \end{bmatrix} = \begin{bmatrix} v_{1,1} & v_{1,2} & \cdots & v_{1,P} \\ v_{2,1} & v_{2,2} & \cdots & v_{2,P} \\ \vdots & \vdots & \ddots & \vdots \\ v_{N,1} & \cdots & \cdots & v_{N,P} \end{bmatrix}, \tag{6.32}$$

and

$$\boldsymbol{Y} = \begin{bmatrix} \boldsymbol{v}^{P_S f_1^1} \\ \boldsymbol{v}^{P_S f_1^2} \\ \vdots \\ \boldsymbol{v}^{P_S f_1^N} \end{bmatrix} = \begin{bmatrix} \upsilon_{1,1} & \upsilon_{1,2} & \cdots & \upsilon_{1,N} \\ \upsilon_{2,1} & \upsilon_{2,2} & \cdots & \upsilon_{2,N} \\ \vdots & \vdots & \ddots & \vdots \\ \upsilon_{N,1} & \upsilon_{N,2} & \cdots & \upsilon_{N,N} \end{bmatrix}, \tag{6.33}$$

The matrix $\boldsymbol{Y}$ is obtained as a solution to a constrained optimisation problem

$$\min_{\{\upsilon_{i,j}\}_{i,j=1}^{N} \ge 0} \left\| \boldsymbol{V} - \boldsymbol{Y} \cdot \boldsymbol{D}^T \right\|_F, \tag{6.34}$$

subject to

$$\sum_{j=1}^{N} \upsilon_{i,j} \lambda(R_j) = 1, \text{ for } i = 1, \ldots, N. \tag{6.35}$$

Let $\boldsymbol{w}^{f_0^i} = [w_{i,1}, \cdots w_{i,N}]$ be the vectors describing f_0^i. From (6.17), the Frobenius-Perron matrix can be obtained by

$$\boldsymbol{M}_S = \boldsymbol{W}^{-1}\boldsymbol{Y}, \tag{6.36}$$

where

$$\boldsymbol{W} = \begin{bmatrix} \boldsymbol{w}^{f_0^1} \\ \boldsymbol{w}^{f_0^2} \\ \vdots \\ \boldsymbol{w}^{f_0^N} \end{bmatrix} = \begin{bmatrix} w_{1,1} & 0 & \cdots & 0 \\ 0 & w_{2,2} & \cdots & 0 \\ \vdots & \vdots & \ddots & \vdots \\ 0 & \cdots & \cdots & w_{N,N} \end{bmatrix}, \tag{6.37}$$

For a continuous nonlinear map *S*, after obtaining a tentative estimated Frobenius-Perron matrix, the same step as introduced in Section 4.2.2 for refining the estimation by specifying the contiguous non-zero entries in each row is needed to be taken here. Since non-zero entries in $\boldsymbol{Y}$ and $\boldsymbol{M}$ have identical indices, the optimisation is re-performed with the following constraints

$$\sum_{k=1}^{p(i)} \upsilon_{i,r(i,k)} = N, \tag{6.38}$$

for $i = 1,\ldots,N$, and $0 \le \upsilon_{i,j} \le N$ if $j = r(i,k), k = 1,..., p(i)$, and $b_{i,j} = 0$ if $j \ne r(i,k), k = 1,..., p(i)$.

The final estimated Frobenius-Perron matrix is then obtained by (6.36) with the new resulting $\boldsymbol{Y}$.

2. F-P matrix identification based on sequences of evolving probability density functions $f_0,\ldots, f_T$

Let $f_0(x)$ be an initial density function that is piecewise constant on the partition $\mathfrak{R} = \{R_1,\ldots,R_N\}$.

$$f_0(x) = \sum_{i=1}^{N} w_{0,i}\chi_{R_i}(x), \tag{6.39}$$

where the coefficients satisfy $\sum_{i=1}^{N} w_{0,i}\lambda(R_i)=1$. The initial density corresponds to the set of initial states $X_0=\{x_{0,j}\}_{j=1}^{\theta}$. The following sets of states $X_t=\{x_{t,j}\}_{j=1}^{\theta}$ at each sampling time *t* can be observed by applying *t* times the transformation with the input samples generated in (6.28), such that $x_{t,j}=S(x_{t-1,k})+u_k \pmod b$ for some initial point $x_{0,k}\in X_0$, $u_k\in U$. $j=1,\ldots,\theta$, $k=1,\ldots,\theta$, $t=1,\ldots,T$. In practice, the correspondences between two continuous states may be not available, i.e. $x_{t,j}\neq S(x_{t-1,j})+u_k \pmod b$.

The density function on $\Re'$ associated with the states X_t is given by

$$f_t(x)=\sum_{i=1}^{P} w'_{t,i}\chi_{R'_i}(x), \tag{6.40}$$

where the coefficients $w'_{t,i}=\dfrac{1}{\lambda(R'_i)\cdot\theta}\sum_{j=1}^{\theta}\chi_{R'_i}(x_{t,j})=\dfrac{P}{b\theta}\sum_{j=1}^{\theta}\chi_{R'_i}(x_{t,j})$.

Let $\boldsymbol{w}^{f_t}=[w_{t,1},...,w_{t,N}]$ be the vector defining $f_t(x)$ $t=0,\ldots,T$ where $T\geq N$. Thus, the sequence of densities estimated on $\Re$ and their images measured on $\Re'$ can be represented by

$$\boldsymbol{W}_0=\begin{bmatrix}\boldsymbol{w}^{f_0}\\ \boldsymbol{w}^{f_1}\\ \vdots\\ \boldsymbol{w}^{f_{T-1}}\end{bmatrix}=\begin{bmatrix} w_{0,1} & w_{0,2} & \cdots & w_{0,N}\\ w_{1,1} & w_{1,2} & \cdots & w_{2,N}\\ \vdots & \vdots & \ddots & \vdots\\ w_{T-1,1} & w_{T-1,2} & \cdots & w_{T-1,N}\end{bmatrix}, \tag{6.41}$$

and

$$\boldsymbol{W}_1=\begin{bmatrix}\boldsymbol{w}'^{f_1}\\ \boldsymbol{w}'^{f_2}\\ \vdots\\ \boldsymbol{w}'^{f_T}\end{bmatrix}=\begin{bmatrix} w'_{1,1} & w'_{1,2} & \cdots & w'_{1,P}\\ w'_{2,1} & w'_{2,2} & \cdots & w'_{2,P}\\ \vdots & \vdots & \ddots & \vdots\\ w'_{T,1} & w'_{T,2} & \cdots & w'_{T,P}\end{bmatrix}, \tag{6.42}$$

The first step of estimating $P_S f_0^i(x)$ which are related with $Q f_0^i(x)$ can be resolved by the following constrained optimisation

$$\min_{0\le\{\upsilon_{i,j}\}_{i,j=1}^{N}\le N} \left\| \boldsymbol{W}_1 - \boldsymbol{Y}\cdot\boldsymbol{D}^T \right\|_F , \tag{6.43}$$

subject to

$$\sum_{j=1}^{N} \upsilon_{i,j}\lambda(R_j) = 1, \text{ for } i = 1,\ldots,N , \tag{6.44}$$

where

$$\boldsymbol{Y} = \begin{bmatrix} \boldsymbol{v}^{P_S f_0} \\ \boldsymbol{v}^{P_S f_1} \\ \vdots \\ \boldsymbol{v}^{P_S f_{T-1}} \end{bmatrix} = \begin{bmatrix} \upsilon_{0,1} & \upsilon_{0,2} & \cdots & \upsilon_{0,N} \\ \upsilon_{1,1} & \upsilon_{1,2} & \cdots & \upsilon_{1,N} \\ \vdots & \vdots & \ddots & \vdots \\ \upsilon_{T-1,1} & \upsilon_{T-1,2} & \cdots & \upsilon_{T-1,N} \end{bmatrix}. \tag{6.45}$$

After obtaining $P_S f_0^i(x)$, the Frobenius-Perron matrix corresponding to S is obtained as a solution to a constrained optimisation problem

$$\min_{\{m_{i,j}\}_{i,j=1}^{N}\ge 0} \| \boldsymbol{Y} - \boldsymbol{W}_0\boldsymbol{M} \|_F , \tag{6.46}$$

subject to

$$\sum_{j=1}^{N} m_{i,j}\lambda(R_j) = \lambda(R_i), \quad \text{for } i = 1,\ldots,N . \tag{6.47}$$

For continuous nonlinear map, by identifying the indices of the non-zero entries from the obtained $\boldsymbol{M}$, the final Frobenius-Perron matrix can be recovered with the re-implemented optimisation as described in Section 4.2.2.

6.2.4 Reconstruction of the underlying transformation

Based on the derived Frobenius-Perron matrix, an approximate piecewise linear semi-Markov transformation can be constructed over $\Re$ as introduced in Section 4.2.3 and finally the smoothed map can be obtained for continuous transformation which was shown in Section 4.2.4.

6.2.5 Numerical example

To demonstrate the applicability of the proposed algorithms, let us consider a numerical simulation example. The aim is to recover the logistic map on $[0, 1]$ (4.17), shown in Figure 4.2. The probability density function of the input variable u_n is given by

$$f_u(u) = \begin{cases} 1.5136, & 0 \le u \le 0.25; \\ 0.4880, & 0.25 < u \le 0.50; \\ 0.2776, & 0.50 < u \le 0.75; \\ 1.7208, & 0.75 < u \le 1, \end{cases} \tag{6.48}$$

shown in Figure 6.1.

The number of intervals of a regular partition of I for the initial conditions is set to N =40. Then 40 constant density functions $f_0^i(x),\ i = 1, 2, \ldots, 40$, compactly

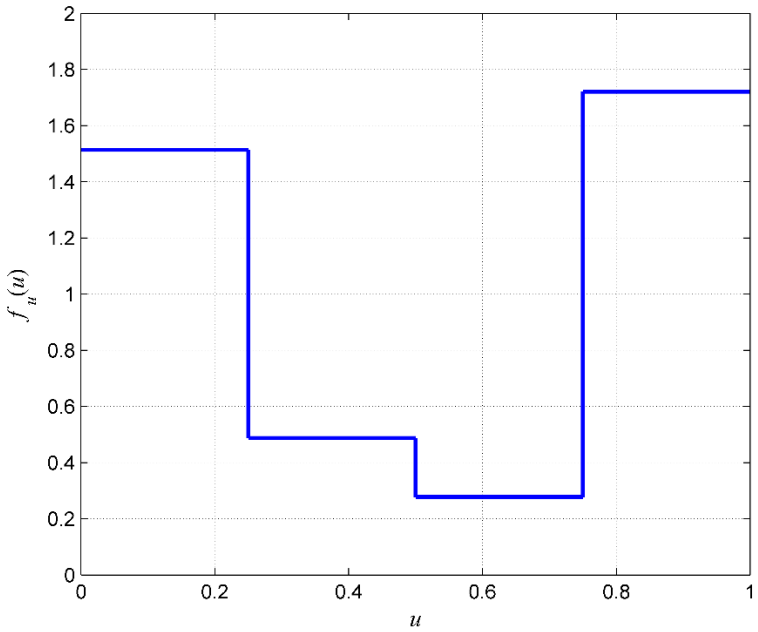

Figure 6.1 Probability density function of the input f_u.

supported on each interval I_i were constructed. To obtain the new densities $f_1^i(x)$, 5×10^3 initial states and a same number of inputs were randomly generated by sampling $f_0^i(x)$ and the input density f_u. The number of intervals of the regular

partition for $f_1^i(x)$ is set to *R*=40. The approximate piecewise linear semi-Markov map constructed based on the estimated Frobenius-Perron matrix is depicted in Figure 6.2. The smoothed map, obtained by fitting a cubic spline (smoothing parameter: 0.999), is shown in Figure 6.3.

To show the identification performance of the algorithms, the relative error between the identified and original maps is calculated for $x \in X = \{0.01, 0.02, ..., 0.99\}$. As shown in Figure 6.4, the relative error is less than 5%.

To evaluate the prediction performance of the identified model, two sets of initial conditions were generated by randomly sampling a uniform distribution $\mathcal{U}(0, 1)$ and a Gaussian distribution $\mathcal{N}(0.5, 0.1^2)$. The new input density was set to a Gaussian density $\mathcal{N}(0.28, 0.035^2)$, shown in Figure 6.5, and sampled to generate the inputs values. The *n*-steps-ahead model predictions where $n = 1, 2, 3, 5, 50, 200$, were used to estimate the predicted density functions which were compared with the density functions generated by the original model.

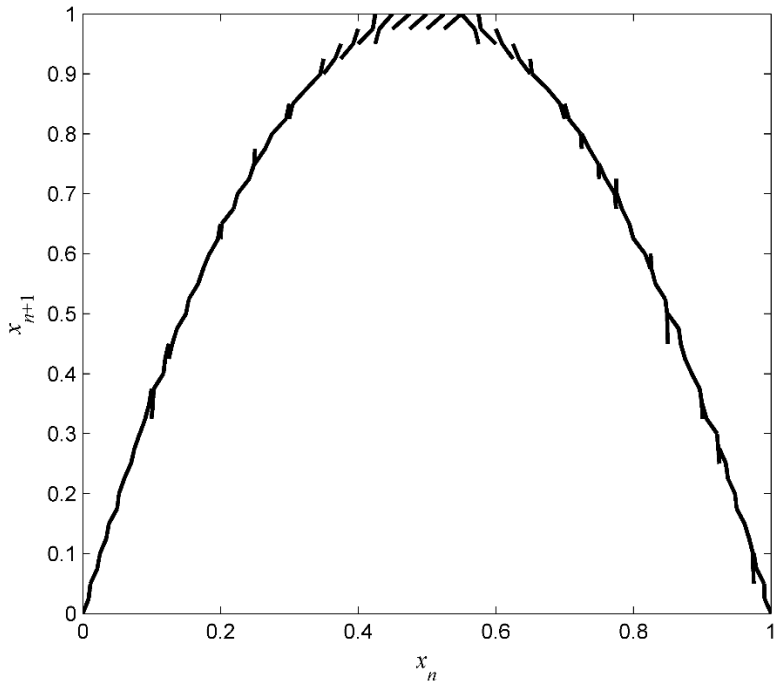

Figure 6.2 Constructed piecewise linear semi-Markov transformation for the underlying system.

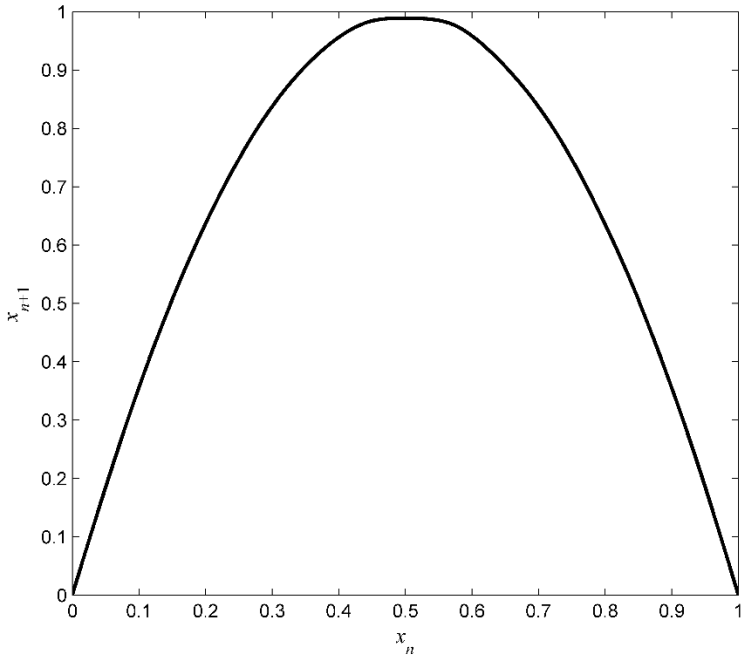

Figure 6.3 Identified smooth map.

The predicted densities for 1, 2, 3, 5, 50, and 200 iterations are shown in Figure 6.6 (uniform initial density) and Figure 6.7 (Gaussian initial density).

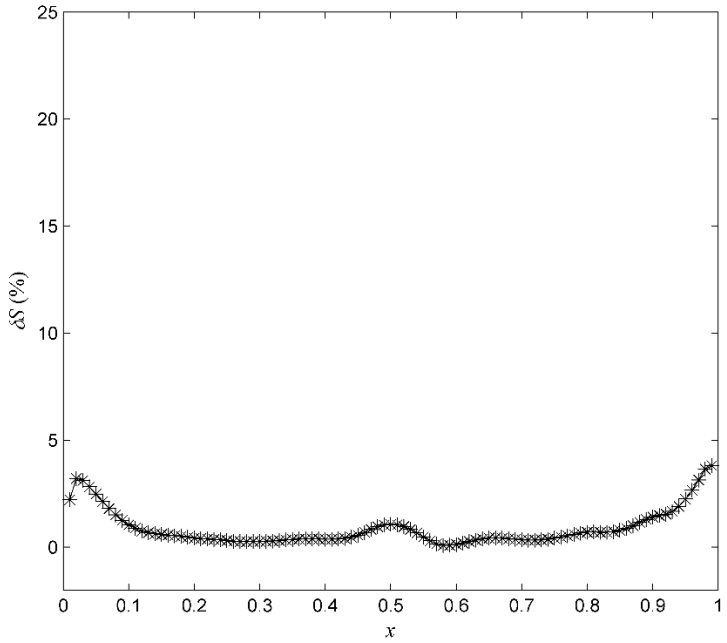

Figure 6.4 Relative error between the original map and the identified map evaluated for 99 uniformly spaced points.

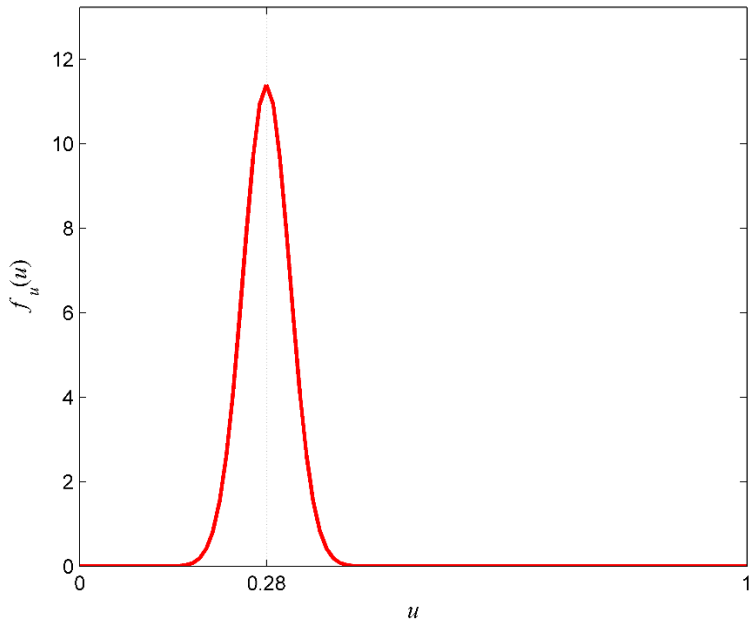

Figure 6.5 The input Gaussian density function used for model validation ($\mu = 0.28$, $\sigma = 0.035$).

The *root mean square error* (RMSE) between the predicted densities and true densities calculated by

$$\text{RMSE} = \sqrt{\frac{1}{R}\sum_{i=1}^{R}(v_i - \hat{v}_i)^2}\,, \tag{6.49}$$

is shown in Table 6.1, from which it can be clearly seen that the reconstructed map has high precision for predicting the evolving probability densities of the considered system.

Table 6.1 Root mean square error of the multiple steps predictions of densities with the identified model.

Initial density	1 Step	2 Steps	3 Steps	5 Steps	50 Steps	200 Steps
$\mathcal{U}(0,1)$	0.0891	0.1037	0.1448	0.1038	0.1173	0.1134
$\mathcal{N}(0.5, 0.1^2)$	0.1951	0.1839	0.1547	0.1341	0.1431	0.1283

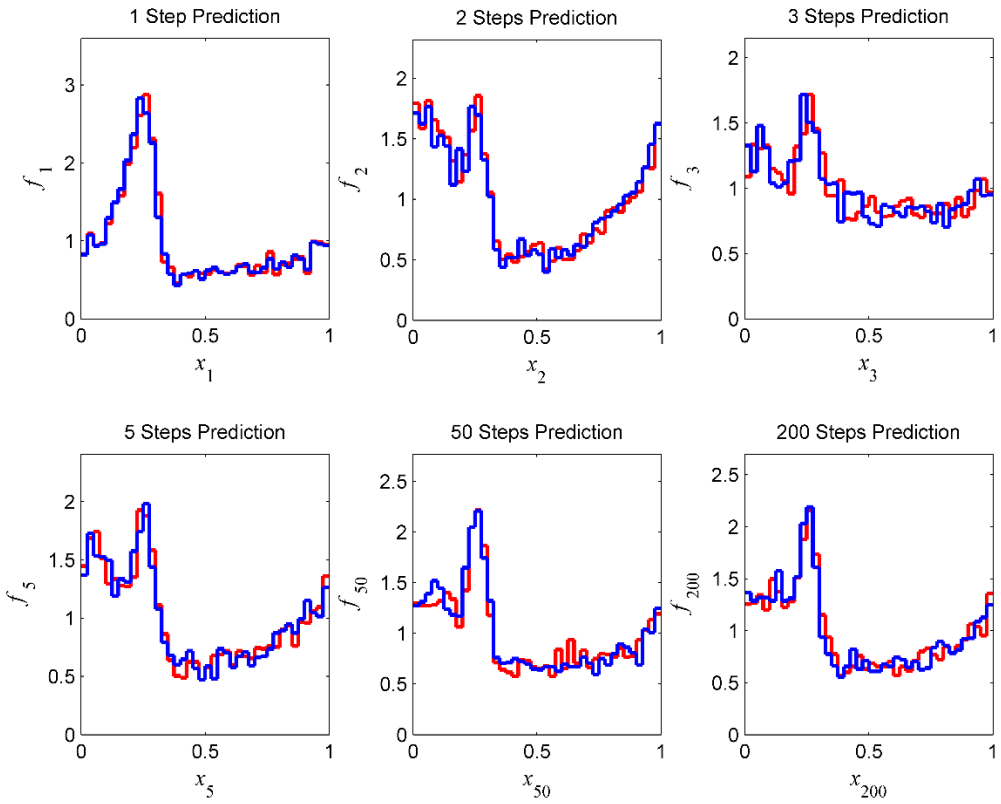

Figure 6.6 Predicted densities (blue lines) and true densities (red lines) of 1, 2, 3, 5, 50, and 200 steps from the initial uniform density $\mathcal{U}(0,1)$.

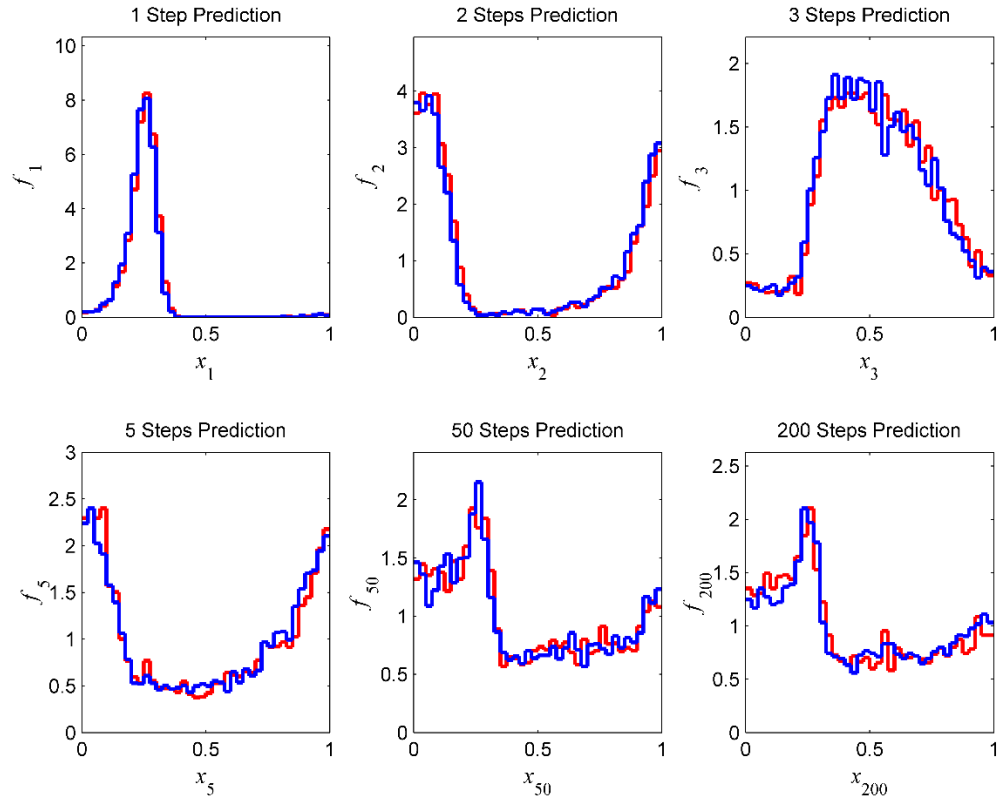

Figure 6.7 Predicted densities (blue lines) and true densities (red lines) of 1, 2, 3, 5, 50, and 200 steps from the initial Gaussian density $\mathcal{N}(0.5, 0.1^2)$.

6.3 Modelling of a one-dimensional dynamical system subjected to an additive stochastic noise

In Chapter 3 and Chapter 4, noise-free dynamical systems were studied. However, in all practical physical situations, systems under consideration are inevitably subjected to stochastic perturbations from external noise. Assuming the noise density function is known, this section rigorously examines reconstructing the one-dimensional chaotic map perturbed by an additive random noise, given observed sequences of probability density functions.

6.3.1 Formulation of the evolution of probability densities

The following one-dimensional non-singular discrete-time dynamical system subjected to an additive small random noise is considered.

$$x_{n+1} = S(x_n) + \omega_n \pmod{b}, \quad n = 0, 1, 2, \ldots, \tag{6.50}$$

where the transformation $S : I \to I$, $I = [0, b]$, x_n is a random variable bounded in I, having probability density function $f_n \in \mathfrak{D}(I, \mathfrak{B}, \mu)$, $\{\omega_n\}$ is i.i.d. noise bounded in $[-\varepsilon, \varepsilon]$ having the probability density function $g \in \mathfrak{D}$ and satisfying the following conditions:

1) $0 < \varepsilon \le b/2$;

2) $g(x) = 0$ for $|x| > \varepsilon$;

3) $\int_{-\varepsilon}^{\varepsilon} \omega_n(x)dx = 1$.

In order to understand the evolution of probability densities, same with the previous section, it is essential to derive the mathematical relationship between the density function f_{n+1} and f_n, g.

For an arbitrary Borel set $B \subset I$, the probability of x_{n+1} falling into B can be given by

$$\text{Prob}\{x_{n+1} \in B\} = \iint\limits_{S(x)+\omega \bmod b} f_n(x) g(\omega) dx d\omega \,, \tag{6.51}$$

Let $y = S(x) + \omega \bmod b$, it can be seen that the noisy system can be represented by

$$y = S(x) + \omega - b\chi_{(b,b+\varepsilon]}(S(x)+\omega) + b\chi_{(-\varepsilon,0)}(S(x)+\omega) \,. \tag{6.52}$$

It follows that

$$\omega = y - S(x) + b\chi_{(-b,\varepsilon-b]}(y - S(x)) - b\chi_{[b-\varepsilon,b]}(y - S(x)) \,. \tag{6.53}$$

Then, (6.51) can be rewritten as

$$\begin{aligned} &\text{Prob}\{x_{n+1} \in B\} \\ &= \int_B \int_I f_n(x) g(y - S(x) + b\chi_{(-b,\varepsilon-b]}(y - S(x)) - b\chi_{(b-\varepsilon,b]}(y - S(x))) dy dx. \end{aligned} \tag{6.54}$$

By changing the variables, it can be obtained that

$$f_{n+1}(x) = \int_I f_n(z) g(x - S(z) + b\chi_{(-b,\varepsilon-b]}(x - S(z)) - b\chi_{[b-\varepsilon,b)}(x - S(z)))\, dz \,. \tag{6.55}$$

This formula indicates the mathematical relationship between f_n and f_{n+1} under the effect of the additive noise.

6.3.2 The Foias operator

Using the Foias operator defined in Section 6.2.2, the formula (6.55) can be expressed as

$$Q f_n(x) = \int_I f_n(z) g(x - S(z) + b\chi_{(-b,\varepsilon-b]}(x - S(z)) - b\chi_{[b-\varepsilon,b)}(x - S(z)))\, dz \,, \tag{6.56}$$

In order to expand the equation, it is supposed that for one single noise value ω_n, there exist N_1 intervals $\{I_i^{(N_1)}\}_{i=1}^{N_1}$ on which $S(x_n) + \omega_n \in (b, b+\varepsilon]$, N_2 intervals $\{I_i^{(N_2)}\}_{i=1}^{N_2}$ on which $S(x_n) + \omega_n \in [-\varepsilon, 0)$, and N_3 intervals $\{I_i^{(N_3)}\}_{i=1}^{N_3}$ on which $S(x_n) + u_n \in [0, b]$. These lead to a partition of I given by $0 = a_0 < a_1 < \ldots < a_{N_1+N_2+N_3} = b$, thus the right side of (6.56) can be transformed in the following way

$$\begin{aligned} Q f_n(x) = &\sum_{i=1}^{N_1} \int_I f_n(z) g(x - S(z) + b) \chi_{I_i^{(N_1)}}(z)\, dz \\ &+ \sum_{i=1}^{N_2} \int_I f_n(z) g(x - S(z) - b) \chi_{I_i^{(N_2)}}(z)\, dz \\ &+ \sum_{i=1}^{N_3} \int_I f_n(z) g(x - S(z)) \chi_{I_i^{(N3)}}(z)\, dz. \end{aligned} \tag{6.57}$$

Let $y = S(z)$, then (6.57) can be written as

$$\begin{aligned} Q f_n(x) = &\sum_{i=1}^{N_1} \int_I \frac{f_n(S^{-1}(y))}{S'(S^{-1}(y))} g(x - y + b) \chi_{S(I_i^{(N_1)})}(y)\, dy \\ &+ \sum_{i=1}^{N_2} \int_I \frac{f_n(S^{-1}(y))}{S'(S^{-1}(y))} g(x - y - b) \chi_{S(I_i^{(N_2)})}(y)\, dy, \\ &+ \sum_{i=1}^{N_3} \int_I \frac{f_n(S^{-1}(y))}{S'(S^{-1}(y))} g(x - y) \chi_{S(I_i^{(N3)})}(y)\, dy. \end{aligned} \tag{6.58}$$

It follows that

$$\begin{aligned} Q f_n(x) = &\int_I g(x - y + b) \sum_{i=1}^{N_1} \left[\frac{f_n(S^{-1}(y))}{S'(S^{-1}(y))} \chi_{S(I_i^{(N_1)})}(y) \right] dy \\ &+ \int_I g(x - y - b) \sum_{i=1}^{N_2} \left[\frac{f_n(S^{-1}(y))}{S'(S^{-1}(y))} \chi_{S(I_i^{(N_2)})}(y) \right] dy \\ &+ \int_I g(x - y) \sum_{i=1}^{N_3} \left[\frac{f_n(S^{-1}(y))}{S'(S^{-1}(y))} \chi_{S(I_i^{(N_3)})}(y) \right] dy. \\ = &\int_I g(x - y + b \chi_{(-b,\, \varepsilon - b]}(x - y) - b \chi_{[b - \varepsilon,\, b)}(x - y)) \\ &\cdot \left\{ \sum_{i=1}^{N_1} \left[\frac{f_n(S^{-1}(y))}{S'(S^{-1}(y))} \chi_{S(I_i^{(N_1)})}(y) \right] + \right. \\ &\sum_{i=1}^{N_2} \left[\frac{f_n(S^{-1}(y))}{S'(S^{-1}(y))} \chi_{S(I_i^{(N_2)})}(y) \right] + \\ &\left. \sum_{i=1}^{N_3} \left[\frac{f_n(S^{-1}(y))}{S'(S^{-1}(y))} \chi_{S(I_i^{(N_3)})}(y) \right] \right\} dy. \end{aligned} \tag{6.59}$$

Let $N = N_1 + N_2 + N_3$, $I = \{I_i^{(N_1)}\}_{i=1}^{N_1} \cup \{I_i^{(N_2)}\}_{i=1}^{N_2} \cup \{I_i^{(N_3)}\}_{i=1}^{N_3} = \{I_1, I_2, \ldots, I_N\}$.

After merging the accumulations on the right side, it is obtained that

$$Q f(x) = \int_I g(x - y + b\chi_{(-b,\,\varepsilon-b]}(x-y) - b\chi_{[b-\varepsilon,\,b)}(x-y)) \cdot \sum_{i=1}^{N}\left[\frac{f_n(S^{-1}(y))}{S'(S^{-1}(y))}\chi_{S(I_i)}(y)\right]dy. \quad (6.60)$$

By submitting the Frobenius-Perron operator P_S associated with the transformation S into right side of (6.60), finally it is obtained that

$$Q f(x) = \int_I g(x - y + b\chi_{(-b,\,\varepsilon-b]}(x-y) - b\chi_{[b-\varepsilon,\,b)}(x-y)) P_S\, f_n(y)dy. \quad (6.61)$$

This formula establishes the mathematical relationship between the Foias operator corresponding to the noisy dynamical system and the Frobenius-Perron operator corresponding to the noise-free chaotic map.

The same assumption in Section 6.2 is made here that S is a piecewise linear semi-Markov transformation on the partition of I, $\Re = \{R_1, R_2, \ldots, R_N\}$. Using the same way of estimating $Q f_n$ on a regular partition $\Re' \square \{R'_1, R'_2, \ldots, R'_P\}$, $P_S f_n$ and f_n both on $\Re$, the resulting matrix is given by $\boldsymbol{D} = (d_{k,j})_{1\le k\le P;\,1\le j\le N}$,where

$$d_{k,j} = \frac{P}{b}\int_{R'_k}\int_{R_j} g(x - y + b\chi_{(-b,\,\varepsilon-b]}(x-y) - b\chi_{[b-\varepsilon,\,b)}(x-y))\, dydx. \quad (6.62)$$

Consequently, the following equation can be obtained

$$\boldsymbol{v}^{f_1} = \boldsymbol{w}^{f_0} \cdot \boldsymbol{M} \cdot \boldsymbol{D}^T, \quad (6.63)$$

where $\boldsymbol{w}^{f_0} = [w_1, \ldots, w_N]$, $\boldsymbol{v}^{f_1} = [v_1, \ldots, v_P]$, $f_n(x) = \sum_{i=1}^{N} w_i \chi_{I_i}(x)$,

$Q f_n(x) = \sum_{k=1}^{P} v_k \chi_{I_k}(x)$.

The Foias operator is represented by the estimated matrix $\boldsymbol{H}$ as follows

$$\boldsymbol{H} = \boldsymbol{M} \cdot \boldsymbol{D}^T. \quad (6.64)$$

6.3.3 Model identification

Based on the derived equality (6.63), the two experimentally designed scenarios described in Section 6.2.3 can be utilised to identify the Frobenius-Perron matrix $\boldsymbol{M}$. A set of noise values

$$\Omega = \{\omega_i\}_{i=1}^{\theta}, \tag{6.65}$$

is generated by sampling the given noise density function *g*. Finally, the map can be constructed in the same way as presented in Section 6.2.4.

6.3.4 Numerical examples

The following two numerical simulation examples are used to demonstrate the applicability of the derived algorithms,

1. Example A:

The piecewise linear chaotic transformation (3.39) which is subjected to an additive stochastic noise

$$x_{n+1} = S(x_n) + \omega_n, \qquad (\text{mod } 1), \tag{6.66}$$

is considered here. $\{\omega_n\}$ is white Gaussian noise of which $\xi = 1/50$. Given the partition of the underlying transformation $\mathfrak{R} = \{R_1, R_2, R_3, R_4\}$ where $R_1 = [0, 0.3]$, $R_2 = (0.3, 0.4]$, $R_3 = (0.4, 0.8]$ and $R_4 = (0.8, 1]$, a set of initial densities f_0^i, $i = 1, \ldots, 4$ shown in Figure 6.8 is used to generate the set of initial conditions X_0^i, $i = 1, \ldots, 4$, and the final density functions f_1^i, $i = 1, \ldots, 4$ shown in Figure 6.8 are estimated from the corresponding final states X_1^i, $i = 1, \ldots, 4$ for T =1 over the uniform partition $\mathfrak{R}'$ containing *P* equal intervals. *P* is set to be equal to *N*.

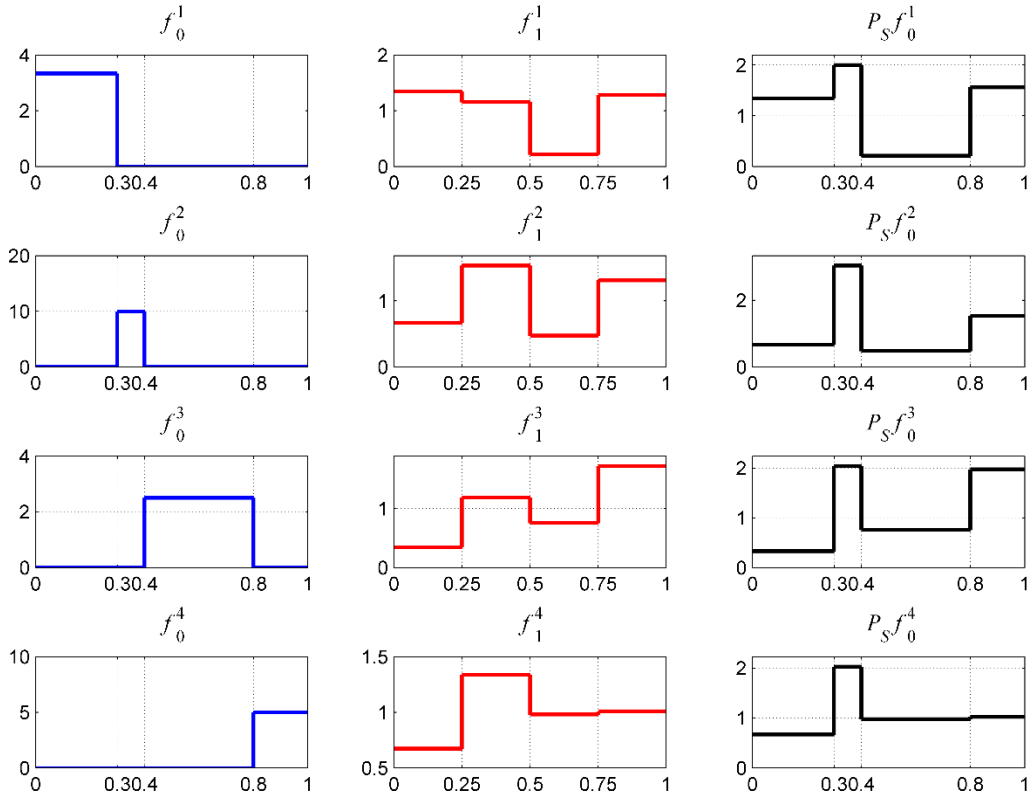

Figure 6.8 The initial and final density functions $f_0^i(x)$ and $f_1^i(x)$, and $P_S f_0^i(x)$

The obtained matrix $\boldsymbol{D}$ is given as follows

$$\boldsymbol{D} = \begin{bmatrix} 0.9921 & 0 & 0 & 0.0080 \\ 0.2000 & 0.4000 & 0.4000 & 0 \\ 0 & 0 & 1 & 0 \\ 0.0079 & 0 & 0.2000 & 0.7920 \end{bmatrix}. \tag{6.67}$$

$P_S f_0^i$, $i = 1, \ldots, 4$ on $\Re$ are obtained and figured in Figure 6.8. The estimated Frobenius-Perron matrix is

$$M = \begin{bmatrix} 0.4034 & 0.5988 & 0.0641 & 0.4674 \\ 0.0665 & 0.3033 & 0.0477 & 0.1533 \\ 0.1317 & 0.8164 & 0.3018 & 0.7907 \\ 0.1340 & 0.4056 & 0.1962 & 0.2039 \end{bmatrix}. \tag{6.68}$$

The corresponding reconstructed map $\hat{S}$ is shown in

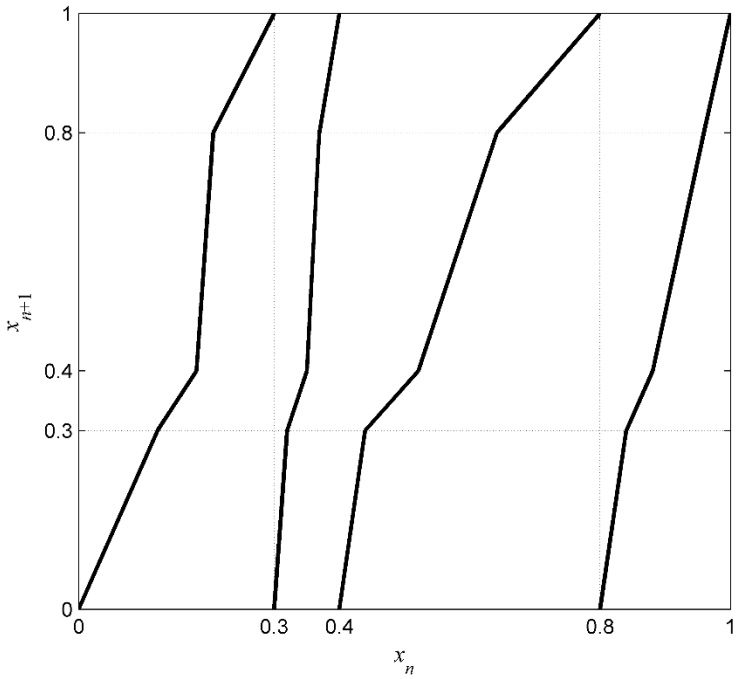

Figure 6.9 The identified transformation $\hat{S}$ of the underlying system.

The estimated coefficients of the identified piecewise linear semi-Markov transformation $\hat{S}\big|_{R_i}(x) = \hat{\alpha}_{i,j}x + \hat{\beta}_{i,j}$ are

$$(\hat{\alpha}_{i,j})_{1\le i,j\le 4} = \begin{bmatrix} 2.48 & 1.67 & 15.61 & 2.14 \\ 15.04 & 3.30 & 20.97 & 6.53 \\ 7.59 & 1.22 & 3.31 & 1.26 \\ 7.46 & 2.47 & 5.10 & 4.91 \end{bmatrix},$$

$$(\hat{\beta}_{i,j})_{1\le i,j\le 4} = \begin{bmatrix} 0 & 0.10 & -2.42 & 0.36 \\ -4.51 & -0.76 & -6.95 & -1.61 \\ -3.04 & -0.24 & -1.33 & -0.01 \\ -5.97 & -1.77 & -4.09 & -3.91 \end{bmatrix}.$$

The relative error for $x \in X = \{0.01, 0.02, ..., 0.99\}$ is plotted in Figure 6.10. It can be seen that $\delta S < 5\%$ on each point *x*.

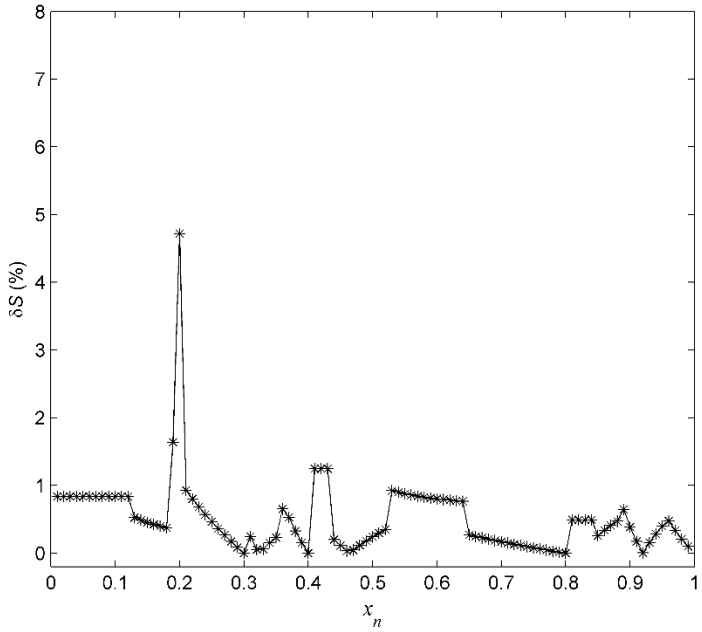

Figure 6.10 Relative error between the original map S and the identified map $\hat{S}$ evaluated for 99 uniformly spaced points.

In order to more fully demonstrate the effectiveness of the developed methodologies for reconstructing the maps of noisy dynamical systems, Table 6.2 shows the MAPE of identified maps for noise of varying magnitudes, compared with the MAPE using the algorithms for noise-free systems, given the partition of the underlying transformation.

Table 6.2 Comparison of MAPE (%) of identified maps for additive noise of different magnitudes ξ using A: the algorithms developed in this section and B: the algorithms for noise-free systems presented in Chapter 3.

ξ	0.02	0.04	0.10	0.15	0.20	0.40	0.50
A	0.5020	0.3267	0.7154	1.6843	1.3168	3.1725	2.9188
B	1.1422	1.4501	2.9156	4.6891	6.4222	9.8031	10.9585

It can be clearly seen that while the partition $\mathfrak{R}$ of the underlying transformation is known, the MAPE of the identified map using the algorithms of this section is apparently lower than 5% for the selected noise levels, and that the accuracy of identified maps using the algorithms is strictly higher than the one by directly applying the developed approach for solving the GIFPP for noise-free systems.

2. Example B:

To show the effectiveness of the developed algorithms for continuous nonlinear systems, the example of the logistic map with an additive random noise

$$x_{n+1} = 4x_n(1-x_n) + \omega_n \quad (\text{mod } 1), \tag{6.69}$$

is considered here. The noise is assumed to be white Gaussian noise with $\xi = 1/50$. A set of noise $\Omega = \{\omega_i\}_{i=1}^{\theta}$, was generated by sampling from a Gaussian probability density function $\mathcal{N}(0, (5\times10^{-3})^2)$. The partition $\mathfrak{R}$ is set to be uniform with $N = 40$ intervals. 100 densities (see Appendix) were randomly sampled to generate 100 sets of initial states $X_0^i = \{x_{0,j}^i\}_{j=1}^{\theta}$, i=1,...,100, $\theta = 5\times10^3$. The initial densities were estimated from the initial states X_0^i and their images $X_1^i = \{x_{i,j}\}_{j=1}^{\theta}$, i=1,...,100 obtained by applying the noise per iteration for each set X_0^i were used to estimate the initial density functions $\{f_{0,i}^{j(i)}\}$ on $\mathfrak{R}$ and the final density functions $\{f_{1,i}^{j(i)}\}$ on $\mathfrak{R}'$. It was set that $\mathfrak{R}' = \mathfrak{R}$, thus, $P = N$. Examples of initial densities $f_{0,i}^{j(i)}$, and the corresponding final densities $f_{1,i}^{j(i)}$, and $Pf_{0,i}^{j(i)}$ transformed from $f_{0,i}^{j(i)}$ under the undisturbed transformation S are shown in Figure 6.11.

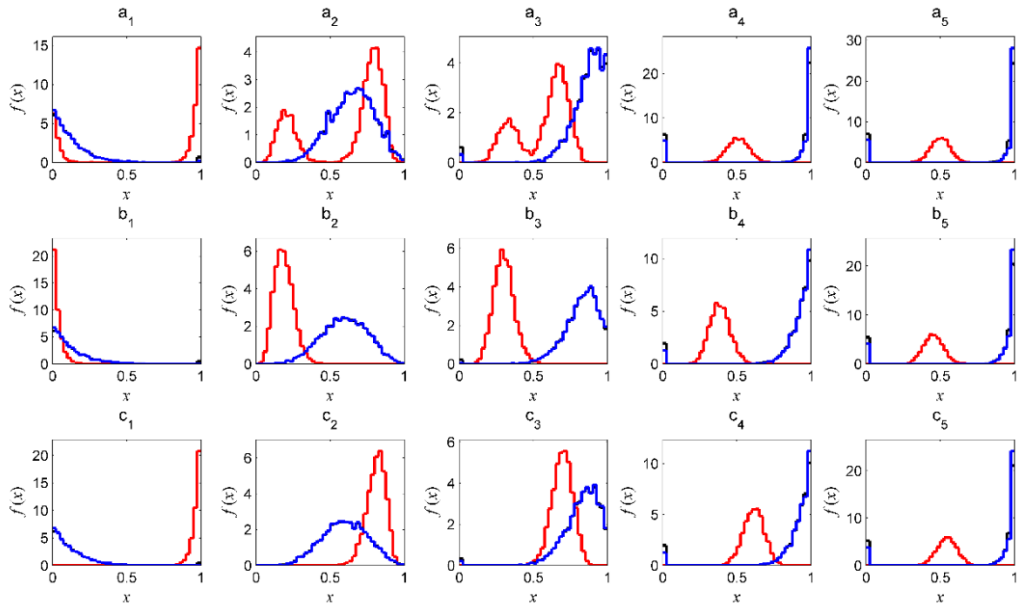

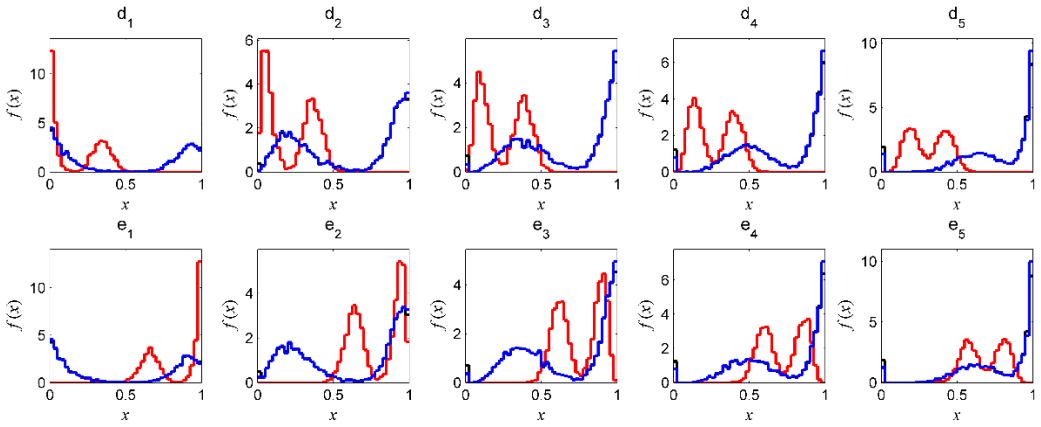

Figure 6.11 Examples of initial densities (red lines) $f_{0,i}^{j(i)}$ and the corresponding densities after one iteration (blue lines) $f_{1,i}^{j(i)}$ and $Pf_{0,i}^{j(i)}$ (black lines):

a1: $f_{0,1}^{1}$, $f_{1,1}^{1}$, $Pf_{0,1}^{1}$; a2: $f_{0,1}^{8}$, $f_{1,1}^{8}$, $Pf_{0,1}^{8}$; a3: $f_{0,1}^{15}$, $f_{1,1}^{15}$, $Pf_{0,1}^{15}$; a4: $f_{0,1}^{27}$, $f_{1,1}^{27}$, $Pf_{0,1}^{27}$; a5: $f_{0,1}^{30}$, $f_{1,1}^{30}$, $Pf_{0,1}^{30}$;

b1: $f_{0,2}^{1}$, $f_{1,2}^{1}$, $Pf_{0,2}^{1}$; b2: $f_{0,2}^{7}$, $f_{1,2}^{7}$, $Pf_{0,2}^{7}$; b3: $f_{0,2}^{13}$, $f_{1,2}^{13}$, $Pf_{0,2}^{13}$; b4: $f_{0,2}^{27}$, $f_{1,2}^{27}$, $Pf_{0,2}^{27}$; b5: $f_{0,2}^{30}$, $f_{1,2}^{30}$, $Pf_{0,2}^{30}$;

c1: $f_{0,3}^{1}$, $f_{1,3}^{1}$, $Pf_{0,3}^{1}$; c2: $f_{0,3}^{7}$, $f_{1,3}^{7}$, $Pf_{0,3}^{7}$; c3: $f_{0,3}^{13}$, $f_{1,3}^{13}$, $Pf_{0,3}^{13}$; c4: $f_{0,3}^{27}$, $f_{1,3}^{27}$, $Pf_{0,3}^{27}$; c5: $f_{0,3}^{30}$, $f_{1,3}^{30}$, $Pf_{0,3}^{30}$;

d1: $f_{0,4}^{1}$, $f_{1,4}^{1}$, $Pf_{0,4}^{1}$; d2: $f_{0,4}^{3}$, $f_{1,4}^{3}$, $Pf_{0,4}^{3}$; d3: $f_{0,4}^{5}$, $f_{1,4}^{5}$, $Pf_{0,4}^{5}$; d4: $f_{0,4}^{7}$, $f_{1,4}^{7}$, $Pf_{0,4}^{7}$; d5: $f_{0,4}^{10}$, $f_{1,4}^{10}$, $Pf_{0,4}^{10}$;

e1: $f_{0,5}^{1}$, $f_{1,5}^{1}$, $Pf_{0,5}^{1}$; e2: $f_{0,5}^{3}$, $f_{1,5}^{3}$, $Pf_{0,5}^{3}$; e3: $f_{0,5}^{5}$, $f_{1,5}^{5}$, $Pf_{0,5}^{5}$; e4: $f_{0,5}^{7}$, $f_{1,5}^{7}$, $Pf_{0,5}^{7}$; e5: $f_{0,5}^{10}$, $f_{1,5}^{10}$, $Pf_{0,5}^{10}$.

It is noticeable that $Pf_{0,i}^{j(i)}$ is close to $f_{1,i}^{j(i)}$ for the noise of the magnitude $\xi = 1/50$.

The identified approximate piecewise linear semi-Markov map is shown in Figure 6.12.

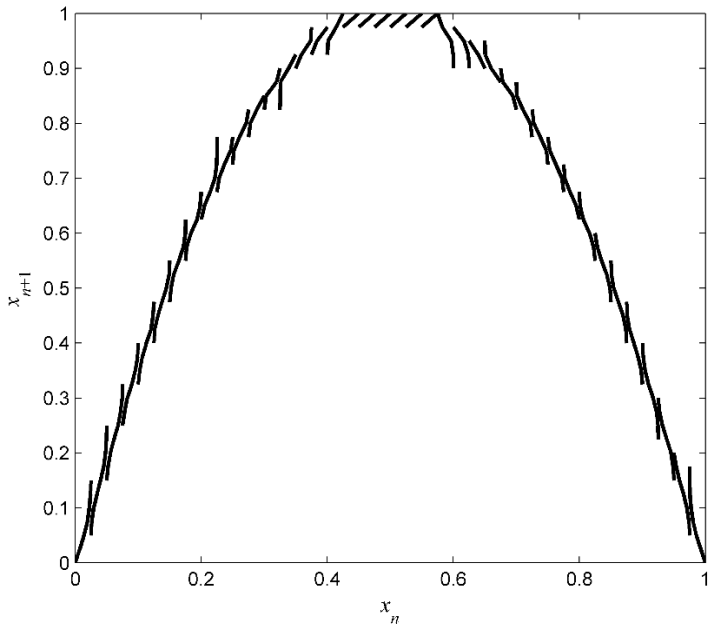

Figure 6.12 Reconstructed piecewise linear semi-Markov map $\hat{S}$ over the uniform partition $\mathfrak{R} = \{R_i\}_{i=1}^{40}$.

The smoothed map obtained with the smoothing parameter 0.999 is shown in Figure 6.13, and the relative error calculated on the uniformly spaces points is shown in Figure 6.14.

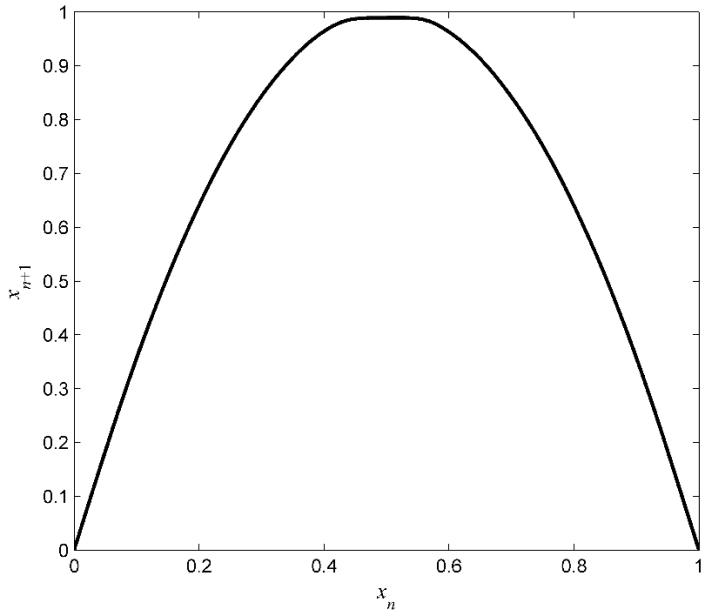

Figure 6.13 Identified smooth map $\overline{S}$ resulted from piecewise linear semi-Markov map in Figure 6.12 with smoothing parameter 0.999.

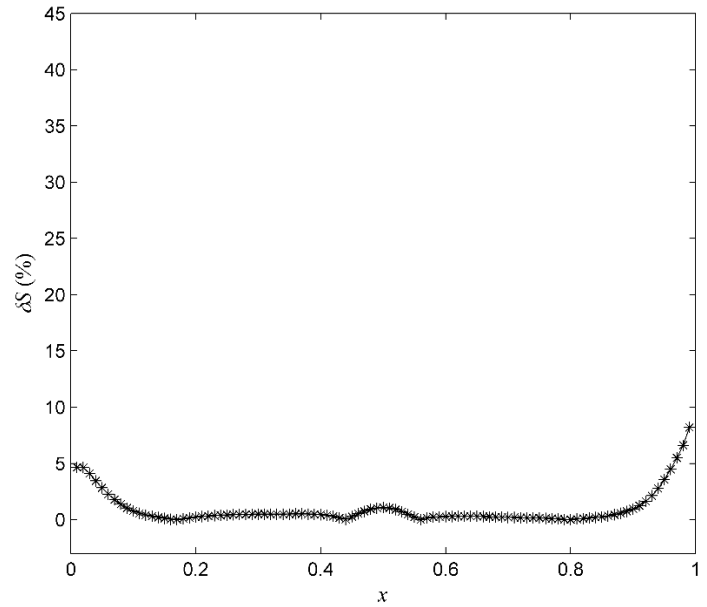

Figure 6.14 Relative error between the original map *S* and the identified smooth map $\overline{S}$ in Figure 6.13 evaluated for 99 uniformly spaced points.

Table 6.3 lists the results of MAPE of between the identified map $\overline{S}$ and the original map S for some different noise magnitudes $\xi = 0.02, 0.04, 0.10, 0.20, 0.40, 0.50$.

Table 6.3 MAPE between the identified and original maps for 7 different noise magnitudes.

ξ	0.02	0.04	0.10	0.15	0.20	0.40	0.50
MAPE (%)	0.9282	0.9809	4.5791	3.1054	2.7850	4.6319	9.7981

It can be clearly seen that satisfactory results have been obtained. Compared with the identification results in Section 4.3.2 where the modelling algorithm for noise-free dynamical systems was directly applied to the same noisy system, the developed algorithm possesses clearly better performance in reconstructing the underlying map, which is exactly the desired objective of modelling for this class of stochastic dynamical systems.

6.4 Conclusions

The chapter introduced new methodologies of reconstructing the maps of one-dimensional dynamical systems subjected to additive perturbations. The evolution of probability density functions was formulated. The approximate matrix representations of the Foias operator corresponding to the perturbed dynamical system was derived as well as the relationship between the Foias operator and the Frobenius-Perron matrix corresponding to the noise-free transformation. Assuming that the partition and probability density functions of perturbation are known, approaches for solving the inverse Foias problem for two cases of additive perturbations (input and noise) were presented. These provides solutions to inverse problems for practical dynamical systems, and modelling scheme used for designing control law of practical systems. Compared with the simulation results of applying the algorithms derived for noise-free dynamical systems to noisy dynamical systems, the proposed techniques have better performance in reconstructing the underlying transformations.

Chapter 7
Control of Invariant Densities for Stochastic Dynamical Systems

7.1 Introduction

Over the past few years there has been a great deal of interest in control of probability density function for dynamical systems. The main purpose is to regulate the statistical long-term behaviour so that it can settle down to a desired stable dynamical behaviour described by probability distribution. The so far developed control algorithms can be generally classified to two groups: 1) the control of output probability density function of a stochastic dynamical system through selecting a deterministic optimal input; 2) the control of the invariant density function for a chaotic dynamical system by virtue of slightly modifying the underlying transformation. The first group focuses on how to generate a crisp control input to make the output density function close to the desired one. Some representative research has been presented from Wang (1999a, 1999c, 2001, 2001, 2003, 2005a, 2008) and Forbes (2002, 2003a, 2003b, 2004a, 2004, 2004b, 2006). The second group looks into reconstructing a transformation by direct modifications (Góra and Boyarsky (1996, 1998, 2001)) or using a small perturbation to affect the original map to achieve a desired invariant density function (Bollt 2000a, Bollt 2000b). In this group, there are no assumption that the dynamical system is subjected to any perturbations.

In contrast to existing control strategies, the objective of controller design approach proposed in this work is to determine probability density function of the input in order to achieve a desired invariant density function for the perturbed chaotic map.

In Section 7.2, the existence and uniqueness of the invariant densities of dynamical systems subjected to additive perturbations (inputs and noise) are proven. The algorithm of estimating the invariant density function over a uniform partition is developed. Section 7.3 studies a more complex stochastic dynamical system which involves a bounded input and a random noise term. The evolution of probability density functions is formulated for the first time and used to prove asymptotic stability. A new algorithm to estimation of the invariant density using the derived approximate matrix representation of Foias operator is introduced. A numerical example is given to show the effectiveness of the proposed algorithms. Section 7.4 presents the control design algorithm for this class of stochastic dynamical system together with a simulated example that is used to demonstrate the applicability of the algorithm. Conclusions are presented in Section 7.5.

7.2 Invariant densities of stochastic dynamical systems

The existence of invariant densities of stochastic dynamical systems can be proven by analysing the asymptotic stability of $\{Q^n f\}$. The associated invariant densities are derived using the approximate matrix representation of the Foias operator.

7.2.1 Asymptotic stability of $\{Q^n\}$

To achieve the control of invariant densities of stochastic dynamical systems, the asymptotic stability of $\{Q^n f\}$ of the following dynamical system with an additive input is firstly examined.

$$x_{n+1} = S(x_n) + u_n \pmod{b}, \quad n = 0, 1, 2, \ldots, \tag{7.1}$$

where $S: I \to I$, $I = [0, b]$, is a measurable nonlinear and non-singular transformation; u_n is the independent random input variable bounded on I having the probability density function $f_u \in \mathfrak{D}(I, \mathfrak{B}, \mu)$. $Q f_n \in \mathfrak{D}$, $Q: L^1(I) \to L^1(I)$ is the Foias operator corresponding to the stochastic dynamical systems.

The asymptotic stability of $\{Q^n f\}$ is defined as follows (Lasota & Mackey 1994).

Definition 7.1 Let $Q: L^1 \to L^1$ be a Markov operator. Then $\{Q^n\}$ is said to be asymptotically stable if there exists a unique $f^* \in \mathfrak{D}$ such that $Q f^* = f^*$ and

$$\lim_{n\to\infty} \left\| Q^n f - f^* \right\| = 0, \tag{7.2}$$

for every $f \in \mathfrak{D}$.

It has been obtained that

$$Q f_n(x) = \int_I f_n(z) f_u(x - S(z) + b\chi_I(S(z) - x)) dz . \tag{7.3}$$

The integration over I is

$$\begin{aligned} \int_I Q f_n(x) dx &= \int_I \int_I f_u(x - S(z) + b\chi_I(S(z) - x)) f_n(z) dz dx \\ &= \int_I f_n(z) \int_I f_u(x - S(z) + b\chi_I(S(z) - x)) dz dx \end{aligned} \tag{7.4}$$

Since $\int_I \int_I f_u(x, z) dx dz = 1$,

$$\int_I Q f_n(x) dx = \int_I f_n(z) dz , \tag{7.5}$$

and $Q f_n(x) \geq 0$. Q is therefore a Markov operator.

The following theorem is proven in (Lasota & Mackey 1994).

Theorem 7.1 *Let $K: I \times I \to I$ be a stochastic kernel and P be the corresponding Markov operator. Assume that there is nonnegative $\zeta < 1$ such that for every bounded $B \subset I$ there is a $\varphi = \varphi(B) > 0$ for which*

$$\int_E K(x,y)dx \le \zeta\,, \tag{7.6}$$

for $\mu(E) < \varphi$, $y \in B$, $E \subset B$. *Assume further there exists a Liapunov function* $V : I \to I$ *such that*

$$\int_I V(x)P\,f(x)dx \le \alpha \int_0^\infty V(x)\,f(x)dx + \beta\,, \tag{7.7}$$

$0 \le \alpha < 1$, $\beta \ge 0$, *holds. Then P is constrictive. Consequently, for every* $f \in \mathfrak{D}$ *the sequence* $\{P^n\}$ *is asymptotically periodic.*

The theorem of asymptotic stability for a constrictive Markov operator is provided in (Lasota & Mackey 1994).

Theorem 7.2 *Let P be a constrictive Markov operator. Assume there is a set* $A \subset I$ *of non-zero measure,* $\mu(A) > 0$, *with the property that for every* $f \in \mathfrak{D}$ *there is an integer* $n_0(f)$ *such that* $P^n f(x) > 0$ *for almost all* $x \in A$ *and all* $n > n_0(f)$. *Then* $\{P^n\}$ *is asymptotically stable.*

A new theorem concerning the asymptotic periodicity of $\{Q^n\}$ is introduced and proven below.

Theorem 7.3 *For the Foias operator* $Q : L^1 \to L^1$ *defined by* (7.3). *If there exists a Liapunov function* $V : I \to I$ *such that*

$$\int_I f_u(x - S(z) + b\chi_I(S(z) - x))V(x)dx \le \alpha V(z) + \beta\,, \tag{7.8}$$

$0 \le \alpha < 1$, $\beta \ge 0$, *for all* $z \in I$, *then the Foias operator is constrictive, and for every* $f \in \mathfrak{D}$, $\{Q^n\}$ *is asymptotically stable.*

Proof. Since f_u is integrable, for every $\zeta > 0$ there is a $\varphi > 0$ such that

$$\int_A f_u(x)dx < \zeta\,, \text{ for } \mu(A) < \varphi\,. \tag{7.9}$$

Then from,

$$\begin{aligned}\int_E K(x,y)dx &= \int_E f_u(x - S(z) + b\chi_I(S(z) - x))dx \\ &= \int_{E-S(z)+b\chi_I(S(z)-x)} f_u(x)dx. \\ &< \zeta,\end{aligned} \tag{7.10}$$

for $\mu(E - S(z) + b\chi_I(S(z) - x)) = \mu(E) < \varphi$. Thus (7.6) holds.

Further,

$$\int_I V(x)Q f_n(x)dx = \int_I V(x)\int_I f_n(z) f_u(x - S(z) + b\chi_I(S(z) - x))dzdx, \tag{7.11}$$

Let $K(x,y) = f_u(x - S(z) + b\chi_I(S(z) - x))$ that is a stochastic kernel. It is given in (Lasota & Mackey 1994) that

$$\int_I K(x,y)V(x)dx \le \alpha V(x) + \beta. \tag{7.12}$$

From the assumption (7.8), it is given that

$$\begin{aligned}\int_I V(x)Q f_n(x)dx &= \int_I V(x)\int_I f_n(z) f_u(x - S(z) + b\chi_I(S(z) - x))dzdx \\ &= \int_I f_n(z)\int_I V(x) f_u(x - S(z) + b\chi_I(S(z) - x))dzdx \\ &\le \int_I f_n(z)[\alpha V(z) + \beta]dz \\ &= \alpha\int_I V(z) f_n(z)dz + \beta.\end{aligned} \tag{7.13}$$

Thus, the inequality (7.8) holds. As a consequence, Q is constrictive.

Since $f_u > 0$, $Q f_n(x) > 0$. From theorem 7.2, the asymptotic stability of $\{Q^n\}$ is thus proven.

Based on the above theorem, the new result of the asymptotic stability is derived as follows.

Theorem 7.4 *Let* $Q : L^1 \to L^1$ *be the Foias operator corresponding to the stochastic dynamical system* (7.1), $\{Q^n\}$ *is asymptotically stable.*

Proof. Let $V(x) = |x|$, then

$$\int_I f_u(x-S(z)+b\chi_I(S(z)-x))V(x)dx = \int_I f_u(x-S(z)+b\chi_I(S(z)-x))|x|dx \quad (7.14)$$

By changing the variables with $y = x - S(z) + b\chi_I(S(z)-x)$, then

$$\begin{aligned}
&\int_I f_u(x-S(z)+b\chi_I(S(z)-x))V(x)dx \\
&= \int_I f_u(y)\left|S(x)+y-b\chi_{(b,2b]}(S(x)+y)\right|dy \\
&\le \int_I f_u(y)(|S(x)|+\left|y-b\chi_{(b,2b]}(S(x)+y)\right|)dy \\
&= |S(x)|\int_I f_u(y)dy + \int_I f_u(y)\left|y-b\chi_{(b,2b]}(S(x)+y)\right|dy \\
&= |S(x)| + \int_I f_u(y)\left|y-b\chi_{(b,2b]}(S(x)+y)\right|dy. \qquad (7.15)
\end{aligned}$$

Since *S* maps *I* to *I*, the following inequality holds

$$|S(x)| \le \alpha|x| + b, \qquad (7.16)$$

where $0 \le \alpha < 1$. And

$$\beta = \int_I f_u(y)\left|y-b\chi_{(b,2b]}(S(x)+y)\right|dy > 0. \qquad (7.17)$$

Thus, (7.8) is satisfied. It is proven that $\{Q^n\}$ is asymptotically stable.

Since the invariant density of the stochastic dynamical system exists, the following new theorem regarding the uniqueness of an invariant density f^* of Q can be proven in the similar way as for the theorem 10.5.2 given in (Lasota & Mackey 1994).

Theorem 7.5 *Let* $Q: L^1 \to L^1$ *be the Foias operator corresponding to the stochastic dynamical system* (7.1). *If an invariant density* f^* *for Q exists, then the* f^* *is unique.*

Proof. Assume there exist two different invariant densities for *Q*, denoted by f_1^* and f_2^*. Let $\Delta f = f_1^* - f_2^*$. Since $Q f_1^* = f_1^*$, $Q f_2^* = f_2^*$,

$$
\begin{aligned}
&Q f_1^*(x) - Q f_2^*(x) \\
&= \int_I [f_1^*(z) - f_2^*(z)] f_u(x - S(z) + b\chi_I(S(z) - x))dz \\
&= \int_I \Delta f^*(z) f_u(x - S(z) + b\chi_I(S(z) - x))dz \\
&= Q\Delta f^*(x).
\end{aligned} \tag{7.18}
$$

Then Q is a linear operator, $Q\Delta f^* = \Delta f^*$. Thus,

$$
\left\| Q\Delta f^* \right\|_{L_1} = \left\| \Delta f^* \right\|_{L_1}. \tag{7.19}
$$

It is defined that $f^+(x) = \max(0, f(x))$, and $f^-(x) = \max(0, -f(x))$, thus $f(x) = f^+(x) - f^-(x)$ (Lasota & Mackey 1994).

$$
Q\Delta f^{*^+}(x) = \int_I \Delta f^{*^+}(z) f_u(x - S(z) + b\chi_I(S(z) - x))dz. \tag{7.20}
$$

Since $f_u > 0$, $Q\Delta f^{*^+}(x) > 0$ for $x \in I$. Also, $Q\Delta f^{*^-}(x) > 0$, for $x \in I$. Therefore,

$$
\begin{aligned}
\left\| Q\Delta f^* \right\|_{L^1} &= \left\| Q\Delta f^{*^+} - Q\Delta f^{*^-} \right\|_{L^1} \\
&= \left\| Q\Delta f^{*^+} \right\|_{L^1} - \left\| Q\Delta f^{*^-} \right\|_{L^1} \\
&< \left\| Q\Delta f^{*^+} \right\|_{L^1} + \left\| Q\Delta f^{*^-} \right\|_{L^1} = \left\| \Delta f^* \right\|_{L^1},
\end{aligned} \tag{7.21}
$$

which contradicts the equality (7.19). Thus, f_1^* and f_2^* should be identical. The stochastic dynamical system preserves a unique invariant density.

Similarly, by extending the above new derived results concerning the existence and uniqueness of invariant density of the dynamical system subjected to an additive input to the dynamical system subjected to an additive random noise, the following new theorem can be proven.

Theorem 7.6 *Let $Q: L^1 \to L^1$ be the Foias operator corresponding to the dynamical system subjective an additive random noise* (6.50), *$\{Q^n\}$ is asymptotically stable and the invariant density f^* for Q is unique.*

Proof. Assume there exist two different invariant densities for *Q*, denoted by f_1^* and f_2^*. Let $\Delta f = f_1^* - f_2^*$. Since $Q f_1^* = f_1^*$, $Q f_2^* = f_2^*$,

$$\begin{aligned} & Q f_1^*(x) - Q f_2^*(x) \\ &= \int_I [f_1^*(z) - f_2^*(z)] g(x - S(z) + b\chi_{(-b,\varepsilon-b]}(x - S(z)) - b\chi_{[b-\varepsilon,b)}(x - S(z)))\, dz \\ &= \int_I \Delta f^*(z) g(x - S(z) + b\chi_{(-b,\varepsilon-b]}(x - S(z)) - b\chi_{[b-\varepsilon,b)}(x - S(z)))\, dz \\ &= Q\Delta f^*(x). \end{aligned} \tag{7.22}$$

Then *Q* is a linear operator, $Q\Delta f^* = \Delta f^*$. Thus,

$$\left\| Q\Delta f^* \right\|_{L_1} = \left\| \Delta f^* \right\|_{L_1}. \tag{7.23}$$

It is still defined that $f^+(x) = \max(0, f(x))$, and $f^-(x) = \max(0, -f(x))$, thus $f(x) = f^+(x) - f^-(x)$ (Lasota & Mackey 1994).

$$\begin{aligned} & Q\Delta f^{*^+}(x) \\ &= \int_I \Delta f^{*^+}(z) g(x - S(z) + b\chi_{(-b,\varepsilon-b]}(x - S(z)) - b\chi_{[b-\varepsilon,b)}(x - S(z)))dz. \end{aligned} \tag{7.24}$$

Since $f_u > 0$, $Q\Delta f^{*^+}(x) > 0$ for $x \in I$. Also, $Q\Delta f^{*^-}(x) > 0$, for $x \in I$. From (7.21), it can be also obtained that

$$\left\| Q\Delta f^* \right\|_{L^1} < \left\| \Delta f^* \right\|_{L^1}, \tag{7.25}$$

which contradicts the equality (7.23). Thus, f_1^* and f_2^* should be identical. Then the chaotic system subjected to an additive random noise preserves a unique invariant density.

7.2.2 Approximation of the invariant density functions

The invariant density functions of the stochastic dynamical systems can be approximated by assuming the partitions $\mathfrak{R}$ and $\mathfrak{R}'$ are uniform and identical. A

new important result concerning the eigenvalue of the matrix $\boldsymbol{H}$ representing the corresponding Foias operator Q is stated and proven as follows.

Theorem 7.7 *Let the transformation S in* (7.1) *be a piecewise linear semi-Markov transformation on a regular partition* $\mathfrak{R} = \{R_1, R_2, \ldots, R_N\}$ *comprised of N equal sized intervals, and it is set that* $\mathfrak{R}' = \mathfrak{R}$, $P = N$. *Then matrix* $\boldsymbol{H}$ *representing the corresponding Foias operator has* 1 *as the eigenvalue of maximum modulus and also has the unique eigenvalue of modulus* 1.

Proof. It has been shown in Section 6.2 that for the stochastic dynamical system the following equality holds

$$\boldsymbol{Q}\,\boldsymbol{f} = \boldsymbol{f} \cdot \boldsymbol{H}, \tag{7.26}$$

where $\boldsymbol{f} = [f^1, f^2, \ldots, f^N]$ is a row vector, the matrix $\boldsymbol{H} = \boldsymbol{M} \cdot \boldsymbol{D}^T$ is a square matrix,

$$\boldsymbol{M} = \begin{bmatrix} m_{11} & \cdots & m_{1,j} & \cdots & m_{1,N} \\ \vdots & \ddots & \vdots & \vdots & \vdots \\ m_{i,1} & \cdots & m_{i,j} & \cdots & m_{i,N} \\ \vdots & \vdots & \vdots & \ddots & \vdots \\ m_{N,1} & \cdots & m_{N,i} & \cdots & m_{N,N} \end{bmatrix}, \tag{7.27}$$

$$\boldsymbol{D} = \begin{bmatrix} d_{11} & \cdots & d_{1,j} & \cdots & d_{1,N} \\ \vdots & \ddots & \vdots & \vdots & \vdots \\ d_{i,1} & \cdots & d_{i,j} & \cdots & d_{i,N} \\ \vdots & \vdots & \vdots & \ddots & \vdots \\ d_{N,1} & \cdots & d_{N,i} & \cdots & d_{N,N} \end{bmatrix}. \tag{7.28}$$

Let

$$\boldsymbol{H} = \begin{bmatrix} h_{11} & \cdots & h_{1,j} & \cdots & h_{1,N} \\ \vdots & \ddots & \vdots & \vdots & \vdots \\ h_{i,1} & \cdots & h_{i,j} & \cdots & h_{i,N} \\ \vdots & \vdots & \vdots & \ddots & \vdots \\ h_{N,1} & \cdots & h_{N,i} & \cdots & h_{N,N} \end{bmatrix}. \tag{7.29}$$

Thus, it can be given that

$$h_{i,j} = \sum_{k=1}^{N} \left(m_{i,k} \cdot d_{j,k} \right). \tag{7.30}$$

The sum of the j-th row of $\boldsymbol{H}$ is given by

$$\begin{aligned}
\sum_{j=1}^{N} h_{i,j} &= \left(h_{i,1} + \ldots h_{i,j} + \ldots + h_{i,N} \right) \\
&= \left(\begin{array}{c} \\ [m_{i,1} \ \cdots \ m_{i,j} \ \cdots \ m_{i,N}] \begin{bmatrix} d_{11} \\ \vdots \\ d_{1,j} \\ \vdots \\ d_{1,N} \end{bmatrix} + \cdots + [m_{i,1} \ \cdots \ m_{i,j} \ \cdots \ m_{i,N}] \begin{bmatrix} d_{j1} \\ \vdots \\ d_{j,j} \\ \vdots \\ d_{j,N} \end{bmatrix} \\ \\ \end{array} \right. \\
&\qquad \left. + \cdots + [m_{i,1} \ \cdots \ m_{i,j} \ \cdots \ m_{i,N}] \begin{bmatrix} d_{N1} \\ \vdots \\ d_{N,j} \\ \vdots \\ d_{N,N} \end{bmatrix} \right), \qquad (7.31) \\
&= [m_{i,1} \ \cdots \ m_{i,j} \ \cdots \ m_{i,N}] \begin{bmatrix} d_{11} + \ldots + d_{j,1} + \ldots + d_{N,1} \\ \vdots \\ d_{1,j} + \ldots + d_{j,j} + \ldots + d_{N,j} \\ \vdots \\ d_{1,N} + \ldots + d_{j,N} + \ldots + d_{N,N} \end{bmatrix}. \qquad (7.32)
\end{aligned}$$

From (6.22), it can be seen that

$$
\begin{aligned}
& d_{1,j} + \ldots + d_{j,j} + \ldots + d_{N,j} \\
&= \sum_{i=1}^{N} d_{i,j} \\
&= \sum_{i=1}^{N} \frac{N}{b} \int_{R_i} \int_{R_j} f_u(x - y + b\chi_I(y - x))\, dydx \\
&= \frac{N}{b} \sum_{i=1}^{N} \int_{R_i} \int_{R_j} f_u(x - y + b\chi_I(y - x))\, dydx \\
&= \frac{N}{b} \int_{I} \int_{R_j} f_u(x - y + b\chi_I(y - x))\, dydx \\
&= \frac{N}{b} \cdot \frac{b}{N} \\
&= 1.
\end{aligned} \tag{7.33}
$$

Thus, (7.32) becomes

$$
\sum_{j=1}^{N} h_{i,j} = [m_{i,1} \ \cdots \ m_{i,j} \ \cdots \ m_{i,N}] \begin{bmatrix} 1 \\ \vdots \\ 1 \\ \vdots \\ 1 \end{bmatrix}_{N \times 1} = \sum_{j=1}^{N} m_{i,j} \tag{7.34}
$$

Since $\Re$ is a uniform partition, $\sum_{j=1}^{N} m_{i,j} = \frac{\sum_{k=1}^{p(i)} Q_k^{(i)}}{\lambda(R_i)} = 1$, then $\sum_{j=1}^{N} h_{i,j} = 1$. Thus $\boldsymbol{H}$ is row stochastic. And $\boldsymbol{H}$ is a positive matrix, so it follows from the Frobenius-Perron Theorem that the matrix $\boldsymbol{H}$ has 1 as the eigenvalue of maximum modulus, and the algebraic and geometric multiplicities of the eigenvalue 1 is 1.

Consequently, the equation $\boldsymbol{f}^* = \boldsymbol{f}^* \boldsymbol{H}$ has a non-trivial solution, which is the left eigenvector associated with the eigenvalue 1. This is the invariant density function of the stochastic dynamical systems, estimated by a step function on the uniform partition $\Re$. It further establishes the existence of the invariant density functions of the stochastic dynamical systems.

Similarly, it can be concluded that the matrix $\boldsymbol{H}$ representing the Foias operator that is corresponding to the dynamical system subjected to an additive random noise

$$x_{n+1} = S(x_n) + \omega_n \pmod{b}, \quad n = 0, 1, 2, \ldots, \tag{7.35}$$

where the transformation $S : I \to I$, $I = [0, b]$, ω_n is the independent noise term bounded in $[-\varepsilon, \varepsilon]$, preserves 1 as the only eigenvalue of the maximum modulus. The associated left eigenvector is the estimated invariant density function.

7.2.3 Simulation example

Recall the numerical example in Section 6.2.5. Let the Gaussian density shown in Figure 6.1 be the probability density function f_u of the input. A set of initial states $X_0 = \{x_{0,j}\}_{j=1}^{\theta}$, $\theta = 5 \times 10^3$ generated by sampling from a uniform probability density function $f_0(x) = \chi_{[0,1]}(x)$ were iterated with the input $U = \{u_i\}_{i=1}^{\theta}$, $\theta = 5 \times 10^3$ sampled from f_u and applied per iteration using the stochastic dynamical system (7.1) to generate a corresponding set of final states $X_T = \{x_{T,j}\}_{j=1}^{\theta}$ where $T = 30{,}000$. The probability density function f_T estimated using the identified map and $\hat{f}_T$ estimated using the original map on $\Re = \{R_i\}_{i=1}^{40}$ are shown in Figure 7.1. The estimated unique invariant density function is given by

$$\boldsymbol{f}^* = \frac{\boldsymbol{\pi}}{\sum_{i=1}^{N} \frac{b\pi_i}{N}}, \tag{7.36}$$

where $\boldsymbol{\pi} = [\pi_1, \ldots, \pi_N]$ is the normalised left eigenvector of $\boldsymbol{H}$, and shown in Figure 7.1 to compare with f_T and $\hat{f}_T$.

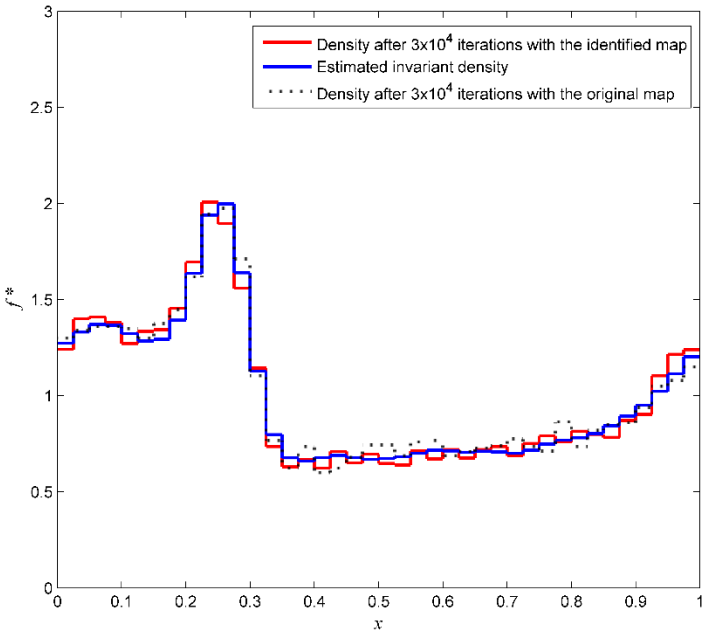

Figure 7.1 Comparison of the resulting density functions after 3×10^4 iterations from a set of 5×10^3 initial states uniformly distributed on [0 1] with the identified map and the original map, and the estimated invariant density.

7.3 Dynamical systems subjected to additive inputs and stochastic noise

The system considered for controlling the invariant density function in this chapter is a more complex one-dimensional dynamical system subjected to an additive input and a stochastic noise, stated as follows.

$$x_{n+1} = S(x_n) + u_n + \omega_n \pmod{b}, \quad n = 0, 1, 2, \ldots, \tag{7.37}$$

where $S : I \to I$, $I = [0, b]$, is a measurable nonlinear and non-singular transformation; x_n is a random variable bounded in I, having probability density function $f_n \in \mathfrak{D}(I, \mathfrak{B}, \mu)$, u_n is the independent random input variable bounded in I having a manipulated probability density function $f_u \in \mathfrak{D}$. The additive random noise $\{\omega_n\}$ bounded in $[-\varepsilon, \varepsilon]$ is i.i.d. (independent and identically distributed) with the probability density function $g \in \mathfrak{D}$.

7.3.1 Formulation of the evolution of probability densities

Since the system is bounded in *I*, assume a measurable function as

$$G(x_n, u_n) = S(x_n) + u_n \pmod{b}, \tag{7.38}$$

which is bounded in *I*. thus (7.37) can be expressed as

$$x_{n+1} = G(x_n, u_n) + \omega_n \pmod{b}, \quad n = 0, 1, 2, \ldots, \tag{7.39}$$

Let $x'_{n+1} = G(x_n, u_n)$, thus $x'_{n+1} \in I$, then it is obtained from (6.14) that the probability density function of x'_{n+1} is

$$f'_{n+1}(x') = \int_I f_u(x' - y + b\chi_I(y - x')) \cdot P_S f_n(y)\, dy. \tag{7.40}$$

where P_S is the Frobenius-Perron operator corresponding to *S*, Thus, (7.39) becomes

$$x_{n+1} = x'_{n+1} + \omega_n \mod b, \quad n = 0, 1, 2, \ldots. \tag{7.41}$$

This can be viewed as a dynamical system only with an additive noise. For an arbitrary Borel set $B \subset I$, the probability of $x_{n+1} \in B$ is given by

$$\text{Prob}\{x_{n+1} \in B\} = \iint\limits_{x'_{n+1}+\omega_n \bmod b} f'_{n+1}(x') g(\omega) dx' d\omega, \tag{7.42}$$

Let $z = x'_{n+1} + \omega \mod b$. Then (7.41) can be rewritten as

$$z = x'_{n+1} + \omega - b\chi_{(b,b+\varepsilon]}(x'_{n+1} + \omega) + b\chi_{(-\varepsilon,0)}(x'_{n+1} + \omega), \tag{7.43}$$

By substituting

$$\omega = z - x'_{n+1} + b\chi_{(-b,\varepsilon-b]}(z - x'_{n+1}) - b\chi_{[b-\varepsilon,b]}(z - x'_{n+1}), \tag{7.44}$$

into (7.42), it is obtained that

$$\begin{aligned} &\text{Prob}\{x_{n+1} \in B\} \\ &= \int_B \int_I f'_{n+1}(x') g(z - x' + b\chi_{(-b,\varepsilon-b]}(z - x') - b\chi_{(b-\varepsilon,b]}(z - x'))dx' dz. \end{aligned} \tag{7.45}$$

By changing the variable, it is further obtained that

$$f_{n+1}(x) = \int_I f'_{n+1}(x') g(x - x' + b\chi_{(-b,\varepsilon-b]}(x - x') - b\chi_{[b-\varepsilon,b)}(x - x'))\, dx'. \quad (7.46)$$

By submitting (7.40) into (7.46),

$$\begin{aligned} f_{n+1}(x) = \int_I \int_I f_u(x' - y + b\chi_I(y - x')) \cdot P_S f_n(y) \\ \cdot g(x - x' + b\chi_{(-b,\varepsilon-b]}(x - x') - b\chi_{[b-\varepsilon,b)}(x - x'))\, dydx'. \end{aligned} \quad (7.47)$$

As a result, the Foias operator corresponding to the system (7.37) is defined by

$$\begin{aligned} Q f_n(x) = \int_I \int_I f_u(x' - y + b\chi_I(y - x')) \\ \cdot g(x - x' + b\chi_{(-b,\varepsilon-b]}(x - x') - b\chi_{[b-\varepsilon,b)}(x - x')) \cdot P_S f_n(y)\, dydx'. \end{aligned} \quad (7.48)$$

It is assumed that S is a piecewise linear semi-Markov transformation on the partition of I, $\Re = \{R_1, R_2, \ldots, R_N\}$ containing N intervals. The density function of x_{n+1}, $Q f_n$ is estimated on a regular partition $\Re' \square \{R'_1, R'_2, \ldots, R'_P\}$.

By integrating both sides of (7.48) over $R'_k \in \Re'$, it is given that

$$\begin{aligned} \int_{R'_k} Q f_n(x)dx = \int_{R'_k} \int_I \int_I \big[f_u(x' - y + b\chi_I(y - x')) \\ \cdot g(x - x' + b\chi_{(-b,\varepsilon-b]}(x - x') - b\chi_{[b-\varepsilon,b)}(x - x')) \\ \cdot P_S f_n(y) \big] dydx'dx. \end{aligned} \quad (7.49)$$

Let $P_S f_n(x) = \sum_{i=1}^{N} \upsilon_i \chi_{I_i}(x)$, and $Q f_n(x) = \sum_{k=1}^{P} v_k \chi_{I_k}(x)$ which is estimated with rectangle method with respect to $\Re'$. Then,

$$\begin{aligned} v_k &= \frac{1}{\lambda(R'_k)} \int_{R'_k} \sum_{j=1}^{N} \Big\{ \int_{R_j} \int_I \big[f_u(x' - y + b\chi_I(y - x')) \\ &\quad \cdot g(x - x' + b\chi_{(-b,\varepsilon-b]}(x - x') - b\chi_{[b-\varepsilon,b)}(x - x')) \cdot \upsilon_j \big] dx'dy \Big\} dx \\ &= \frac{P}{b} \sum_{j=1}^{N} \Big\{ \int_{R'_k} \int_{R_j} \int_I \big[f_u(x' - y + b\chi_I(y - x')) \\ &\quad \cdot g(x - x' + b\chi_{(-b,\varepsilon-b]}(x - x') - b\chi_{[b-\varepsilon,b)}(x - x')) \big] dx'dydx \cdot \upsilon_j \Big\}. \end{aligned} \quad (7.50)$$

The matrix $\boldsymbol{D} = (d_{k,j})_{1\le k\le P;\,1\le j\le N}$ is defined by

$$\begin{aligned} d_{k,j} = \frac{P}{b}\int_{R_k'}\int_{R_j}\int_I \big[f_u(x'-y+b\chi_I(y-x')) \\ \cdot g(x-x'+b\chi_{(-b,\varepsilon-b]}(x-x')-b\chi_{[b-\varepsilon,b)}(x-x'))\big]dx'dydx. \end{aligned} \tag{7.51}$$

Then, (7.50) can be converted into the following equation.

$$\begin{bmatrix} v_1 \\ v_2 \\ \vdots \\ v_k \\ \vdots \\ v_P \end{bmatrix} = \begin{bmatrix} d_{11} & d_{12} & \cdots & d_{1j} & \cdots & d_{1N} \\ d_{21} & d_{22} & \cdots & d_{2j} & \cdots & d_{2N} \\ \vdots & \vdots & \ddots & \vdots & \vdots & \vdots \\ d_{k1} & d_{k2} & \cdots & d_{kj} & \cdots & d_{kN} \\ \vdots & \vdots & \vdots & \vdots & \ddots & \vdots \\ d_{P1} & d_{P2} & \cdots & d_{Pj} & \cdots & d_{PN} \end{bmatrix} \cdot \begin{bmatrix} \upsilon_1 \\ \upsilon_2 \\ \vdots \\ \upsilon_j \\ \vdots \\ \upsilon_N \end{bmatrix}. \tag{7.52}$$

By submitting (6.17) into (7.52), it can be obtained that

$$\begin{aligned} \boldsymbol{v}^{f_1} &= \boldsymbol{w}^{f_0}\cdot\boldsymbol{M}\cdot\boldsymbol{D}^T \\ &= \boldsymbol{\upsilon}^{P_S f_0}\cdot\boldsymbol{D}^T, \end{aligned} \tag{7.53}$$

where $\boldsymbol{w}^{f_0} = [w_1,\ldots,w_N]$, $\boldsymbol{v}^{f_1} = [v_1,\ldots,v_P]$, $\boldsymbol{\upsilon}^{P_S f_0} = [\upsilon_1,\ldots,\upsilon_N]$.

7.3.2 Invariant densities

The result concerning the asymptotic stability of $\{Q^n f\}$ of the stochastic dynamical systems (7.37) is stated as follows.

Theorem 7.8 *Let $Q: L^1 \to L^1$ be the Foias operator corresponding to the stochastic dynamical system* (7.37). *$\{Q^n\}$ is asymptotically stable and the invariant density f^* for Q is unique.*

Proof. The system (7.37) can be represented by (7.39). Since $G: I \to I$, the original system can be viewed as a dynamical system with an additive noise. From Theorem 7.6, it readily can be seen that the system admits a unique invariant density, and $\{Q^n\}$ is asymptotically stable.

Similarly, given a uniform partition $\mathfrak{R}$, the Foias operator can be represented by a square matrix $\boldsymbol{H}$. The result concerning the eigenvalue of the matrix $\boldsymbol{H}$ is stated as follows.

Theorem 7.9 *Let the transformation S in* (7.37) *be a piecewise linear semi-Markov transformation on a regular partition* $\mathfrak{R} = \{R_1, R_2, \ldots, R_N\}$, *and* $\mathfrak{R}' = \mathfrak{R}$, $P = N$. *Then matrix* $\boldsymbol{H}$ *representing the corresponding Foias operator has* 1 *as the eigenvalue of maximum modulus and also has the unique eigenvalue of modulus* 1.

Proof. In fact, (7.51) can be further expanded in the following way.

$$\begin{aligned} & d_{k,j} \\ & = \frac{P}{b}\int_{R_k'}\int_{R_j}\sum_{i=1}^{P}\left\{\int_{R_i'}\left[f_u(x'-y+b\chi_I(y-x'))\right.\right. \\ & \left.\left.\cdot g(x-x'+b\chi_{(-b,\varepsilon-b]}(x-x')-b\chi_{[b-\varepsilon,b)}(x-x'))\right]dx'\right\}dydx \\ & = \frac{P}{b}\sum_{i=1}^{P}\left\{\int_{R_i'}dx'\int_{R_k'}g(x-x'+b\chi_{(-b,\varepsilon-b]}(x-x')-b\chi_{[b-\varepsilon,b)}(x-x'))dx\right. \\ & \left.\cdot\int_{R_j}f_u(x'-y+b\chi_I(y-x'))dy\right\}. \end{aligned} \tag{7.54}$$

Then,

$$\begin{aligned} d_{k,j} &= \frac{\frac{b}{P}\sum_{i=1}^{P}(d_{k,i}^{\omega}\cdot d_{i,j}^{u})}{\int_{R_i'}dx'} = \frac{\frac{b}{P}\sum_{i=1}^{P}(d_{k,i}^{\omega}\cdot d_{i,j}^{u})}{\lambda(R_i')} \\ &= \frac{\frac{b}{P}\sum_{i=1}^{P}(d_{k,i}^{\omega}\cdot d_{i,j}^{u})}{b/P} \\ &= \sum_{i=1}^{P}(d_{k,i}^{\omega}\cdot d_{i,j}^{u}), \end{aligned} \tag{7.55}$$

where

$$d_{k,i}^{\omega} = \frac{P}{b}\int_{R_k'}\int_{R_i'}g(x-x'+b\chi_{(-b,\varepsilon-b]}(x-x')-b\chi_{[b-\varepsilon,b)}(x-x'))\,dx'dx, \tag{7.56}$$

$$d_{i,j}^{u} = \frac{P}{b}\int_{R_i'}\int_{R_j} f_u(x' - y + b\chi_I(y - x'))\, dydx' . \tag{7.57}$$

They forms the following two matrices:

$$\boldsymbol{D}^{\omega} = \begin{bmatrix} d_{1,1}^{\omega} & \cdots & d_{1,i}^{\omega} & \cdots & d_{1,P}^{\omega} \\ \vdots & \ddots & \vdots & \vdots & \vdots \\ d_{k,1}^{\omega} & \cdots & d_{k,i}^{\omega} & \cdots & d_{k,P}^{\omega} \\ \vdots & \vdots & \vdots & \ddots & \vdots \\ d_{P,1}^{\omega} & \cdots & d_{P,i}^{\omega} & \cdots & d_{P,P}^{\omega} \end{bmatrix}, \tag{7.58}$$

which is equivalent to the matrix $\boldsymbol{D}$ (6.62) while $N = P, \Re = \Re'$ for the noisy system considered in Section 6.3;

$$\boldsymbol{D}^{u} = \begin{bmatrix} d_{1,1}^{u} & \cdots & d_{1,j}^{u} & \cdots & d_{1,N}^{u} \\ \vdots & \ddots & \vdots & \vdots & \vdots \\ d_{i,1}^{u} & \cdots & d_{i,j}^{u} & \cdots & d_{i,N}^{u} \\ \vdots & \vdots & \vdots & \ddots & \vdots \\ d_{P,1}^{u} & \cdots & d_{P,j}^{u} & \cdots & d_{P,N}^{u} \end{bmatrix}, \tag{7.59}$$

which is equivalent to the matrix $\boldsymbol{D}$ (6.22) for the dynamical system with an additive input considered in Section 6.2.

From (7.55), it can be seen that

$$\boldsymbol{D} = \boldsymbol{D}^{\omega} \cdot \boldsymbol{D}^{u}, \tag{7.60}$$

Thereby, for a Frobenius-Perron matrix induced by the piecewise linear semi-Markov transformation *S*, (7.53) can rewritten as

$$\begin{aligned} \boldsymbol{v}^{f_1} &= \boldsymbol{w}^{f_0} \cdot \boldsymbol{M} \cdot (\boldsymbol{D}^{\omega} \cdot \boldsymbol{D}^{u})^{T} \\ &= \boldsymbol{w}^{f_0} \cdot \boldsymbol{M} \cdot \boldsymbol{D}^{u^T} \cdot \boldsymbol{D}^{\omega^T}. \end{aligned} \tag{7.61}$$

Thus, the Foias operator can be represented by the estimated matrix $\boldsymbol{H}$ as

$$\boldsymbol{H} = \boldsymbol{M} \cdot \boldsymbol{D}^{u^T} \cdot \boldsymbol{D}^{\omega^T}. \tag{7.62}$$

Alternatively, this can be obtained in the following way. Firstly only consider the dynamical systems with an additive input $x_{n+1} = S(x_n) + u_n \pmod b$,

$n = 0, 1, 2, \ldots$, which can be expressed as $x_{n+1} = G(x_n, u_n)$, $G : I \to I$. It has been obtained in (6.24) that

$$\boldsymbol{v}^{f_1} = \boldsymbol{w}^{f_0} \cdot \boldsymbol{M} \cdot \boldsymbol{D}^{u^T}. \tag{7.63}$$

From (6.25),

$$\boldsymbol{H} = \boldsymbol{M} \cdot \boldsymbol{D}^{u^T}. \tag{7.64}$$

is a row stochastic matrix, which satisfies the definition of a Frobenius-Perron matrix. Thus, *G* can be regarded as a piecewise linear semi-Markov transformation corresponding to the Frobenius-Perron matrix $\boldsymbol{M}_G = \boldsymbol{H}$. Therefore, (7.63) can be given by

$$\boldsymbol{v}^{f_1} = \boldsymbol{w}^{f_0} \cdot \boldsymbol{M}_G. \tag{7.65}$$

Then, for a dynamical system with an additive noise $x_{n+1} = G(x_n, u_n) + \omega_n, \bmod b$, $n = 0, 1, 2, \ldots$, from (6.63) it is obtained that

$$\boldsymbol{v}^{f_1} = \boldsymbol{w}^{f_0} \cdot \boldsymbol{M}_G \cdot \boldsymbol{D}^{\omega^T}. \tag{7.66}$$

Submitting (7.64) into (7.66) gives rise to the result of (7.61).

Then,

$$h_{i,j} = \sum_{k=1}^{N} \left(\sum_{t=1}^{N} (m_{i,t} \cdot d_{k,t}^{u}) \cdot d_{j,k}^{\omega} \right). \tag{7.67}$$

The sum of the *j*-th row of $\boldsymbol{H}$ is given by

$$\begin{aligned}
&\sum_{j=1}^{N} h_{i,j} \\
&= \left(h_{i,1} + \ldots h_{i,j} + \ldots + h_{i,N} \right) \\
&= \left(\left[\sum_{t=1}^{N} m_{i,t} d_{1,t}^{u} \;\; \cdots \;\; \sum_{t=1}^{N} m_{i,t} d_{k,t}^{u} \;\; \cdots \;\; \sum_{t=1}^{N} m_{i,t} d_{N,t}^{u} \right] \begin{bmatrix} d_{11}^{\omega} \\ \vdots \\ d_{1,j}^{\omega} \\ \vdots \\ d_{1,N}^{\omega} \end{bmatrix} \right.
\end{aligned}$$

$$+\cdots+[\sum_{t=1}^{N} m_{i,t}d_{1,t}^{u} \ \cdots \ \sum_{t=1}^{N} m_{i,t}d_{k,t}^{u} \ \cdots \ \sum_{t=1}^{N} m_{i,t}d_{N,t}^{u}]\begin{bmatrix} d_{j,1}^{\omega} \\ \vdots \\ d_{j,j}^{\omega} \\ \vdots \\ d_{j,N}^{\omega} \end{bmatrix}$$

$$+\cdots+[\sum_{t=1}^{N} m_{i,t}d_{1,t}^{u} \ \cdots \ \sum_{t=1}^{N} m_{i,t}d_{k,t}^{u} \ \cdots \ \sum_{t=1}^{N} m_{i,t}d_{N,t}^{u}]\begin{bmatrix} d_{N,1}^{\omega} \\ \vdots \\ d_{N,j}^{\omega} \\ \vdots \\ d_{N,N}^{\omega} \end{bmatrix}\Bigg), \tag{7.68}$$

$$=[\sum_{t=1}^{N} m_{i,t}d_{1,t}^{u} \ \cdots \ \sum_{t=1}^{N} m_{i,t}d_{k,t}^{u} \ \cdots \ \sum_{t=1}^{N} m_{i,t}d_{N,t}^{u}]\begin{bmatrix} d_{11}^{\omega}+\ldots+d_{j,1}^{\omega}+\ldots+d_{N,1}^{\omega} \\ \vdots \\ d_{1,j}^{\omega}+\ldots+d_{j,j}^{\omega}+\ldots+d_{N,j}^{\omega} \\ \vdots \\ d_{1,N}^{\omega}+\ldots+d_{j,N}^{\omega}+\ldots+d_{N,N}^{\omega} \end{bmatrix}. \tag{7.69}$$

From (7.33), it can be obtained that $\sum_{k=1}^{N} d_{k,j}^{\omega} = 1$, (7.69) becomes

$$\sum_{j=1}^{N} h_{i,j} = [\sum_{t=1}^{N} m_{i,t}d_{1,t}^{u} \ \cdots \ \sum_{t=1}^{N} m_{i,t}d_{k,t}^{u} \ \cdots \ \sum_{t=1}^{N} m_{i,t}d_{N,t}^{u}]\begin{bmatrix} 1 \\ \vdots \\ 1 \\ \vdots \\ 1 \end{bmatrix} \tag{7.70}$$

$$=\left(\sum_{t=1}^{N} m_{i,t}d_{1,t}^{u} \ +\ldots+ \ \sum_{t=1}^{N} m_{i,t}d_{k,t}^{u} \ +\ldots+ \ \sum_{t=1}^{N} m_{i,t}d_{N,t}^{u}\right) \tag{7.71}$$

$$=[m_{i,1}\cdots m_{i,j}\cdots m_{i,N}]\left(\begin{bmatrix} d_{1,1}^{u} \\ \vdots \\ d_{1,j}^{u} \\ \vdots \\ d_{1,N}^{u} \end{bmatrix}+\ldots+\begin{bmatrix} d_{k,1}^{u} \\ \vdots \\ d_{k,j}^{u} \\ \vdots \\ d_{k,N}^{u} \end{bmatrix}+\ldots+\begin{bmatrix} d_{N,1}^{u} \\ \vdots \\ d_{N,j}^{u} \\ \vdots \\ d_{N,N}^{u} \end{bmatrix}\right) \tag{7.72}$$

$$= [m_{i,1} \cdots m_{i,j} \cdots m_{i,N}] \begin{bmatrix} \sum_{k=1}^{N} d_{k,1}^{u} \\ \vdots \\ \sum_{k=1}^{N} d_{k,j}^{u} \\ \vdots \\ \sum_{k=1}^{N} d_{k,N}^{u} \end{bmatrix}. \tag{7.73}$$

From (7.33), $\sum_{k=1}^{N} d_{k,j}^{u} = 1$. Then,

$$\sum_{j=1}^{N} h_{i,j} = \sum_{j=1}^{N} m_{i,j} = 1. \tag{7.74}$$

Hence, the matrix representation ***H*** is a row stochastic matrix, then it has 1 as the eigenvalue of maximum modulus, and also has the unique eigenvalue of modulus 1. Consequently, Theorem 7.9 is proved.

The left eigenvector associated with the eigenvalue 1 of ***H*** is the invariant density function of the stochastic dynamical system (7.37) that is estimated with a step function on a regular partition.

7.3.3 Model identification

Given the probability density functions of the input u_n and the noise ω_n, f_u and g, and the partition $\Re$ on which the transformation is to be constructed, the matrix ***D*** can be obtained from (7.60). It is set that $P \geq N$. The Frobenius-Perron matrix associated with the piecewise linear semi-Markov transformation $\hat{S}$ is identified using the approaches described in Section 6.3.2. θ random input values $U = \{u_i\}_{i=1}^{\theta}$ and noise values $\Omega = \{\omega_i\}_{i=1}^{\theta}$ are sampled from f_u and g, respectively. To generated the final densities, each input and noise value are applied per iteration to yield the final states by $x_{t,j} = S(x_{t-1,j}) + u_k + \omega_k \pmod b$, $j = 1,\ldots,\theta$, $k = 1,\ldots,\theta$, $t = 1,\ldots,T$.

7.3.4 Numerical example

To show the effectiveness of the developed modelling algorithms in this section, consider the logistic map with an additive input and an additive noise that is stated as follows.

$$x_{n+1} = 4x_n(1-x_n) + u_n + \omega_n \pmod 1, \quad n = 0, 1, 2, \ldots, \tag{7.75}$$

where $x_n \in I = [0, 1]$, $u_n \in I$, and $\omega_n \in [-0.2, 0.2]$, the input density function is given by

$$f_u(u) = \frac{1}{2}\left(\frac{1}{\sigma_1\sqrt{2\pi}} e^{-\frac{(u-\mu_1)^2}{2\times\sigma_1^2}} + \frac{1}{\sigma_2\sqrt{2\pi}} e^{-\frac{(u-\mu_2)^2}{2\times\sigma_2^2}} \right), \tag{7.76}$$

where $\mu_1 = 0.30$, $\sigma_1 = 0.07$, $\mu_2 = 0.60$, $\sigma_2 = 0.10$, plotted in Figure 7.2; the noise density function shown in Figure 7.3 is step function given by

$$g(\omega) = \begin{cases} 4, & -0.20 \le \omega \le -0.10; \\ 4/3, & -0.10 < \omega \le 0.05; \\ 20/7, & 0.05 < \omega \le 0.12; \\ 2.5, & 0.12 < \omega \le 0.20. \end{cases} \tag{7.77}$$

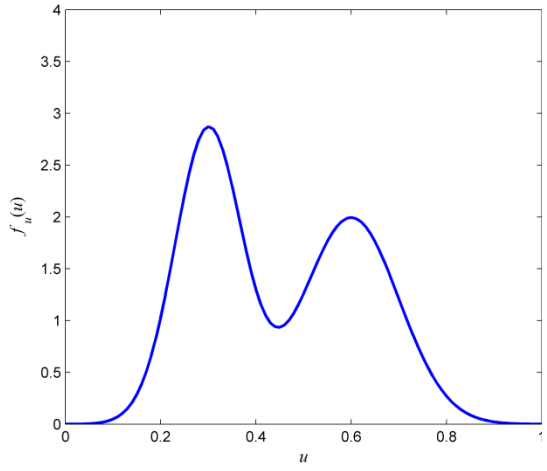

Figure 7.2 Probability density function of the input f_u

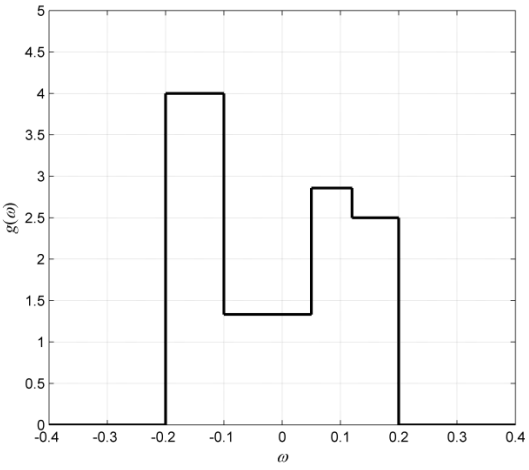

Figure 7.3 Probability density function of the noise f_ω

The partition $\Re$ is set to be a uniform partition containing $N = 40$ intervals. Partition $\Re'$ is set to be same with $\Re$, thus $P = N$. 40 constant density functions

$f_0^i(x)$, $i = 1, 2, \ldots, 40$, compactly supported on each interval I_i were constructed. To obtain the new densities $f_1^i(x)$, $\theta = 5\times10^3$ initial states, θ random inputs and θ random noise were generated by sampling $f_0^i(x)$, the given input density function f_u and the noise density function g_ω respectively. The Frobenius-Perron matrix recovered leads to the approximate piecewise linear semi-Markov transformation with respect to $\Re$ that is shown in Figure 7.4. The smoothed map, obtained by fitting a cubic spline (smoothing parameter: 0.999), is shown in Figure 7.5.

Using the same way in the preceding examples, the relative error between the identified smooth map and the original map is shown in Figure 7.6. It is obtained that $\text{MAPE} = 0.6692\%$. Starting at a set of initial states $X_0 = \{x_{0,j}\}_{j=1}^{\theta}$, $\theta = 5\times10^3$ uniformly distributed on *I*, the final states were arrived after $T = 30{,}000$ iterations. The obtained density function f_T is shown in Figure 7.7, compared with the resulting density function after same iterations with the original map, and the calculated invariant density function from (7.36) and (7.62).

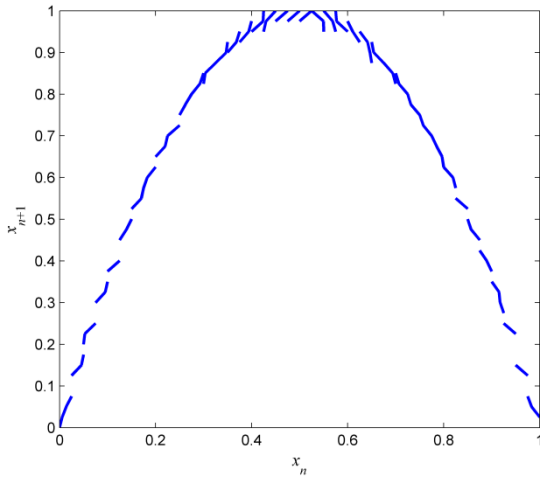

Figure 7.4 Constructed piecewise linear semi-Markov transformation for the dynamical system subjected to an additive random input having the probability density function (7.76) and an additive random noise with the probability density function (7.77).

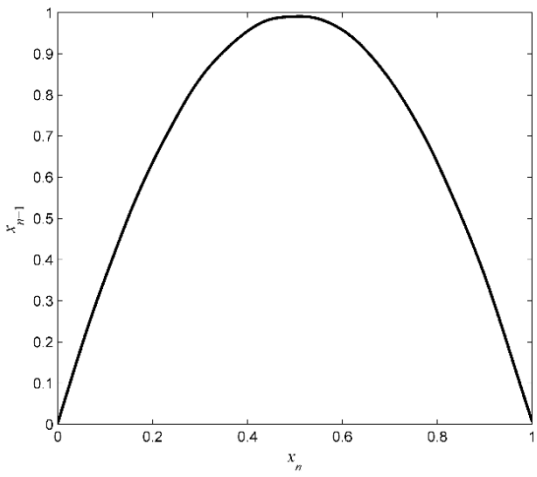

Figure 7.5 Smooth map identified from the constructed semi-Markov transformation shown in Figure 7.4.

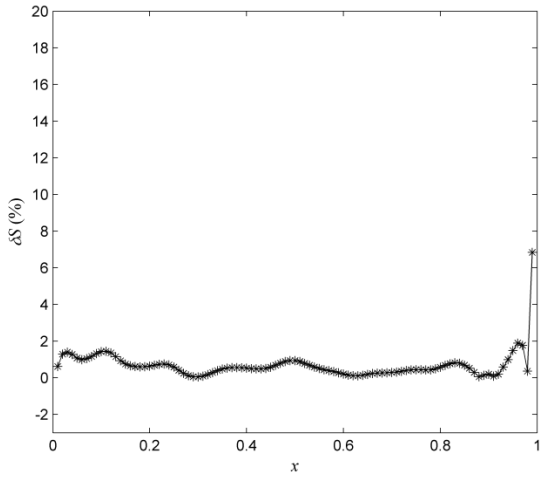

Figure 7.6 Relative error between the original map and the identified map Figure 7.5 evaluated for 99 uniformly spaced points.

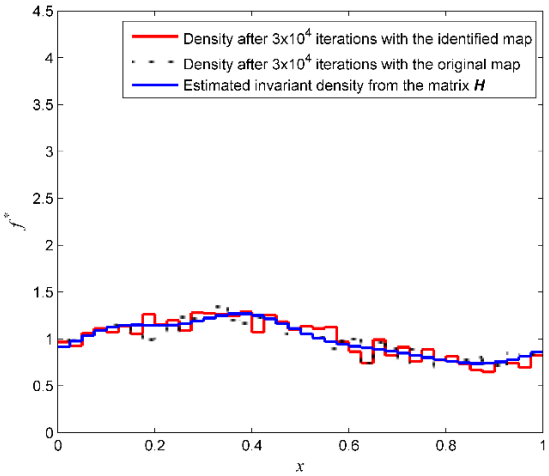

Figure 7.7 Comparison of the resulting density functions after 3×10^4 iterations from a set of 5×10^3 initial states uniformly distributed on [0 1] with the identified map Figure 7.5 (red line) and the original map (black dotted line), and the estimated invariant density (blue line).

It can be clearly seen that the estimated invariant density function of the identified map and the step function corresponding to the eigenvector associated with eigenvalue 1 of the matrix $\boldsymbol{H}$ are both very close to f_T.

7.4 Controller design

The above work lays the foundation for the design of control law. In this section, the controller design will be presented.

7.4.1 Design algorithm

The purpose of the controller design is to determine the probability density function of the input, $f_u(x)$, so that the invariant density function of the stochastic dynamical system (7.38) is made as close as possible to a desired distribution function, which is defined on *I*. This can be achieved by minimising the following performance function

$$J = \int_I (f^*(x) - f_d^*(x))^2 dx, \tag{7.78}$$

where $f^*(x)$ is the invariant density of the stochastic dynamical system, and $f_d^*(x)$ is the targeted distribution function.

Figure 7.8 shows the block diagram of the control system where the stochastic dynamical system is controlled by the designed controller that provides the optimal input density function.

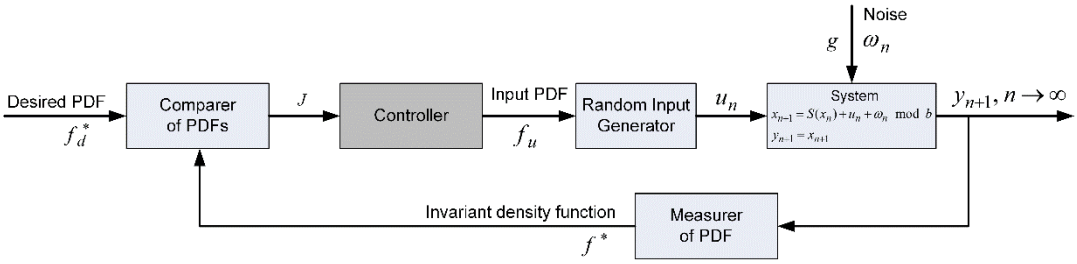

Figure 7.8 The block diagram of the control system.

The assumed measurable function *G* (7.38) can be also only related with *S* and the noise term ω_n, written as follows

$$G(x_n, \omega_n) = S(x_n) + \omega_n \pmod{b}, \tag{7.79}$$

thus, (7.37) can be expressed as

$$x_{n+1} = G(x_n, \omega_n) + u_n \pmod{b}, \quad n = 0, 1, 2, \ldots. \tag{7.80}$$

Since *G* still maps *I* into itself, and is independent with u_n, it can be shown that the matrix representing the Foias operator in (7.62) is equivalent to right side of the following equality

$$\boldsymbol{H} = \boldsymbol{M} \cdot \boldsymbol{D}^{\omega^T} \cdot \boldsymbol{D}^{u^T}. \tag{7.81}$$

Let $\boldsymbol{v}^{f_d^*} = [v_1^{d*}, v_2^{d*}, \ldots, v_N^{d*}]$ be the vector form of the desired invariant density function on $\Re$, then $f_d^*(x) = \sum_{i=1}^{N} v_i^{d*} \chi_{R_i}(x)$. Thus, the ideal situation is to find an input density function f_u which can make the following equation satisfied

$$\boldsymbol{v}^{f_d^*} = \boldsymbol{v}^{f_d^*} \cdot \boldsymbol{H}, \tag{7.82}$$

By substituting (7.81) into (7.82), it follows that

$$\boldsymbol{v}^{f_d^*} = \boldsymbol{v}^{f_d^*} \cdot \boldsymbol{M} \cdot \boldsymbol{D}^{\omega^T} \cdot \boldsymbol{D}^{u^T}. \tag{7.83}$$

Since $\Re$ is a uniform partition, from (7.57) and (7.59), it can be obtained that

$$\begin{aligned}
&d_{1,1}^u = d_{2,2}^u = \ldots = d_{i,i}^u = \ldots = d_{N,N}^u;\\
&d_{1,2}^u = d_{2,3}^u = \ldots = d_{i,i+1}^u = \ldots = d_{N-1,N}^u;\\
&\vdots\\
&d_{1,j}^u = d_{2,j+1}^u = \ldots = d_{i,i+j-1}^u = \ldots = d_{N-j+1,N}^u;\\
&\vdots\\
&d_{1,N-1}^u = d_{2,N}^u,
\end{aligned} \tag{7.84}$$

where $2 \le j \le N-1$, $j \le i \le N-j+1$, and

$$\begin{aligned}
&d_{2,1}^u = d_{3,2}^u = \ldots = d_{i+1,i}^u = \ldots = d_{N,N-1}^u;\\
&\vdots\\
&d_{j,1}^u = d_{j+1,2}^u = \ldots = d_{i,i-j+1}^u = \ldots = d_{N,N-j+1}^u;\\
&\vdots\\
&d_{N-1,1}^u = d_{N,2}^u,
\end{aligned} \tag{7.85}$$

where $2 \le j \le N-1$, $j \le i \le N$.

Moreover, it can be seen that

$$d_{1,i}^u = d_{N-i+2,1}^u, \tag{7.86}$$

for $2 \le i \le N$. This implies that the matrix $\boldsymbol{D}^u$ contains N unique values, which are $\{d_{i,1}^u\}_{i=1}^N$. Let $\alpha_i = d_{i,1}^u$ for $i = 1, \ldots, N$. Then the matrix $\boldsymbol{D}^u$ can be represented by

$$\boldsymbol{D}^{u}=\begin{bmatrix}\alpha_1 & \alpha_N & \alpha_{N-1} & \alpha_{N-2} & \dots & \alpha_5 & \alpha_4 & \alpha_3 & \alpha_2\\ \alpha_2 & \alpha_1 & \alpha_N & \alpha_{N-1} & \ddots & \ddots & \alpha_5 & \alpha_4 & \alpha_3\\ \alpha_3 & \alpha_2 & \alpha_1 & \alpha_N & \ddots & \ddots & \ddots & \alpha_5 & \alpha_4\\ \alpha_4 & \alpha_3 & \alpha_2 & \alpha_1 & \ddots & \ddots & \ddots & \ddots & \alpha_5\\ \vdots & \ddots & \ddots & \ddots & \ddots & \ddots & \ddots & \ddots & \vdots\\ \alpha_{N-3} & \ddots & \ddots & \ddots & \ddots & \alpha_1 & \alpha_N & \alpha_{N-1} & \alpha_{N-2}\\ \alpha_{N-2} & \alpha_{N-3} & \ddots & \ddots & \ddots & \alpha_2 & \alpha_1 & \alpha_N & \alpha_{N-1}\\ \alpha_{N-1} & \alpha_{N-2} & \alpha_{N-3} & \ddots & \ddots & \alpha_3 & \alpha_2 & \alpha_1 & \alpha_N\\ \alpha_N & \alpha_{N-1} & \alpha_{N-2} & \alpha_{N-3} & \cdots & \alpha_4 & \alpha_3 & \alpha_2 & \alpha_1\end{bmatrix}. \quad (7.87)$$

Let $\boldsymbol{v}^{f_d^*}\cdot\boldsymbol{M}\cdot\boldsymbol{D}^{\omega^T}=[\beta_1,\beta_2,\dots,\beta_i,\dots,\beta_N]$. Then

$$\beta_i=\sum_{j=1}^{N}\left(d_{i,j}^{\omega}\sum_{i=1}^{N}v_i^*m_{i,k}\right). \quad (7.88)$$

Thus,

$$\begin{aligned}&\boldsymbol{v}^{f_d^*}\cdot\boldsymbol{M}\cdot\boldsymbol{D}^{\omega^T}\cdot\boldsymbol{D}^{u^T}\\ &=\begin{bmatrix}\beta_1\alpha_1+\beta_2\alpha_N+\beta_3\alpha_{N-1}+\dots+\beta_N\alpha_2\\ \beta_1\alpha_2+\beta_2\alpha_1+\beta_3\alpha_N+\dots+\beta_N\alpha_3\\ \vdots\\ \beta_1\alpha_N+\beta_2\alpha_{N-1}+\beta_3\alpha_{N-2}+\dots+\beta_N\alpha_1\end{bmatrix}^T.\end{aligned} \quad (7.89)$$

By extracting the N unique values α_i, it is further obtained that

$$\begin{aligned}&\boldsymbol{v}^{f_d^*}\cdot\boldsymbol{M}\cdot\boldsymbol{D}^{\omega^T}\cdot\boldsymbol{D}^{u^T}\\ &=\begin{bmatrix}\alpha_1 & \alpha_2 & \alpha_3 & \cdots & \alpha_N\end{bmatrix}\cdot\begin{bmatrix}\beta_1 & \beta_N & \beta_{N-1} & \cdots & \beta_2\\ \beta_2 & \beta_1 & \beta_N & \cdots & \beta_3\\ \beta_3 & \beta_2 & \beta_1 & \cdots & \beta_4\\ \vdots & \vdots & \vdots & \ddots & \vdots\\ \beta_N & \beta_{N-1} & \beta_{N-2} & \cdots & \beta_1\end{bmatrix}^T.\end{aligned} \quad (7.90)$$

Thereby, the problem of minimising the performance function (7.78) is converted to the following constrained optimisation problem to solve for the unique values α_i in the first instance.

$$\min_{\{\alpha_i\}_{i=1}^N \geq 0} \left\| \boldsymbol{\beta}\boldsymbol{\alpha} - (\boldsymbol{v}^{f_d^*})^T \right\|_F^2, \tag{7.91}$$

subject to

$$\sum_{i=1}^{N} \alpha_i = 1, \tag{7.92}$$

where $\boldsymbol{\beta} = \begin{bmatrix} \beta_1 & \beta_N & \beta_{N-1} & \cdots & \beta_2 \\ \beta_2 & \beta_1 & \beta_N & \cdots & \beta_3 \\ \beta_3 & \beta_2 & \beta_1 & \cdots & \beta_4 \\ \vdots & \vdots & \vdots & \ddots & \vdots \\ \beta_N & \beta_{N-1} & \beta_{N-2} & \cdots & \beta_1 \end{bmatrix}, \boldsymbol{\alpha} = \begin{bmatrix} \alpha_1 \\ \alpha_2 \\ \alpha_3 \\ \vdots \\ \alpha_N \end{bmatrix}$.

Let $f_u(x)$ be approximated over the partition $\mathfrak{R}$, represented by

$$f_u(x) = \sum_{i=1}^{N} \psi_i \chi_{R_i}(x) dx. \tag{7.93}$$

Given the obtained $\{\alpha_i\}_{i=1}^N$, the coefficients $\{\psi_2, \psi_3, \ldots, \psi_N\}$ can be estimated by

$$\psi_k = \frac{\alpha_k}{\iint_{R_k \times R_1} dxdy} \cdot \frac{b}{N} = \frac{N\alpha_k}{b}, \tag{7.94}$$

for $k = 2, 3, \ldots, N$, and

$$\psi_1 = \frac{b}{N} \cdot \frac{\alpha_1 - \frac{1}{2}\alpha_N}{\frac{1}{2}\iint_{R_1 \times R_1} dxdy} = \frac{(2\alpha_1 - \alpha_N)N}{b}. \tag{7.95}$$

As a consequence, $f_u(x)$ estimated with the coefficients in (7.94) and (7.95) is the obtained probability density function of the control input that aims at attaining the targeted invariant density function $f_d^*(x)$.

It has been proven that $\{Q^n\}$ for the stochastic dynamical system is asymptotically stable. Given the input density function $f_u \in \mathfrak{D}$ defined on *I*, the system has a unique invariant density function $f^*(x)$. In other words, $Q^n f \to f^*$, as $n \to \infty$.

7.4.2 Numerical example

To demonstrate the use of the proposed control algorithm, the following stochastic dynamical system is considered

$$x_{n+1} = S(x_n) + u_n + \omega_n \pmod 1, \quad n = 0, 1, 2, \ldots, \tag{7.96}$$

where $S(x_n) = 4x_n(1 - x_n)$ is the logistic map of which the approximate Frobenius-Perron matrix has been identified in Section 6.3.4, $\omega_n \in [-0.02, 0.02]$ is a Gaussian noise of which the density function is shown in Figure 7.9. The desired invariant density is shown in Figure 7.10.

$$\begin{aligned} \boldsymbol{v}^{f_d^*} = [&0.14,0.16,0.18,0.19,0.25,0.28,0.35,0.44,0.55,0.67,\\ &0.75,0.93,1.19,1.37,1.54,1.72,1.78,1.78,1.71,1.52,\\ &1.25,1.04,1.04,1.09,1.36,1.65,1.96,2.24,2.50,2.27,\\ &1.84,1.56,1.02,0.62,0.35,0.21,0.11,0.11,0.12,0.13]. \end{aligned} \tag{7.97}$$

$\boldsymbol{D}^{\omega}$ for the given noise density function has been obtained, thus

$$\begin{aligned} &[\beta_1, \beta_2, \ldots, \beta_N]\\ &= [0.824,0.072,0.070,0.071,0.076,0.075,0.079,0.079,0.080,0.079,\\ &\ 0.086,0.086,0.091,0.107,0.123,0.137,0.162,0.182,0.204,0.246,\\ &\ 0.292,0.346,0.411,0.502,0.581,0.735,0.869,0.979,1.107,1.257,\\ &\ 1.456,1.678,1.891,2.099,2.272,2.459,2.703,3.133,4.061,8.239]. \end{aligned} \tag{7.98}$$

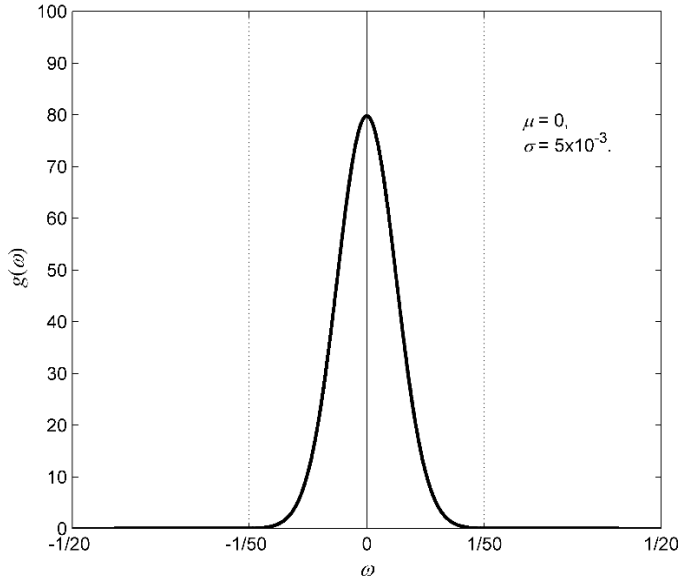

Figure 7.9 Probability density function of the noise ω_n of the stochastic dynamical system.

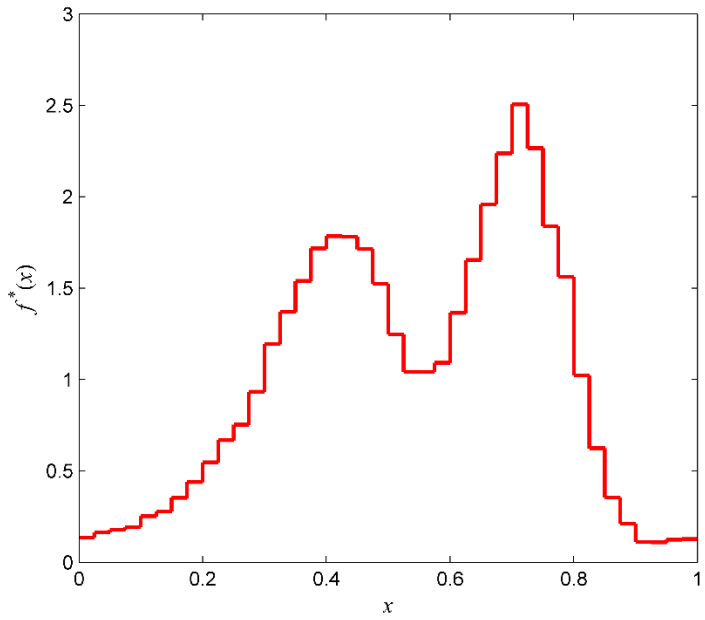

Figure 7.10 The target density function.

By solving the linear least-squares (7.91) problem, it is obtained that

$$
\begin{aligned}
&[\alpha_1, \alpha_2, \ldots, \alpha_N] \\
&= [0, 0, 0, 0, 0, 0, 0, 0, 0, 0, \\
&\ 0, 0, 0, 0, 0, 0.0169, 0.0415, 0.0549, 0.0644, 0.0719, \\
&\ 0.0641, 0.0339, 0, 0, 0, 0, 0, 0.0168, 0.0534, 0.116, \\
&\ 0.1202, 0.098, 0.109, 0.0702, 0.0424, 0.0203, 0.006, 0, 0, 0].
\end{aligned}
\tag{7.99}
$$

Then the optimal input density function is obtained, as shown in Figure 7.11.

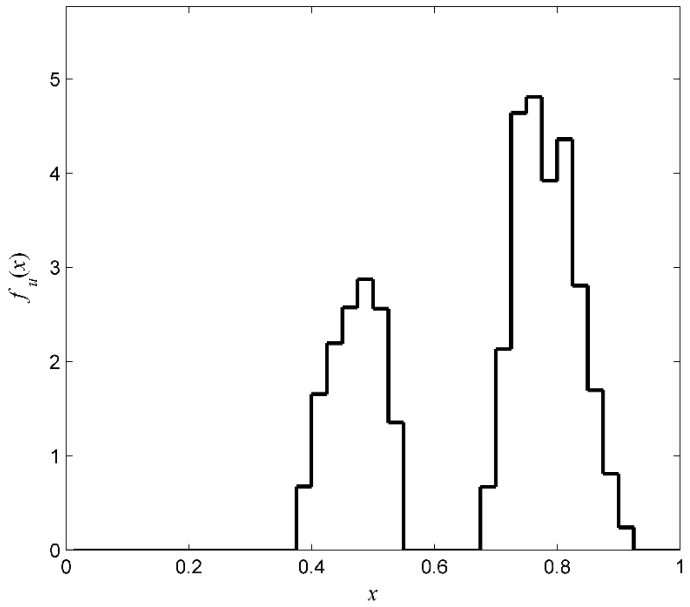

Figure 7.11 Optimal density function of the input.

$$
\begin{aligned}
&[\psi_1, \psi_2, \ldots, \psi_N] \\
&= [0, 0, 0, 0, 0, 0, 0, 0, 0, 0, \\
&\quad 0, 0, 0, 0, 0, 0.6769, 1.6582, 2.1956, 2.5768, 2.8757, \\
&\quad 2.5648, 1.3554, 0, 0, 0, 0, 0, 0.6713, 2.1365, 4.6390, \\
&\quad 4.8088, 3.9206, 4.3607, 2.8074, 1.6977, 0.8129, 0.2419, 0, 0, 0].
\end{aligned} \tag{7.100}
$$

As a result, this leads to the responds of the invariant density function as shown in Figure 7.12.

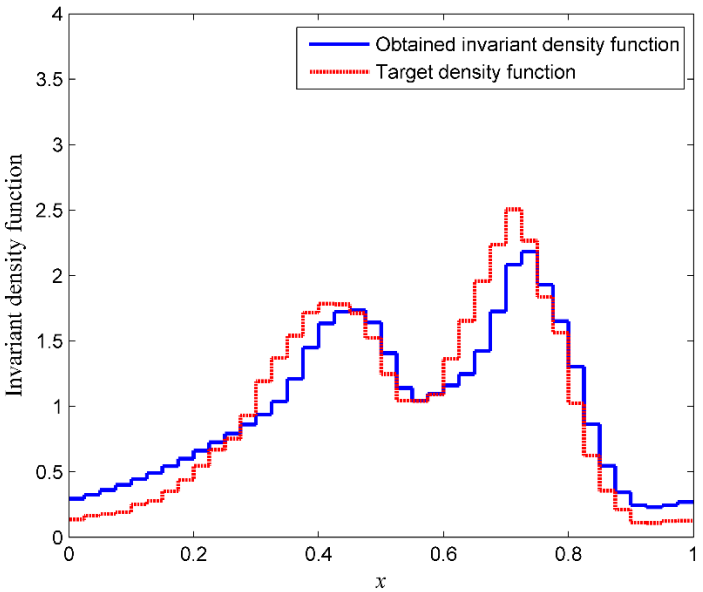

Figure 7.12 Comparison of the resulting invariant density function and the target density function.

7.5 Conclusions

In this chapter, new theorems regarding the asymptotic stability of $\{Q^n f\}$ for the dynamical systems subjected to additive inputs or random noise, and the uniqueness of the existing invariant densities have been proven. It has been proven that the invariant densities can be estimated from the left eigenvector associated with the eigenvalue 1 of matrix $\boldsymbol{H}$ representing the corresponding Foias operator. Based on the derivation of formulation of $\{Q^n f\}$ for the two cases of perturbed chaotic systems (by an additive input or an additive noise), the evolution of probability density functions of a more extensive stochastic dynamical system that involves an additive input and a random input has been inferred mathematically. Also, the statistical stability of such systems has been proven, and the invariant density functions have been estimated with the approaximate matrix representation of the associated Foias operator. Identifying the model of such stochastic dynamical systems has been addressed based on the earlier developed modelling methodologies.

The above work laid the theoretical foundation for addressing the control problem. A new control strategy has been developed which aims for controlling the shape of the invariant density function of the stochastic dynamical system so as to make it as close as possible to a given density function. To minimise the established performance function, connection between the input density function and the desired invariant density function is derived. The optimisation problem for determining the input density function can be formulated as a constrained least-squares problem to solve for the vector that corresponds to the optimal input density function. A simulated example is used to illustrate the effectiveness of the proposed algorithm.

Chapter 8

Conclusions and Future Work

8.1 Contributions

Chaotic dynamical systems can exhibit complex and random-like behaviour which is not predictable in general (Kellert & Sklar 1997). This phenomenon can be characterised by probability density function as an alternative to study individual point trajectories, particularly in some situations when probability density functions are more convenient to be measured than individual point trajectories. The main purpose of the thesis is that modelling for one-dimensional chaotic dynamical systems from sequences of probability density functions, and controlling the invariant density functions of such systems. The work of this thesis focused on the development of new methods and algorithms of reconstruction of one-dimensional chaotic maps from sequences of probability density functions. The methods were successfully applied to model the dynamical evolution of heterogeneous human embryonic stem cell populations. The reconstruction for dynamical systems subjected to additive perturbations from sequences of probability density functions and the design of control laws to achieve desired invariant density function were also considered. The main contributions are summarised as follows:

- **A novel approach to solving the generalised inverse Frobenius-Perron problem**

  In Chapter 3 a novel matrix-based approach was proposed to solve the generalised inverse Frobenius-Perron problem and was extended to general nonlinear systems in Chapter 4. These addressed in a systematic manner the

problem of inferring one-dimensional chaotic maps based on sequences of probability density functions. Compared with previous solutions to solving the inverse Frobenius-Perron problem, it has been rigorously demonstrated that the proposed approach can uniquely identify the unknown transformation sufficient conditions, of which sufficient conditions have been derived. Specifically, the reconstructed maps can exhibit the same dynamics as the original systems and therefore can be used to predict the long term dynamical evolution, infer dynamical invariants and to control the dynamical behaviour of the underlying system of interest. The applicability of the proposed methodology and its performance for different levels of noise was demonstrated using numerical simulations involving a piecewise linear and expanding transformations as well as a continuous one-dimensional nonlinear transformation.

- **Modelling heterogeneous populations of human embryonic stem cell**

  In Chapter 5 the developed solution to the GIFPP was successfully applied to infer the dynamical model that characterises the dynamical evolution of heterogeneous stem cell populations (pluripotent carcinoma cell line NTERA2), using densities generated experimentally by fluorescence-based flow cytometry. The model described the transition of SSEA3 cell surface marker expression over a single day interval. The reconstructed dynamical model enables us to characterise and compare rigorously the dynamics of different cell populations, predict the long term evolution of SSEA3-sorted cell fractions, as well as identify the particular stationary points which have biological relevance.

- **A novel approach to modelling chaotic dynamical systems subjected to additive perturbations from sequences of probability density functions**

  In Chapter 6 a novel method of inferring models of one-dimensional chaotic dynamical systems with additive perturbations was proposed based on sequences of probability density functions measured from the perturbation-corrupted data. Two forms of additive perturbations were analysed respectively: a chaotic map subjected to an additive input; a chaotic map subjected to an additive random noise, for which probability density function of the input and

noise were both assumed to be known. The evolution of probability densities was formulated, which gives rise to the description of Foias operator corresponding to the perturbed dynamical system. An approximate matrix representation of Foias operator was derived by assuming the chaotic map to be a piecewise linear semi-Markov transformation. In this way, the density evolution equation was transformed into a matrix equation that links two successive density functions and the Frobenius-Perron matrix associated with the transformation. The modelling problem was then reduced to an inverse problem to recover the Frobenius-Perron matrix based on the new developed two-step matrix-based method. Numerical examples were provided to demonstrate the effectiveness of the developed approaches to modelling for chaotic dynamical systems subjected to additive perturbation from density functions.

- **A new algorithm of controlling the invariant densities of chaotic dynamical systems subjected to additive stochastic perturbations**

  In Chapter 7 the asymptotic stability of probability density functions, equivalently statistical stability, of chaotic dynamical systems subjected to additive stochastic perturbations was proven, which reveals the unique existence of invariant densities of such systems. Estimation of the corresponding invariant density functions was derived. For a stochastic dynamical system, given the additive input and random noise densities, the mathematical characterisation of the evolution of densities was inferred, resulting in the estimated matrix representing the Foias operator. Using the developed matrix-based approach, the chaotic maps of the perturbed underlying systems can be reconstructed from the probability density functions measured from the observed perturbation-corrupted data. Based on the derived mathematical relationship connecting the control input density function and the invariant density function, the control algorithm was designed for the objective of determining the control input density function to manipulate the invariant density function to be as close as possible to a desired one. A simulation example was given to illustrate the effectiveness of proposed control strategy.

8.2 Future work

As an alternative to the traditional data-based methodology of modelling and controlling dynamical systems with individual point orbits, the strategies developed in this thesis have mainly addressed the generalised inverse problem and the problem of designing control law for one-dimensional chaotic dynamical systems. Considering the complexity of real systems and potential application prospects of the achieved results, the following issues can be further investigated in the future research.

- The methods presented in the thesis can be extended to higher-dimensional maps but this is not necessarily straightforward. As noted in (Bollt 2000a), for higher-dimensional systems the Ulam's conjecture has been proven for some special cases (Boyarsky & Lou 1991, Ding & Zhou 1995, Froyland 1995, Froyland 1997). A possible solution would be to convert the N-dimensional problem to a 1-D problem, approximate the Frobenius-Perron operator by a stochastic matrix (Rogers, Shorten et al. 2008b) and then use Bollt's approach (Bollt 2000a) to construct a piecewise linear transformation which approximates the original map.

- The inverse problem for stochastic dynamical systems considered a typical form of additive perturbations. There are other forms of perturbation appearance in a multiplicative fashion, and a both additive and multiplicative way. For these cases, the proposed algorithms provide a starting point to derive the mathematical description of the evolution of density functions and the matrix representation of the corresponding Foias operator. Using the matrix-based approach described in Chapter 6, the Frobenius-Perron matrix associated with the chaotic map can be identified. Therefore, the proposed method can be applied to solve the inverse problem for general stochastic dynamical systems.

- In Chapter 5 there are five fractions divided by the FACS machine. Fractions of these cells expressing different levels of SSEA3 generate the whole population but at differing rates. The equilibrium points can be predicted from the reconstructed dynamical model. Further experiments can be conducted to

investigate the regeneration of the cells on the equilibrium points. The cell sorting can be refined from the predicted equilibrium points. Experimental results can be used to validate the stability of these fractions which need to take longer time to regenerate the parent distribution, and on the other hand, this provides a new way to demonstrate the validity of the model.

- Based on the inferred dynamical model of heterogeneous stem cell populations, the developed control algorithm can be used to design the control strategy. The control objective is to optimise the cell culture conditions so as to manipulate the differentiation of the heterogeneous embryonic stem cells into desired cells that can be used in regenerative therapies.

Appendix: Initial states generation

The 100 sets of initial states used in the example are obtained by sampling the following density functions.

$$f_{0,1}^{\beta_1}(x,\beta_1)=\frac{7}{10}\cdot\frac{x^{29}(1-x)^{\beta_1-1}}{\mathrm{B}(30,\beta_1)}+\frac{3}{10}\cdot\frac{x^{\beta_1-1}(1-x)^{29}}{\mathrm{B}(\beta_1,30)},\quad \beta_1=1,2,\ldots,30;$$

$$f_{0,2}^{\beta_2}(x,\beta_2)=\frac{x^{\beta_2-1}(1-x)^{29}}{\mathrm{B}(\beta_2,30)},\quad \beta_2=1,2,\ldots,25;$$

$$f_{0,3}^{\beta_3}(x,\beta_3)=\frac{x^{29}(1-x)^{\beta_3-1}}{\mathrm{B}(30,\beta_3)},\quad \beta_3=1,2,\ldots,25;$$

$$f_{0,4}^{\beta_4}(x,\beta_4)=\frac{1}{2}\cdot\frac{x^{39}(1-x)^{\beta_4+19}}{\mathrm{B}(40,\beta_4)}+\frac{1}{2}\cdot\frac{x^{39}(1-x)^{\beta_4+19}}{\mathrm{B}(40,\beta_4)},\quad \beta_4=1,2,\ldots,10;$$

$$f_{0,5}^{\beta_5}(x,\beta_5)=\frac{1}{2}\cdot\frac{x^{\beta_5+19}(1-x)^{39}}{\mathrm{B}(\beta_5,40)}+\frac{1}{2}\cdot\frac{x^{\beta_5+19}(1-x)^{39}}{\mathrm{B}(\beta_5,40)},\quad \beta_5=1,2,\ldots,10;$$

where $\mathrm{B}(\cdot,\cdot)$ is beta function.

Bibliography

Abarbanel, H. D. I., R. Brown and J. B. Kadtke (1989). "Prediction and system identification in chaotic nonlinear systems: Time series with broadband spectra." Physics Letters A **138**(8): 401-408.

Ackerman, S. L., B. B. Knowles and P. W. Andrews (1994). "Gene regulation during neuronal and non-neuronal differentiation of NTERA2 human teratocarcinoma-derived stem cells." Molecular Brain Research **25**(1–2): 157-162.

Aguirre, L. A. and S. A. Billings (1995a). "Identification of models for chaotic systems from noisy data: implications for performance and nonlinear filtering." Physica D: Nonlinear Phenomena **85**(1–2): 239-258.

Aguirre, L. A. and S. A. Billings (1995b). "Retrieving dynamical invariants from chaotic data using NARMAX models." International Journal of Bifurcation and Chaos **05**(02): 449-474.

Aherne, F. J., N. A. Thacker and P. I. Rockett (1998). "The Bhattacharyya metric as an absolute similarity measure for frequency coded data." Kybernetika **34**(4): [363]-368.

Altschuler, S. J. and L. F. Wu (2010). "Cellular Heterogeneity: Do Differences Make a Difference?" Cell **141**(4): 559-563.

Andrews, P., I. Damjanov, D. Simon, G. Banting, C. Carlin, N. Dracopoli and J. Føgh (1984). "Pluripotent embryonal carcinoma clones derived from the human teratocarcinoma cell line Tera-2. Differentiation in vivo and in vitro." Laboratory investigation; a journal of technical methods and pathology **50**(2): 147-162.

Andrews, P. W. (1984). "Retinoic acid induces neuronal differentiation of a cloned human embryonal carcinoma cell line in vitro." Developmental Biology **103**(2): 285-293.

Andrews, P. W. (1998). "Teratocarcinomas and human embryology: pluripotent human EC cell lines." Apmis **106**(1 - 6): 158-168.

Åström, K. J. (1970). Introduction to stochastic control theory. New York ; London, Academic Press.

Åström, K. J. and B. Wittenmark (1989). Adaptive Control. Reading, MA, Addison-Wesley.

Bani-Yaghoub, M., J. M. Felker and C. C. Naus (1999). "Human NT2/D1 cells differentiate into functional astrocytes." Neuroreport **10**(18): 3843-3846.

Baranovsky, A. and D. Daems (1995). "Design of one-dimensional chaotic maps with prescribed statistical properties." International Journal of Bifurcation and Chaos **5**(6): 1585-1598.

Billings, S. A. and D. Coca (1999). "Dsicrete wavelet models for identification and qualitative analysis of chaotic systems " International Journal of Bifurcation and Chaos **09**(07): 1263-1284.

Billings, S. A., H. B. Jamaluddin and S. Chen (1992). "Properties of neural networks with applications to modelling non-linear dynamical systems." International Journal of Control **55**(1): 193-224.

Bollt, E., P. Góra, A. Ostruszka and K. Zyczkowski (2008). "Basis Markov partitions and transition matrices for stochastic systems." SIAM Journal on Applied Dynamical Systems **7**(2): 341-360.

Bollt, E. M. (2000a). "Controlling chaos and the inverse Frobenius-Perron problem: Global stabilization of arbitrary invariant measures." International Journal of Bifurcation and Chaos **10**(5): 1033-1050.

Bollt, E. M. (2000b). "Controlling invariant density: An l(infinity) solution to the inverse Frobenius-Perron problem." ISCAS 2000: IEEE International Symposium on Circuits and Systems: 112-115.

Boyarsky, A. and P. Góra (1997). Laws of chaos : invariant measures and dynamical systems in one dimension. Boston, Mass., Birkhäuser.

Boyarsky, A. and P. Góra (2002). "Chaotic maps derived from trajectory data." Chaos: An Interdisciplinary Journal of Nonlinear Science **12**(1): 42-48.

Boyarsky, A. and P. Góra (2008). "An Irreversible Process Represented by a Reversible One." International Journal of Bifurcation and Chaos **18**(07): 2059-2061.

Boyarsky, A. and Y. Lou (1991). "Approximating measures invariant under higher-dimensional chaotic transformations." Journal of Approximation Theory **65**(2): 231-244.

Brown, R., N. F. Rulkov and E. R. Tracy (1994). "Modeling and synchronizing chaotic systems from time-series data." Physical Review E **49**(5): 3784-3800.

Casdagli, M. (1989). "Nonlinear prediction of chaotic time series." Physica D: Nonlinear Phenomena **35**(3): 335-356.

Chambers, I., J. Silva, D. Colby, J. Nichols, B. Nijmeijer, M. Robertson, J. Vrana, K. Jones, L. Grotewold and A. Smith (2007). "Nanog safeguards pluripotency and mediates germline development." Nature **450**(7173): 1230-1234.

Chang, H. H., M. Hemberg, M. Barahona, D. E. Ingber and S. Huang (2008). "Transcriptome-wide noise controls lineage choice in mammalian progenitor cells." Nature **453**(7194): 544-547.

Chang, T. P. (2011). "Estimation of wind energy potential using different probability density functions." Applied Energy **88**(5): 1848-1856.

Coca, D. and S. A. Billings (2001). "Non-linear system identification using wavelet multiresolution models." International Journal of Control **74**(18): 1718-1736.

Coen, E. M., R. G. Gilbert, B. R. Morrison, H. Leube and S. Peach (1998). "Modelling particle size distributions and secondary particle formation in emulsion polymerisation." Polymer **39**(26): 7099-7112.

Crespo, L. G. and J. Q. Sun (2002). Nonlinear stochastic control via stationary probability density functions. Proceedings of the American Control Conference, Anchorage, AK.

Crespo, L. G. and J. Q. Sun (2003). "Non-linear stochastic control via stationary response design." Probabilistic Engineering Mechanics **18**(1): 79-86.

Crowley, T. J., E. S. Meadows, E. Kostoulas and F. J. Doyle Iii (2000). "Control of particle size distribution described by a population balance model of semibatch emulsion polymerization." Journal of Process Control **10**(5): 419-432.

Diakonos, F. K., D. Pingel and P. Schmelcher (1999). "A stochastic approach to the construction of one-dimensional chaotic maps with prescribed statistical properties." Physics Letters A **264**(2–3): 162-170.

Diakonos, F. K. and P. Schmelcher (1996). "On the construction of one-dimensional iterative maps from the invariant density: the dynamical route to the beta distribution." Physics Letters A **211**(4): 199-203.

Ding, J. and A. H. Zhou (1995). "Piecewise linear Markov approximations of Frobenius-Perron operators associated with multi-dimensional transformations." Nonlinear Analysis: Theory, Methods & Applications **25**(4): 399-408.

Draper, J. S., C. Pigott, J. A. Thomson and P. W. Andrews (2002a). "Surface antigens of human embryonic stem cells: changes upon differentiation in culture." Journal of anatomy **200**(3): 249-258.

Draper, J. S., C. Pigott, J. A. Thomson and P. W. Andrews (2002b). "Surface antigens of human embryonic stem cells: changes upon differentiation in culture*." Journal of Anatomy **200**(3): 249-258.

Enver, T., M. Pera, C. Peterson and P. W. Andrews (2009). "Stem Cell States, Fates, and the Rules of Attraction." Cell Stem Cell **4**(5): 387-397.

Enver, T., S. Soneji, C. Joshi, J. Brown, F. Iborra, T. Orntoft, T. Thykjaer, E. Maltby, K. Smith, R. A. Dawud, M. Jones, M. Matin, P. Gokhale, J. Draper and P. W. Andrews (2005). "Cellular differentiation hierarchies in normal and culture-adapted human embryonic stem cells." Human Molecular Genetics **14**(21): 3129-3140.

Ershov, S. V. and G. G. Malinetskii (1988). "The solution of the inverse problem for the Perron-Frobenius equation." USSR Computational Mathematics and Mathematical Physics **28**(5): 136-141.

Farmer, J. D. and J. J. Sidorowich (1987). "Predicting chaotic time series." Physical Review Letters **59**(8): 845-848.

Fenderson, B. A., P. W. Andrews, E. Nudelman, H. Clausen and S.-i. Hakomori (1987). "Glycolipid core structure switching from globo-to lacto-and ganglio-series during retinoic acid-induced differentiation of TERA-2-derived human embryonal carcinoma cells." Developmental biology **122**(1): 21-34.

Forbes, M., J. F. Forbes and M. Guay (2003a). Control design for discrete-time stochastic nonlinear processes with a nonquadratic performance objective. Decision and Control, 2003. Proceedings. 42nd IEEE Conference on.

Forbes, M., M. Guay and J. F. Forbes (2004a). Probabilistic control design for continuous-time stochastic nonlinear systems: a PDF-shaping approach. Intelligent Control, 2004. Proceedings of the 2004 IEEE International Symposium on, IEEE.

Forbes, M. G., J. F. Forbes and M. Guay (2003b). "Regulatory control design for stochastic processes: Shaping the probability density function." Proceedings of the 2003 American Control Conference, Vols 1-6: 3998-4003.

Forbes, M. G., J. F. Forbes and M. Guay (2004). "Regulating discrete-time stochastic systems: focusing on the probability density function." DYNAMICS OF CONTINUOUS DISCRETE AND IMPULSIVE SYSTEMS SERIES B **11**: 81-100.

Forbes, M. G., J. F. Forbes and M. Guay (2006). "Controller design for discrete-time stochastic processes with nonquadratic loss." Technometrics **48**(3): 361-372.

Forbes, M. G., M. Guay and J. F. Forbes (2002). PDF-shaping control design. World Congress on Automatic Control, Barcelona, Spain.

Forbes, M. G., M. Guay and J. F. Forbes (2004b). "Control design for first-order processes: shaping the probability density of the process state." Journal of Process Control **14**(4): 399-410.

Friedman, N. and A. Boyarsky (1981). "Matrices and Eigenfunctions Induced by Markov Maps." Linear Algebra and Its Applications **38**(Jun): 141-147.

Friedman, N. and A. Boyarsky (1982). "Construction of Ergodic Transformations." Advances in Mathematics **45**(3): 213-254.

Froyland, G. (1995). "Finite approximation of Sinai-Bowen-Ruelle measures for Anosov systems in two dimensions." Random and Computational Dynamics **3**(4): 251-264.

Froyland, G. (1997). Computing physical invariant measures. Int. Symp. Nonlinear Theory and its Applications, Japan, Research Society of Nonlinear Theory and its Applications (IEICE).

Gleick, J. (2008). Chaos: Making a new science. New York, Penguin.

Goodwin, G. and K. S. Sin (1984). "Adaptive filtering, prediction and control." Englewood Clifs: Prentice Ha lI.

Góra, P. and A. Boyarsky (1993). "A Matrix Solution to the Inverse Perron-Frobenius Problem." Proceedings of the American Mathematical Society **118**(2): 409-414.

Góra, P. and A. Boyarsky (1996). "An algorithm to control chaotic behavior in one-dimensional maps." Computers & Mathematics with Applications **31**(6): 13-22.

Góra, P. and A. Boyarsky (1998). "A new approach to controlling chaotic systems." Physica D **111**(1-4): 1-15.

Góra, P. and A. Boyarsky (2001). "Optimal control of chaotic systems." International Journal of Bifurcation and Chaos **11**(07): 2007-2018.

Götz, M., A. Abel and W. Schwarz (1997). What is the Use of Frobenius-Perron Operator for Chaotic Signal Processing? in Proc. NDES, Citeseer.

Guo, L. and H. Wang (2003). Pseudo-PID tracking control for a class of output PDFs of general non-Gaussian stochastic systems. American Control Conference, 2003. Proceedings of the 2003.

Guo, L. and H. Wang (2005a). "Generalized discrete-time PI control of output PDFs using square root B-spline expansion." Automatica **41**(1): 159-162.

Guo, L. and H. Wang (2005b). "PID controller design for output PDFs of stochastic systems using linear matrix inequalities." Systems, Man, and Cybernetics, Part B: Cybernetics, IEEE Transactions on **35**(1): 65-71.

Guo, L., H. Wang and A. Wang (2008). "Optimal probability density function control for NARMAX stochastic systems." Automatica **44**(7): 1904-1911.

Hayashi, K., S. M. Lopes, F. Tang and M. A. Surani (2008a). "Dynamic equilibrium and heterogeneity of mouse pluripotent stem cells with distinct functional and epigenetic states." Cell stem cell **3**(4): 391-401.

Hayashi, K., S. M. C. d. S. Lopes, F. Tang and M. A. Surani (2008b). "Dynamic Equilibrium and Heterogeneity of Mouse Pluripotent Stem Cells with Distinct Functional and Epigenetic States." Cell Stem Cell **3**(4): 391-401.

Holmes, P. and F. Moon (1983). "Strange attractors and chaos in nonlinear mechanics." Journal of Applied Mechanics **50**(4b): 1021-1032.

Hong, W. and P. Afshar (2006). Radial Basis Function based Iterative Learning Control for stochastic distribution systems. Computer Aided Control System Design, 2006 IEEE International Conference on Control Applications, 2006 IEEE International Symposium on Intelligent Control, 2006 IEEE.

Hsu, C. S. (1987). Cell-to-cell mapping: a method of global analysis for nonlinear systems, Springer New York.

Huang, W. (2006). "Constructing chaotic transformations with closed functional forms." Discrete Dynamics in Nature and Society **2006**.

Huang, W. (2009a). "Constructing Multi-Branches Complete Chaotic Maps That Preserve Specified Invariant Density." Discrete Dynamics in Nature and Society **2009**: 14.

Huang, W. (2009b). On the complete chaotic maps that preserve prescribed absolutely continuous invariant densities. Topics on Chaotic Systems: Selected Papers from CHAOS 2008 International Conference.

Iourtchenko, D. V. (2000). "Stochastic Optimal Bounded Control for a System With the Boltz Cost Function." Journal of Vibration and Control **6**(8): 1195-1204.

Isabelle, S. H. and G. W. Wornell (1997). "Statistical analysis and spectral estimation techniques for one-dimensional chaotic signals." Signal Processing, IEEE Transactions on **45**(6): 1495-1506.

Islam, M. S. and P. Góra (2011). "Invariant measures of stochastic perturbations of dynamical systems using Fourier approximations." International Journal of Bifurcation and Chaos **21**(01): 113-123.

Jabłoński, M., P. Góra and A. Boyarsky (1996). "A general existence theorem for absolutely continous invariant measures on bounded and unbounded intervals." Nonlinear World **3**: 183-200.

Karny, M. (1996). "Towards fully probabilistic control design." Automatica **32**(12): 1719-1722.

Kárný, M. and T. V. Guy (2006). "Fully probabilistic control design." Systems & Control Letters **55**(4): 259-265.

Kellert, S. H. and L. Sklar (1997). "In the wake of chaos: Unpredictable order in dynamical systems." Philosophy of Science **64**(1): 181.

Koga, S. (1991). "The inverse problem of Flobenius-Perron equations in 1D difference systems—1D map idealization." Progress of Theoretical Physics **86**(5): 991-1002.

Kuske, P. and G. Papanicolaou (1998). "The invariant density of a chaotic dynamical system with small noise." Physica D: Nonlinear Phenomena **120**(3–4): 255-272.

Lai, Y.-C. and C. Grebogi (1993). "Synchronization of chaotic trajectories using control." Physical Review E **47**(4): 2357.

Laskar, J. (1989). "A numerical experiment on the chaotic behaviour of the solar system."

Laskar, J. (1994). "Large-scale chaos in the solar system." Astronomy and Astrophysics **287**: L9-L12.

Laslett, A., S. Grimmond, B. Gardiner, L. Stamp, A. Lin, S. Hawes, S. Wormald, D. Nikolic-Paterson, D. Haylock and M. Pera (2007). "Transcriptional analysis of early lineage commitment in human embryonic stem cells." BMC Developmental Biology **7**(1): 12.

Lasota, A. and M. C. Mackey (1994). Chaos, fractals, and noise : stochastic aspects of dynamics. New York, Springer-Verlag.

Lasota, A. and J. A. Yorke (1973). "On the existence of invariant measures for piecewise monotonic transformations." Transactions of the American Mathematical Society **186**: 481-488.

Lee, V. M.-y. and P. Andrews (1986). "Differentiation of NTERA-2 clonal human embryonal carcinoma cells into neurons involves the induction of all three neurofilament proteins." The Journal of neuroscience **6**(2): 514-521.

Li, T.-Y. (1976). "Finite approximation for the Frobenius-Perron operator. A solution to Ulam's conjecture." Journal of Approximation Theory **17**(2): 177-186.

Lorenz, E. N. (1995). The essence of chaos, University of Washington Press.

Lozowski, A. G., M. Lysetskiy and J. M. Zurada (2004). "Signal Processing with temporal sequences in olfactory systems." Neural Networks, IEEE Transactions on **15**(5): 1268-1275.

Lu, J. and R. R. Skelton (1998). "Covariance control using closed-loop modelling for structures." Earthquake Engineering and Structural Dynamics **27**(11): 1367-1383.

MacArthur, B. D. and I. R. Lemischka (2013). "Statistical Mechanics of Pluripotency." Cell **154**(3): 484-489.

Medio, A. and G. Gallo (1995). Chaotic dynamics: Theory and applications to economics, Cambridge University Press.

Miyazono, M., V. Lee and J. Q. Trojanowski (1995). "Proliferation, cell death, and neuronal differentiation in transplanted human embryonal carcinoma (NTera2) cells depend on the graft site in nude and severe combined immunodeficient mice." Laboratory investigation; a journal of technical methods and pathology **73**(2): 273-283.

Mondragó C., R. J. (1999). "A model of packet traffic using a random wall model." International Journal of Bifurcation and Chaos **09**(07): 1381-1392.

Olariu, V., D. Coca, S. A. Billings, P. Tonge, P. Gokhale, P. W. Andrews and V. Kadirkamanathan (2009). "Modified variational Bayes EM estimation of hidden Markov tree model of cell lineages." Bioinformatics **25**(21): 2824-2830.

Ostruszka, A. and K. Życzkowski (2001). "Spectrum of the Frobenius–Perron operator for systems with stochastic perturbation." Physics Letters A **289**(6): 306-312.

Ott, E. (1993). Chaos in Dynamical Systems. Cambridge, Cambridge University Press.

Papoulis, A. (1991). "Probability, random variables and stochastic processes." McGraw-Hill.

Pera, M. F., S. Cooper, J. Mills and J. M. Parrington (1989). "Isolation and characterization of a multipotent clone of human embryonal carcinoma cells." Differentiation **42**(1): 10-23.

Philips, M. F., J. K. Muir, K. E. Saatman, R. Raghupathi, V. M.-Y. Lee, J. Q. Trojanowski and T. K. McIntosh (1999). "Survival and integration of transplanted postmitotic human neurons following experimental brain injury in immunocompetent rats." Journal of neurosurgery **90**(1): 116-124.

Pigeon, B., M. Perrier and B. Srinivasan (2011). "Shaping probability density functions using a switching linear controller." Journal of Process Control **21**(6): 901-908.

Pikovsky, A. and O. Popovych (2003). "Persistent patterns in deterministic mixing flows." EPL (Europhysics Letters) **61**(5): 625.

Pingel, D., P. Schmelcher and F. K. Diakonos (1999). "Theory and examples of the inverse Frobenius-Perron problem for complete chaotic maps." Chaos **9**(2): 357-366.

Pleasure, S. and V. Y. Lee (1993). "NTera 2 cells: a human cell line which displays characteristics expected of a human committed neuronal progenitor cell." Journal of neuroscience research **35**(6): 585-602.

Potthast, R. (2012). "Implementing Turing Machines in Dynamic Field Architectures." arXiv preprint arXiv:1204.5462.

Principe, J. C., A. Rathie and J.-M. Kuo (1992). "Prediction of chotic time series with neural networks and the issue of dynamic modeling." International Journal of Bifurcation and Chaos **02**(04): 989-996.

Rendt, J., S. Erulkar and P. Andrews (1989). "Presumptive neurons derived by differentiation of a human embryonal carcinoma cell line exhibit tetrodotoxin-sensitive sodium currents and the capacity for regenerative responses." Experimental cell research **180**(2): 580-584.

Rényi, A. (1957). "Representation for real numbers and their ergodic properties." Acta Mathematica Hungarica **8**: 477-493.

Rogers, A., R. Shorten and D. M. Heffernan (2004). "Synthesizing chaotic maps with prescribed invariant densities." Physics Letters A **330**(6): 435-441.

Rogers, A., R. Shorten and D. M. Heffernan (2008a). "A novel matrix approach for controlling the invariant densities of chaotic maps." Chaos Solitons & Fractals **35**(1): 161-175.

Rogers, A., R. Shorten, D. M. Heffernan and D. Naughton (2008b). "Synthesis of Piecewise-Linear Chaotic Maps: Invariant Densities, Autocorrelations, and Switching." International Journal of Bifurcation and Chaos **18**(8): 2169-2189.

Rovatti, R., G. Mazzini, G. Setti and A. Giovanardi (2002). "Statistical modeling and design of discrete-time chaotic processes: advanced finite-dimensional tools and applications." Proceedings of the IEEE **90**(5): 820-841.

Rozenholc, Y., T. Mildenberger and U. Gather (2010). "Combining regular and irregular histograms by penalized likelihood." Computational Statistics & Data Analysis **54**(12): 3313-3323.

Schütte, C., W. Huisinga and P. Deuflhard (2001). Transfer Operator Approach to Conformational Dynamics in Biomolecular Systems. Ergodic Theory, Analysis, and Efficient Simulation of Dynamical Systems. B. Fiedler, Springer Berlin Heidelberg**:** 191-223.

Setti, G., G. Mazzini, R. Rovatti and S. Callegari (2002). "Statistical modeling of discrete-time chaotic processes-basic finite-dimensional tools and applications." Proceedings of the IEEE **90**(5): 662-690.

Shevinsky, L. H., B. B. Knowles, I. Damjanov and D. Solter (1982). "Monoclonal antibody to murine embryos defines a stage-specific embryonic antigen expressed on mouse embryos and human teratocarcinoma cells." Cell **30**(3): 697-705.

Shinbrot, T., C. Grebogi, E. Ott and J. A. Yorke (1992). "Using chaos to target stationary states of flows." Physics Letters A **169**(5): 349-354.

Solter, D. and I. Damjanov (1979). Teratocarcinoma and the expression of oncodevelopmental genes, Academic Press.

Srivastava, R., P. K. Srivastava and J. Chattopadhyay (2013). "Chaos in a chemical system." The European Physical Journal Special Topics **222**(3-4): 777-783.

Stevens, L. (1966). "The biology of teratomas." Advances in morphogenesis **6**: 1-31.

Stewart, M. H., M. Bossé, K. Chadwick, P. Menendez, S. C. Bendall and M. Bhatia (2006). "Clonal isolation of hESCs reveals heterogeneity within the pluripotent stem cell compartment." Nature methods **3**(10): 807-815.

Tonge, P. D., V. Olariu, D. Coca, V. Kadirkamanathan, K. E. Burrell, S. A. Billings and P. W. Andrews (2010). "Prepatterning in the stem cell compartment." PloS one **5**(5): e10901.

Tonge, P. D., M. Shigeta, T. Schroeder and P. W. Andrews (2011). "Functionally defined substates within the human embryonic stem cell compartment." Stem Cell Research **7**(2): 145-153.

Ulam, S. M. (1960). A collection of mathematical problems: Interscience Tracts in Pure and Applied Mathematics. New York, Interscience.

Ulam, S. M. and J. von Neumann (1947). "On combinations of stochastic and deterministic processes." Bulletin of the American Mathematical Society **53**: 1120.

van Wyk, M. A. and J. Ding (2002). "Stochastic analysis of electrical circuits." Chaos in Circuits and Systems], edited by G. Chen and T. Ueta: 215-236.

Voss, H. U., J. Timmer and J. Kurths (2004). "Nonlinear dynamcial system identification from uncertain and indrect measurements." International Journal of Bifurcation and Chaos **14**(06): 1905-1933.

Walsh, J. and P. W. Andrews (2003). "Expression of Wnt and Notch pathway genes in a pluripotent human embryonal carcinoma cell line and embryonic stem cells." Apmis **111**(1): 197-211.

Wang, A., P. Afshar and H. Wang (2008). "Complex stochastic systems modelling and control via iterative machine learning." Neurocomputing **71**(13–15): 2685-2692.

Wang, H. (1999a). Bounded dynamic stochastic distribution: modelling and control. London, Springer-Verlag.

Wang, H. (1999b). "Model reference adaptive control of the output stochastic distributions for unknown linear stochastic systems." International Journal of Systems Science **30**(7): 707-715.

Wang, H. (1999c). "Robust control of the output probability density functions for multivariable stochastic systems with guaranteed stability." Ieee Transactions on Automatic Control **44**(11): 2103-2107.

Wang, H. (2000). Bounded dynamic stochastic systems : modelling and control. London, Springer.

Wang, H. (2002). "Minimum entropy control of non-Gaussian dynamic stochastic systems." IEEE Transactions on Automatic Control **47**(2): 398-403.

Wang, H. (2003). "Control of conditional output probability density functions for general nonlinear and non-Gaussian dynamic stochastic systems." Iee Proceedings-Control Theory and Applications **150**(1): 55-60.

Wang, H., H. Baki and P. Kabore (2001). "Control of bounded dynamic stochastic distributions using square root models: an applicability study in papermaking systems." Transactions of the Institute of Measurement and Control **23**(1): 51-68.

Wang, H., P. Kabore and H. Baki (2001). "Lyapunov-based controller design for bounded dynamic stochastic distribution control." Iee Proceedings-Control Theory and Applications **148**(3): 245-250.

Wang, H., J. Zhang and H. Yue (2005a). "Multi-step predictive control of a PDF-shaping problem." ACTA AUTOMATICA SINICA **31**(2): 274-279.

Wang, H., J. F. Zhang and H. Yue (2005b). "Iterative learning control of output PDF shaping in stochastic systems." 2005 IEEE International Symposium on Intelligent Control & 13th Mediterranean Conference on Control and Automation, Vols 1 and 2: 1225-1230.

Wang, H. and J. H. Zhang (2001). "Bounded stochastic distributions control for pseudo-ARMAX stochastic systems." IEEE Transactions on Automatic Control **46**(3): 486-490.

Wigren, T. (2009). "Soft Uplink Load Estimation in WCDMA." Vehicular Technology, IEEE Transactions on **58**(2): 760-772.

Wojtkiewicz, S. F. and L. A. Bergman (2001). "Moment specification algorithm for control of nonlinear systems driven by Gaussian white noise." Nonlinear Dynamics **24**(1): 17-30.

Wyk, M. A. v. and J. Ding (2002). Stochastic Analysis of Electrical Circuits. Chaos in Circuits and Systems**:** 215-236.

Yang, Y., G. Lei and W. Hong (2009). "Constrained PI Tracking Control for Output Probability Distributions Based on Two-Step Neural Networks." Circuits and Systems I: Regular Papers, IEEE Transactions on **56**(7): 1416-1426.

Yue, H., A. J. A. Leprand and H. Wang (2005). "Stochastic distribution control of singular systems: output PDF shaping." ACTA AUTOMATICA SINICA **31**(1): 151-161.

Yue, H., J. Zhang, H. Wang and L. Cao (2004). Shaping of molecular weight distribution using B-spline based predictive probability density function control. American Control Conference, 2004. Proceedings of the 2004.

Zhiwei, S. and H. Min (2007). "Support Vector Echo-State Machine for Chaotic Time-Series Prediction." Neural Networks, IEEE Transactions on **18**(2): 359-372.

Zhu, C. X. and W. Q. Zhu (2011). "Feedback control of nonlinear stochastic systems for targeting a specified stationary probability density." Automatica **47**(3): 539-544.

Zhu, C. X. and W. Q. Zhu (2012). "Control of stationary probability density of nonlinear systems subject to Poisson white noise excitation." Journal of Vibration and Control.